Application of High Resolution Seismic Technique in Precambrian Terrain (Sudbury, Ontario)

Mulugeta H. Serzu

A Thesis
Presented to The University of Manitoba
in Partial Fullfilment of the Requirement for the Degree of
Master of Science
in
Geophysics

Department of Geological Sciences
The University of Manitoba
Winnipeg, Canada

April, 1990

ISBN 0-315-63263-1

APPLICATION OF HIGH RESOLUTION SEISMIC TECHNIQUE IN PRECAMBRIAN TERRAIN (SUDBURY, ONTARIO)

BY

MULUGETA H. SERZU

A thesis submitted to the Faculty of Graduate Studies of the University of Manitoba in partial fulfillment of the requirements of the degree of

MASTER OF SCIENCE

I hereby declare that I am the sole author of this thesis.

I authorize the University of Manitoba to lend this thesis to other institutions or individuals for the purpose of scholarly research.

Mulugeta Hailu Serzu

I further authorize the University of Manitoba to produce this thesis by photocopying or by other means, in total or in part, at the request of other institutions or individuals for the purpose of scholarly research.

Mulugeta Hailu Serzu

Abstract

Use of the High Resolution Reflection Seismic Technique in the precambrian crystalline environment has gained increased application in the past few years. The conventional seismic data processing technique developed by the petroleum industry for sedimentary basins is often not appropriate to analyse data recorded over geologically complex crystalline environment. The development of new processing techniques discussed in this thesis are specifically aimed at high resolution seismic data collected over precambrian terrain.

In this study Prestack Partial Migration (dip-moveout) algorithm was developed to correct for the geometrical effects associated with dipping and curved reflectors on the recorded seismic data (Serzu and Moon, 1989(b)). The dip-moveout (DMO) correction via partial prestack migration is performed in the $f-k$ domain. The DMO algorithm developed in this study requires an efficient FFT program. The FFT subroutines available in user subroutine libraries require the whole dataset to reside in the computer real memory. Reflection seismic datasets are extremely large, and require very large amount of computer real memory to Fourier transform the data. In time sharing systems such as the University of Manitoba Amdhal mainframe Computer, there is a limited core memory a user is allowed to access. The memory and input/output (I/O) count restriction imposed by the time sharing systems, make the in-place FFT subroutines ineffective as far as large datasets are concerned. For this reason an efficient Stepwise 2-D FFT software has been developed to handle large datasets that performs very well in limited core memory (Serzu and Moon, 1989(a)).

To test the prestack partial migration software, a wave equation modeling and a post stack migration programs have also been developed in this study. These al-

gorithms are tested with point diffractors and other simple geological models. The synthetic tests showed promising results. Upon completion of the prestack and post-stack migration experiments on synthetic data, the high resolution reflection seismic data from Sudbury, Ontario, was processed using the newly developed prestack processing technique. The final section with prestack partial migration showed marked improvement compared to the section without prestack DMO.

Results of the high resolution seismic experiment with DMO processing revealed observable discontinuities in the form of reflectors and faults. However, contrary to the conclusions of previous study (Messfin and Moon, 1984), direct mapping of the massive sulphide was not feasible due to the relative small thickness of the ore bodies with respect to the wavelength of the signal. In spite of the improved and careful data processing algorithms developed and tested in this study, improvement in the final result was not as significant as anticipated. This is perhaps due to low S/N ratio in the original field records. It is the recommendation of this study that future high resolution seismic data aquisition strategy in crystalline environment be carefully designed for the most optimum field aquisition parameters, and that more suitable receivers and recording instruments appropriate for hard rock terraines be utilized to record the desired high frequency signal bandwidth with integrity.

Acknowledgments

The author wishes to express his sincere gratitude to Dr. Wooil M. Moon for his advice and guidance during the course of this thesis research. Many thanks to Mr. Joong-Sun Won for helpfull suggestions during the programming stage of the prestack partial migration.

Financial support of this research by the Natural Sciences and Engineering Research Council (NSERC) of Canada is thankfully acknowledged. Logistic support provided by INCO Gold Inc. (Coppercliff, Ontario) is also greatefully acknowledged.

Most of all I would like to acknowledge the tremendous support I received from all my family members during the course of my studies.

Contents

List of Figures

List of Tables

Chapter 1

Introduction and Background

1.1 Seismic Prospecting in the Precambrian Crystalline Terrain

Seismic reflection prospecting is the most commonly used and the most popular method in *Exploration Geophysics* mainly because of its effectiveness in oil and gas exploration. Reflection seismic surveys are primarily designed to map subsurface geological structures from data recorded at the surface of the Earth. Seismic sources (dynamite, vibroseis on land, airgun on marine surveys ...etc.) when activated, generate seismic waves which propagate through the Earth. In the presence of a diffractor or a reflector the wavefield is backscattered. Some of the backscattered energy propagates upward toward the surface where it is recorded by a string of geophones which are laid along the line of profile. The seismic data collected in this manner undergo extensive *digital processing* steps. These processing steps enhance the signal-to-noise (S/N) ratio and aid in the construction of the final digital image which is geologically meaningful.

Reflection seismic prospecting in younger sedimentary basins have been extremely successful. Most of the present oil fields of the world owe their discoveries to some

form of reflection seismic prospecting technique. One of the main reasons behind the great success of seismic methods in hydrocarbon exploration is that : the younger sedimentary rocks are less complex geologically, and the acoustic impedance contrast is much higher across sedimentary formations, compared to igneous and metamorphic rocks. On the other hand, older crystalline rocks normally are geologically more ambiguous for seismic wave phenomena. Crystalline rocks do not have structural sorting and have often undergone chemical reworking as well as structural deformation, usually related to earlier tectonic events. In hard rock environments, the acoustic impedance contrast across any rock types is relatively low and there is often a gradual change in physical properties across rock units. Because of the afore-mentioned problems, seismic data collected over crystalline environment contain low S/N ratio and are more difficult to process and interpret.

Recently, with the advent of new technologies, recording instruments have been improved. Seismic data processing also advanced tremendously over the last ten years. Computers for data processing are much faster and contain large real and virtual memory. New algorithms for data processing are also reported frequently. Over the last few years, a number of high resolution reflection seismic surveys have been conducted in Europe and North America (Ziolkowski and Lerwill (1979); Green (1981); Applegate et al. (1982); Green and Mair(1983); Dahle et al.(1985); Palmer (1987); Carswell and Moon (1989)) with varying degree of success.

In the summer of 1985, the University of Manitoba conducted a *High Resolution Reflection Seismic Survey* in the North Range of the Sudbury Basin of Ontario, Canada. The aim of the project was to estimate the poorly understood seismic parameters and to test the seismic imaging technique for mapping the deep seated nickel

sulphide mineralized zones in the area. The survey was designed on the basis of the conclusions and recommendation from an earlier theoretical study by Messfin and Moon (1984). Laboratory tests on core samples from the area revealed significant acoustic impedance contrast at the depth of interest for mining. Synthetic seismogram modeling, making use of the laboratory obtained acoustic parameters, showed strong reflections associated with sulphide mineralization (Messfin, 1983).

1.2 Review of Conventional Seismic Data Processing

Conventional seismic data processing consists among others of three basic processing steps, namely : surface corrections including static correction, the zero dip normal moveout (NMO) correction, and common midpoint (CMP) stacking. Sometimes post-stack migration is included for better imaging.

In regions of relatively simple geology, this conventional method yields good results for interpretation. However, when the geology becomes very complex, the principle behind NMO and CMP stacking (zero dip assumption) breaks down and the final processed section often leads to incorrect interpretation.

One step processing such as the full *migration before stack* is ideally the choise for imaging subsurface features from data collected at the surface. Prestack migration as it is also sometimes called, is based on wave theory and can handle conflicting dips and lateral changes in velocity correctly. However, this method requires the whole volume of data to be on hand for processing, and it is very unattractive, because the demand placed on computer resources is enormous and it is very expensive. Another alternative is, to improve the conventional method by including a *prestack partial*

migration step into the seismic processing sequence. Prestack partial migration (Dip-moveout) is a processing step which corrects the dip filtering action of NMO and CMP stacking (Hale, 1984). Dip-moveout eliminates reflection point scattering associated with dipping events, correctly handles conflicting dips, and improves lateral resolution.

The aim of seismic data processing is to enhance the S/N ratio, to sort and focus and to display the data in such a way that the displayed data are geologically meaningful. The conventional seismic data processing includes several processing steps of which the zero dip normal moveout (NMO), CMP stacking, and the zero-offset migration play important part in improving the interpretability of the field collected seismic data.

In multi-channel and multi-offset seismic experiments such as the one depicted in figure 1.1, the observed travel time from a particular shot-receiver pair is given by :

$$t = \left({t_n}^2 + \frac{x^2}{v^2} \right)^{1/2} \tag{1.1}$$

where,

x – $(= 2h)$ source-receiver separation

h – is the half offset

t_n – $(= 2h/v)$ vertival two way travel time

v – average velocity of the medium.

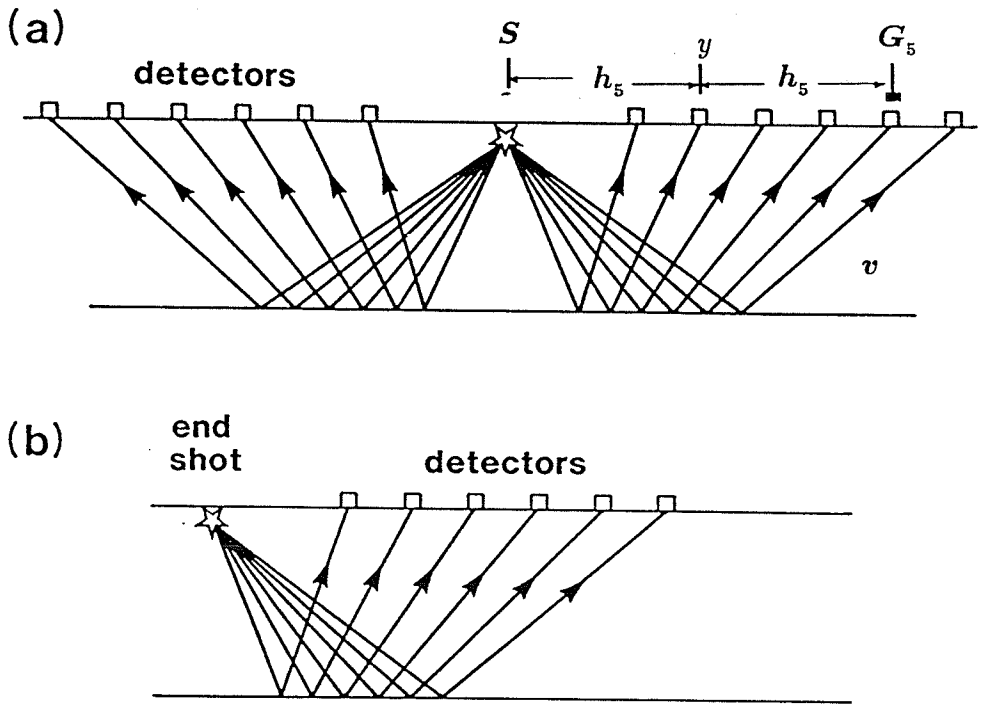

Figure 1.1: Geometry of a multi-channel seismic reflection experiment, (a) is a split spread, (b) end on shooting. Seismic reflection surveys are conducted in source-receiver *(s,r)* coordinate.

To estimate the depth to a particular reflector one needs to know the vertical travel time below the line of profile. The difference between the observed two way travel time t and the zero-offset two way time t_n is the normal moveout correction and it is given by :

$$\Delta t = t - t_n \tag{1.2}$$

$$= \left({t_n}^2 + \frac{x^2}{v^2} \right)^{1/2} - t_n \tag{1.3}$$

$$= \frac{2h}{t_n v} \tag{1.4}$$

NMO removes the effect of source-receiver separation by reducing the observed slanted two way travel time to vertical two way travel time. The NMO correction is variable with respect to offset as well as travel time. Thus, it is sometimes refered to the *dynamic correction.* The dynamic correction is large for early arrivals and for far offset traces. The correction decreases with increasing travel time. NMO correction brings about unequal stretching of the time axis. As a result, the frequency content of the seismic data is shifted to lower frequencies. Figure 1.2 shows the original field geometry and NMO corrected geometry.

In multi-offset and multiple coverage experiment the surface collected data can be sorted and displayed in a number of ways. Figure 1.3 shows the relationship among the various horizontal coordinates involved in sorting and processing of seismic data. The horizontal coordinates are all measured along the line of profile with respect to an established origin. The primary spatial coordinates are r and s and they represent the source and receiver coordinates respectively. The time coordinate is given by t.

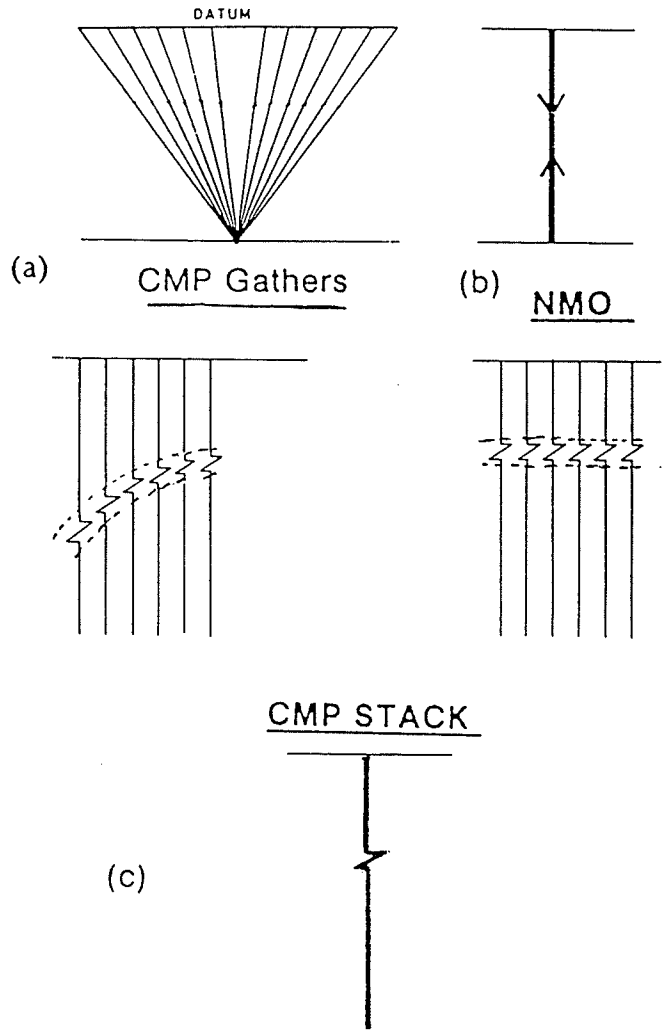

Figure 1.2: Traces of a CMP gather, (a) before and (b) after NMO correction. The top sketches are ray diagram representation of (a) and (b). (c) Shows the stacked trace obtained by summation of the NMO corrected traces of the CMP gather (modified after Al Sadi, 1980).

Conventional seismic data processing makes use of two other spatial coordinates, the source-receiver midpoint m and the half offset h. These four spatial coordinates are related by the following expression :

$$m = \frac{s+r}{2} \tag{1.5}$$

$$h = \frac{r-s}{2} \tag{1.6}$$

Seismic data collected in multiple coverage experiment can be sorted into sections or gathers where one of the spatial coordinate is constant. Let p represent the surface recorded data, then,

$p(s, r = constant, t)$ – common receiver gather

$p(s = constant, r, t)$ – common source gather

$p(h, m = constant, t)$ – common midpoint gather

$p(h = constant, m, t)$ – common offset section, and

$p(h = 0, m, t)$ – zero offset (stacked) section.

The multi-fold coverage seismic data are reduced by CMP stacking, and as a result, handling of the data during processing becomes less cumbersome. Mathematically, CMP stacking is expressed as summation over offset. Practically, however, this is accomplished, first, the data is sorted into common midpoint gathers. Then, each CMP gather is analysed to estimate the stacking velocity. After NMO correction, the traces of the CMP gather are summed up to give a trace with improved S/N amplitude. The stacking of all CMP gathers one at a time yields the CMP stacked

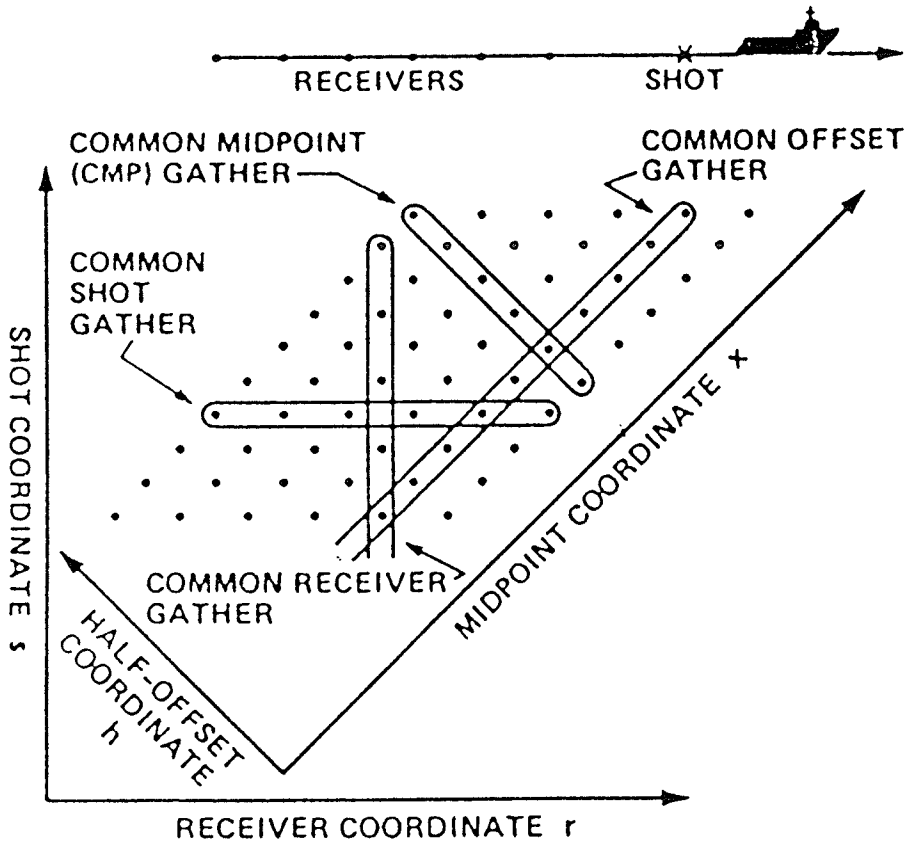

Figure 1.3: Coordinate system for seismic data aquisition. All axes are measured alog the seismic line. Seismic surveys are conducted in shot-receiver *(s,r)* coordinate, on the other hand seismic data processing is performed in mid point-half offset *(y,h)* coordinate, (after Gazdag and Squazzero, 1984(b)).

section, where, each CMP point gather contributes only a single trace to the *stacked section*. In this manner, the CMP stacking decimates the volume of data into a section, a reduction proportional to the fold coverage. Figure 1.2 (b) and (c) illustrates a CMP gather before and after stacking. A CMP stacked section is assumed to be equivalent to data obtained with coincident sources and receivers located at the midpoint (*zero-offset*).

In conventional seismic data processing, normally, the processing stops after the CMP stacked section is obtained, however if there exist complex structures with steep dips, and if better imaged section is required, then, poststack migration should be performed.

Poststack (zero-offset) migration repositions the events observed on the stacked time section into their correct lateral positions provided that the zero dip assumption made by the NMO and CMP stacking is reasonably acceptable. Poststack migration involves two steps ; *downward continuation* and *imaging*. Most of the zero offset wave equation algorithms are based on the *Exploding Reflector Model* (Loewenthal et al., 1976). The model assumes that sources are located along the reflecting surfaces and are activated in unison at time *t=0*. The energy propagates upward toward the surface where it is picked up by a string of geophones (receivers). The resulting time section is equivalent to zero-offset data. According to the exploding reflector model migration involves depropagation of the surface collected data back to the reflector depth location. The downward continued data is imaged at time t=0.

In regions of relatively simple geology, the conventional seismic data processing gives good results for interpretation. However, if the region under investigation is geologically complex, then, the *improved conventional seismic data processing* with

an additional prestack partial migration step is the alternative to the one step full prestack migration. Migration before stack is superior compared to multi-step seismic data processsing techniques. However, with this method data handling is very cumbersome. The method also requires accurate velocity field and it can be very expensive.

Prestack partial migration (dip-moveout) and poststack migration will be discussed in detail in chapters 4 and 5 respectively.

The geometry of Sudbury high resolution seismic survey consisted of a 48 channel split spread on most part of the line. Because of the rugged nature of the topography, nine geophones were arranged in a circular pattern to simulate a response from a single receiver. The geophone group interval was 10 m while shot spacing ranged from 20 to 40 m.

Preliminary processing of the Sudbury high resolution reflection seismic data showed low S/N ratio. This could be due to a number of reasons : gradational instead of sharp contacts, near surface velocities anomaly or could be attributed to the breakdown of conventional CMP seismic data processing technique.

Near surface velocity estimated from the first arrivals showed significant change in lateral velocity along the survey line. It was also known from previous studies (Card and Hutchinson, 1972; Dressler, 1984) that there exist steeply dipping reflectors in the region. Taking into account the above mentioned problems it was concluded that surface velocity dependent static correction and prestack partial migration (dip-moveout) be applied to the Sudbury seismic data to improve the quality of final stacked section.

The reasearch project to be discussed in this thesis was initiated with main ob-

jectives of developing a prestack partial migration program, which will in turn be inserted in conventional seismic processing sequence. Application of this improved prestack processing step on the Sudbury reflection data was expected to enhance the resolution of final processed section.

The prestack partial migration algorithm requires an efficient fast Fourier transform (FFT) subroutines. The FFT subroutines available publicly or through the IMSL subroutine library are in-place algorithms by design. They require that the data to be trasformed reside in the real memory of the system in its entirety for processing. In a time sharing system such as the one owned by the University of Manitoba Computer Services, the real memory available to the user is just over 4 Mbytes. This maximum limit is only available during late night and/or weekends. There is also restriction on *CPU time, and Input/Output counts.* Processing of high resolution reflection seismic data in general involves millions of digital data points. The minimum core memory requirement to perform a prestack partial migration is twice the maximum memory imposed by a time sharing system such as the Amdahl main frame at the University of Manitoba. Because of these limitations, the in-place FFT algorithms were impractical for our purpose. To overcome some of these problems it was decided that the thesis should include a development of a multi-purpose 2-D fast Fourier transform program that is capable of handling large square and rectangular datasets. To test the prestack partial migration program, synthetic datasets were required, and as a result a *Modeling and Migration* programs were also developed for this thesis research. They are discussed in detail in the following chapters.

Chapter 2

Sudbury High Resolution Seismic Reflection Survey

The Sudbury high resolution reflection seismic survey was conducted in mid August of 1985. The main goal of the survey was to investigate the feasibility of adapting the high resolution reflection seismic method as a mineral exploration tool in the Sudbury Basin of Ontario. The survey was conducted with prior velocity and theoretical modeling information on the basis of the earlier theoretical works by Messfin (1983), and Messfin and Moon (1984).

One of the recommendations of the theoretical work was to conduct high resolution reflection survey to map the Norite-Micropegmatite contact. Site selection was conducted in the North Range of the Sudbury Basin. At this part of the Basin the Norite-Micropegmatite contact was believed to be shallower. The topography of North Range is very rugged, heavily forested, and swampy at places. Therefore vehicle access was an important factor in selecting an appropriate site within the North Range. A suitable area for the seismic survey was found in the Wisner Municipality along an old abandoned north-south running Ontario Hydro transmission line. Access for drilling machinery and recording equipment was possible via an access road.

In this chapter, the setting of the Sudbury Basin, important field parameters, and

instrumentation are discussed.

2.1 General Geology of the Sudbury Basin

The Sudbury Basin is an elliptical shaped structure located near the junction of the Superior, Southern and Grenville Provinces of the Canadian Shield. The major and minor axes of the basin trend northeast and northwest parallel to the Murray and the Onaping fault systems respectively (figure 2.1).

On map view the *Nickel Irruptive* intrusion makes the outer ring of the elliptical basin (figure 2.2) . The Nickel Irruptive itself consists of two primary units. The lower part is the granitic unit known as the *Micropegmatite*, while the upper part is the gabbroid *Norite*. The contacts of the Nickel Irruptive in the south, dip steeply at about 50 to 70 degrees northward while in the north, the dip is approximately 30 to 50 degrees toward the centre of the basin. Enclosed within the Nickel Irruptive unit are the rocks of the Onaping formation which consist of a brecciated sequence. The Onwatin slate unit overlays the brecciated sequence. The upper unit is the turbidites sandstone sequence of the Chelmsford formation. The sedimentary formations which compose the central part of the Sudbury Basin are collectively known as the *Whitewater group* (Dietz, 1972).

The economically important nickel-iron-sulphide ore bodies are sulphide and inclusion-bearing facies of the irruptive unit. They occur as discontinuous sublayers around the outer margin and in some case in dikes which intrude the host rock.

There are a couple of hypotheses on the origin of the Sudbury Basin. The older hypothesis is based on *Volcanic-tectonic explosion* (Speers 1957, and Dence 1978). According to this hypothesis a volcanic irruption followed by the collapse of the

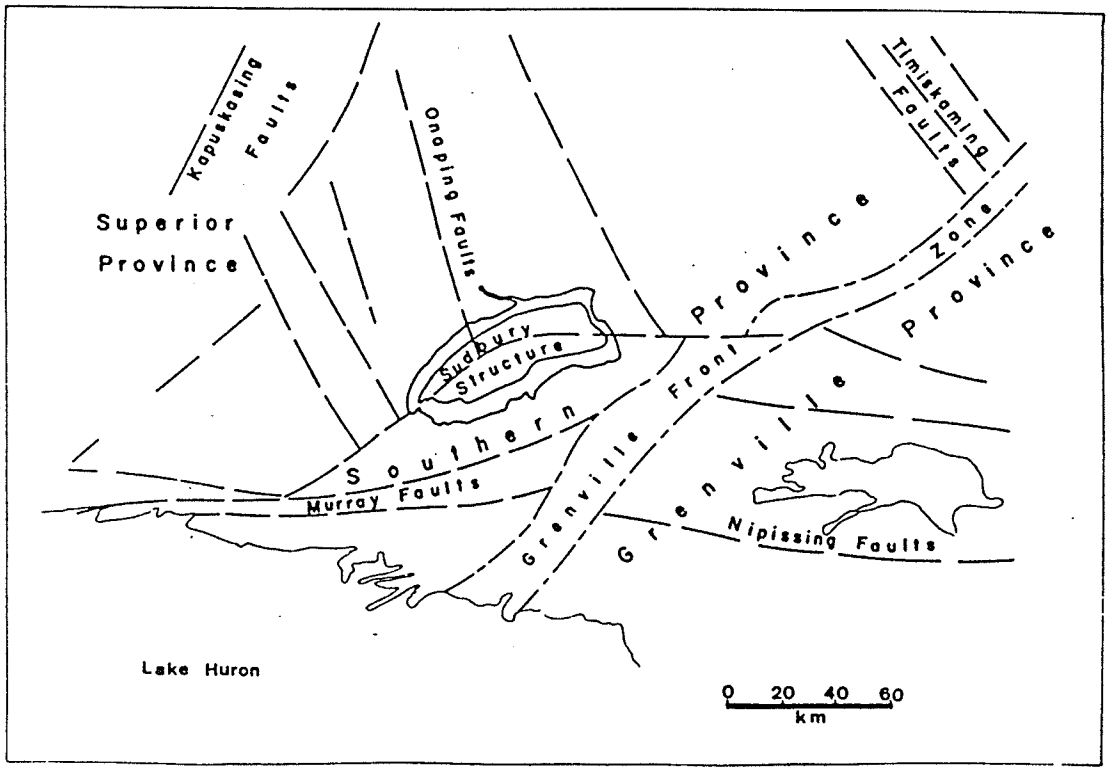

Figure 2.1: The location of the Sudbury Basin in relation to the Murray and Onaping fault system and the structural provinces of the Canadian Shield (after Card and Hutchinson, 1972).

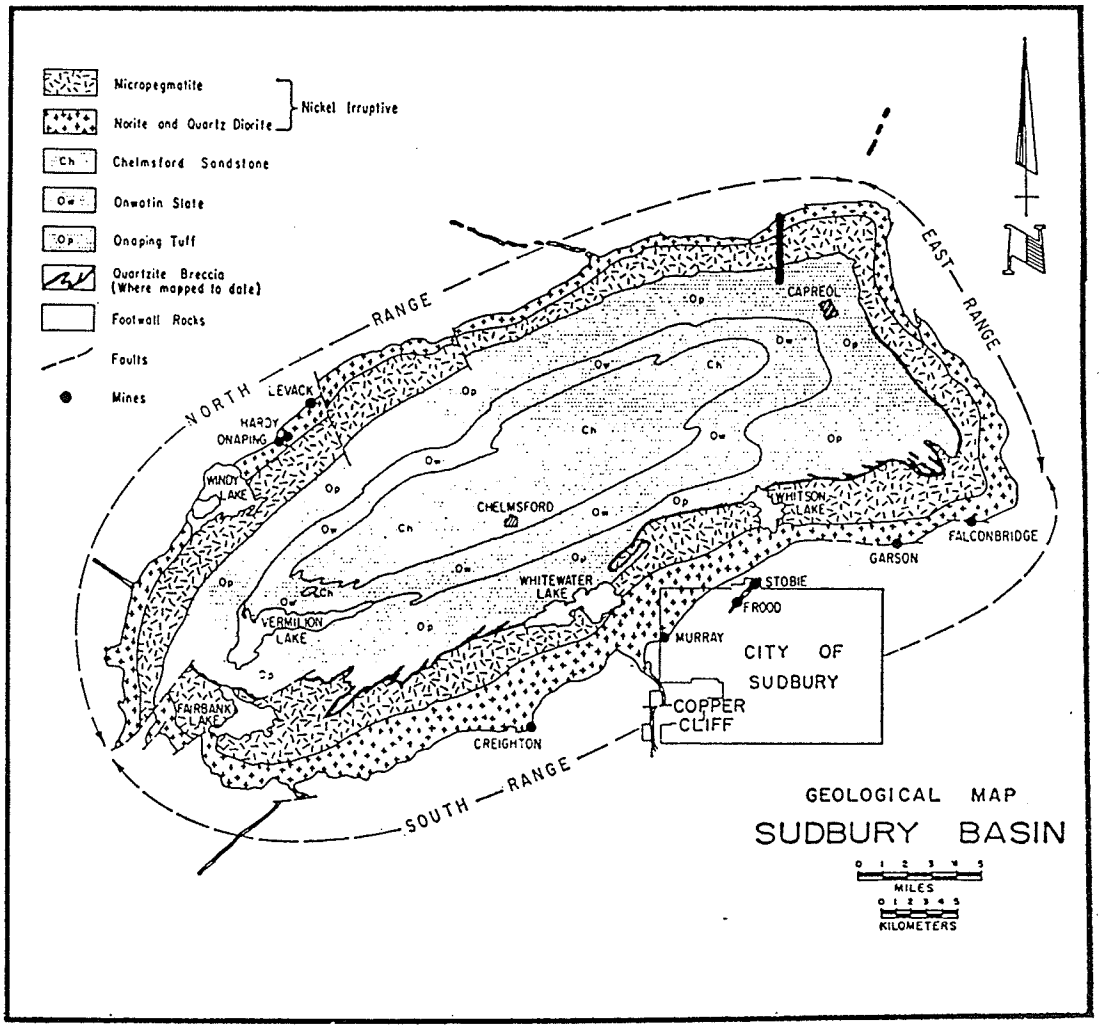

Figure 2.2: Geology of the Sudbury Basin showing the sedimentary formations of the Whitewater group being enclosed by Nickel irruptive unit. The short thick line on the North Range part of the basin shows line L85S1 in relation to the Sudbury structure (after French, 1967).

caldera allowed magma to escape around the rim forming the Onaping formation. The Nickel irruptive was emplaced between the caldera walls and the Onaping volcanics. The Onwatin and Chelmsford formations are believed to have been formed in the lake within the caldera.

The more recent hypothesis Dietz (1964, 1972) points out that the circularity and brecciation of the Sudbury basin could be better explained by *explosive meteorite impact.* More recently, French (1967) has found collaborating evidence to Dietz hypothesis. The meteorite impact hypothesis is currently more widely accepted. According to this hypothesis, a meteorite impact produced shock waves which radiated outward from the point of impact and produced brecciation, melting and excavated a circular crater. Part of the material blasted from crater fell back to form the breccia of the Onaping formation. The magma produced by the impact was emplaced between the brecciated crater and the crater wall forming the outer irruptive unit. Subsequently, the basin was covered by water in which the sediments of the Onwatin and Chelmsford formation were deposited. The original structure of the Sudbury Basin (lapolith) is believed to have been influenced by rebound, isostasy and the tectonic events (Penokean and Grenville) and finally by erosion, to aquire its present day structure.

2.2 Theoretical Study

The Sudbury high resolution seismic survey was conducted on the basis of the results of the theoretical study conducted by Messfin and Moon (1984). The theoretical forward modeling was done to determine seismic response to geological models having rock properties typical of a crystalline environment, in this case, that of the Sudbury

Basin.

In the theoretical study, parameters such as velocity and density were determined from actual rock samples taken from depths ranging from 15 to 2000 meters. Figure 2.3 - 2.5 are reproduction of the laboratory tests (Messfin, 1983). Figure 2.3 and 2.4 illustrate velocity measurements for mafic and felsic rocks respectively. These measurements are translated to velocity-depth model for synthetic seismogram generation. The acoustic impedance for the significant rock types in the area is shown in figure 2.5. The massive sulphide, the oxide rich quartz gabbro, and the mafic norite exhibit the highest acoustic impedances in the region. The theoretical study predicted that the interfaces involving these particular rocks to yield reflection coefficients of sufficient magnitude to be detected using seismic reflection techniques. Figure 2.6 show a model for a North Range mineralized zone. The model includes a 200 meters mafic sublayer between the felsic norite and the granitic country rock. The corresponding synthetic seismogram is given in figure 2.7. There is a strong reflection associated with the micropegmatite-quartz gabbro interface. Good reflection is also observed from the base of the mineralized zone.

Some of the conclusions reached in the theoretical study are:

(1) Strong reflections should be possible from the contact of the micropegmatite-quartz gabbro interface. This key reflector should be used as a marker horizon.

(2) The strong reflection from the base of the mafic sublayer will be of great significance as far as mineral prospecting is concerned, as this layer is closely associated with sulphide mineralization.

(3) The presence of thick massive sulphide showed strong reflection, however, sul-

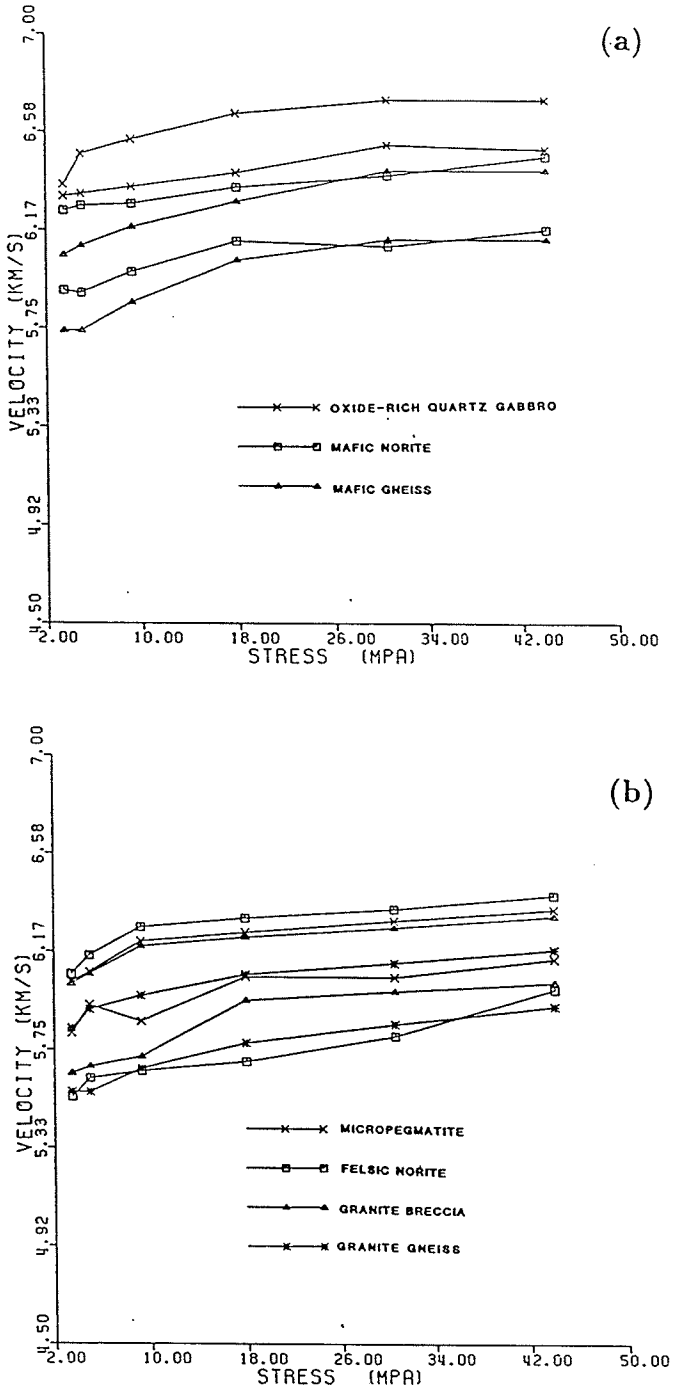

Figure 2.3: Velocity measurement for rock samples obtained from the Sudbury Basin, (a) for mafic and (b) for felsic rocks, after (Messfin and Moon, 1984).

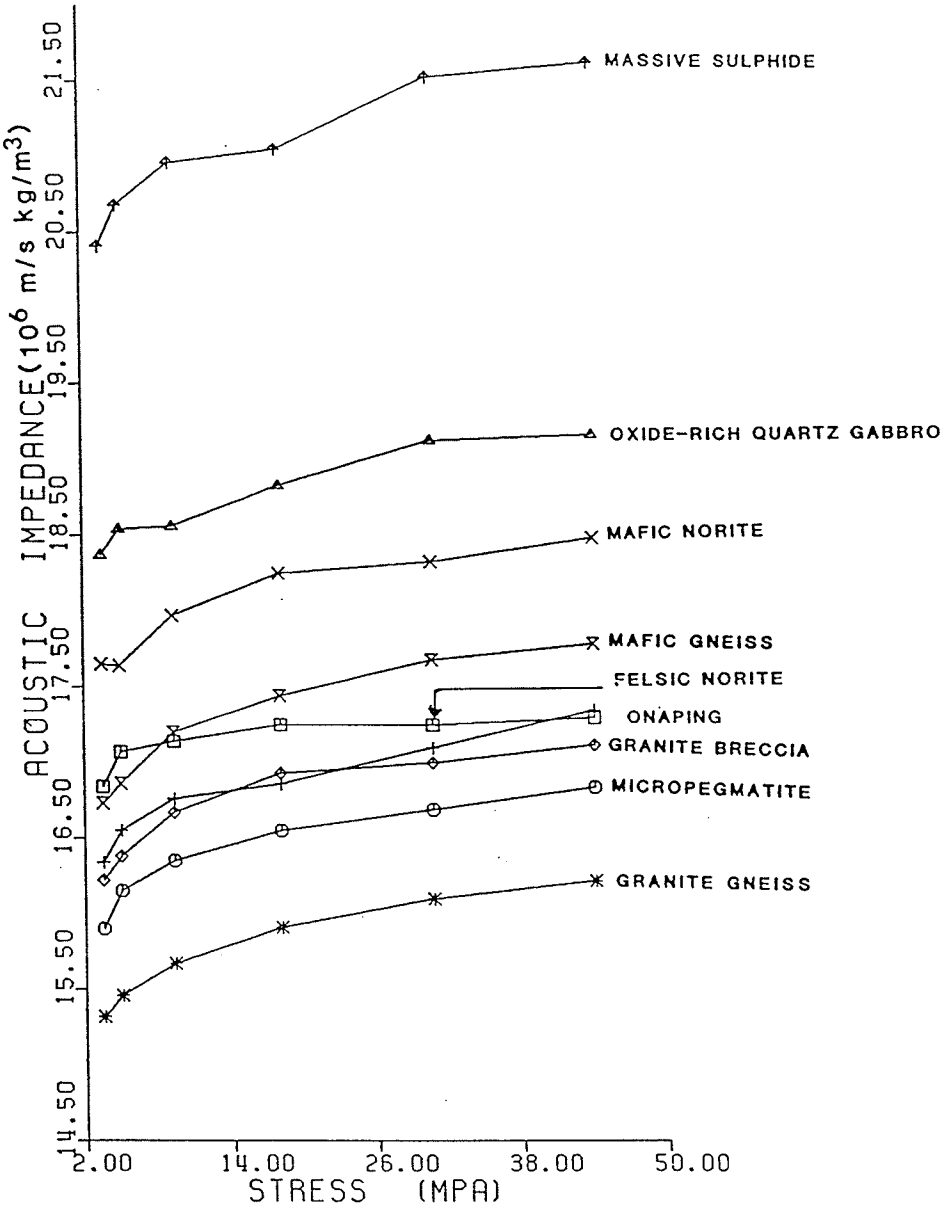

Figure 2.4: Acoustic impedances for the major rock types found in the Sudbury Basin. The massive sulphide, the quartz gabbro and the mafic norite show the high acoustic impedances, after (Messfin and Moon, 1984).

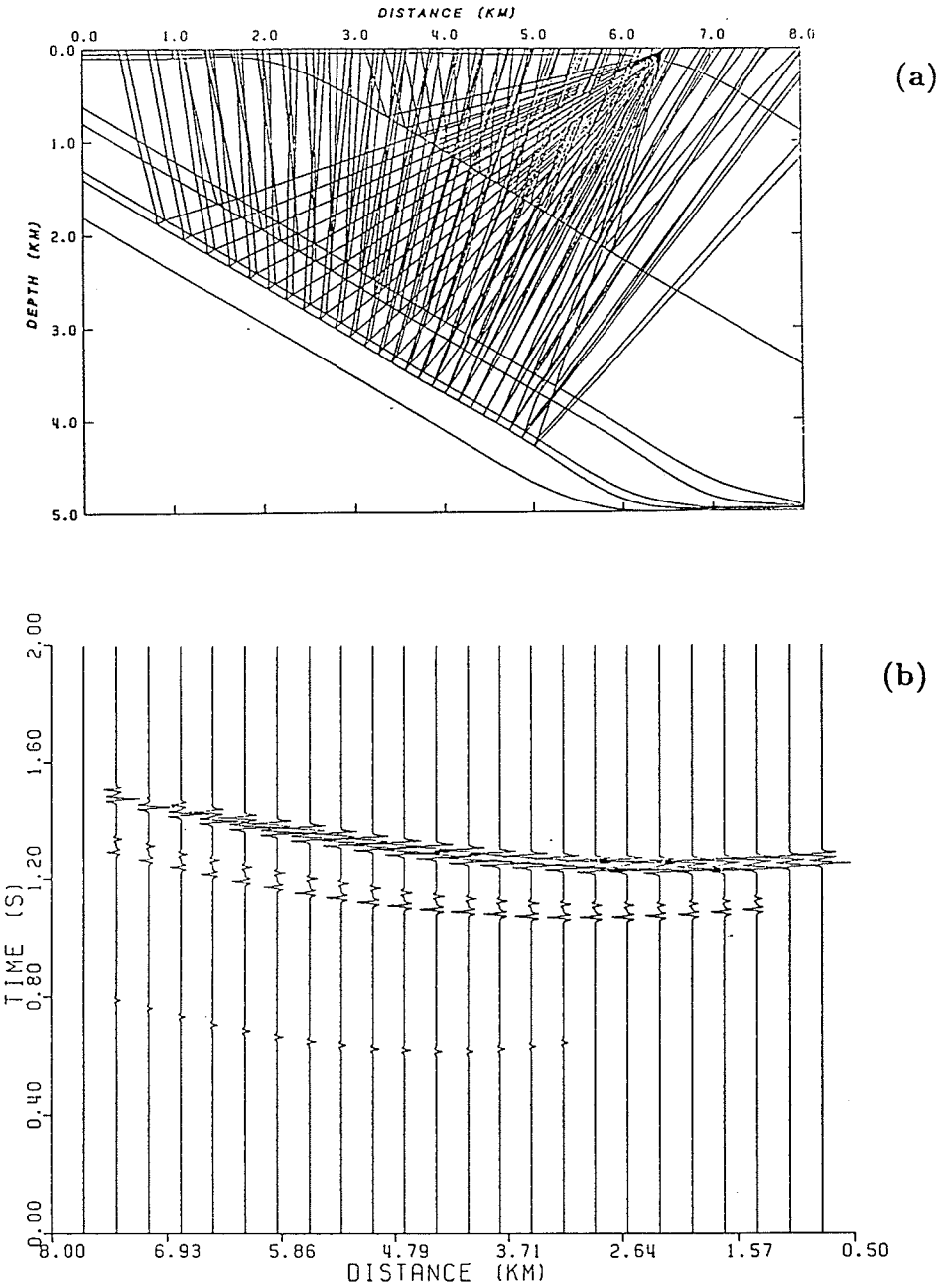

Figure 2.5: Mineralized zone North Range model and the corresponding synthetic seismogram, (a) geologic model with 200 m of mafic sublayer sundwiched between the felsic norite and the granitic country rock. The superimposed ray tracing shows reflection from several interfaces. (b) synthetic sesismogram for the model in (a). Note most of the reflection arrivals are under 2 s. after (Messfin, 1983).

phide ore bodies in the area being of limited lateral extent and thickness less than 45 meters, it would be difficult to detect them in the presence of steep dips and depth of burial of hundreds of meters.

(4) The study also recommended the use of high resolution seismic reflection method with frequencies greater than 100 Hz in the crystalline environment of the Sudbury region.

To substantiate the result of the theoretical study, a high resolution seismic survey was undertaken in the North Range of the Sudbury Basin. The survey opted for a high resolution seismic in order to resolve ore bodies which are too thin or too small to be detected by conventional seismic.

To ensure the high frequency content in the recorded data, some modification were made to the conventional seismic data aquisition technique (Ziolkowski and Lerwill, 1979):

(1) Reduce charge size to shift the spectrum of the recorded signal toward the high frequency end of the spectrum.

(2) Use single geophone instead of geophone groups. The rational of using single geophone is double-fold. First, Geophone arrays although attenuate coherent noise such as ground roll, they also act as frequency filters which affect the high frequency signal. Second, to attenuate surface waves an array greater than 30 meters in length have to be used. This exceeds the geophone group interval required for high resolution seismic survey.

(3) Shorten sampling rate in time and space to avoid temporal and spatial aliasing.

2.3 Preliminary Field Work

The preliminary field work involved choosing a suitable site for the survey, obtaining permission to access selected location and permit to conduct a seismic survey.

The actual field work started in the early part of 1985 with a search for a site suitable for survey. The site selection was conducted in the North Range of the Sudbury Basin, as the dips of igneous complex were shallower at this part of the structure compared to the South Range (Dressler, 1984). The terrain of the North Range was known to be rugged and heavily forested with very few access roads. Therefore, the search was limited to the north-south running municipal boundaries and the north-south running right of ways along power transmission lines.

In Wisner municipality a north-south running right of way along transmission line was considered, and initial reconnaissance in February of 1985 indicated that the site was suitable for the desired seismic survey. The right of way was free from shrubs and trees. The terrain appeared accessible, and based on the initial inspection it seemed possible to run a six kilometer north-south line from the granitic outcrops of the Superior Province to the Onwatin shales in the interior of the Sudbury Basin. However, subsequent reconnaissance after the snow cover was gone revealed some problems within the selected site. A large area south of the Wisner Creek was found to be too swampy for drilling and recording tracks to operate. Thus, the northern end of the proposed line was moved southward to avoid the swamp. In the south, the proposed line was routed along the access road to avoid the rugged terrain of the southern portion of the line, and joined the transmission line near Hamner lake. The revised line is located on the eastern part of the North range, and it is just under 5 km in length. The location of the line is highlighted as thick north-south line on the

regional map of the Sudbury Basin shown in figure 2.2. The line in great detail is given in figure 2.8. Note, the irregular pattern of the southern portion of the line.

In order to procceed with the actual field work, written permissions were obtained fron Ontario Hydro, Inco, and Falconbridge to have access to and to use the selected location for the purpose of conducting seismic survey. A permit was also obtained from the Provincial Government of Ontario, to carry out a seismic survey in the province.

2.4 Site Preparation

The next stage of the actual field work involved, identifying and marking of stations, line cutting and smoothing, surveying and flagging of stations, drilling of shot holes, laying out of cables, and finally, shooting and recording.

Laying out of the seismic survey line was the responsibility of the University of Manitoba. Identification and marking of stations was conducted by a two man crew equipped with a tape measurement and a clinometer. Station positions were located at every ten meter intervals. The clinometer was essential in the rugged terrain to ensure a ten meter horizontal spacing between adjacent stations.

Line cutting and smoothing the access road was the responsibily of the contractors. A caterpillar and an operator were provided to smooth the access road, and, where necessary, provide suitable access along the seismic line. This consisted of removing boulders, filling holes, and providing a few access roads to the proposed seismic line.

Surveying was done by a two man crew. The base for the control was taken from an INCO baseline approximately 1 km north of the northern end of the seismic line. Measurements were taken at every station as well at some offset shot holes from which

UTM coordinates and elevation were computed.

2.4.1 Drilling and Casing

The choice of dynamite as an energy source for the survey necessitated the drilling of shot holes in the subsurface. It was decided that the charge be detonate at depth of 2 to 3 m within the bedrock. Drilling was contracted to Carman Construction of Lively, Ontario,. which provided a track mounted self-propelled air drill and a two man crew. Most of the shot holes were drilled with a two and one-half inch wide bit. Holes drilled through overburden were cased in with a one and one-half inch PCV pipe to prevent collapsing.

The major problem in drilling was the presence of the overburden, which for the most part was made up of glacial till consisting of mud, sand, gravel, and boulders. Some of the problems associated with the overburden was the drill bit being stuck in boulders, sand and gravel caving into the hole or the sides of hole collapsing. As a result of the drilling problems encountered in the southern half of the line, it was decided to cut the number of holes by drilling every fourth, rather than every second station. Other changes made to the initial plan include, drilling into outcrops if they are located within a reasonable distance from the proposed location, to terminate holes within the overburden depending on the degree of difficulty, and to shorten the line by simply cutting off the southern end of the proposed line. Altogether, 200 holes were drilled, half of them through overburden. Shot hole depths ranged from 1.9 to 5.5 m with an average depth of 3 m.

2.5 The Seismic Survey

2.5.1 Survey Tools and Equipment

The University of Manitoba did not have all the required recording equipment for the high resolution seismic survey, and it was decided to contract the recording part of the project to Cangeo of Oil Spring, Ontario, which supplied equipment and personnel for the survey.

The survey equipment consisted of a DFS V recording system, Mark 30 Hz geophones and marsh phones (9 per group), seismic cables, explosives and detonation equipment.

Three type of geophones were employed during the survey of line L85S1, the flat based were used whenever the shot point location coincided with an outcrop where they could be cemented for better acoustic coupling. The spiked geophones were planted in overburden and the marsh-phones were employed in wet swampy areas. Table 2.1 summarizes instrumentation and source configaration.

2.5.2 Geometry and Field Parameters

The geometry of the survey consisted of a 48 channel *split spread* on most part of the line. Few shots at each end of the line were *end on shooting.* This was done to obtain equal coverage.

In line geophone group arrangement could not be justified for two reasons; first, high resolution survey requires a single geophone per station instead of geophone groups, and second, there was significant elevation differnce within geophone group interval along the survey line. As a result, nine geophones were arranged in a circular

tight pattern approximately one meter in diameter to simulate response of a single receiver. The theoretical response for the circularly arranged geophones is given in figure 2.6. The diagram on the top shows the tight circular array and its equivalent linear array. The equivalent array shown in (b) is nonuniform weighted and unequal spaced pattern. The lower diagram of figure 2.6 is the impulse response of the geophone group. Horizontally travelling waves such as ground roll have wavelengths greater than seventy meters. The tight circular pattern will do little to eliminate surface waves. On the other hand, conventional linear arrays such as the one shown in figure 2.7 with array length of 30 m will minimize the presence of ground roll in the field record. The drawback of linear array is, it behaves as a frequency filter and reduce the high frequency content of the data due to averaging. Therefore, in a high resolution seismic reflection survey attenuation of horizontally travelling waves is left to be taken care off during processing stage. The Sudbury seismic experiment was conducted using the following field parameters; the geophone group spacing was set 10 m while the shot spacing ranged from 20 to 40 m. The shot-receiver gap ranged from no gap to 20 m to the nearest geophone. The coverage of the recorded data ranged from 6 to 12 fold with 1 *ms* sampling rate. The geometry and the important field parameters are summarizes on table 2.2.

2.5.3 Shooting and Recording

During actual survey, holes were loaded just prior to shooting. Charge depth was estimated at time of loading. Most holes were tamped with either sand or water after loading.

The initial test profiles recorded significant 60 Hz noise. A 60 Hz notch filter

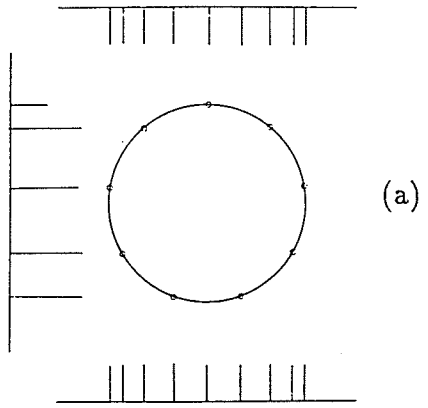

(a)

(b)

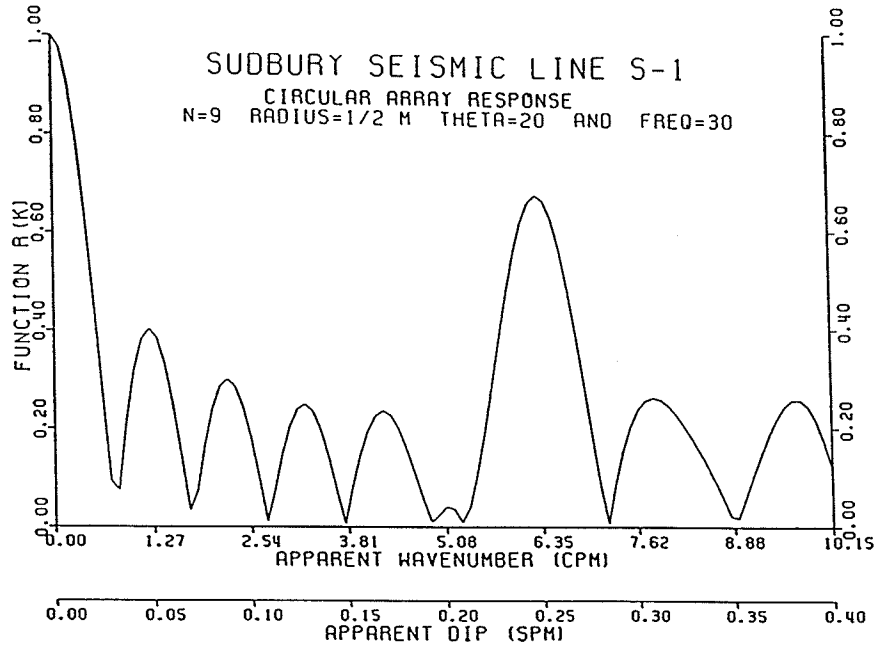

(c)

Figure 2.6: (a) Tight circular array of geophones with 1.0 m diameter, (b) linear array equivalent to the one shown in (a). The linear array is a nonuniformly spaced and nonuniformly weighted. The theoretical respone of the circular array is given in (c).

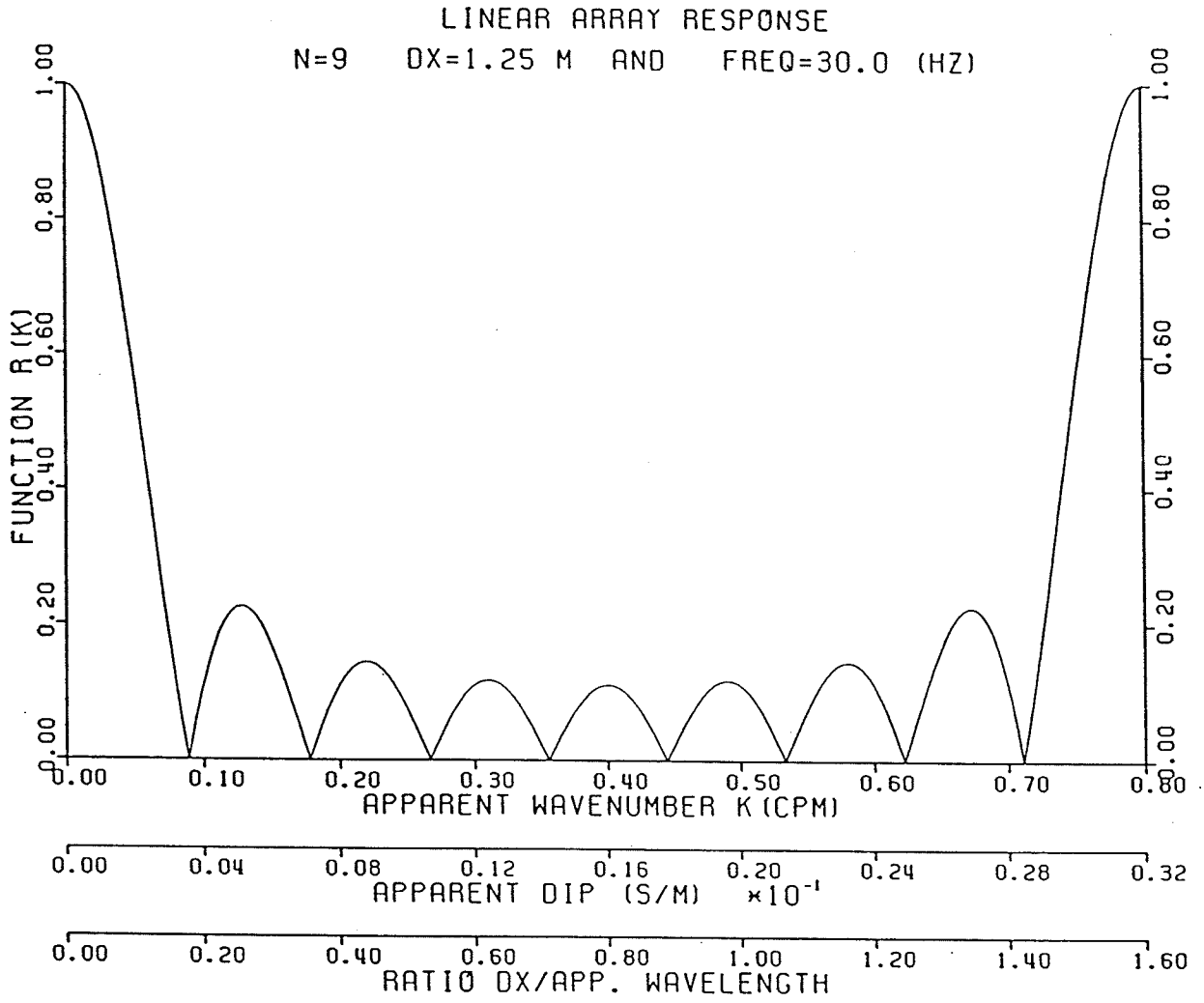

Figure 2.7: Response of conventional linear array of geophones with array length of 10 m.

was switched on to suppress this particular noise. Surface waves and air blasts were also quite evident in the field records. The high near surface noise in the near offset traces in particular prompted change in spread configation. As a result the near offset distance was changed from 0 to 20 m for a good portion of the survey.

Test conducted in the field to find the optimal charge size did not establish a clear-cut choice between the charge size of 9, 18, and 45 gm. However, it was decided that 18 gm be used for the northern portion and 45 gm for the southern portion of the line.

Instrumentation and Source Specification

Recording Instrument

Recorder	-	DFS-V (48 Channel)
Geophone (flat based & spiked)	-	Mark 30 Hz
Marsh geophone	-	Mark 30 Hz

Hole Configuration and Charge Size

Hole Array	-	1 Hole per shot location
Normal Charge Depth		
In Outcrop	-	$\sim$ 2 m
In Overburden	-	$\sim$ 4 m
Charge Size		
North end of the line	-	9 and 18 gm
Central part of the line	-	18 gm
South end of the line	-	45 gm and two 100 gm
Type of Explosive	-	Deta Primer

Table 2.1: Summary of instrumentation, hole configaration, and source specification (Moon et al. 1990).

Field Parameters		
Line Name	-	L85S1
Line Length	-	4.65 km
		Spread Description
Normal Group Interval	-	10 m
Geophones per Group	-	9
Array Pattern	-	Circular with 1 m in diameter
Normal Near Offset	-	20 m
Normal Far Offset	-	250 m
Normal Shot Offset	-	20 m (North end of the line)
	-	40 m (South end of the line)
		Spread Configuration
Normal 3 Group Gap	-	$250 - - * - - 250$ m
No Gap	-	$240 - - * - - 230$ m

Table 2.2: Summary of geometry and field parameters (Moon, et al., 1990).

Chapter 3

Fast Fourier Transform for Large Data Matrices

In many branches of sciences and engineering certain applications are easy to understand in terms of frequency. The Fourier transform is a mathematical tool which transforms a set of data from one domain to another. In the process it makes a difficult problem in the original domain, into a much easier problem in the transform domain.

Computation of the Fourier transform using its discrete version known as *the Discrete Fourier transform* had been known for quite a long time. However, the widespread application of the discrete Fourier transform became possible, only, after the discovery of *fast Fourier transform (FFT)* algorithm (Cooley and Tukey, 1965). The Fast Fourier Transform is an efficient method of computing the discrete Fourier transform (DFT). Because of its computational advantage, the discrete Fourier transform have gained wide application in many fields of quantitative science such as Statistics, Communication Engineering, Image processing, Seismic data processing, and many more (Bracewell, 1986).

The familiar Cooley–Tuckey algorithm as well as the canonic FFT algorithms

require that the whole data matrix to be on hand (core memory) during computation (Brigham, 1974). When the data matrix to be transformed is small enough to fit into the system's core memory, the two-dimensional discrete Fourier transform is computed by repeated use of the one-dimensional in-place FFT algorithm, both in column and row direction. However, if the data matrix can not be accommodated in the system's core memory, then, the in-place FFT algorithms are not suitable to compute the discrete Fourier transform of the data matrix.

In 1980, G.L Anderson developed a stepwise fast Fourier transform algorithm for large multi-dimensional arrays with limited core memory. A review of the two dimensional discrete Fourier Transform and the stepwise approach of computing the 2-D discrete Fourier Transform is given in this chapter. A copy of a paper by Serzu and Moon (1989(a)), which is a long write-up of the stepwise FFT program (SW2DFFT) is given in Appendix D.

SW2DFFT is the practical implementation of the Anderson's method for 2-D case. The Fortran program is capable of handling large data matrices both square and rectangular in limited core memory. The program uses a stepwise approach in computing large matrices. It is based on the decomposed Cooley–Tukey (decimation in time) algorithm (Anderson, 1980). It was written to perform Fourier transform on a large seismic dataset in mind, however, it can be used with any kind large dataset which requires Fourier transformation.

3.1 Two Dimensional Fourier Transform

A two-dimensional function $f(x, y)$ has a Fourier trasform $F(k_x, k_y)$, and the relation between these two transform pair can be expressed as,

$$F(k_x, k_y) = \int\int f(x,y)\, e^{-2\pi i(xk_x + yk_y)}\, dx\, dy \tag{3.1}$$

and,

$$f(x,y) = \frac{1}{4\pi^2} \int\int F(k_x, k_y)\, e^{2\pi i(k_x x + k_y y)}\, dk_x\, dk_y \tag{3.2}$$

Equation (3.1) and (3.2) represent the continuous Fourier transform pair, and they are know as the *direct and inverse* Fourier Transform respectively. The continuous form has a limited practical application, it is normally used for analytic purposes by physicists and engineers. The *discrete Fourier transform* which is discussed in section (3.2) is suitable for digital computer implementation, and it is evaluated efficiently with the help of fast Fourier transform algorithm.

3.2 The Stepwise FFT Algorithm

Following the notation by Anderson (1980), the two-dimensional discrete Fourier transform is given by :

$$X_{kl} = \sum_{j=0}^{N-1} \sum_{i=0}^{M-1} x_{ij}\, W_M^{ik}\, W_N^{jl} \tag{3.3}$$

$$for \quad k = 0, 1, \cdots, M-1 \quad , \quad l = 0, 1, \cdots, N-1 \tag{3.4}$$

where,

$$W_N = e^{\frac{-2\pi i}{N}}, \qquad W_M = e^{\frac{-2\pi i}{M}}. \tag{3.5}$$

$\{x_{ij} |\ 0 \leq i \leq M-1 \quad and \quad 0 \leq j \leq N-1\}$ are complex data samples. (3.6)

The inner sum in equation (3.3)

$$y_{kj} = \sum_{j=0}^{M-1} x_{ij} W_M^{ik} \quad for \quad k = 0, 1, \cdots, M-1 \tag{3.7}$$

is the columnwise Fourier transform. Since the data matrix is stored columnwise, a record from the data matrix may be read and computed using any one of the familiar 1-D FFT algorithms. The outer sum in equation (3.3)

$$X_{kl} = \sum_{j=0}^{N-1} y_{kj} W_M^{jl} \quad for \quad k = 0, 1, \cdots, M-1;\ l = 0, 1, \cdots, N-1 \tag{3.8}$$

is the discrete Fourier transform over the rows of the matrix. A one-dimensional row transform runs through every sample in the k^{th} row. In other words, if the data matrix does not fit into the core memory of the system, to obtain one row from the data matrix, one has to read every record (column) in the disk. This makes the in-place FFT algorithms expensive as well as unsuitable for large data matrices. Anderson (1980) presented an algorithm which does not require the entire row to be in-place at one time. This was done by rearrangement of the Cooley–Tukey FFT algorithm (Anderson, 1980).

Let a single row from the matrix (dropping the column index) be represented by a sequence, such that,

$$x_l = \{x_1, x_2, x_2, \cdots, x_{N-1}\} \tag{3.9}$$

then one-dimensional discrete Fourier transform of the single row is defined as,

$$X_m = \sum_{l=0}^{N-1} x_l W_N^{lm} \quad for \quad m = 0, 1, \cdots, N-1 \tag{3.10}$$

for $N = 2^r$, and $p = lm$, the binary representation of the integer variables l, m, and p is given by,

$$\begin{aligned} l &= 2^{r-1}l_{r-1} + 2^{r-2}l_{r-2} + \cdots + l_o = [l_{r-1}, l_{r-2}, \cdots, l_o] \\ m &= 2^{r-1}m_{r-1} + 2^{r-2}m_{r-2} + \cdots + m_o = [m_{r-1}, m_{r-2}, \cdots, m_o] \end{aligned} \tag{3.11}$$

$$p = lm = (2^{r-1}l_{r-1} + 2^{r-2}l_{r-2} + \cdots + l_o) \times (2^{r-1}m_{r-1} + 2^{r-2}m_{r-2} + \cdots + m_o) \tag{3.12}$$

where each l_i and m_i can take only the values 0 or 1. In binary format the row vector (of length $N = 2^r$) given in equation (3.9) can be expressed as

$$x[j_{r-1}, \cdots, j_0] \qquad \text{where,} \qquad j = [j_{r-1}, \cdots, j_0] \tag{3.13}$$

then the *bit reversed* input sequence is given by

$$y_0([j_{r-1}, \cdots, j_0]) = x[j_0, \cdots, j_{r-1}] \tag{3.14}$$

The 1-D Fourier transform of the bit reversed input sequence given in equation (3.14) can be written as

$$\begin{aligned} y_r([l_{r-1}, l_{r-2}, \cdots, l_0]) &= \sum_{j_{r-1}=0}^{1} \cdots \sum_{j_0=0}^{1} y_0([j_{r-1}, \cdots, j_0] \\ &\quad \times W_N^{[l_0]j_0 2^{r-1}} \cdots W_N^{[l_{r-1}, \cdots, l_0]\, j_{r-1}} \end{aligned} \tag{3.15}$$

equation (3.14) can be rewritten compactly as follows,

$$y_r([l_{r-1}, \cdots, l_0]) = \sum_{j_{r-1}=0}^{1} y_{r-1}([j_{r-1}, l_{r-2}, \cdots, l_0])\, W_N^{[l_{r-1}, \cdots, l_0]j_{r-1}} \tag{3.16}$$

If $n = 2^s (> 2)$ is the number of samples that can be stored in real memory, then

for each row we have N/n subsets. Each subset is composed of samples required to advance the data (row) s steps in the FFT algorithm. The equation required to do the partial transform is given below (Anderson, 1980).

$$y_s([j_{r-1},\cdots,j_s,l_{s-1},\cdots,l_0]) = \sum_{j_{s-1}=0}^{1}\cdots\sum_{j_0=0}^{1} y_0([j_{r-1},\cdots,j_s,j_{s-1},\cdots,j_0] \times W_N^{[l_0]2^{r-s}}\cdots W_N^{[l_{s-1},\cdots,l_0]j_{s-1}2^{r-s}} \quad (3.17)$$

At stage one, equation (3.17) partially transforms each subset and the result is written back to direct access mass storage. On the next stage the samples are chosen to allow each subset to advance another s steps in FFT algorithm. The process is repeated using equation (3.17). If the number of stages (r/s) is equal to two, on the first stage each subset is composed of $r-s$ common high order bits. At the second stage, each subset is made up of samples that can be advanced to the very last step of the FFT algorithm and it is given by

$$\{y_s([j_{r-1},\cdots,j_0]) \mid j_{2s-1},\cdots,j_s \text{ arbitrary; all other index bits constant }\}\ .$$

However, if the number of stages (r/s) is not an integer, there are fewer computational steps on the last stage. For instance, if the number of samples in each row is 32 which is equal to 2^5 and the number of samples in each subset is 8 (2^3) then r/s is less than 2 which is rounded to 2. Two stages of three steps each make six steps greater than the five required. Hence, at the second stage we have to make sure that we calculate one less step, because for N equals to 2^r samples the full FFT algorithm requires only r computational steps.

3.3 The Programing Consideration

(1) The program reads the data matrix stored in bit reverse order in a random access mass storage one subset at a time. At every stage the program chooses records that would allow stepwise computation of the large data matrix.

At Stage 1

(2) A record from the chosen subset is passed to any of the familiar FFT subroutines to compute the column transform

(3) Use Equation (3.17) to partially transform each row of the subset. Write the subset with their intermediate results back to the direct access mass storage

(4) Repeat 2 to 3 for each subset

Stage 2

(5) The full column transform is performed in the first stage, therefore, only row transform is required in the second and subsequent stages.

(6) At stage 2 choose records that would allow computation of the row transform to advance another s steps

(7) repeat steps 3 for each subset

(8) If the calculated total number of stages is 2, then by end step (7) the data will be fourier transformed completely. However, if the total number of stages is greater than 2 then, repeat steps (1) and (3) till the number of stages are completed.

3.3.1 Core Memory Requirement

For 1024 by 1024 complex data matrix, the core memory requirement is about 32 $\times$ 1024 complex words (if each subset consists of 32 records). It is possible to minimize the core memory requirement by decreasing the size of a subset, hence, increasing the number stages.

3.3.2 Application and Performance Tests

The two-dimensional stepwise FFT program discussed above should be used when a need arises to perform FFT on large data matrix on limited core memory. Seismic data processing such as dip-moveout, and migration are good examples. For small and medium size matrices it is slightly slower compaperd to the in-place FFT subroutines. This is due to extra read/write pass required over the data. This program is much faster compared to similar programs which employ several tapes as external mass storage (Singleton, 1967). Unlike method (Eklundh, 1972), the stepwise FFT algorithm is suitable for both square and rectangular matrices and there is no need to transpose the data matrix after processing is completed. The table (3.1) summarizes the CPU time and real memory requirement for two-dimensional complex transforms.

CPU Time for two dimensional complex matrices

(for direct Fourier transform only)

Original matrix	*Size of one subset*	*Minimum core requirement*	*CPU Time (sec)*
64×64	64×8	76Kb	2.31
256×64	256×8	—	7.60
256×256	256×16	120Kb	33.90
1024×256	1024×16	—	121.73
1024×1024	1024×32	368Kb	597.88

Table 3.1: Summarizes the efficiency of the Stepwise 2-D FFT. Column 2 and 3 show the minimum memory requirement for the subsets given in column 2. Column 4 is the CPU time required to Fourier transform the selected matrices on Amdahl 5870 main frame computer running under IBM MVS3 operating system.

Chapter 4

Prestack Partial Migration (Dip-moveout)

In the multi-channel data processing, horizontal stacking consists of the summation of the traces of each common mid–point (CMP) gather after the normal moveout (NMO) correction. This CMP stacking improves S/N ratio by enhancing reflections with a particular slope while attenuating reflections with different slopes. The failure of the CMP stacking with regard to curved and steeply dipping reflectors lie with the zero dip normal moveout correction. The conventional NMO assumes that the reflection point of none zero offset data to be the same reflection point associated with the source-receiver CMP. For dipping layer case this assumption is not valid figure 4.1. The NMO velocity for a dipping reflector is greater than that for a horizontal reflector. This has been shown by Levin (1971) :

$$v_{NMO} = \frac{v}{\cos\phi} \tag{4.1}$$

where, ϕ is the reflector dip associated with the direction of source receiver offset. Equation (4.1) implies that the NMO correction for dipping events is best performed using a velocity v_{NMO} that is higher than the true velocity v. Unfortunately the con-

ventional NMO and stack allow one choice of v for a particular CMP and traveltime. Another problem with the dip dependent NMO velocity is that, the dip a reflector is not known before hand. In dipping layer case, reflection arrivals from a CMP gather do not have a common reflection, instead the reflection points are dispersed in the updip direction. Deregowski (1982) has shown that the reflection point dispersal to increases as square of the half offset (figure 4.2). In structurally complex formations, the correction of all dip angles becomes impossible and horizontal stacking loses its usefulness, and a fewer number of stacks are permitted before the quality of the data is deteriorated rather than being enhanced (Tucker, 1982). Under these circumstances, migration before stack is an alternative.

Migration before stack has a sound theoretical foundation. However, direct implementation requires simultaneous migration of large sets of common offset gathers. The large amount of computer memory and computing time required in migration before stack makes the technique very expensive and less practical. Migration before stack is a one-step process, and does not provide any intermediate results such as a CMP stacked section, which helps to identify false events on the migrated section.

To overcome some of the disadvantages of migration before stack a number of special purpose prestack techniques such as *DEVILISH* (dipping events velocity inequality licked by Sherwood), *prestack partial migration* (PSPM), *offset continuation*, *dip-moveout by Fourier transform*...etc. have been developed to suppress the dip selectivity of the NMO and stacking. Prestack partial migration process when combined with the conventional processing sequence yields approximately the result of the costly full migration before stack.

The *finite-difference* techniques (PSPM, offset continuaion, ... etc) make a number

of approximations in deriving the DMO algorithms (Yilmaz and Claerbout, 1980; Bolondi et al., 1982; and Deregowski and Rocca, 1981) These algorithms break down at large offsets and steep dips. The pre-stack partial migration being introduced in the following sections is based on Fourier transform implementation of the DMO theory (Hale, 1983, 1984). Constant NMO velocity is the only assumption made in developing DMO by Fourier transform. Unlike the finite difference counterparts, this algorithm is accurate for all dips and offsets.

4.1 Dip-moveout by Fourier Transform

The prestack partial migration discussed in this chapter is based on the alorithm by Hale (1984). This DMO algorithm is designed to work in the *frequency–wavenumber domain* and is known as *Dip-moveout by Fourier Transform.* The advantage of this algorithm over the rest DMO algorithms is that it can handle large offsets and dips up to 90 degrees.

4.1.1 Dip-moveout Theory

Consider a seismic experiment conducted over a constant velocity half–space having a single dipping reflector as shown in figure 4.1. Let us define the following variables :

ϕ – dip of reflector

h – source-receiver half offset

t_o – zero-offset two way traveltime

t – slanted two way traveltime

v – velocity of the medium.

y – source receiver mid-point

y_o – the point where the dipping reflector meets the surface.

From triangle $ss'r$, the travel time t of the reflection from the dipping reflector can be written as (following the notation by Hale, 1984) :

$$t^2 = \frac{1}{v^2}\left[(\overline{ss'})^2 + (\overline{sr})^2 - 2(\overline{ss'})(\overline{sr})\cos\left(\frac{\pi}{2} + \phi\right)\right]. \tag{4.2}$$

At the zero offset $s = r = y$, the travel time t_o is obtained from the triangle $y'yy_o$ where $\overline{yy'} = vt_o/2$ and

$$\sin\phi = \frac{t_o v}{2(y - y_o)} \quad , \tag{4.3}$$

and the zero offset travel time becomes

$$t_o = \frac{2}{v}(y - y_o)\sin\phi. \tag{4.4}$$

If we substitute equation (4.3) into (4.2) we obtain the Levin's NMO expression corrected for dip :

$$t = \sqrt{t_o^2 + \frac{4h^2\cos^2\phi}{v^2}}. \tag{4.5}$$

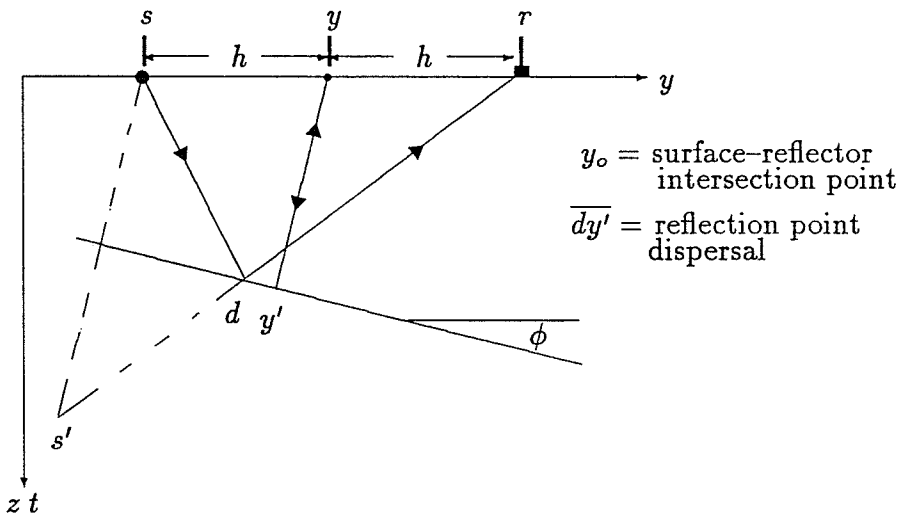

Figure 4.1: Seismic experiment conducted over a half-space with a constant velocity medium and a dipping reflector.

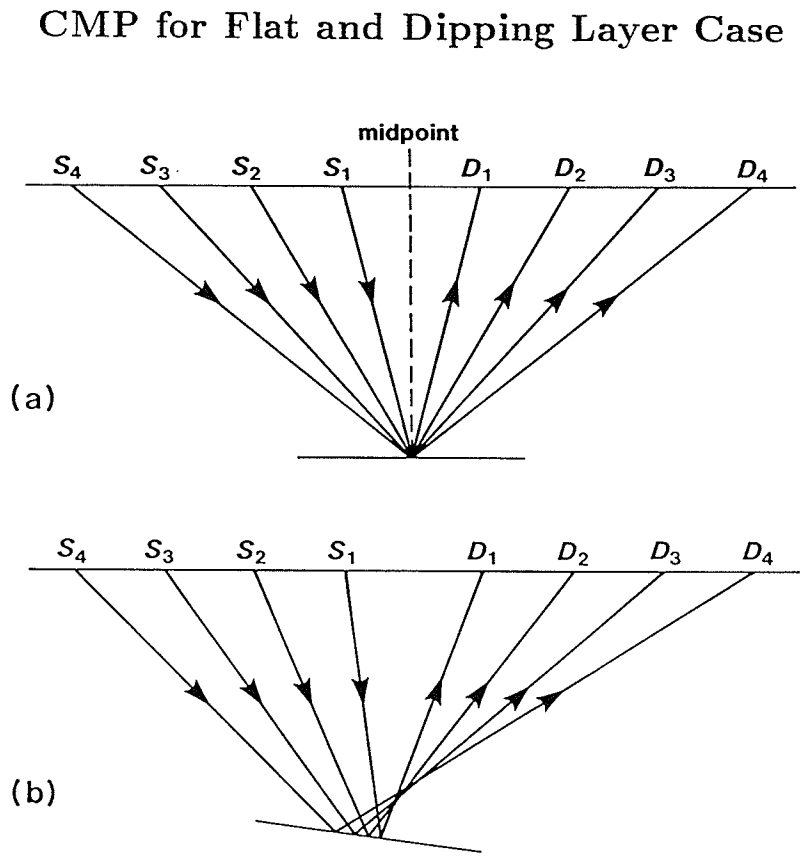

Figure 4.2: Ray diagram representation of a CMP gather for a flat reflector (a) and dipping reflector (b). For the flat reflector all reflection arrivals have a common reflection point (CDP), for a dipping reflector however, the reflections of a CMP gather do not have a common reflection point, instead, the reflection points are dispersed in the updip direction.

Let $p(t, y, h)$ denote seismograms recorded as a function of time t, midpoint y, and half offset h. Equation (4.5) then leads to the following transformation to zero offset from non-zero offset seismograms $p(t, y, h)$

$$p_o(t_o, y, h) = p\left(\sqrt{t_o^2 + \frac{4h^2 \cos^2 \phi}{v^2}}, y, h\right) \tag{4.6}$$

The dip corrected NMO may be performed in two steps. First we rewrite equation (4.5), the dip corrected NMO, as follows :

$$t = \sqrt{t_o^2 + \frac{4h^2}{v^2} - \frac{4h^2 \sin^2 \phi}{v^2}}. \tag{4.7}$$

No approximation have been made in deriving the above expression and it is accurate for small ϕ and dips up to 90°. The dip-moveout term in equation (4.7) is significant for large offsets and steep dips and very minor for a gently dipping reflector. Substituting equation (4.4) into equation (4.5) and taking

$$\sin^2 \phi + \cos^2 \phi = 1 \tag{4.8}$$

NMO without dip correction becomes :

$$t = \sqrt{t_n^2 + \frac{4h^2}{v^2}} \tag{4.9}$$

where, t_n is the NMO time. From equation (4.5) and (4.9) we obtain another expression for dip corrected NMO time t_o :

$$t_n = \sqrt{t_o^2 - \frac{4h^2 \sin^2 \phi}{v^2}} \tag{4.10}$$

Equations (4.9) and (4.10) imply that the dip corrected NMO given in equation (4.6) may be evaluated in two steps : First use equation (4.9) to define NMO as :

$$p_n(t_n, h, y) = p\left(\sqrt{t_n^2 + \frac{4h^2}{v^2}}, y, h\right) \tag{4.11}$$

and then use equation (4.10) to define dip-moveout (DMO) as :

$$p_o(t_o, y, h) = p_n\left(\sqrt{t_o^2 + \frac{4h^2 \sin^2\phi}{v^2}}, y, h\right). \tag{4.12}$$

NMO is the transformation from recording time t to NMO time t_n . DMO is the transformation from NMO time t_n to zero offset time t_o .

Consider an example shown in Fig. 4.3 as a zero-offset section. The slope of the reflection is given by :

$$\frac{\Delta t_o}{\Delta y} = \frac{2\sin\phi}{v}. \tag{4.13}$$

Substituting equation (4.13) into equation (4.12) we have

$$p_o(t_o, y, h) = p\left(\sqrt{t_o^2 - (\Delta t_o/\Delta y)^2 h^2}, y, h\right) \tag{4.14}$$

Evaluation of the dip-moveout equation (4.14) does not require knowledge of velocity or dip. However, equation (4.14) is impractical as the slope $\Delta t_o/\Delta y$ must be obtained from the zero offset data. In practice, we record the multi-offset data. The stacked data ($\sim$ zero offset) is obtained by processing the non-zero offset records. Another problem with the above expression is that, conflicting dips may exist for different events at particular (t_o, y).

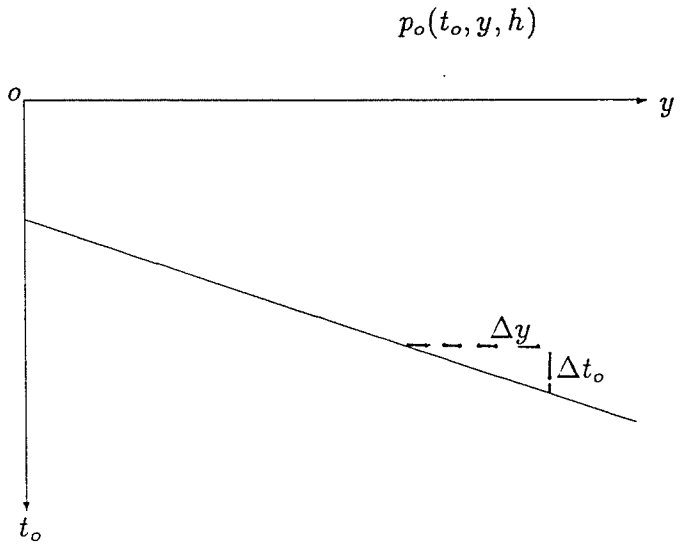

Figure 4.3: Zero offset section

Equation (4.14) implies that a different DMO correction is needed for each different zero-offset slope $\Delta t_o/\Delta y$. The 2-D Fourier transform of t_o–y provides a particularly useful domain to apply to a dip-dependent process, because events having a particular dip in the (t_o,y) domain map into a single radial line in the (ω_o, k) domain (Hale, 1984). The radial lines in the frequency-wavenumber domain are giver by :

$$\frac{k}{\omega_o} = \frac{\Delta t_o}{\Delta y} = \frac{2\sin\phi}{v} \tag{4.15}$$

2-D Fourier transform of $p_o(t_o, y, h)$ (ie. zero offset) is defined by :

$$P_o(\omega_o, k_y, h) = \int dt_o \exp(i\omega_o t_o) \int dy \exp(-ik_y y)\, p_o(t_o, y, h) \tag{4.16}$$

Since we don't measure zero-offset data (dip and velocity being unknown), we can express the above Fourier transform in terms of NMO data. Substituting equation (4.15) into (4.10) we obtain :

$$
\begin{aligned}
t_o &= \sqrt{t_n^2 + \frac{4h^2 \sin^2 \phi}{v^2}} \\
&= \sqrt{t_n^2 + \left(\frac{\Delta t_o}{\Delta y}\right)^2 h^2} \\
&= \sqrt{t_n^2 + \frac{(k_y h)^2}{\omega_o^2}} \quad . \qquad (4.17)
\end{aligned}
$$

Define

$$
\begin{aligned}
A &= \frac{dt_n}{dt_o} = \frac{t_o}{t_n} \\
&= \sqrt{1 + \frac{k^2 h^2}{\omega_o^2 t_n^2}} \qquad (4.18)
\end{aligned}
$$

and

$$
\begin{aligned}
B &= \omega_o t_n A \\
&= \omega_o \sqrt{t_n^2 + \frac{(kh)^2}{\omega_o^2}} \quad . \qquad (4.19)
\end{aligned}
$$

Substitution of equation (4.18) into equation (4.16) gives

$$
P_o(\omega_o, k_y, h) = \int dt_n \, A^{-1} \exp(iB) \int dy \, \exp(-ik_y y) p_n(t_n, y, h) \qquad (4.20)
$$

The right hand integral can be recognized as a Fourier transform with respect to the midpoint coordinate, then equation (4.16) can be written as :

$$P_o(\omega_o, k_y, h) = \int dt_n \, A^{-1} \exp(iB) P_n(t_n, k_y, h) \tag{4.21}$$

Equation (4.15) provides a method for applying DMO correction for each slope $\Delta t_o/\Delta y = k/\omega_o$ in the zero offset section. Inverse Fourier transform of (4.21) gives the zero offset section $p_o(t_o, y, h)$, that is :

$$p_o(t_o, y, h) = \frac{1}{4\pi_2} \int d\omega_o \, \exp(-i\omega_o t_o) \int dk_y \, \exp(ik_y y) \, P_o(\omega_o, k_y, h). \tag{4.22}$$

4.2 Implementation of DMO by Fourier Transform

(1) Apply NMO using equation (4.9) with velocity estimated from velocity analysis.

(2) Reorder the data into common offset section

(3) Take 1-D FFT of the NMO corrected data with respect to midpoint y.

$$p_n(t_n, y, h) \cdots \text{1–D FFT} \cdots > p_n(t_n, k_y, h)$$

(4) Integrate over t_n for the left hand integral in (4.20) for all ω_o and k to obtain $P_o(\omega_o, k_y, h)$.

(5) Inverse 2-D FFT of $P_o(\omega_o, k_y, h)$ to obtain $p_o(t_o, y, h)$ which is the zero offset section.

$$P_o(\omega_o, k_y, h) \cdots \text{2–D FFT}^{-1} \cdots > p_o(t_o, y, h).$$

(6) Repeat steps 3–5 until all the common offset sections are processed.

4.3 Prestack Partial Migration of Synthetic Data

It is a common practice to test a migration operator for a single isolated wavelet. A common offset section, in which the data consist of zeros everywhere except a single arrival at the centre trace, geometrically corresponds to a reflection from a buried semi-elliptical reflector as shown in figure 4.4. The dip-moveout program developed based on Hale's method was tested for synthetic common offset section. Figure 4.5 is a constant offset section with a single arrival at $t = 2.5\ s$. The data was obtained by convolving the trace containing the spike with 5.0 Hz Ricker wavelet. Hale (1984) showed that the dip-moveout and normal moveout do not comute, therefore, NMO has to be performed before DMO. The NMO corrected data is shown in figure 4.6. Applying DMO to the NMO corrected data given in figure 4.6 yields the impulse response shown in figure 4.7. The impulse response of the DMO by Fourier transform is *smile* which traces a lower segment of an ellipse. The NMO and DMO computation was performed assuming a constant offset of 2000 m and medium velocity 3000 m/s. The trace spacing and time sampling interval were 50 m and 50 ms respectivelly. As will be shown in the next chapter, zero-offset migration of the DMO ellipse is the the theoretically expected simi-elliptical reflector.

To investigate the properties of the DMO operator with regard to offset and traveltime a number of tests were conducted. Figure 4.8 is a constant offset section with seven isolated arrivals 650 ms apart. Figure 4.9 shows the common offset section given in Fig. 4.8 after NMO correction using medium velocity of $v = 2000$ m/s and

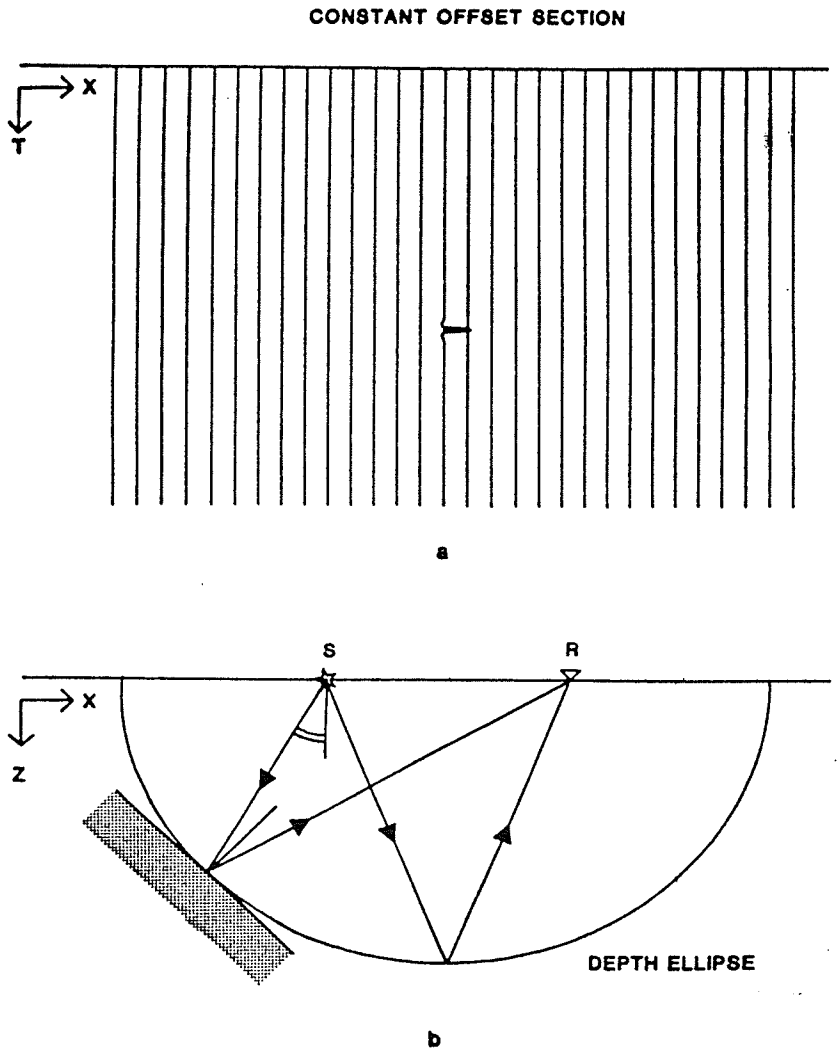

Figure 4.4: An elliptical shaped subsurface model (b), and its corresponding common offset seismic response (a).

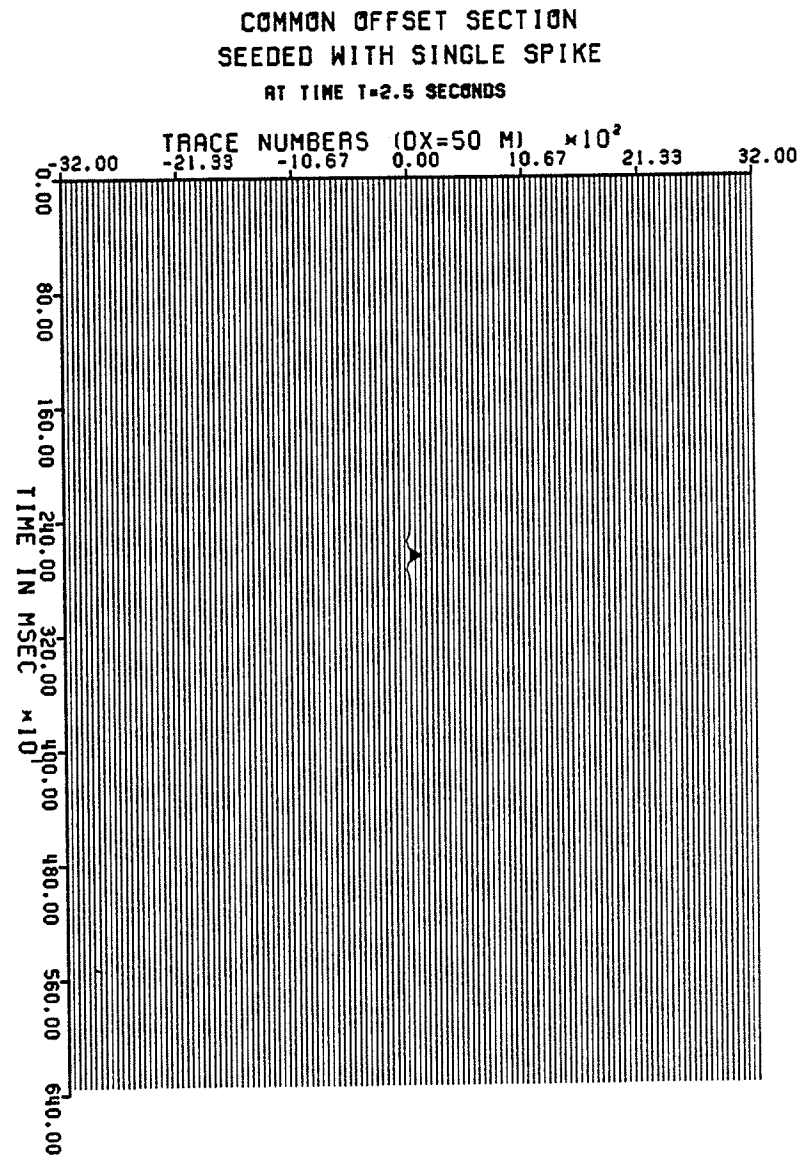

Figure 4.5: (a) Common offset section with single isolated arrival at time $t = 2.5$ s.

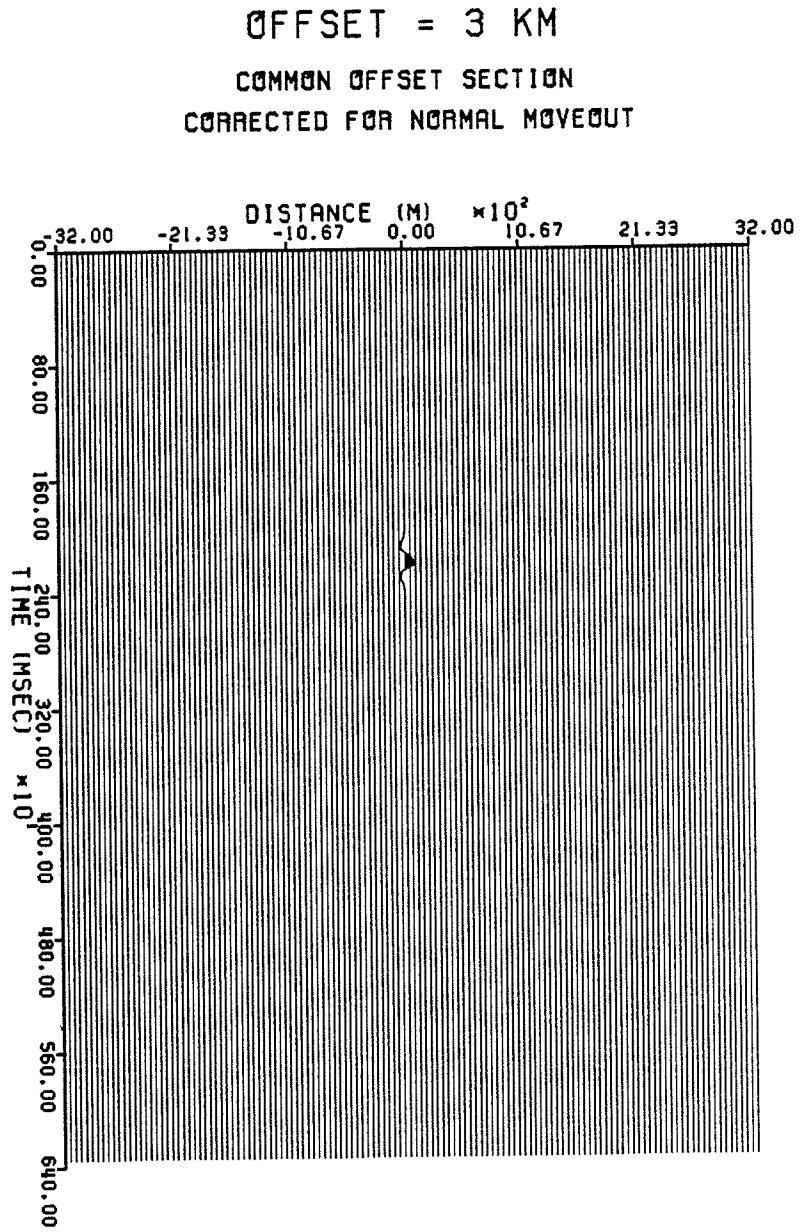

Figure 4.6: The common offset section after NMO correction (with a medium velocity $v = 2000$ m/s and offset= 3000 m).

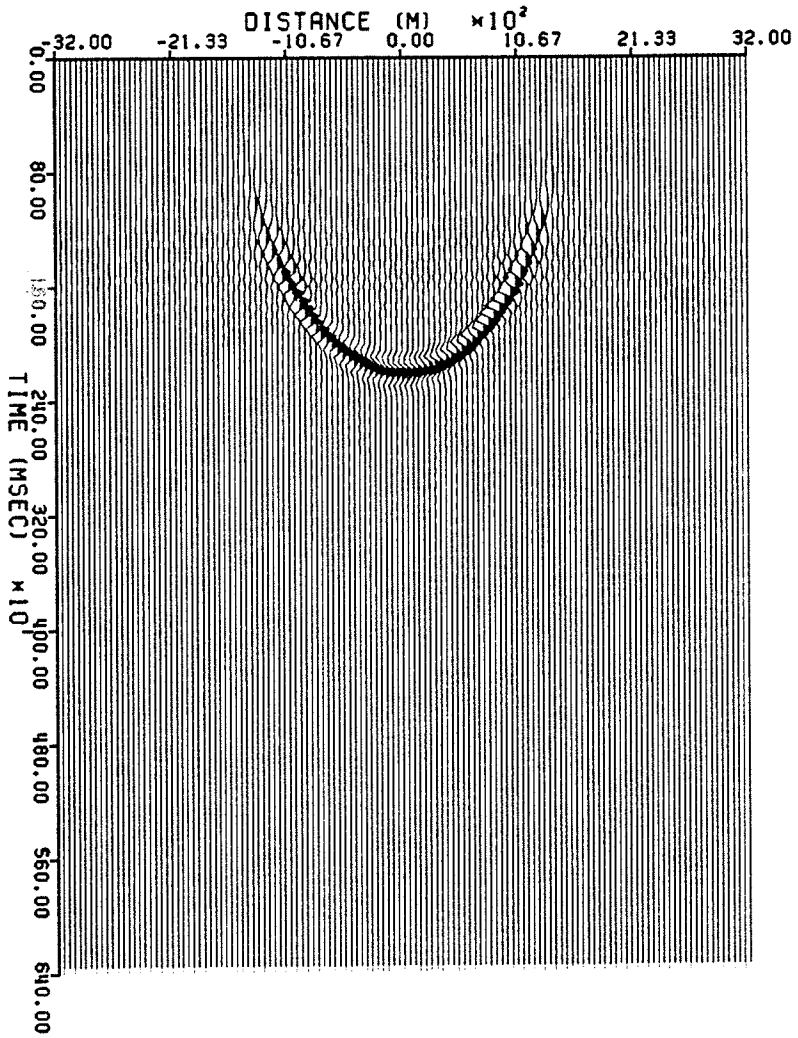

Figure 4.7: Hale's DMO operator obtained by applying prestack partial migration to the NMO corrected common offset section shown in figure 4.6.

half offset $h = 1500$ m. The early arrivals show the normal moveout stretch, which has the effect of lowering the signal frequency. The normal moveout stretch decreases with increasing travel time. The DMO corrected data given in figure 4.10, illustrates the theoretically expected ellipses. From figure 4.10 one can see that DMO is very significant for early arrival times. Figure 4.11 and 4.12 shows the NMO and DMO correction for $h = 500$ m respectively. The medium velocity v is 2000 m/s the same as for the offset 3000 m. Comparing the dip-moveout corrected sections given in figure 10 and 12 it is easily noticeable that DMO correction is very significant for early arrivals and large offsets. As the reflection time increases the DMO response curve becomes sharper and sharper. At shorter offsets and longer travel times the DMO operator reduces to a spike.

4.4 Dip-moveout Performance

The dip-moveout process involves time shift in the f–k domain. In the forward direction, the two dimensional data is fast Fourier transformed with respect to spatial variable and numerically integrated with respect to time. Mapping back to the *time–space* domain is performed using 2-D FFT. This DMO program is slower, but more accurate compared to the approximated DMO algorithms which are being proposed recently and employ the 2-D FFT to move in and out of the f-k space (Biondi and Ronen, (1986, 1987); Notfors and Godfrey, 1987; and Lines and Bleistein, 1988). Table 4.1 shows sample CPU times for selected data matrices.

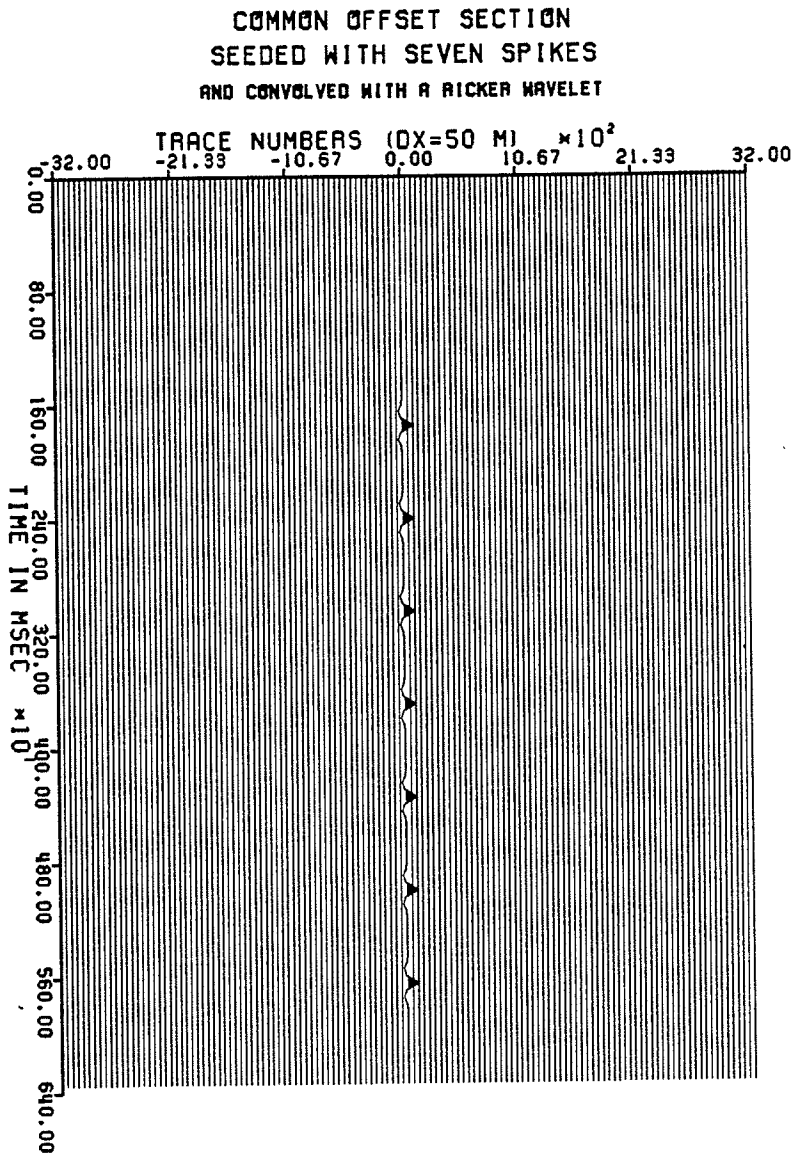

Figure 4.8: Common offset section seeded with seven spikes and convolved with a Ricker wavelet, the arrivals are separated 650 ms apart.

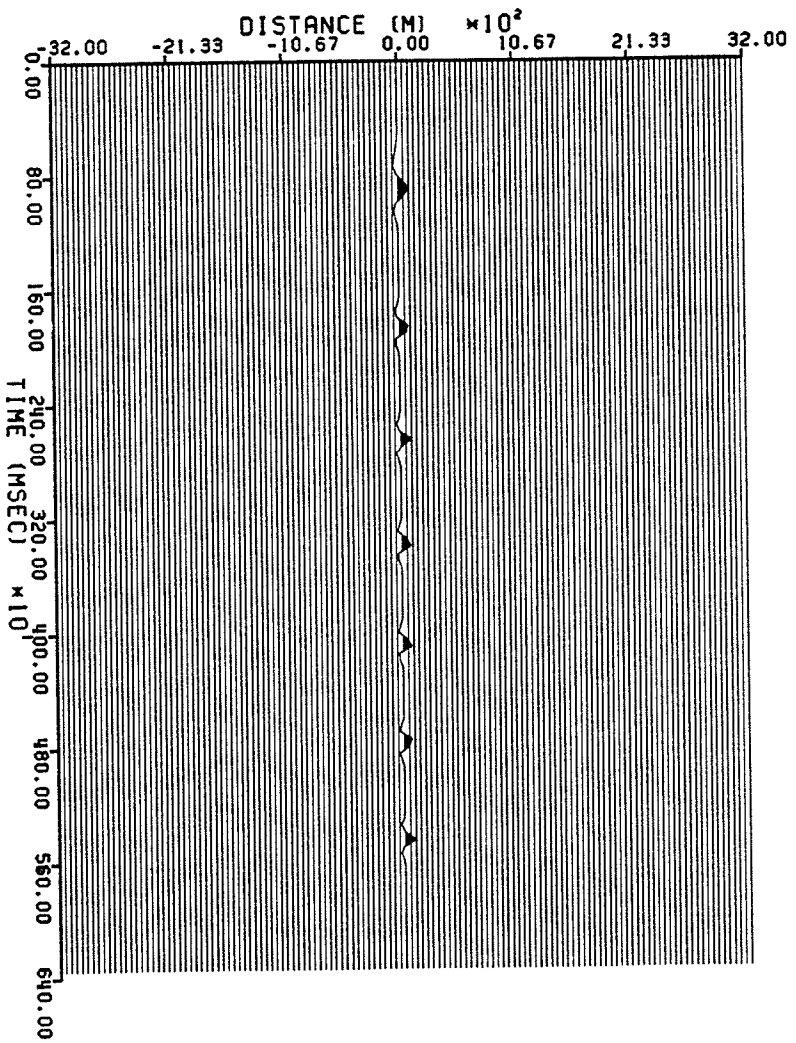

Figure 4.9: The common offset section given in figure 4.8 after NMO correction ($v = 2000$ m/s,and halfoffset $h = 1500$ m).

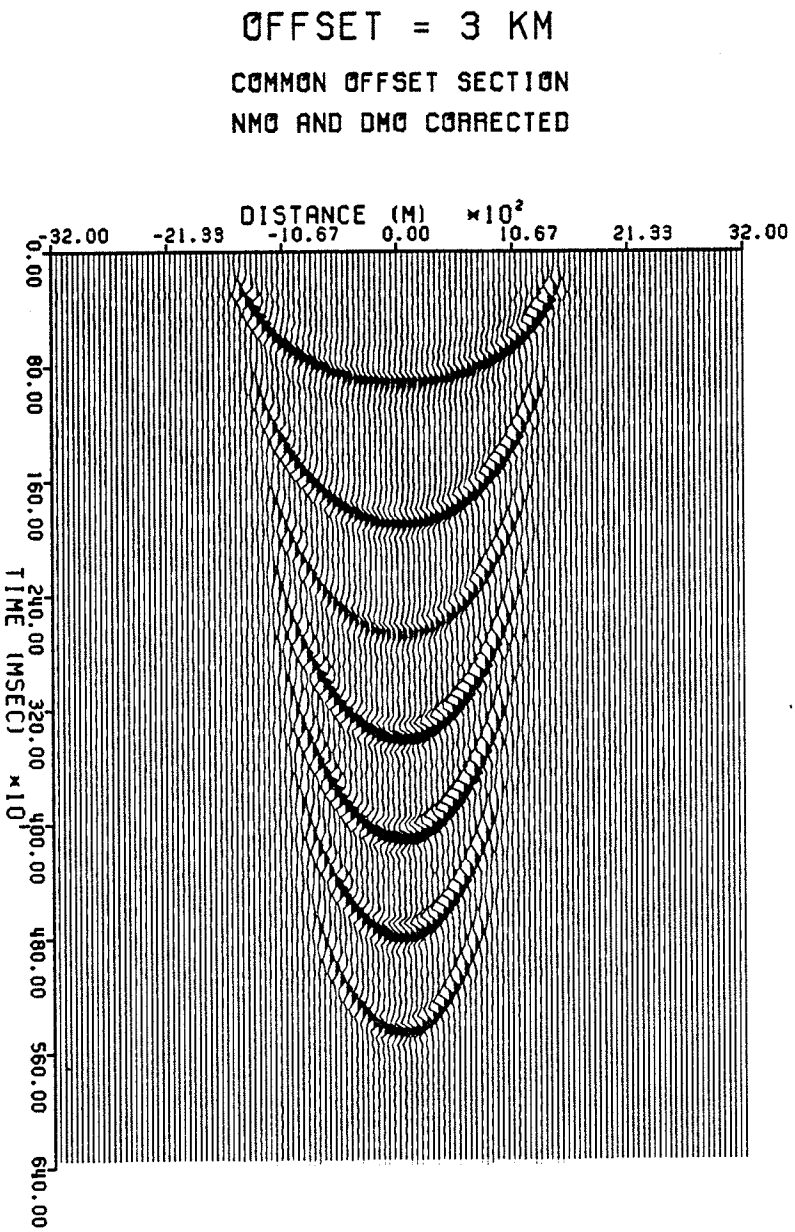

Figure 4.10: Common offset section after NMO and DMO correction. The shallower ellipses encompase large number of traces compared to the deeper ellipses, which means dip-moveout correction is larger for early arrivals as compared to late arrivals.

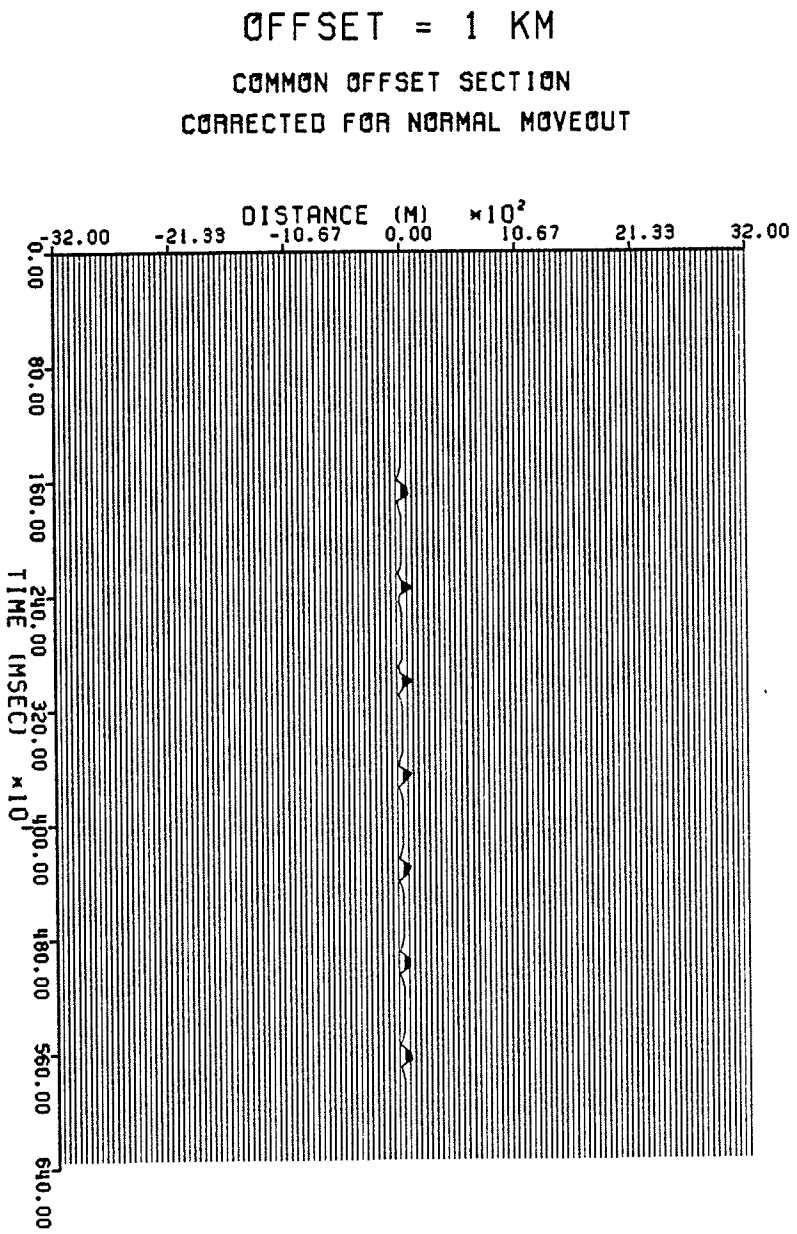

Figure 4.11: The common offset section given in figure 4.10 after NMO correction ($v = 2000$ m/s,and halfoffset $h = 500$ m).

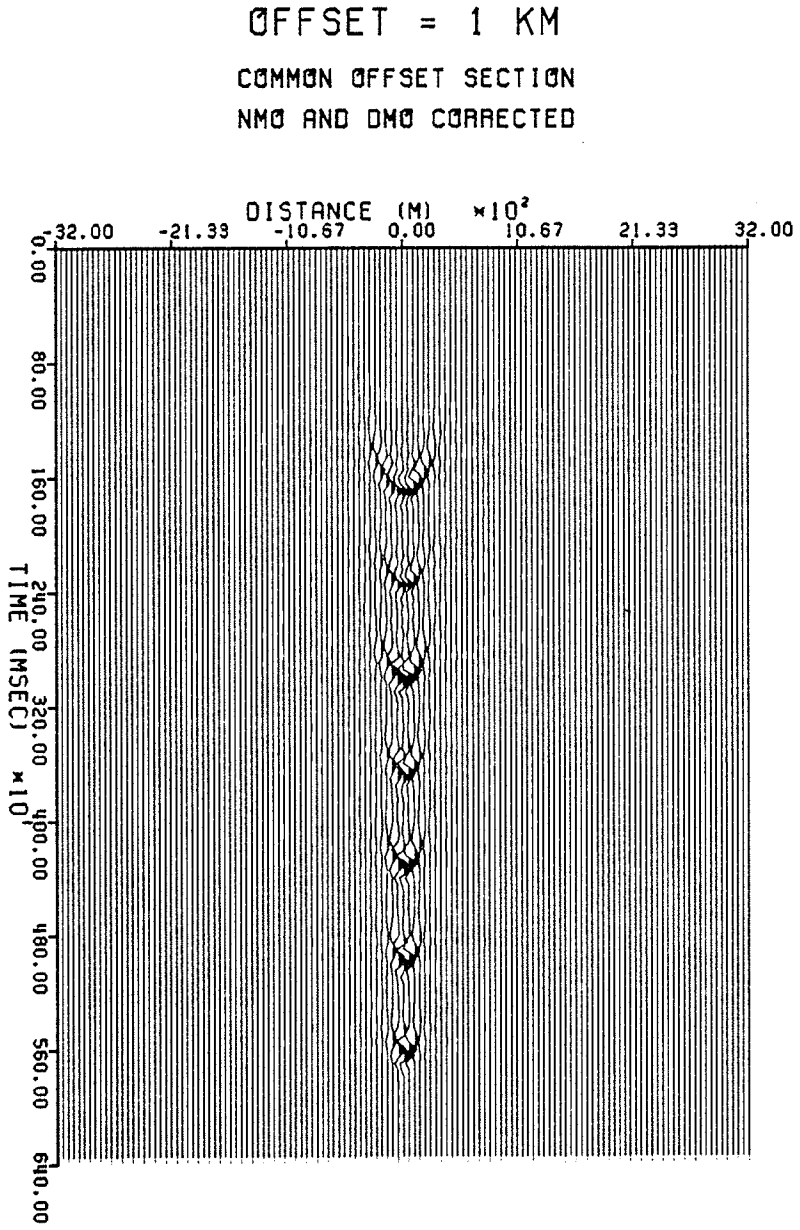

Figure 4.12: Common offset section after NMO and DMO correction. For shorter offsets and late arrivals DMO correction is small.

DMO CPU time for three data matrices

Matrix size	*CPU Time (including plotting)*
64×64	17.0 s
128×128	1.0 min and 18.0 s
256×256	7.0 min and 21.15 s

Table 4.1: DMO CPU Time on Amdahl 5870 with MVS3 operating system (Serzu and Moon, 1989(b)).

Chapter 5

Migration of Seismic Data

In Seismology the term *migration* is synonymous with focusing in optical imaging. In literature we find several definitions and descriptions of seismic migration. Sometimes migration is described as a seismic processing step by which events observed in time section are repositioned in their correct subsurface spatial locations. Others describe seismic migration in mathematical terms as an inverse problem which involves numerical solution to the partial differential equation which governs wave propagation. According to the latter and recent understanding migration consists of two steps : *Downward continuation* (wave extrapolation) and *Imaging.*

Until 1970 seismic migration was often performed using wavefront charts and diffraction summation. This method was based on ray theoretical consideration, and was concerned mainly with repositioning of reflectors. In the early 1970's migration algorithms based on the wave equation were introduced through the work of Claerbout (1970). Since then, several efficient algorithms have been developed based on the solution of the scalar equation of motion.

Wave equation migration algorithms are divided into two main categories : *Migration Before Stack* and *Poststack Migration.* The two main divisions are further

subdivided based on the domain of application and the type of numerical solution employed in solving scalar equation of motion.

In this chapter zero-offset (poststack) migration algorithms will be reviewed and special attention will be given to the *Phase-Shift Migration* (Gazdag, 1978 (a)).

5.1 Poststack Wave Equation Migration

Normally, the CMP stacked section discussed in Chapter 1 is where most of the conventional seismic data processing ends. This vertical section is time representation of the subsurface below the seismic line. The CMP stacked section contains geometrical effects of wave propagation, and diffractions from faults and discontinuities in reflectors. Curved and dipping events in the CMP stacked section are always misplaced and distorted. Shoulders of anticlines appear broader and synclines are sharper than what actually are. A syncline with a large curvature is characterized by a *bow-tie* reflection configaration in a CMP stacked section . The bow-tie shows 180° phase-shift (Stolt and Benson, 1986). All the above undesirable effects on the CMP stacked section have to be corrected using migration.

The CMP stacked section is approximately equivalent to the zero-offset section. Therefore, the poststack (zero-offset) migration is appropriate for stacked data. At present, the majority of migration methods are based on the scalar wave equation, and migration itself is achieved with the help of the *Exploding Reflector Model* (Lowenthal et al., 1976).

Wave equation migration can be implemented in several different domains : space-time (x,t), frequency-wavenumber (ω,k_x), Space-frequency (x,ω), wavenumber-time (k_x,t), and the intercept time-ray parameter domain (τ,p). There are advantages

and disadvantages associated with each of these methods. The space-time domain algorithms are divided into integral and differential methods migration.

The Kirchoff (Summation) method is based on the integral solution of the wave equation. According to this method, the stacked data which is a wavefield recorded at the surface can be expressed at any depth in terms of its value at the surface using a weighted integral. The main advantage of the Kirchoff migration is that, subsurface points can be imaged independently. The method can also handle irregular grid spacing. The disadvantages associated with the Kirchoff integral method include ; poor performance under low S/N ratio, and difficult to accommodate lateral velocity variations.

The differential migration algorithms use the *finite-difference* approximations to obtain a solution of the scalar wave equation. This method was first introduced by Claerbout (1970). The advantage of this technique over the rest of the migration methods is, its ability to handle lateral changes in velocity. The finite-difference method performs well under low S/N ratio (Whitmore et al., 1988). The main disadvantage of the finite-difference methods is frequency dispersion at steep dips. The frequency dispersion is manifested as ghost reflectors accompanying the actual reflector in the migrated section. Other disavantages include lack of specialization for $v(x,z) = v(z)$ and high computational cost.

The frequency-space (ω, x) migration is hybrid in nature and employs the Fourier transform and finite-difference approximation to obtain the solution of scalar wave equation. This method is suitable for depth migration in geologically complex region. Unfortunately, depth migration requires detailed velocity, which is difficult to obtain in structurally complex areas where it is most needed (Gazdag, 1980; Kelamis and

Kjartansson, 1985).

The f–k migration and the Phase-Shift methods are implemented in the transform (ω, k_x) domain. These two methods were introduce by Stolt (1978) and Gazdag (1978(a)) respectively. Stolt's f–k migration involves 2-D Fourier transform of surface recorded data into frequency-wavenumber (ω, k_x) domain, change of variable from ω to k_z, and inverse Fourier transform to (x, t) domain. The main advantage of this method is speed. Migration is performed at the speed of the fast Fourier trasform. The $f-k$ migration can handle dips up to 90°. The serious drawback of the $f-k$ migration is failure to handle both vertical and lateral changes in velocity.

The phase-shift migration such as the f–k method involves 2-D FFT of the CMP stacked data into (ω, k_x) domain. The transformed data is extrapolated from depth z to $z + \Delta z$ simply by rotating the phase of the wavefield by a specified amount $(\exp(-ik_z\Delta z)$ (Gazdag, 1978(a)). The *imaging* principle involves summation with respect to ω. Inverse FFT with respect k_x maps the migrated data in the transform domain back to the (x, z) space. The phase-shift migration handles steep-dips up to 90°. Vertically varying velocity is easily handled by the Phase-shift method. Laterally changing velocity is accomodated by The *Phase-Shift Plus Interpolation* (PSPI). The PSPI is a modification of phase-shift suitable for laterally varying media. The PSPI migration method uses both the (ω, k_x) and (ω, x) domains. In its simplest form involves 2-D FFT of the CMP data $(P(t, x, z = 0)$ to $P(\omega, k_x, z = 0))$, downward continuation of the wavefield $P(\omega, k_x, z)$ to $P(\omega, k_x, z + \Delta z, t)$ as many times as there are velocities between z and $z+\Delta z$. Each extrapolated wavefields P_i is inverse Fourier transformed to time-space domain $(\tilde{p}_i)$ from which a single $\tilde{p}$ is to reconstructed at each x. $\tilde{p}_1$ is reconstructed if $v(x, z + \Delta z) = v_1$ and $\tilde{p}_2$ if $v(x, z + \Delta z) = v_2$ and so

on (Whitmore et al., 1988; Gazdag and Squazzero, 1984(a)). Compared to phase-shift migration, the PSPI method is slow. However, the PSPI method gives accurate results in the presence of laterally varying media .

For the purpose of this *thesis* phase-shift method is the prefered migration algorithm. The criteria used in choosing the migration algorithm is : speed, accuracy, real memory requirement, ability to handle steep dips, and ability to accomadate vertical as well as lateral changes in velocity. The phase-shift method can satisfy all of the above criteria, except, lateral changes in velocity. This last criteria can be handled by increased computational cost using the modified phase-shift (PSPI) method.

In the following few sections the zero-offset concept and the exploding reflector model will be reviewed. These two models play an important role in migration of zero-offset data. The phase-shift migration will be presented in detail, and its performance will be evaluated using synthetic seismograms.

5.2 Zero-offset Concept

In reflection seismic method the zero-offset concept implies coincident source-receiver position. According to this model a disturbance from a coincident source-receiver location at the surface travels through the Earth and upon encountering a discontinuity or a reflecting surface it is reflected back upward toward the surface. The receiver records the reflected energy which originated from the same source-receiver point, which implies the downgoing and upgoing energy followed the same raypath. According to this model the raypath is assumed to be normal to the reflecting surface and the zero-offset section can be regarded as energy recorded by moving the coincident source-receiver along a seismic line. Physically the zero-offset concept is not

realizable. Figure 5.1 (a) illustrates the zero-offset concept schematically.

The CMP stacked section which had undergone several digital processing step is approximately equivalent to a zero-offset section. Hence, zero-offset migration can be understood with the help of a hypothetical model known as the *Exploding Reflector Model.*

5.3 The Exploding Reflector Model

The zero-offset migration uses the exploding reflector concept to reconstruct a wavefield within the earth from data recorded at the surface. According to this model sources are located in the subsurface along the reflecting surface and are set off simultaneously at time $t = 0$. The energy propagates upward where it gets recorded by receivers located at the surface (forward modeling). Migration is an inverse problem, and can be visualized as propagation of the wavefield observed at the surface back to the reflector at depth. In other words, migration extrapolates the observed field to *increasing* depths in *reverse* time. The *imaging* principle is invoked at time t=0. Figure 5.1 (b) shows the exploding reflector model. This model is practically same as the zero-offset concept. The main difference between the two models is ; zero-offset section is recorded in *two way* traveltime while the exploding reflector involves only the *one way* traveltime. Poststack migration is achieved with the help of the exploding reflector model, hence, the two way travel time of CMP stacked (zero-offset) data has to be converted into one way time. However, in practice the traveltimes of the recorded section are left unaltered, instead, one half velocity of the media is used during the wave extrapolation step.

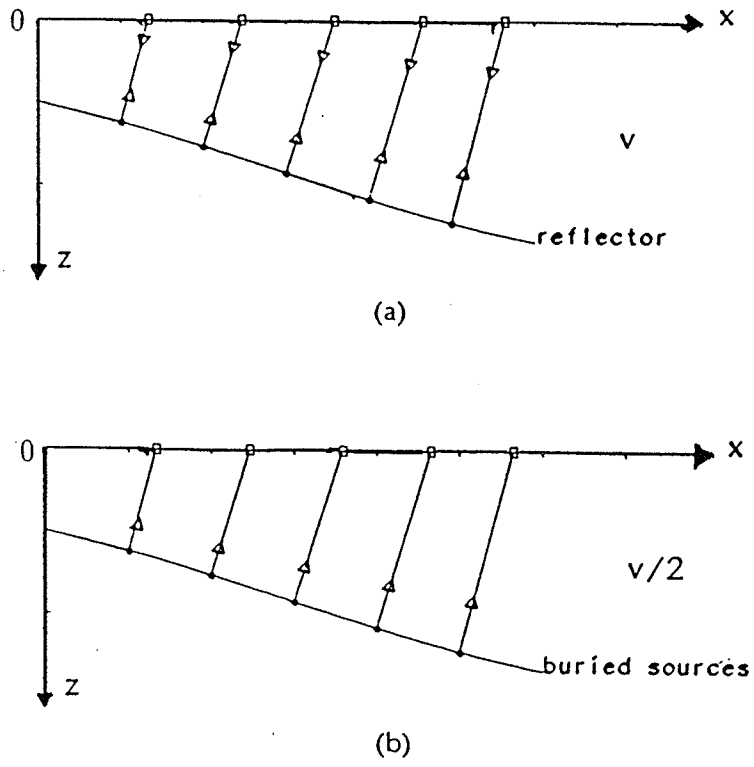

Figure 5.1: (a) Zero-offset section obtained by coincident source-receiver location. (b) Exploding reflector model, contains only upgoing energy. To compensate for traveltime the exploding reflector model propagates the waves with half the medium velocity.

5.4 Phase-Shift Migration

In the last 15 years, several papers have been published on *wave equation migration* of zero-offset data; to name few, Claerbout (1970, 1976, 1985), French (1975), Schneider (1978), Stolt (1978), and Gazdag (1978(a)). The phase-shift migration which is the topic of this section was the work of Gazdag (1978(a)). This method, like many other methods of migration, employs the exploding reflector model to approximate the zero-offset concept which is closely associated with the CMP stacked section.

The phase-shift migration is implemented in the frequency-wavenumber (ω, k_x) domain, and uses discrete Fourier transform to solve the scalar equation of motion. If we take density ρ to be constant, then, the two-dimensional equation for acoustic wave propagation can be written as,

$$\frac{\partial^2 p}{\partial x^2} + \frac{\partial^2 p}{\partial z^2} = \frac{1}{[v(z)^2]} \frac{\partial^2 p}{\partial t^2} \tag{5.1}$$

where, $p(x, z, t)$ is the acoustic wavefield in this case, the variable z represents depth, variable x is the horizontal distance along the seismic line, and $v(z)$ represents velocity of the media. For our purpose velocity varies only with depth. Taking Fourier transform of equation (5.1) with respect to x and t gives,

$$\frac{\partial^2 P}{\partial z^2} + k_z^2 P = 0 \tag{5.2}$$

$P(k_x, z, \omega)$ is the wavefield in $\omega - k_x$ domain. k_x, k_z, and ω are the Fourier dual variables of x, z, and t. The vertical wavenumber k_z is the *dispersion relation* and it is given as follows,

$$k_z = \frac{\omega}{v(z)}\left[1 - \frac{(v(z)k_x)}{\omega^2}\right]^{1/2} \tag{5.3}$$

Following the notation of Robinson (1983), equation (5.2) can be split into two first order partial differential equations representing waves going in opposite directions, the upgoing wave is given by

$$\frac{\partial P}{\partial z} - k_z P = 0 \tag{5.4}$$

and the downgoing wave is expressed as

$$\frac{\partial P}{\partial z} + k_z P = 0 \quad . \tag{5.5}$$

The exploding reflector model is concerned only with the upgoing wave. Assuming $v(z)$ to be constant within a single extrapolation step, the solution of equation (5.4) can be expressed analitically as,

$$P(k_x, z_o + \Delta z, \omega) = P(k_x, z_o, \omega)e^{ik_z \Delta z} \quad . \tag{5.6}$$

Equation (5.6) represent extrapolation of the wavefield from depth z_o to $z_o + \Delta z$. From the expression one can see that the wavefiled extrapolation is achieved by rotating the phase (ie. multiplying by $\exp(ik_z \Delta z)$). Therefore, the phase-shift migration lends its name to the extrapolation principle discussed above. The extrapolated wavefield in the object space (x, z) is obtained by inverse Fourier transformation of equation (5.6), that is

$$p(x, z, t) = \frac{1}{4\pi^2} \int\int P(k_x, z = 0, \omega) \exp[-i(k_x x + k_z z - \omega t)]\, dk_x\, d\omega \quad . \tag{5.7}$$

Imaging is accomplished by setting the time variable $t = 0$, and equation (5.7) can be simplified as follows

$$p(x, z, t = 0) = \frac{1}{4\pi^2} \int \int P(k_x, z = 0, \omega) \exp[-i(k_x x + k_z z)] \, dk_x \, d\omega \quad . \tag{5.8}$$

Equation (5.8) represent the continuous form of the phase-shift migration.

5.5 Numerical Representation of the Migration Integral

Computation using digital computers, requires data to be in digital form. The phase-shift migration integral given by equation (5.8) can be expressed in numerical form as follows

$$p(x, z, t = 0) = \sum_{k_x} \sum_{\omega} P(k_x, z = 0, \omega) \exp[-i(k_x x + k_z z)] \quad . \tag{5.9}$$

Evaluation of equation (5.9) involves :

- 2-D Fourier Transform with respect to x and t
- extrapolation by the phase-shift (ie. multiplication by $\exp[-ik_z z]$)
- summation with respect to ω (imaging) and
- inverse Fourier transform with respect to k_x.

5.6 Approximation of Dispersion Relation (k_z)

The vertical wavenumber for upcoming wave is

$$k_z = \frac{2\omega}{v(z)} \left[1 - \frac{(v(z)k_x)^2}{4\omega^2} \right]^{1/2} \quad . \tag{5.10}$$

The dispersion relation can be rewritten as a function of the vertical travel time τ,

$$k_\tau = \frac{v(z)k_z}{2} = \omega \left[1 - \frac{(v(z)k_x)^2}{4\omega^2}\right]^{1/2} \tag{5.11}$$

provided that velocity $v(z)$ is constant within interval $(z, z + \Delta z)$. The vertical wavenumber k_τ can be approximated as follows :

- 2^{nd} order approximation

$$k_\tau = \omega \left[1 - \frac{(v(z)k_x)^2}{8\omega^2}\right] \tag{5.12}$$

- 4^{th} order approximation

$$k_\tau = \omega \left[1 - \frac{(v(z)k_x)^2}{8\omega^2} - \frac{(v(z)k_x)^4}{128\omega^4}\right] \tag{5.13}$$

- and/or asymptotic (high order) approximation

$$k_\tau \approx \omega \left[\frac{(v(z)k_x)^2}{\omega^2}\right]^{1/2} . \tag{5.14}$$

The asymptotic (high order) approximation closely approximates the dispersion relation of the full wave equation (Gazdag, 1978(a)). In the next section the approximations given above will be tested in synthetic seismogram modeling and migration, and their merits will be discussed.

5.7 Synthetic Seismogram Modeling of the Zero-offset Data

Synthetic seismogram modeling of zero-offset data is a *forward* problem in which seismic waves propagate through the depth model and generate amplitude-traveltime

pairs. The amplitude-traveltime pairs represent the zero-offset response of the model. Zero-offset modeling like migration is based on the exploding reflector model. Wave extrapolation is done with respect to the time variable t using the depth model $p(x, z, t = 0)$ as an input. The *imaging* principle is invoked when depth $z = 0$. The final output of the synthetic seismogram modeling is a zero-offset time section, $p(x, z = 0, t)$. As one may have noticed, the output of modeling process corresponds to the input of migration, and vice versa.

$$p(x, z, t = 0) \quad \underset{\text{Modeling}}{\overset{\text{Migration}}{\Longleftrightarrow}} \quad p(x, z = 0, t) \ .$$

There are as many modeling techniques as there are migration methods. Here we are concerned only with the phase-shift modeling. Section 5.8 deals with phase-shift migration of synthetic data.

5.8 Phase-Shift Migration of Synthetic Data

The zero offset phase-shift migration operator was tested for a single isolated arrival on the zero-offset section shown in figure 5.2 (a). Geometrical optics predicts that a single arrival on the zero-offset section to correspond to the depth model given in figure 5.2 (b). The phase-shift impulse response is shown figure 5.3. Migration smeared the single arrival into a semi-circular shaped reflection.

Several synthetic examples have been generated to test the phase-shift migration, including; a diffraction hyperbola, a truncated flat reflector, a dipping reflector, as well as a curved reflector. Figure 5.4 is a depth model for constant velocity media.

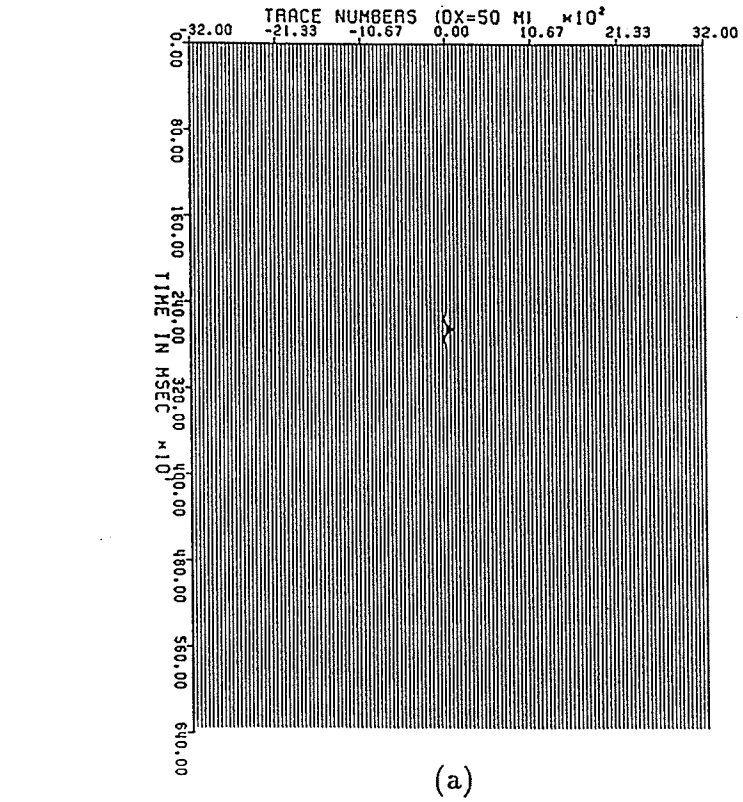

(a)

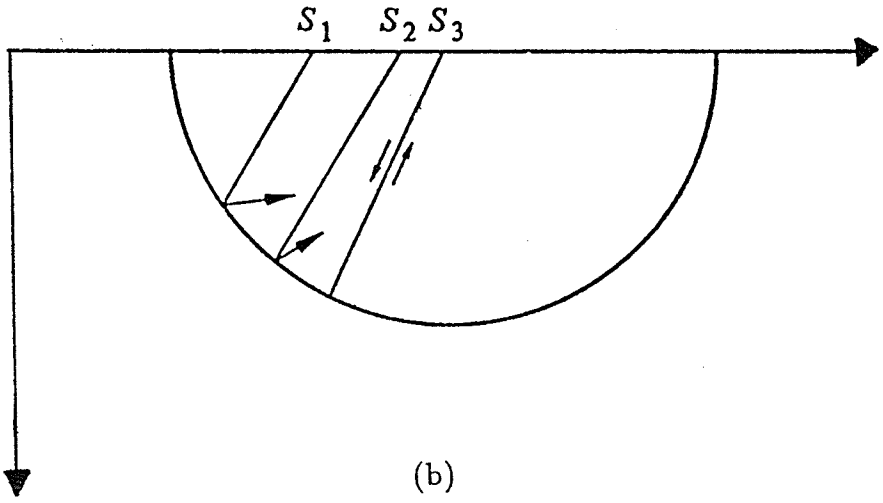

(b)

Figure 5.2: (a) A single arrival on the zero offset section, and (b) corresponding depth model predicted by geometrical optics. The model shows that the response given in (a) can only be recorded when both the shot and receiver are located at the centre of the semi-circular reflector.

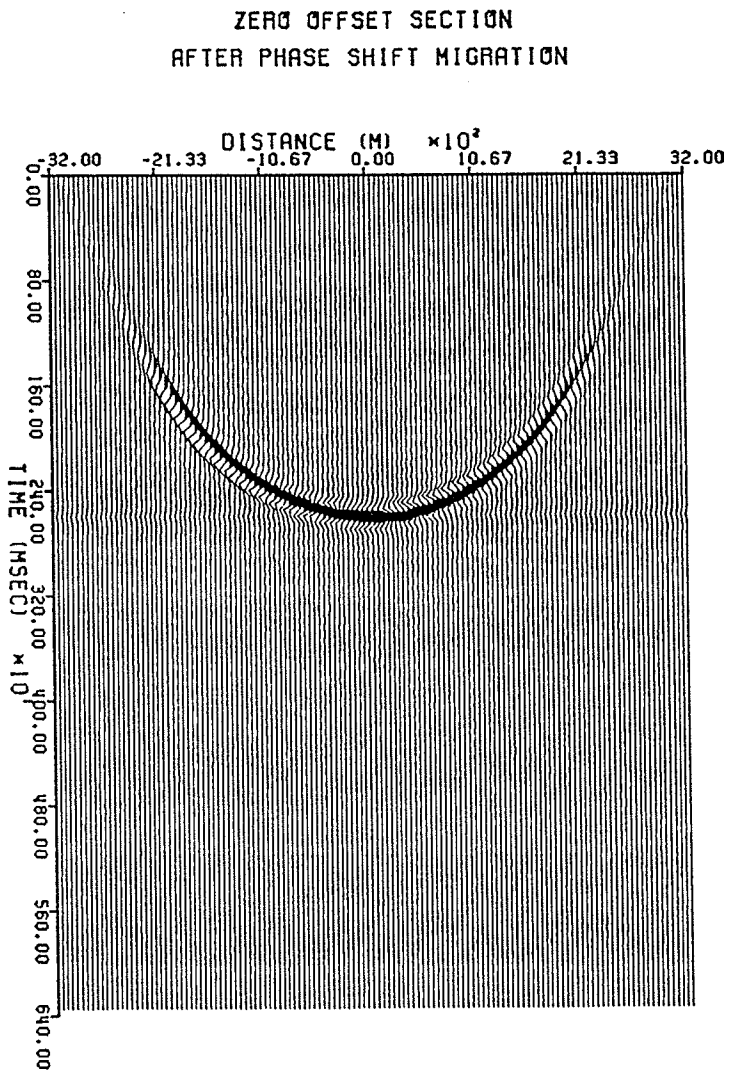

Figure 5.3: (a) Phase-shift migration operator obtained using the zero offset-section given in figure 5.2 (a) as an input to the migration program.

Four point diffractors are buried at regular depths intervals. The zero-offset response corresponding to the model in figure 5.4 is given in figure 5.5. The phase-shift migration of figure 5.5 is shown in figure 5.6. Note, the hyperbolas had been collapsed to their point of origin. Figure 5.7 shows a truncated horizontal reflector model. The seismic response is given figure 5.8. The diffractions at both ends of the reflector in figure 5.8 are due to abrupt truncation. Migration has removed the edge effects shown on the zero-offset section, (figure 5.9). Figure 5.10 is a model for a 45° dipping reflector, the zero-offsest seismic response is shown in figure (5.11). Migration of figure 5.11 is displayed in 5.12. Phase-shift migration moved the elongated dipping event towards the original location in the updip direction, and the reflector has been shortened back to the original shape. Comparing figure 5.11 and 5.12 we notice that the reflector dip is steeper in the migrated section. Figure 5.13 shows a model with a synclinal shaped reflector, and the zero offset section given in figure 5.14 shows the familiar bow-tie responce. Migration have untied the bow-ties, and the shoulders of the anticline have been sharpened, (figure 5.15). The last example given in figure 5.16 is a two layer realistic geologic model in which bottom layer is a faulted horizontal, and the top layer has an irregural shaped topography. The zero-offset response which is a superposition of diffractions, bow-ties, and linear and curved events shown in figure 5.17. Migration has moved the events to their proper vertical and horizontal locations, figure 5.18.

The time section shown in figure 5.19 (a) is an NMO and DMO corrected zero-offset section. The section was migrated using different approximations (equations through (5.12 - 5.14)) of the vertical wavenumber. The migrated section given figure 5.19 (b) was migrated using the 2^{nd} order approximation, the steeply dipping events

had been truncated. Figure 5.19 (c) is migration using the 4^{th} order approximation, compared to (b) shows improvement with regard to the steeply dipping events. Figure 5.19 (d) shows superior result, it was migrated using the asymptotically approximated dispersion relation given in equation (5.14).

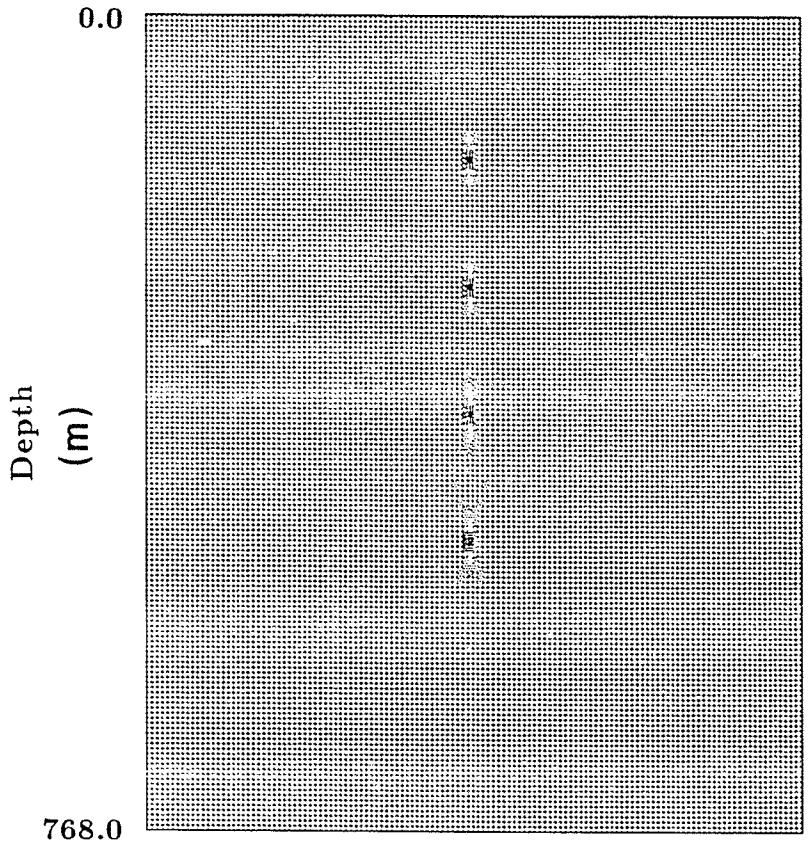

Figure 5.4: Depth model for four point diffractors, the velocity of the medium is assumed to be 3000 m/s

Synthetic Seismic Section

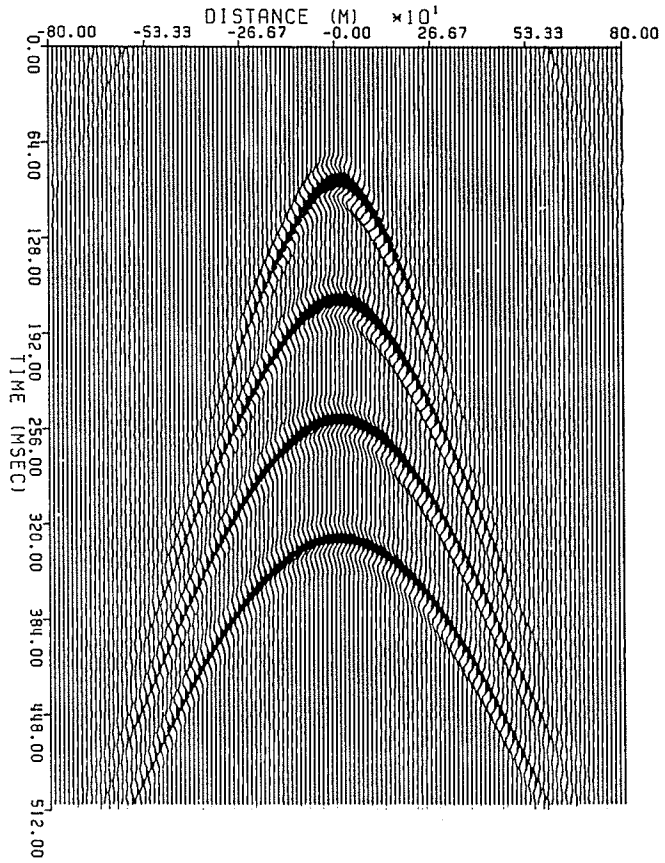

Figure 5.5: Zero offset section corresponding to the model given in figure 5.4. The seismic response to a point scatterer is diffraction hyperbola.

Migrated Synthetic Seismic Section

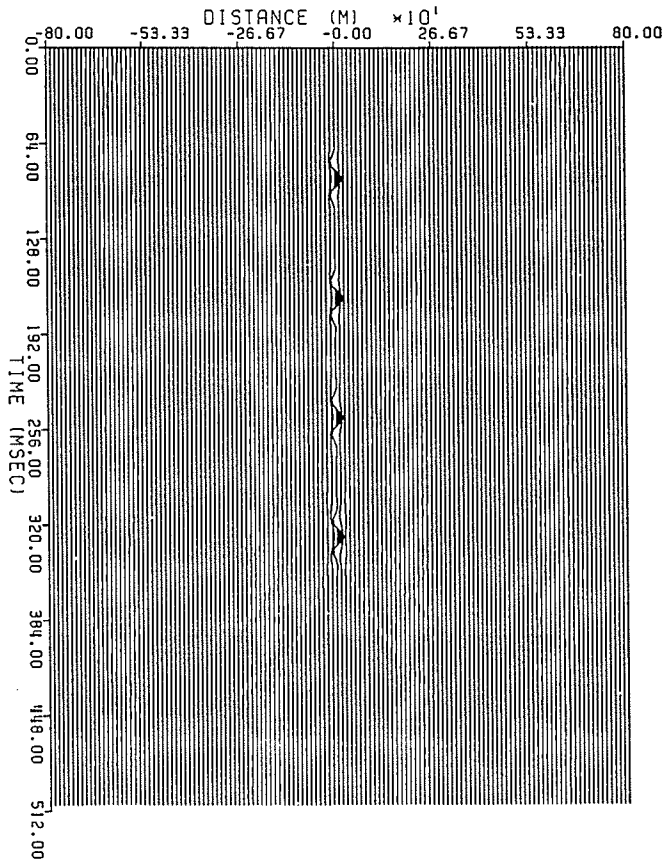

Figure 5.6: Migration collapsed the diffraction hyperbolas shown in in figure 5.5

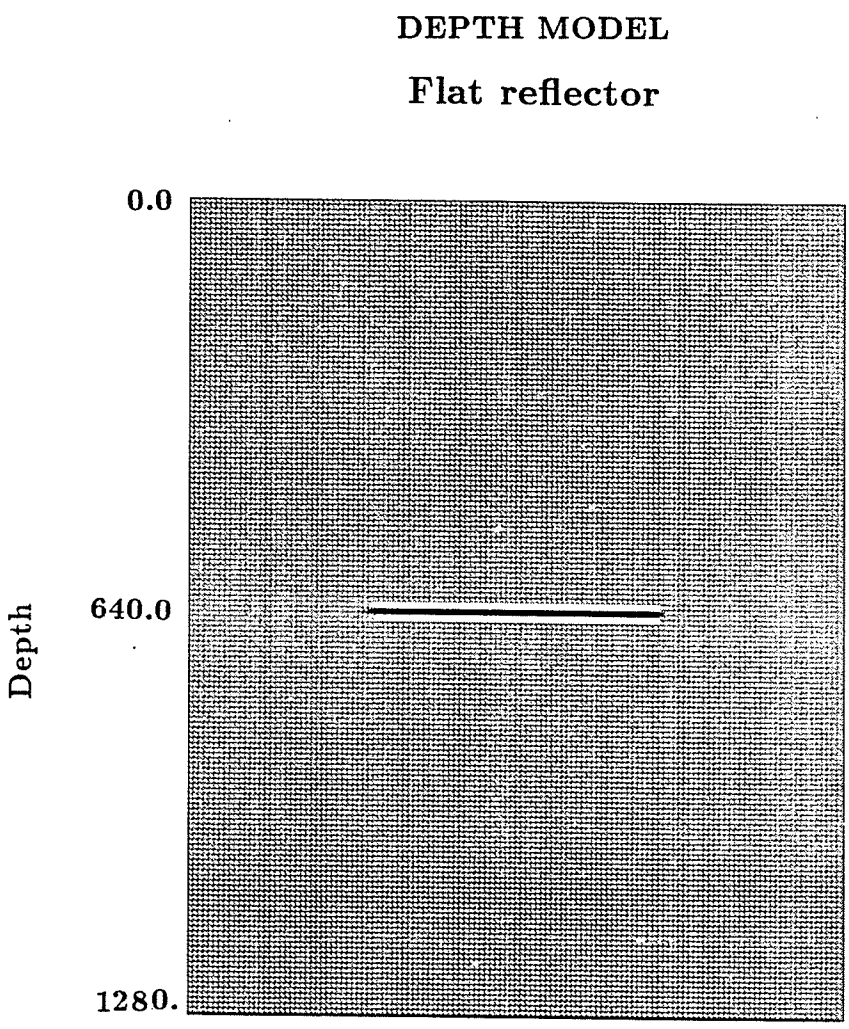

Figure 5.7: Depth model for a truncated horizontal reflector.

Synthetic Seismic Section

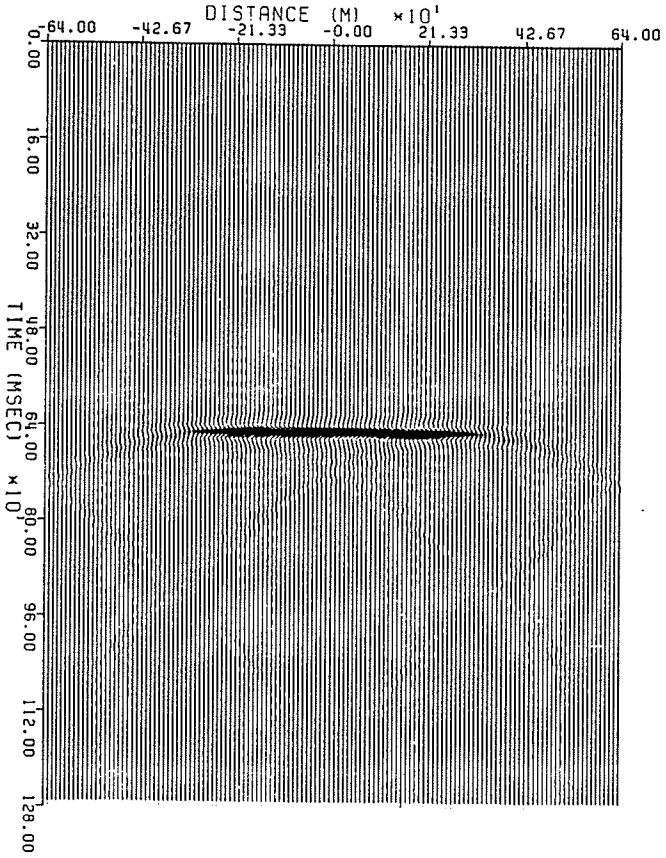

Figure 5.8: Zero-offset section corresponding to the model given in figure 5.7. The seismic response shows diffraction at both ends of reflector related sudden to discontinuity of the reflector.

Migrated Synthetic Seismic Section

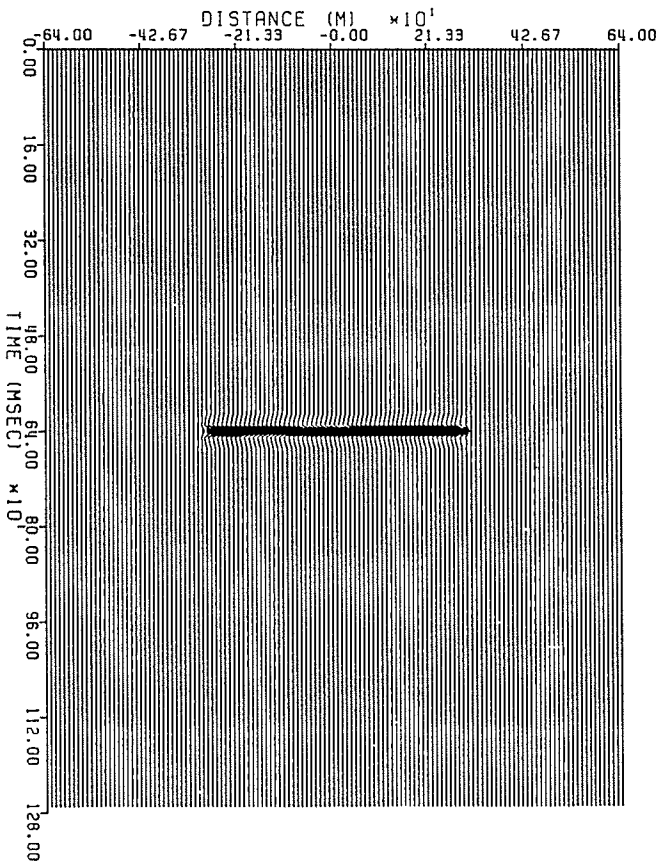

Figure 5.9: Migration removed the edge effets from the zero offset section.

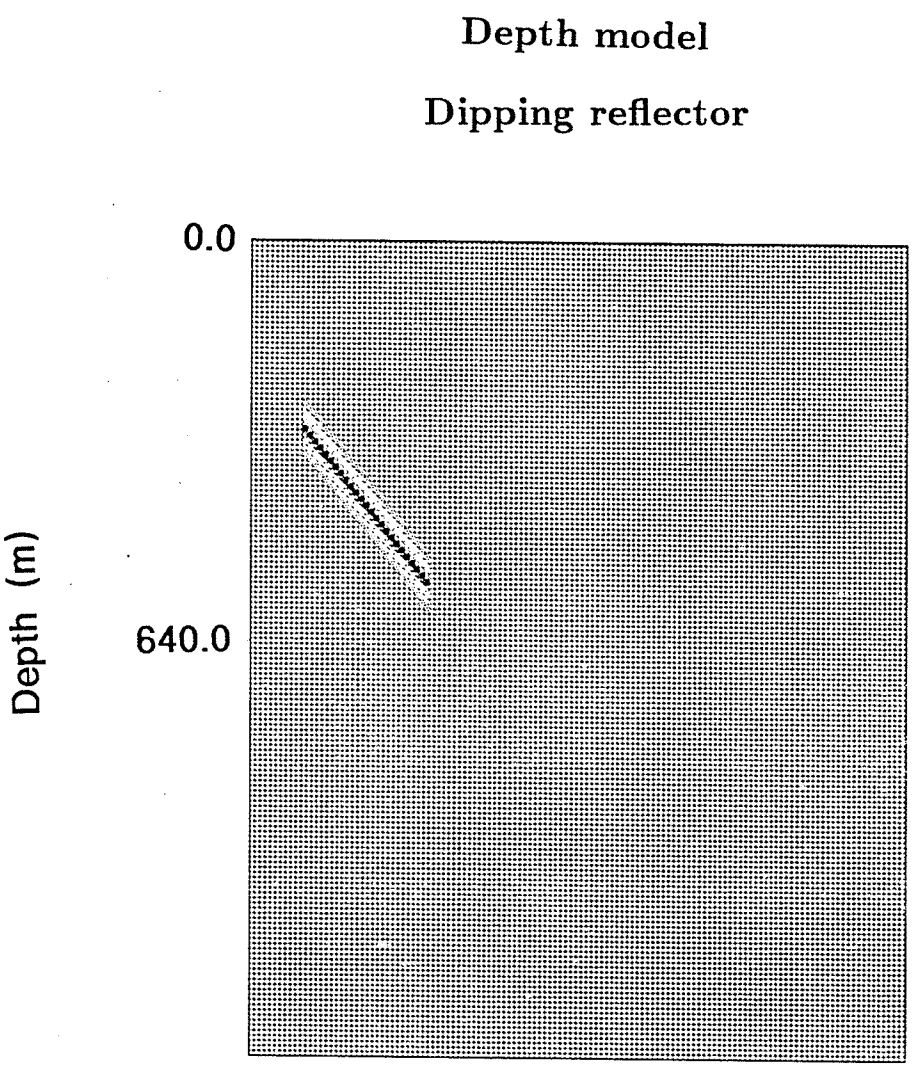

Figure 5.10: Depth model for a 45° dipping truncated reflector.

Synthetic Seismic Section

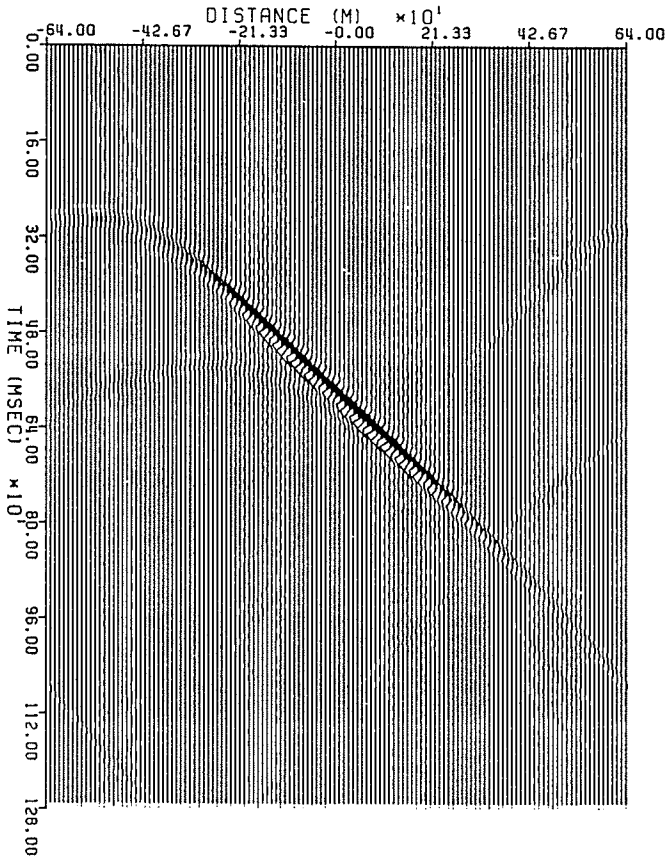

Figure 5.11: Zero offset response to the model given in figure 5.10 shows diffractions and elongation of the reflector.

Migrated Synthetic section

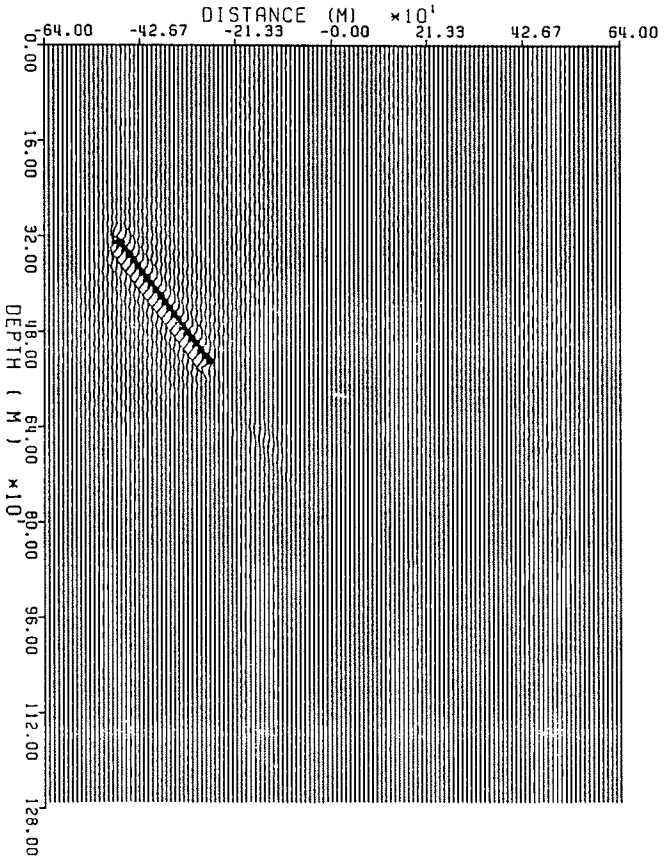

Figure 5.12: Phase-shift migration removed the edge effets and shortened the elongated reflector.

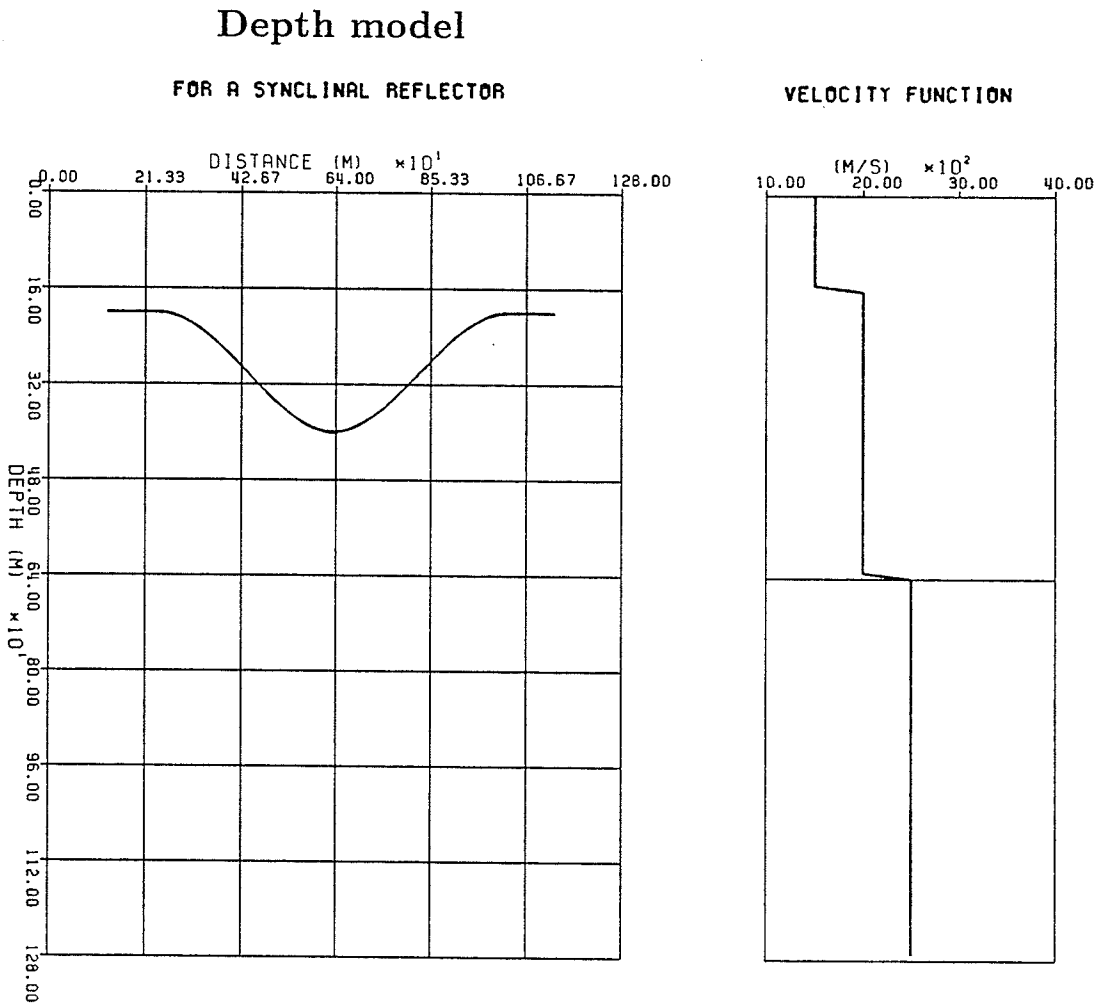

Figure 5.13: A depth model for a synclinal shaped reflector. The velocity of the medium is variable with respect to depth.

Synthetic Seismic Section

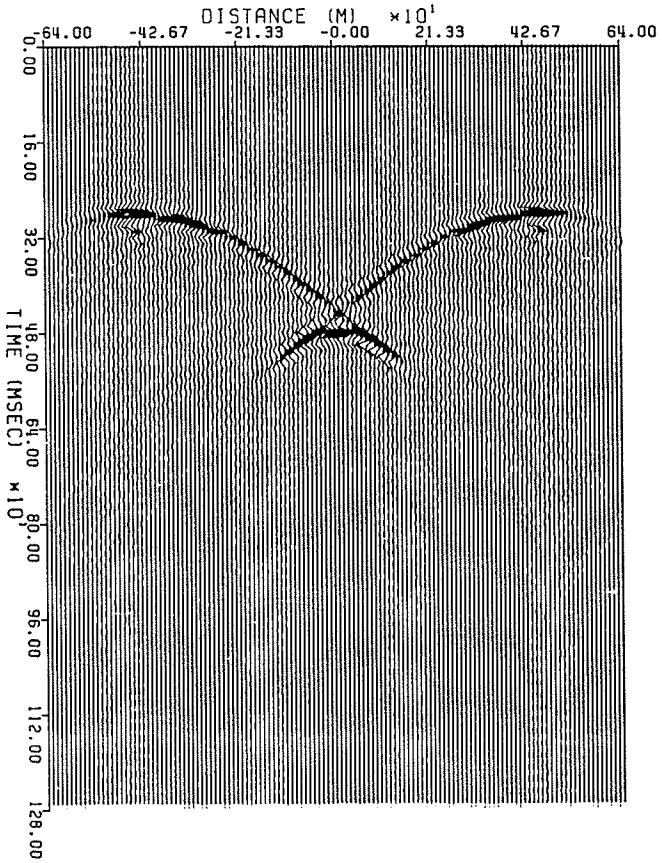

Figure 5.14: The seismic response shows a bow-tie shaped zero offset section to the model given in figure 5.13.

Migrated Synthetic Seismic Section

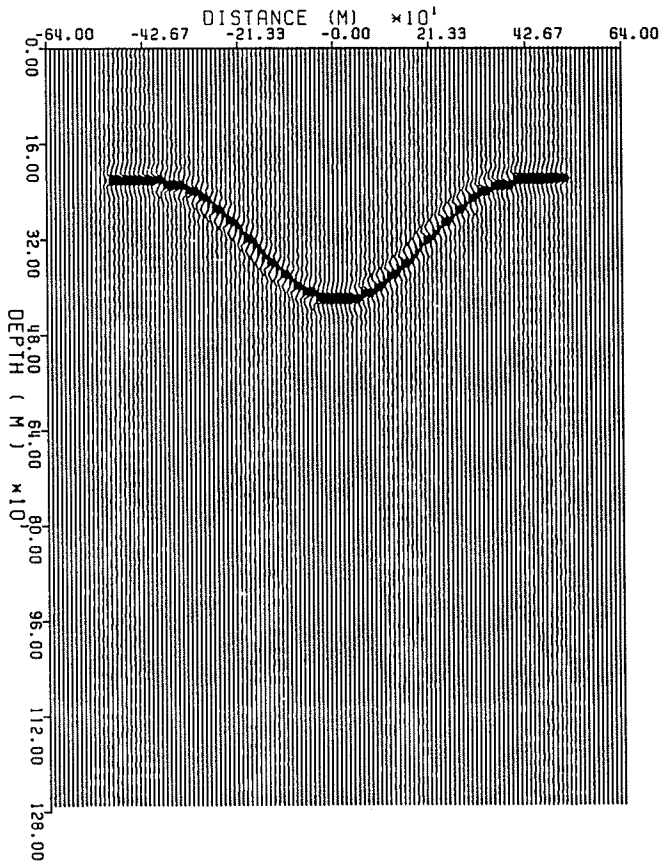

Figure 5.15: Migration of figure 5.14 , the bow-tie had been untied.

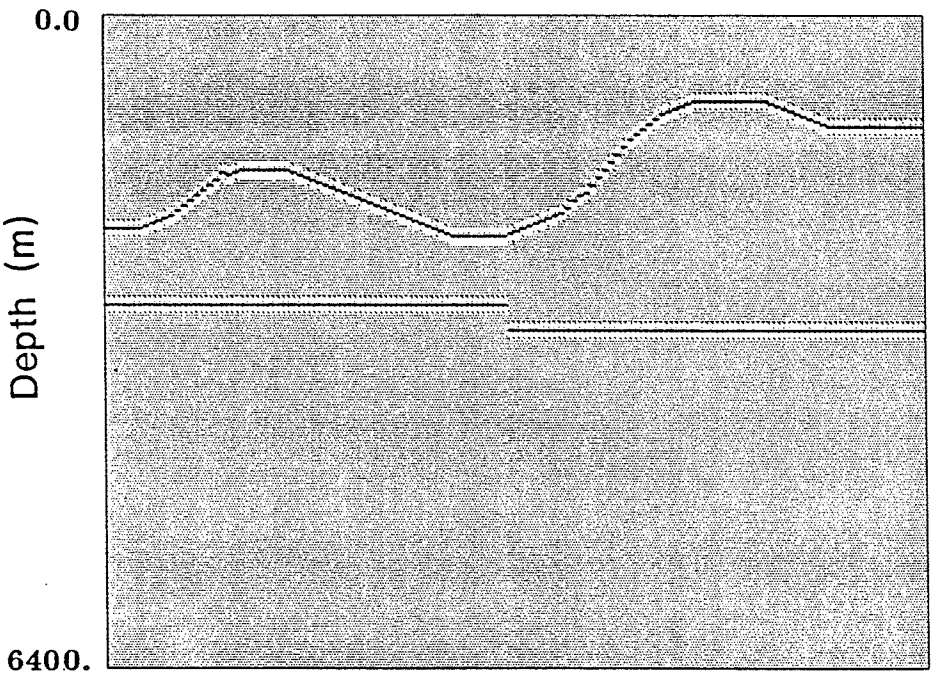

Figure 5.16: A two layer case geologic model the top layer is very irregular. Velocity varries vertically with depth.

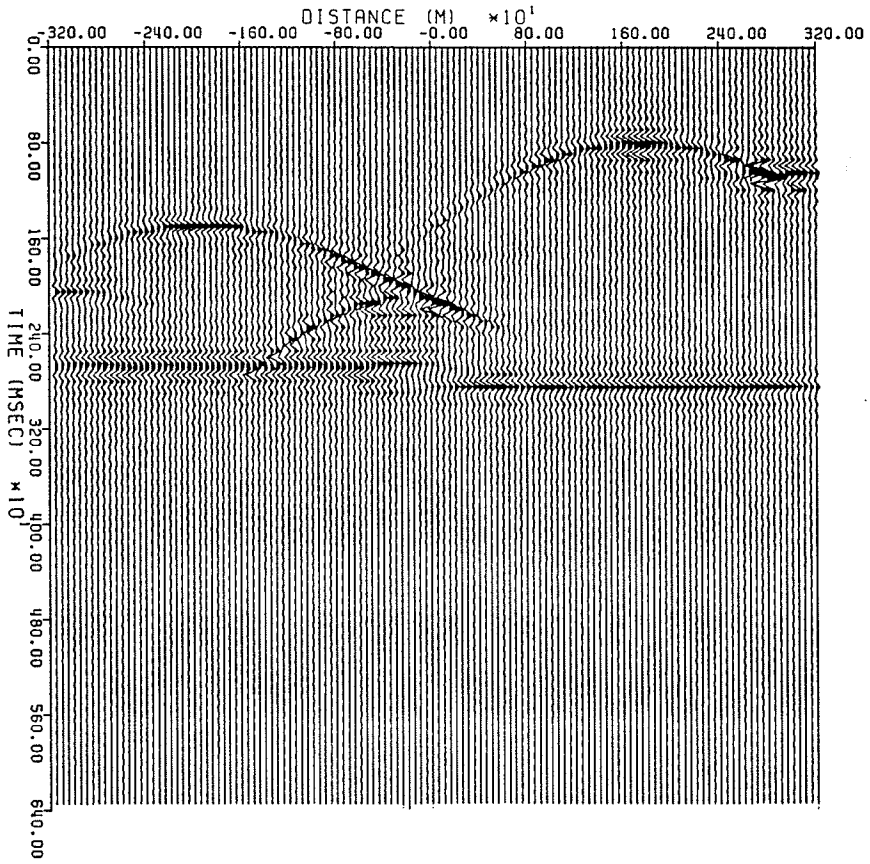

Figure 5.17: The seismic response of the model given in figure 5.16 shows a complex zero-offset section.

Migrated Synthetic Seismic Section

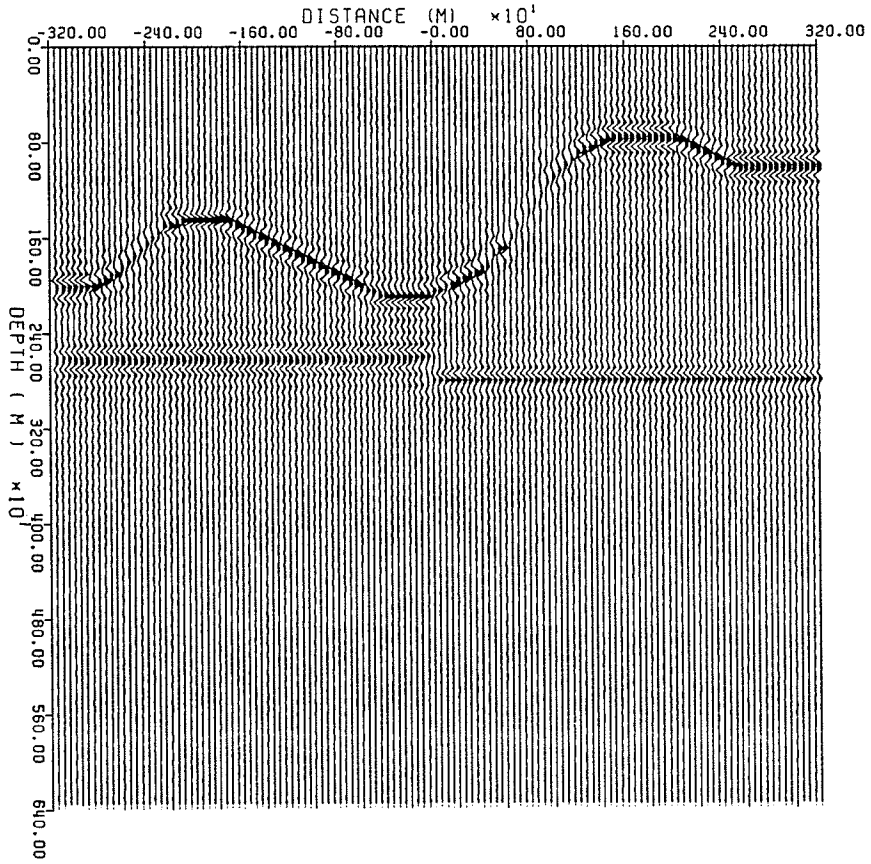

Figure 5.18: Migration of the zero-offset section shown in figure 5.18. Events has been moved to their proper spatial position.

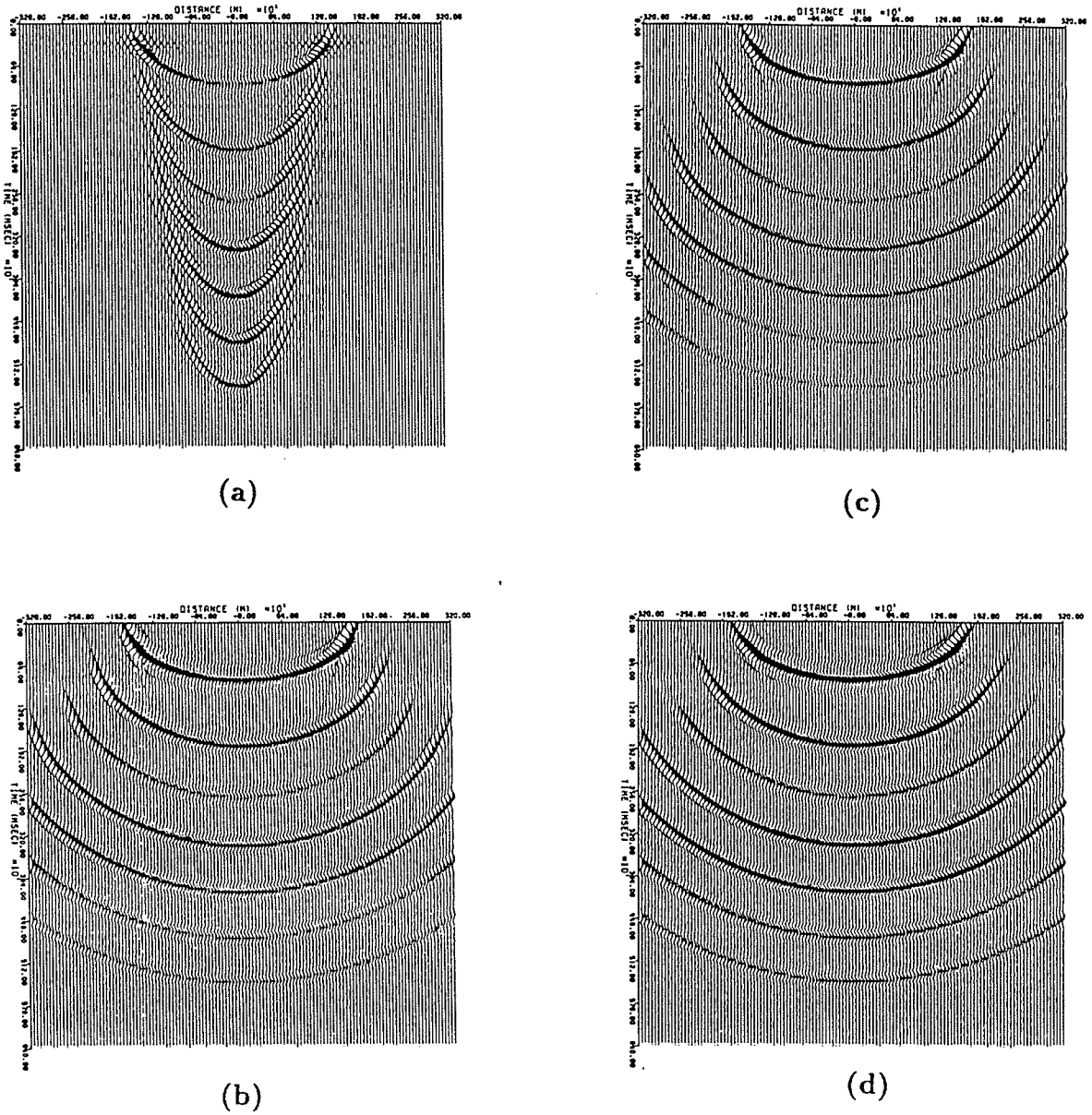

Figure 5.19: (a) NMO and DMO corrected zero-offset section from chapter 4 shows the DMO ellipses. Migration of the zero-offset section shown (a), (b) using the 2^{nd} order approximation to the vertical wavenumber k_z, (c) using the 4^{th} order approximation, (d) using the high order asymptotic approximation. The 4^{th} order approximation shows improvement compared to 2^{nd} order with regard to steep dips. The asymptotic approximation handles steeply dipping events correctly.

Chapter 6

Processing of the Sudbury High Resolution Seismic Reflection Data

In addition to the conventional seismic data processing routinely used by the petroleum industry, a number of special purpose programs suitable for processing the Sudbury data, collected over a crystalline environment, were developed. Processing of the field records was done in three steps. During *preprocessing* stage, necessary preparations were made with regard to the field data and parameters were set for the actual processing to start. The second stage of *Preliminary processing* included tests and trial processing, to obtain the optimum processing parameters. During the *final processing*, the seismic records were subjected to a series of processing steps, in which the final output was carried through. For the most part, the processing sequence applied to the data was typical, except the near surface velocity dependent static correction and the partial prestack migration (DMO) processing steps. These latter steps were applied to the data to increase the S/N ratio and improve the quality of the final stack. Figure 6.1 illustrates the flow chart adopted in processing of the Sudbury high resolution seismic reflection data.

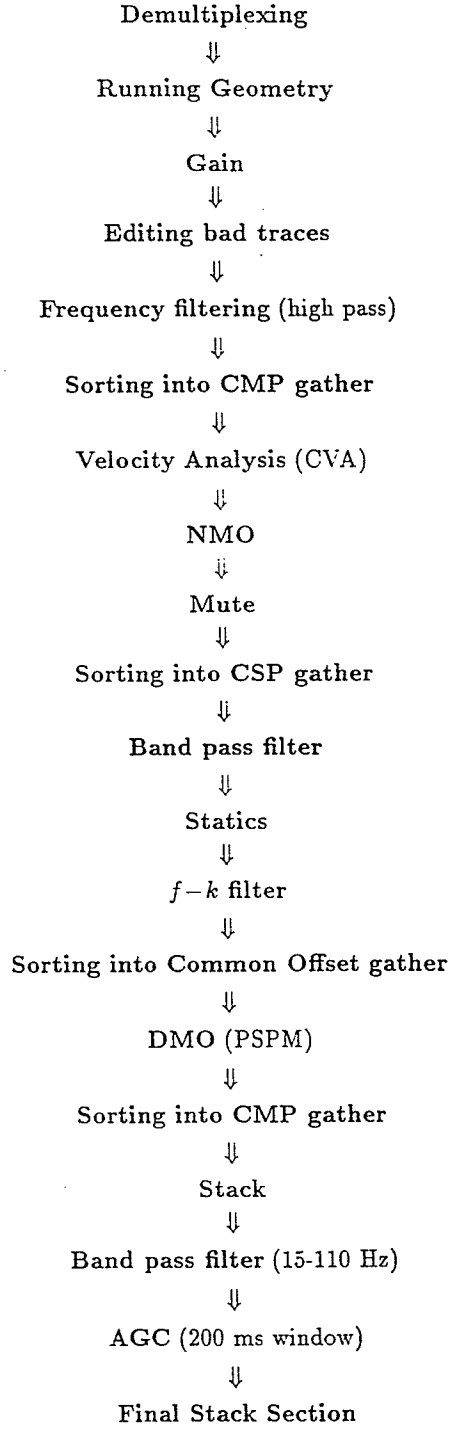

Figure 6.1: Flow chart outlining the processing of the Sudbury high resolution seismic reflection data.

6.1 Preprocessing

The original field data were recorded in the multiplexed (time sequential) SEG-B format. However, conventional CMP processing requires trace sequential data as input. Therefore, the field records were demultiplexed into trace sequential SEG-Y format. Mathematically, this procedure is equivalent to matrix transposition in which the columns of the transposed matrix are the seismic traces.

Gain recovery is a step which is normally done during preprocessing. With this particular dataset, a time variant exponential scaling operator was designed to recover amplitude losses due to spherical divergence and attenuation.

Two other steps which were performed during the initial stage were data editing and generation of the seismic data base of the field geometry. During the editing phase, CSP gathers were displayed and reviewed. Noisy traces were edited or muted. To process the seismic data recorded in the source-receiver coordinate, requires transformation into the midpoint-offset coordinate. The required coordinate transformation is accomplished by sorting the CSP gathers into CMP gathers or into common offset sections. For this task the coordinates of each shot and receiver are computed and stored in the seismic data base and in the header of each trace. This last step is sometimes referred to "running the geometry". The geometry of line L85S1 is given in figure 6.2. The southern half of the line is very irregular. The line shown in figure 6.2 with its corresponding elevation and CDP scatter plot is shown in figure 6.3. Note the violation of the CMP assumption which states that the reflection points lie half way between shot-receiver location. The CDP locations as shown in figure 6.3 are badly scattered in the southern half of the line and computation of CDP gathers for an equivalent straight line involves binning of the scattered CDPs by extending the

definition of common mid-point to cover a small area.

6.2 Preliminary processing

The preliminary processing of the Sudbury high resolution seismic reflection data was focused on spectra analysis and determination of optimum processing parameters. For this purpose, bandpass filtering, AGC (automatic gain control), and velocity filter tests were carried out and the most effective parameters were chosen.

6.2.1 Data presentation and spectra analysis

Figure 6.4 shows typical field records prior to processing. The data has a very low S/N ratio, and it is completely dominated by low frequency coherent noise such as ground rolls and air waves, and some high frequency noise. Amplitude, power and phase spectra of selected traces are shown on the next few figures. Traces recorded using spiked geophones as compared to traces which employed flat base cemented geophones differ in strength and in the frequency bandwidth. Figure 6.5 (a) is a seismic trace which represents data recorded with spiked geophones. The amplitude spectrum is given in (b) and the corresponding power and phase spectra are given in (c) and (d) respectively. The amplitude spectrum shows recorded signal in the frequency range of 20 - 120 Hz in which the dominant frequency is about 65 Hz. This is slightly lower than the anticipated frequency. The lower than expected frequency content of the recorded signal could be explained by bad shot and/or receiver ground coupling. Previous studies (Ziolkowski and Lerwill, 1979; Palmer, 1987) concluded that the lower natural frequency of the geophones employed in the field would limit the higher frequency end of the spectrum and suggested geophones with natural frequency of

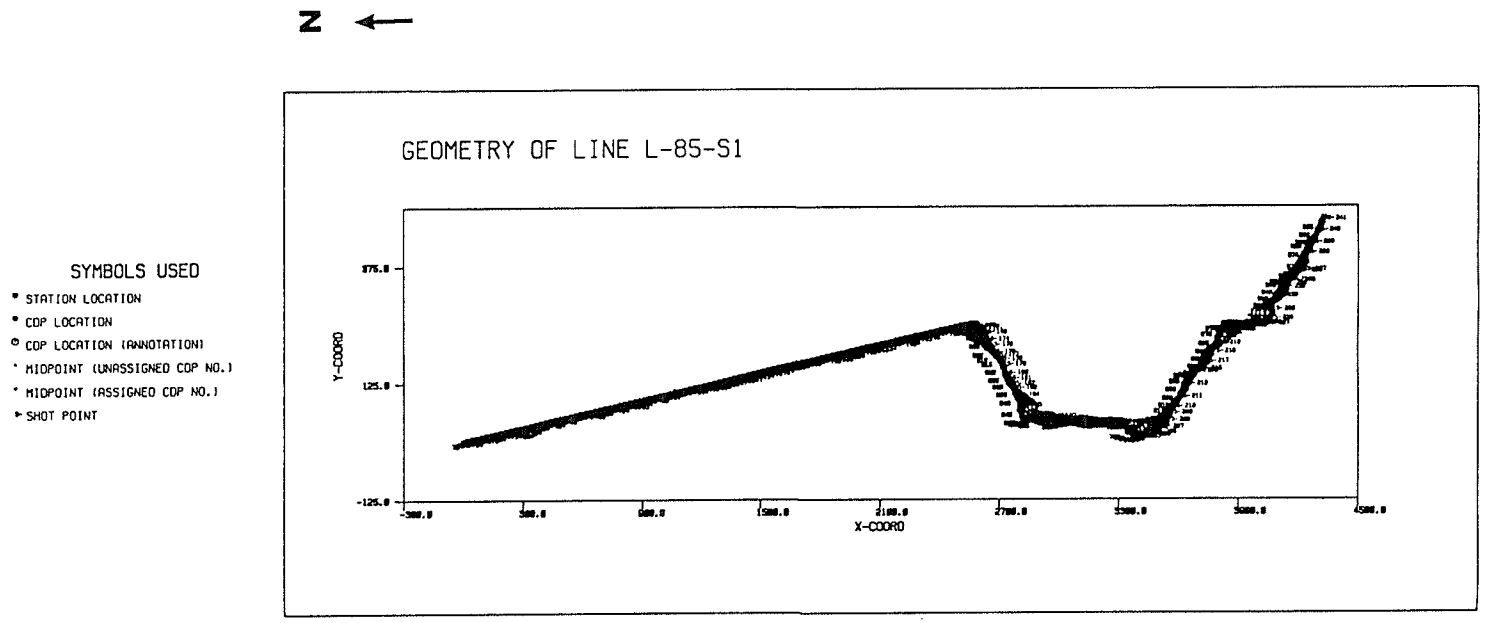

Figure 6.2: The geometry of the Sudbury seismic line L85S1.

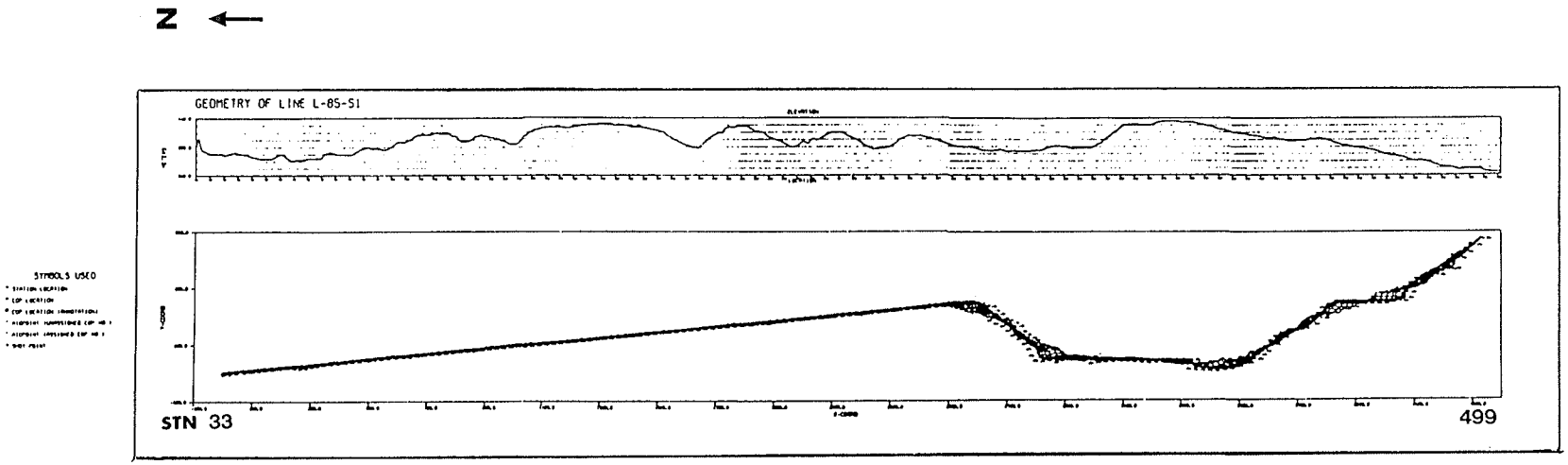

Figure 6.3: Elevation of the crooked line shown in figure 6.2 with its associated CDP scatter plot.

100 - 110 Hz for a high resolution seismic survey. The straightened phase spectrum shows a linear phase. Figure 6.6 illustrates a trace collected with a flat base cemented geophone and its corresponding spectra. Comparing the amplitude spectrum for the spiked and cemented flat base geophones, one can see that the flat base cemented geophone has recorded higher frequency (20-220 Hz) signal. Multiple peaks in the spectrum might indicate better geophone-ground coupling at these frequencies. The effect of the 60 Hz notch filter is shown as a low in the amplitude spectrum. The phase spectrum for cemented geophone also shows linearity similar to the spiked geophone.

6.2.2 Determination of optimum processing parameters

Generally the data exhibited low S/N ratio, and the first processing strategy was, to improve the S/N ratio as much as possible while retaining the useful bandwidth of the recorded signal. During preliminary processing, a number of frequency filter tests were performed on selected common shot gathers. Figures 6.7-6.9 are the filter test panels. The low and high frequency cut-offs (in Hz) are annotated in top of the panels. The panel displaying the result of $20-80$ Hz bandpass filter shows that the attenutation of the high frequency part of the data. Figure 6.9 is a panel for $40-120$ Hz bandpass filter test, from which one can notice that, this filter with the higher low cut frequency than the previous panels, does not eliminate the low frequency surface waves completely. This was expected since both signal and noise overlap over wide range of frequency and wavenumbers. Normally, combination of frequency and $f-k$ filters would be effective in removing surface waves. Figure 6.8 is a bandpass filter test with a pass band in the range of $15-110$ Hz. This filter was found to be

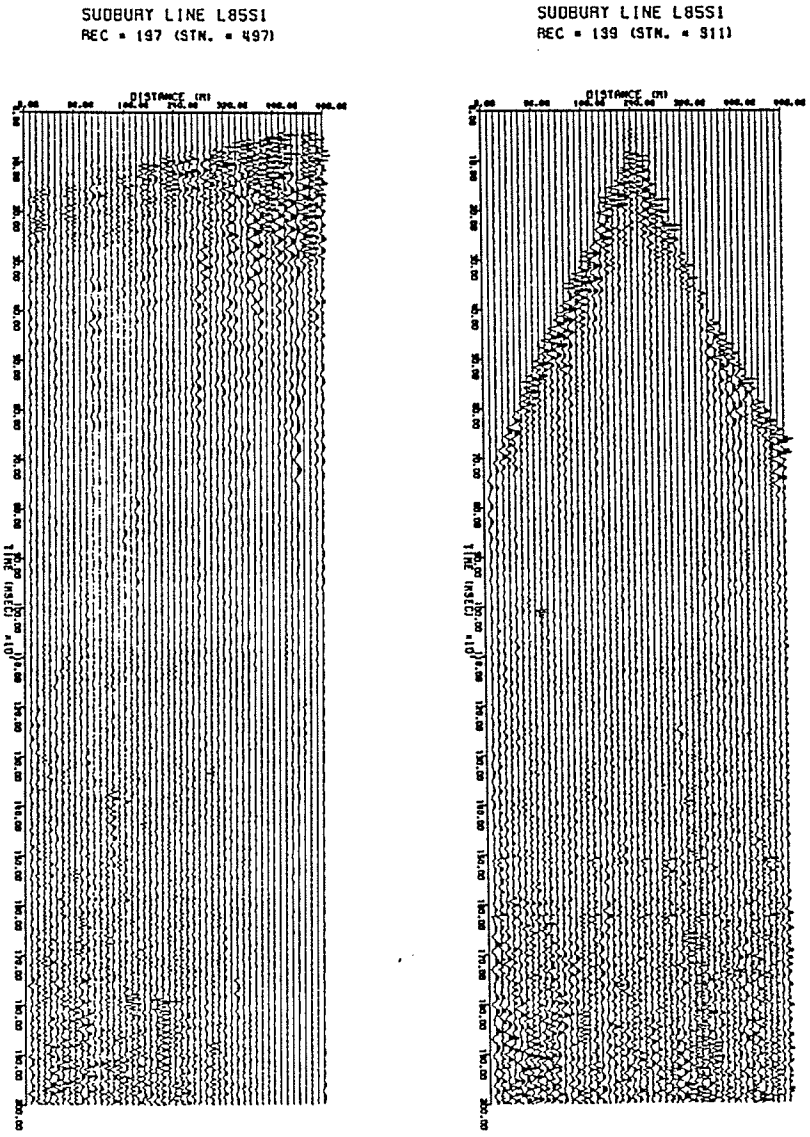

Figure 6.4: Typical shot records dominated by low frequency surface waves and high frequency noise.

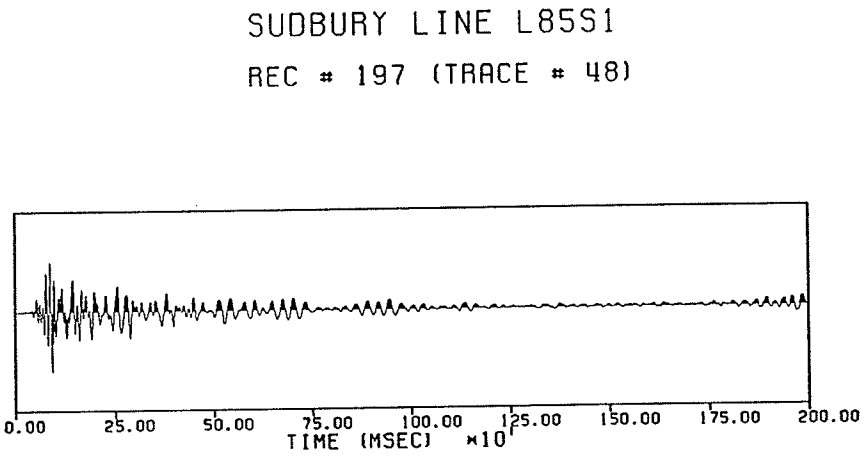
SUDBURY LINE L85S1
REC # 197 (TRACE # 48)
0.00
25.00
50.00
75.00
100.00
125.00
150.00
175.00
200.00
TIME (MSEC) ×10

(a)

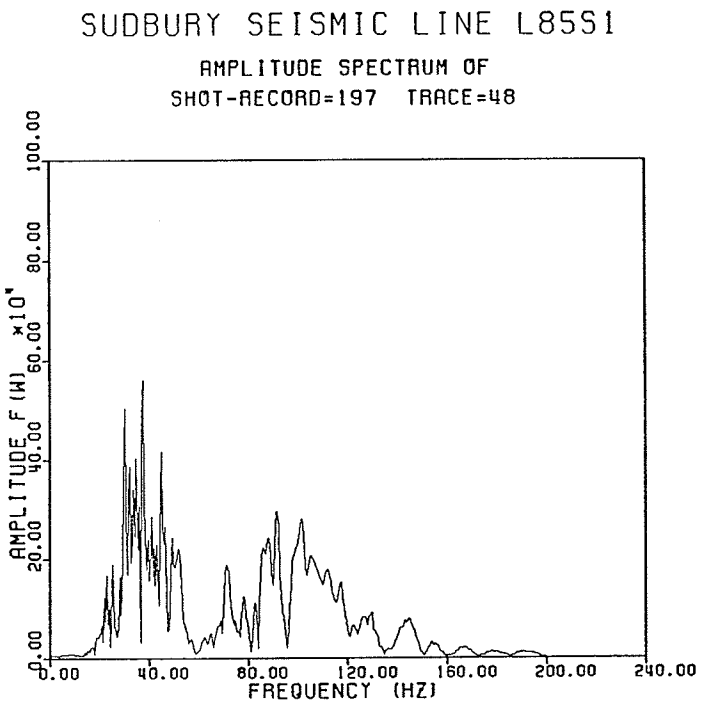
SUDBURY SEISMIC LINE L85S1
AMPLITUDE SPECTRUM OF
SHOT-RECORD=197 TRACE=48
AMPLITUDE F(W) ×10
0.00
20.00
40.00
60.00
80.00
100.00
0.00
40.00
80.00
120.00
160.00
200.00
240.00
FREQUENCY (HZ)

(b)

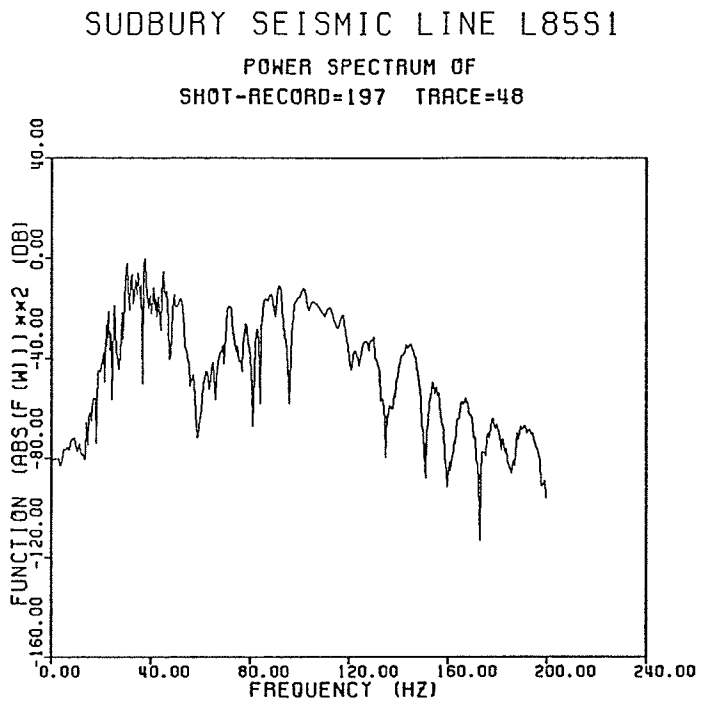

(c)

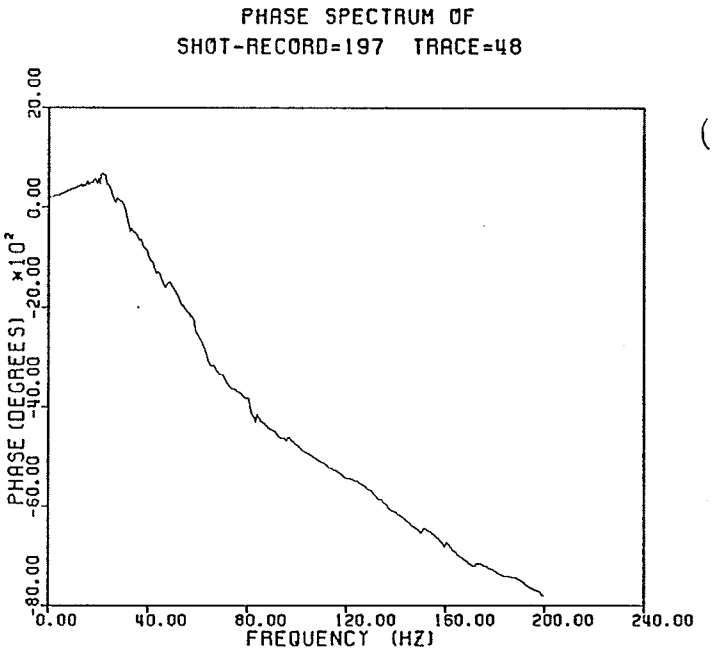

(d)

Figure 6.5: (a) Trace collected with a spiked geophone, (b) the amplitude spectrum, (c) the corresponding power spectrum in decibel, and (d) the unwrapped phase spectrum. The amplitude spectrum shows the recorded data to be band limited in the frequency range of 15-120 Hz. The power spectrum indicates attenuation about 20.0 dB per one octave frequency. The phase spectrum illustrates the linear phase change.

SUDBURY LINE L85S1

REC # 197 (TRACE # 36)

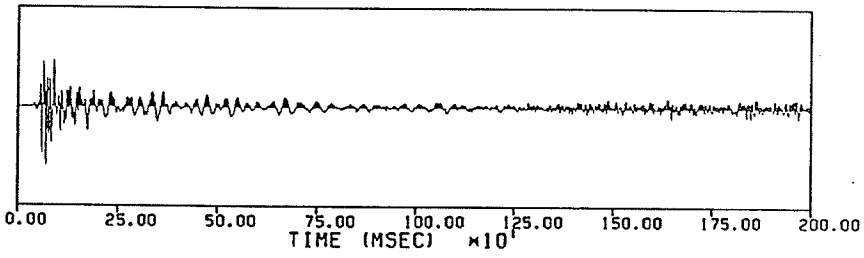

(a)

SUDBURY SEISMIC LINE L85S1

AMPLITUDE SPECTRUM OF

SHOT-RECORD=197 TRACE=36

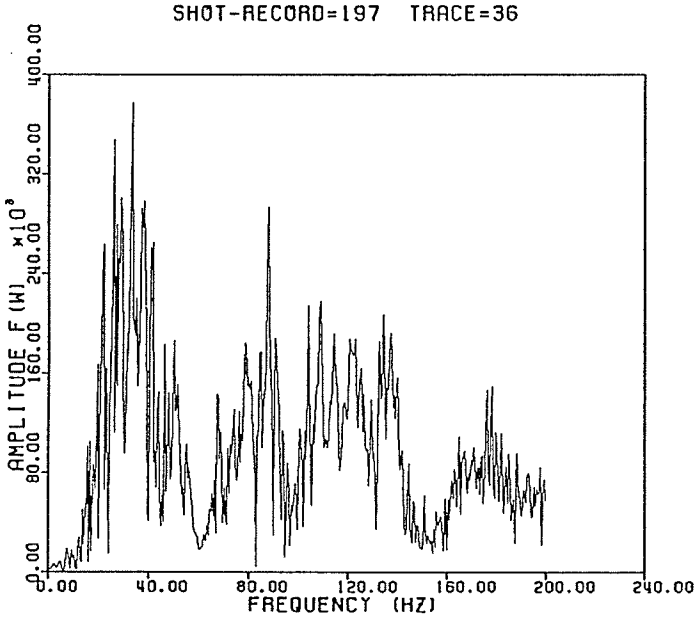

(b)

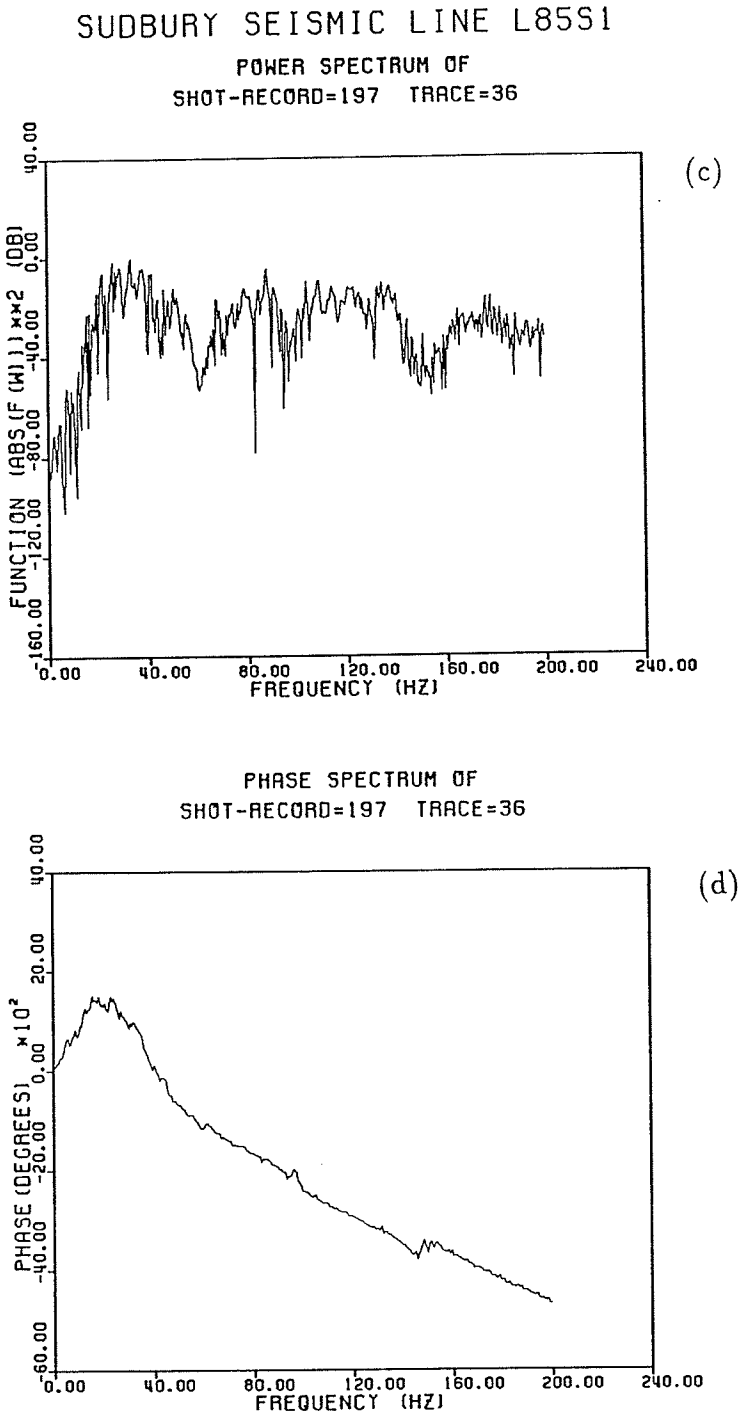

Figure 6.6: (a) and (b) Trace and its amplitude spectrum for cemented circular group of geophone. The corresponding power spectrum (in dB.), and the unwrapped phase spectrum are given in (c) and (d) respectively. The amplitude spectrum shows the recorded signal to be in the frequency range of 20-220 Hz. The phase spectrum illustrates the linear phase change similar to the one for spiked geophones.

most adequate since it retains the high frequency signal while attenuating the low frequency coherent noise.

Velocity (or $f-k$) filter tests were also conducted on the CSP gather shown in figure 6.10 (a). Velocity or dip filters are known to perform very poorly if the data contains low S/N ratio (Claerbout, 1985). This is exemplified by the panel in figure 6.10 (b). The $f-k$ filter attenuated the undesirable coherent noise however the noise at large travel times have been organized and spilled over large number of traces. The organized noise sometimes depicts false reflection arrivals.

To bring the data within a displayable dynamic range, automatic gain control (AGC) scaling and signed cube and square root tests were conducted on selected CSP gathers. Figure 6.11 shows AGC test panels. The panel in (a) is an AGC test for a 42 ms window. As this panel illustrates, short sliding windows introduce extreme equalization of the samples of the given traces and consequently destroyed the original character of the original traces. The 150 ms window shows significant improvement over the 42 ms window. The 200 ms window brings the data within the preferred dynamic range without sacrificing the original character of the data. Increasing the AGC window over 200 ms does not show significant improvement besides increasing the computational cost.

Figure 6.12 is a signed n^{th} root display of the shot gather shown in figure 6.11. The signed cube root panel boosted the low amplitude signal, however, compared to the 200 ms AGC window display given in figure 6.11 the n^{th} root display is less effective.

Velocity analysis was performed at selected common depth points along the line of profile. Velocity spectrum (sembleance analysis) was known to perform very poorly

under low S/N ratio, hence, constant velocity analysis was carried out instead. The selected CMP gathers were repeatdly NMO corrected and stacked using constant velocities in the range of 2000 - 6800 m/s with velocity increment of 100 m/s. Figure 6.13 shows two velocity profiles obtained from the constant velocity stacks. The velocity profiles dispaly a vertically increasing stacking velocity from 4500 m/s at the early traveltimes to about 6400 m/s at two way traveltime of 2 s.

The effective processing parameters (frequency filter, gain and f–k filter) obtained during the preliminary processsing were used during the main processing pass. In order to perform NMO correction, velocity analysis and CMP stacking, the data initially stored as common shot records have to be sorted into CMP gathers. Figure 6.14 illustrates three such gathers prior to NMO correction. Note the lack of any reflection hyperbolas which are normally observed on CMP gathers.

Because of the sheer size of the seismic dataset, it was very crucial to conduct the preliminary processing on selected part of the line, to reduce the waiting time, and to minimize the CPU time and other computer resources associated with processing a large dataset. For this reason, the northern half of the line (SP. 33 to SP. 192) was chosen for detail analysis before the final production run. Two sets of brute stack sections were produced when performing stack tests. The results of stack tests were different from each other as a result of interchanging steps on the processing sequence or due to an omitted processing step altogether. For all the preliminary stacks, datum elevation was chosen at 450 m above sea level and replacement velocity of 5000 m/s was used for static corrections. To obtain the first brute stack section a wide band pass filter, a time gain, datum and NMO correction were applied before stacking. The undesirable noise such as ground roll and air waves dominate this brute

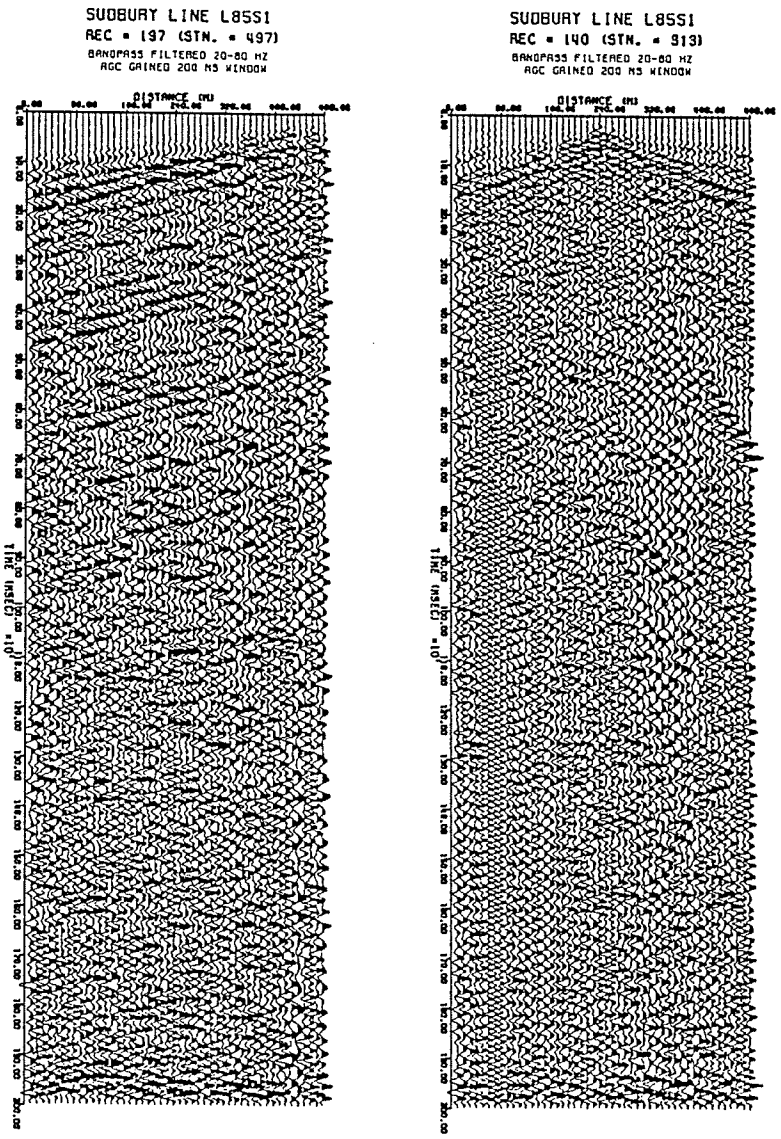

Figure 6.7: A bandpass filter ($20-80$ Hz) test of selected CSP gathers. The high frequency part of signal have beeen attenuated.

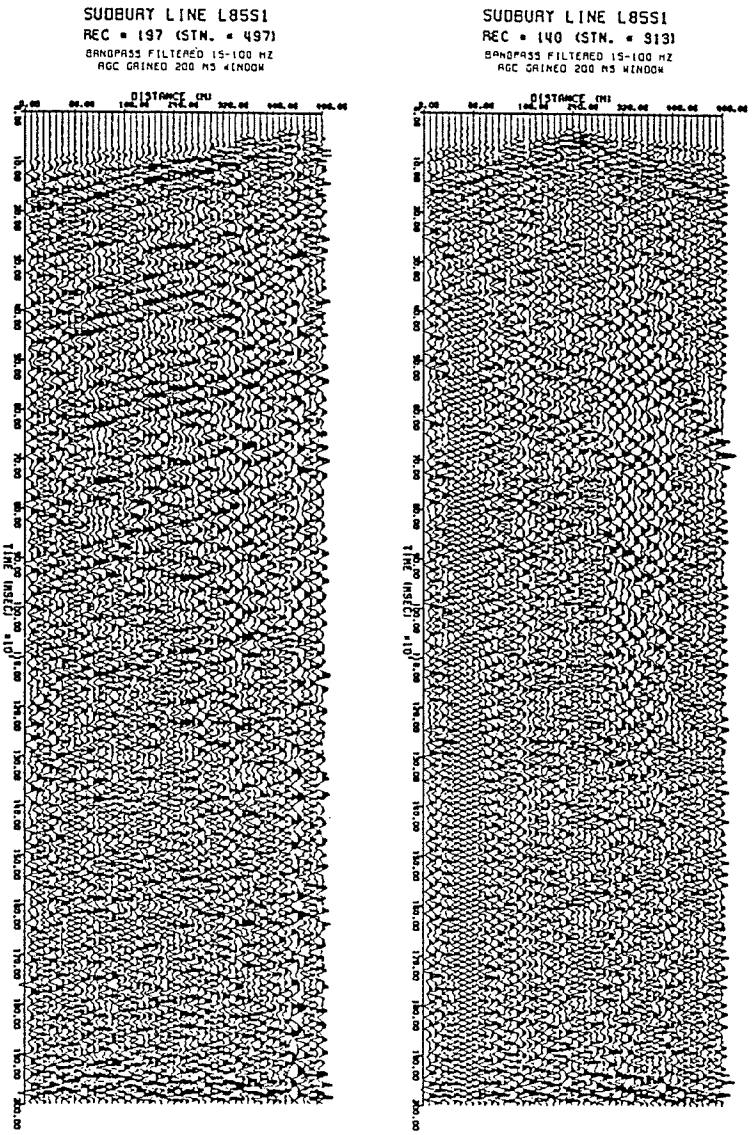

Figure 6.8: A bandpass filter (15 – 100 Hz) test of selected CSP gathers. This filter attenuates the low frequency noise while retaining the high frequency part of the data.

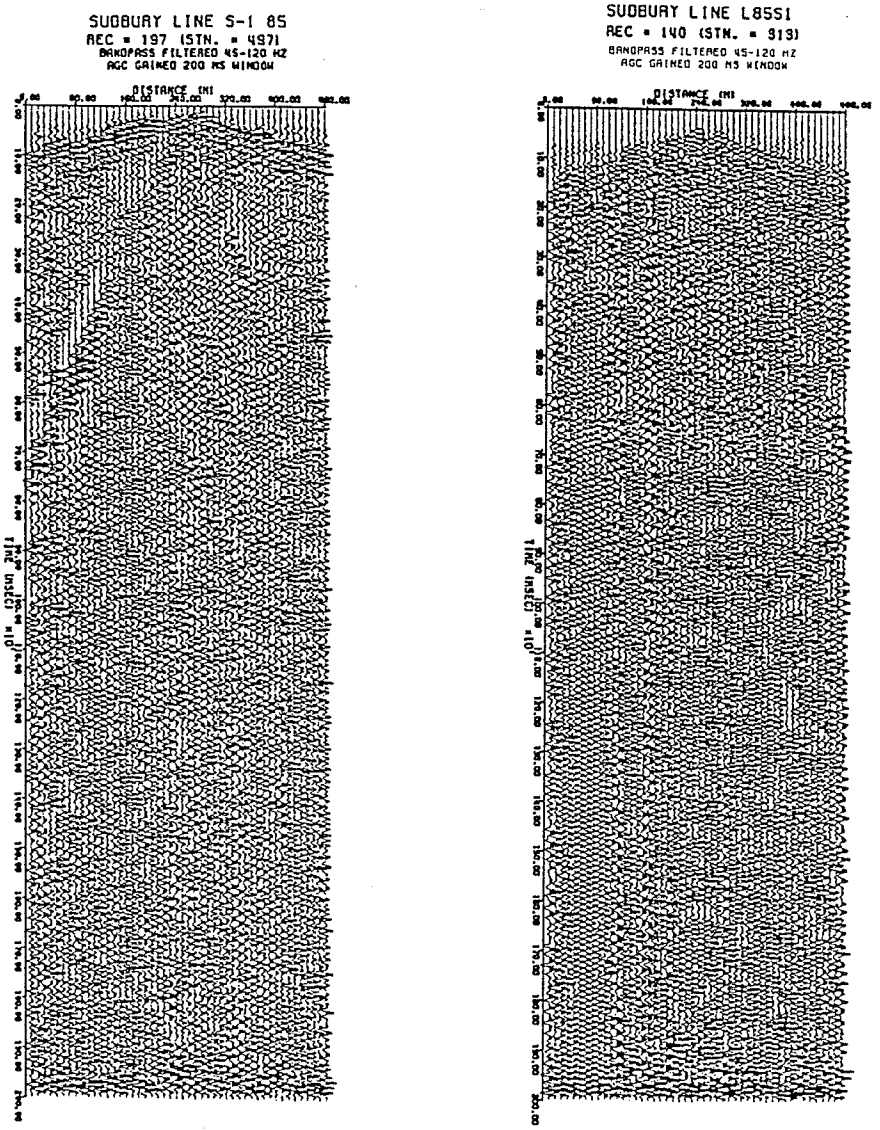

Figure 6.9: A bandpass filter ($45-120$ Hz) test of selected CSP gathers. Note, increasing the low cut frequency does not appear to eliminate the surface waves significantly.

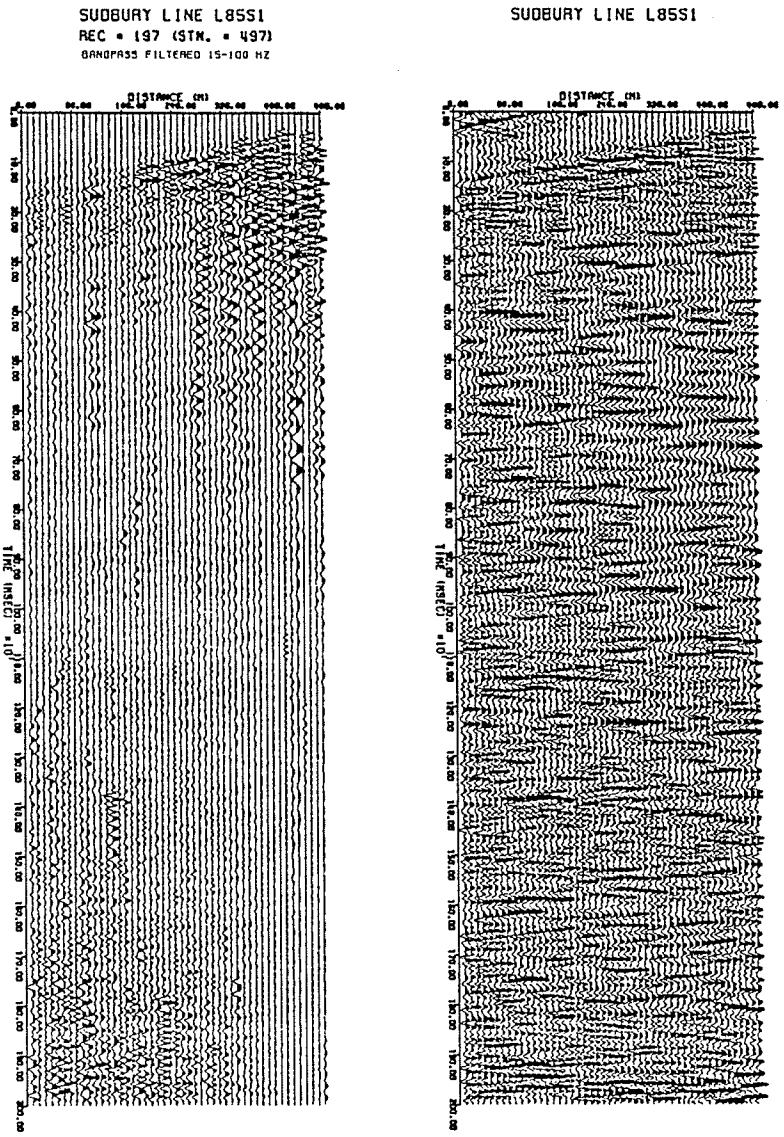

Figure 6.10: The panel in (b) is a velocity filter test of the CSP gather shown in (a). The filter attenuated the surface waves significantly, however, it also introduced ringing and false events to the data. Velocity filtering is not effective if the data contains poor S/N.

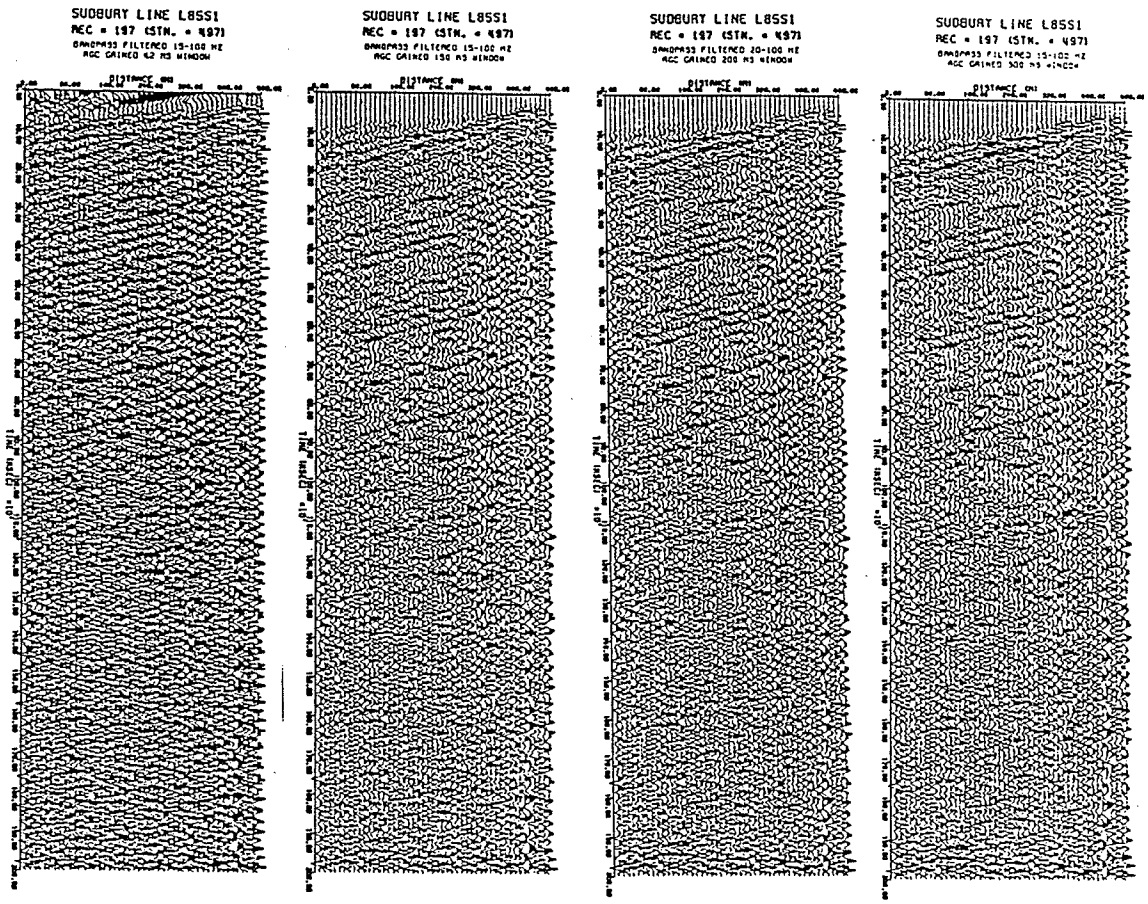

(a) (b) (c) (d)

Figure 6.11: AGC tests for selected shot gathers. Note, the noisy appearance resulting from poor choice of AGC window in (a). The 200 ms AGC window shown in (c) brings the data within the displayable dynamic range.

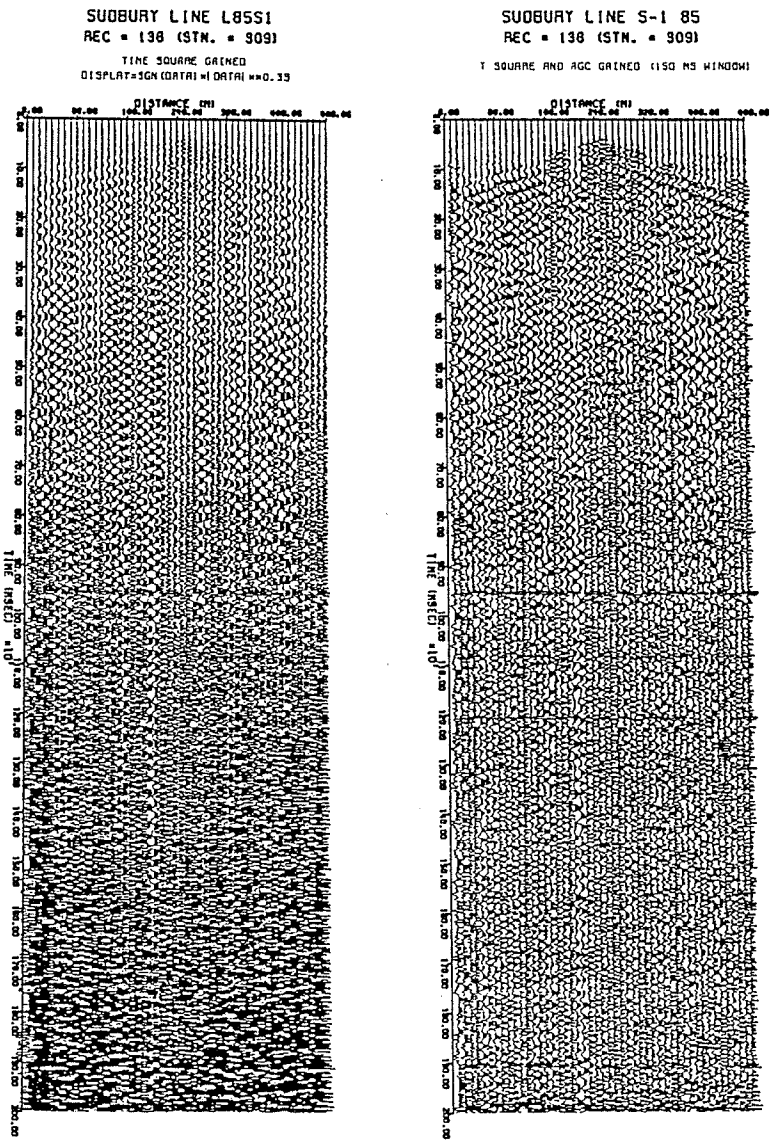

Figure 6.12: Gain test of a CSP gather using the signed cube root is shown in (a). The panel in (b) is a combination of time squared AGC. These gain tests appear to be less effective compared the pure AGC display in figure 6.10 (c)

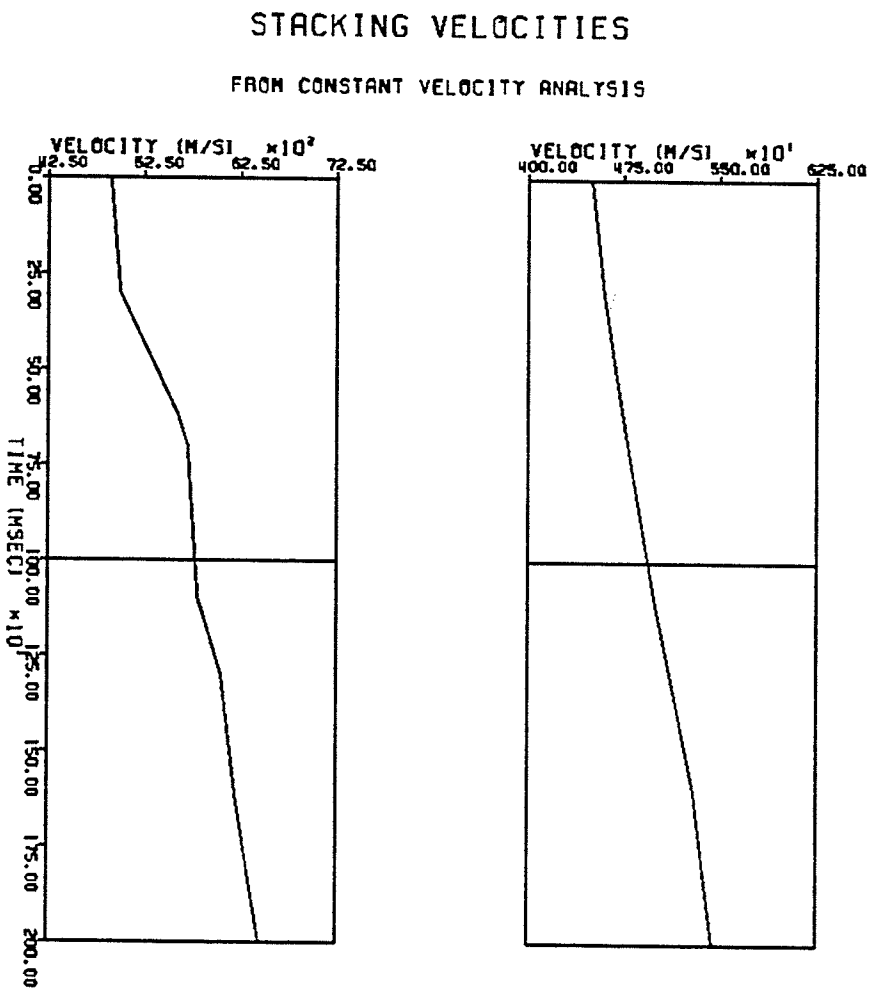

Figure 6.13: Stacking velocity profiles obtained from constant velocity analysis of selected CMP gathers along the sesmic line L85S1.

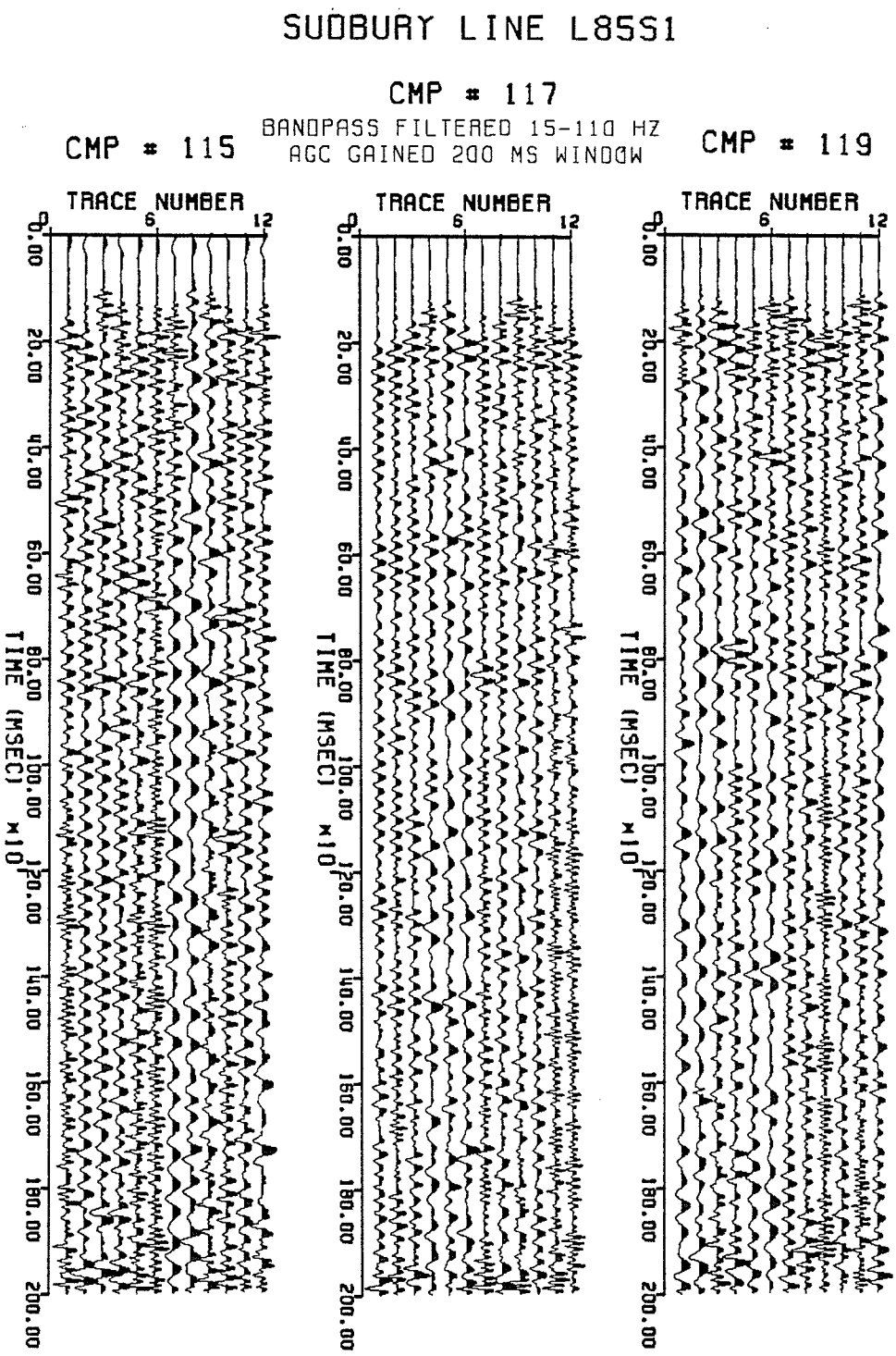

Figure 6.14: Three CMP gather before NMO correction. These gathers show lack of any observable reflections.

stack section. To obtain the second set of the brute stack section given in figure 6.15, frequency filter, and AGC gain was applied to the data before stacking in addition to the steps applied to the first brute stack. Low frequency noise such as ground roll and air wave has been attenuated to some degree, however, the high frequency noise still dominated the section. Besides few short segments, this brute stack section does not reveal any significant reflections.

6.3 Main processing pass

Preliminary processing of the Sudbury high resolution reflection seismic data showed no identifiable continuous reflections on the Brute Stack section. The final stack sections without DMO went through rigorous processing including datum and NMO corrections, bandpass filtering ($20-110$ Hz), *f-k* filtering, and statics. AGC scaling was also applied after stacking. The processed section without DMO is displyed in figure 6.16. The linear features noticeable on this section are processing artifacts, mainly caused $f-k$ filtering which perform poorly under low S/N ratio. This section revealed some minor reflection segments dipping southward. Generally however, the final stack section without prestack partial migration showed low S/N ratio.

In a hard rock environment such as the Sudbury structure one is faced with near surface velocity anomalies, low impedance contrast along rock boundaries, in addition to the breakdown of conventional CMP seismic data processing technique due to complex geology of the region. From previous studies (Card and Hutchinson, 1972; Dressler, 1984) it was known that the limbs of the igneous complex in the North Range dip of up to 30°–50° southward. In view of the above mentioned problems, it was concluded that surface velocity dependent static correction, and partial prestack mi-

N ←

Brute Stack

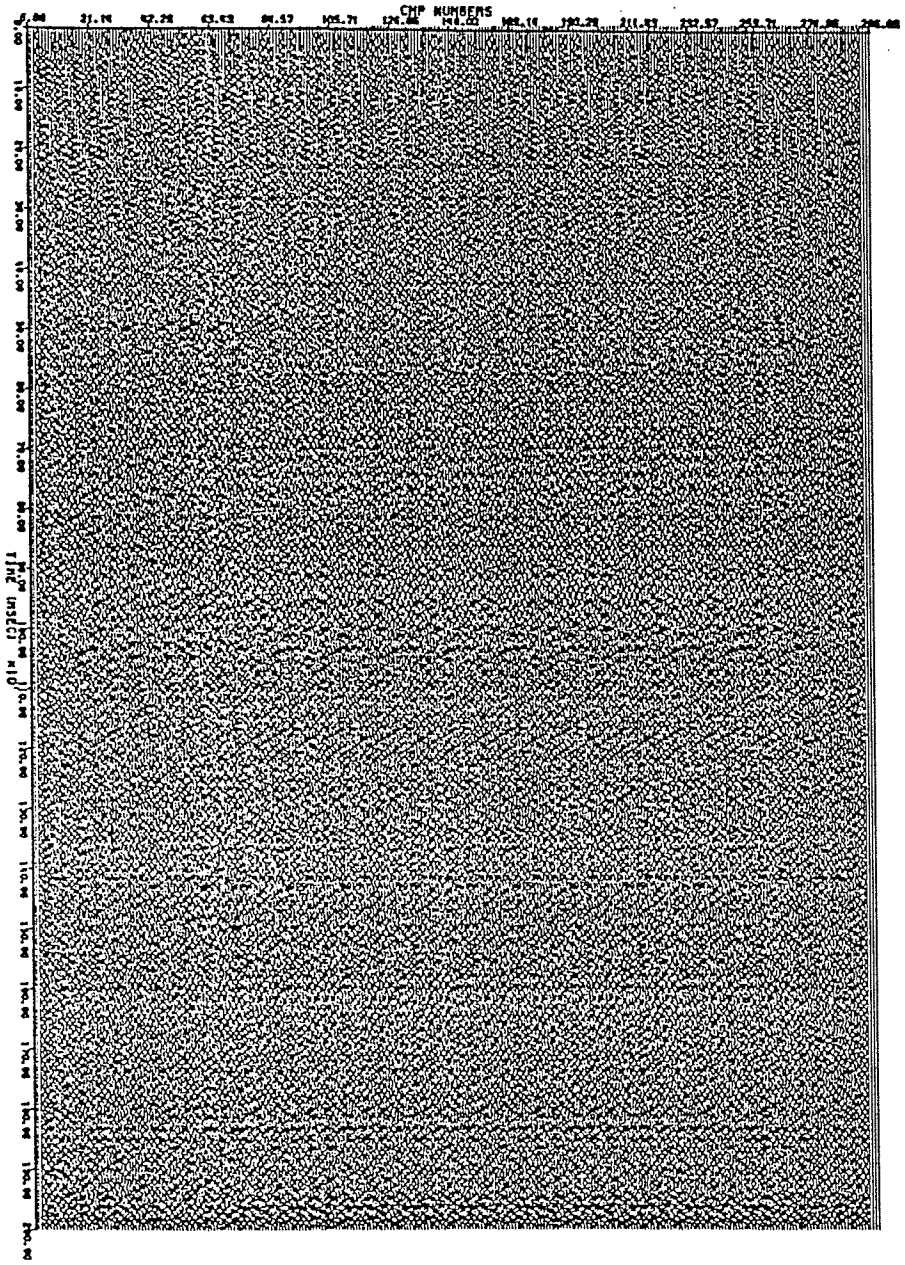

Figure 6.15: Brute stack section of the northern segment (SP. 33-192) of line L85S1. The section was obtained by processing the data using preliminary estimated parameters. As you may have noticed this brute stack section is very noisy and does not reveal any significant reflection arrivals.

CMP

Stack Section

z ←

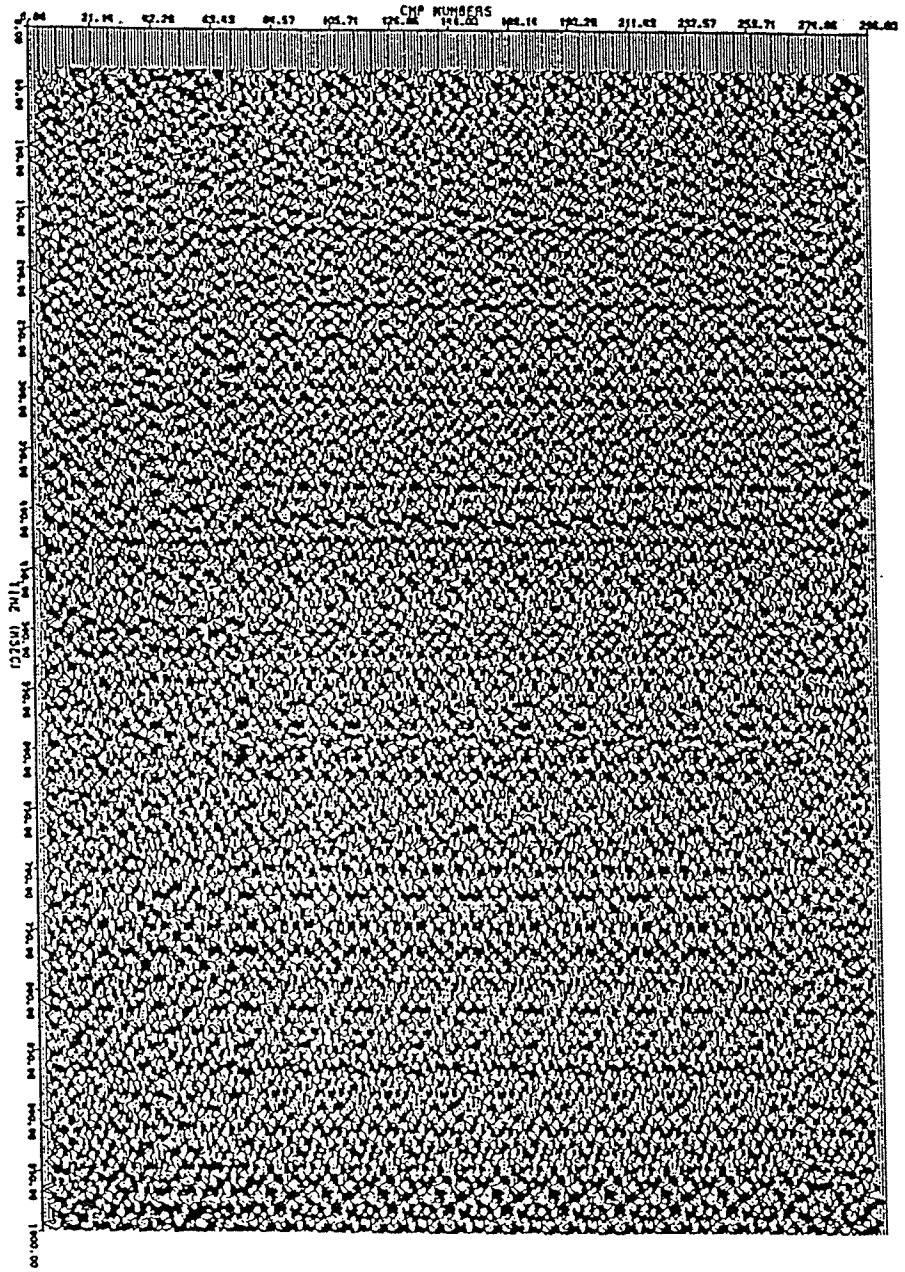

Figure 6.16: Stack section without partial prestack migration shows some reflection segment. This section slightly improved compared to the previous brute stack sections. The horizontal linear features on this section are believed to be processing artifacts.

gration (dip-moveout) be applied to the Sudbury seismic data to improve the quality of final stacked section.

6.3.1 Near surface velocity anomaly and refraction statics

Near surface velocity estimated from the first arrivals showed significant change laterally along the survey line. Near surface velocities obtained from first arrivals are shown in the next few figures. The near surface velocity for the northern part of the line is given in figure 6.17. The average near surface velocity at this location (eg. shot point 63) is about 4955 m/s. Figure 6.18 illustrates the plot of the first arrivals for a shot record obtained from the central portion of the line, and the computed average velocity is (eg. shot point 187) 4660 m/s. The first arrival traveltime curve for the southern portion of the line is displayed in figure 6.19. The average velocity at this particular location is about (eg. shot point 453) 5370 m/s. To obtain the near surface velocity, the first arrivals were hand picked as accurately as possible and the corresponding travel time curve were constructed. From inverse slope of the RMS best fit line, average near surface velocity estimates were obtained. Then, the traces of the given shot record were repeatedly corrected for shot-receiver elevation difference using updated velocity. The process involved few iterations until the best estimates of the near surface velocity were obtained.

Figure 6.20 shows near surface velocities obtained from laboratory and velocities estimated from first arrivals. The dots represent the result of the first arrivals. The solid lines represent laboratory results. Velocities obtained from laboratory tests were generally 20% higher in comparison to the ones obtained from the first arrivals.

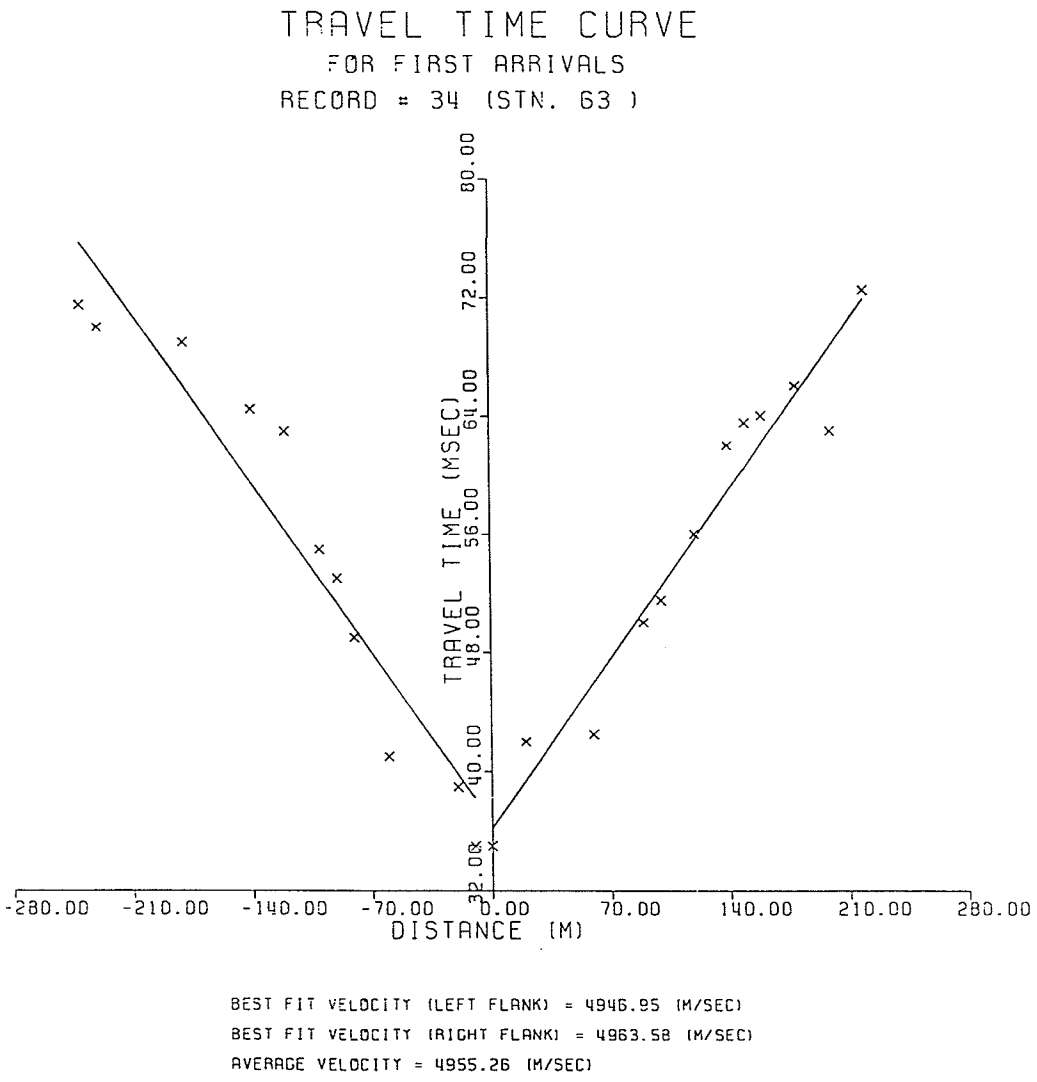

Figure 6.17: Traveltime curve of the first arrivals for the northern portion of the line. The computed average near surface velocity is given at the bottom of the figure.

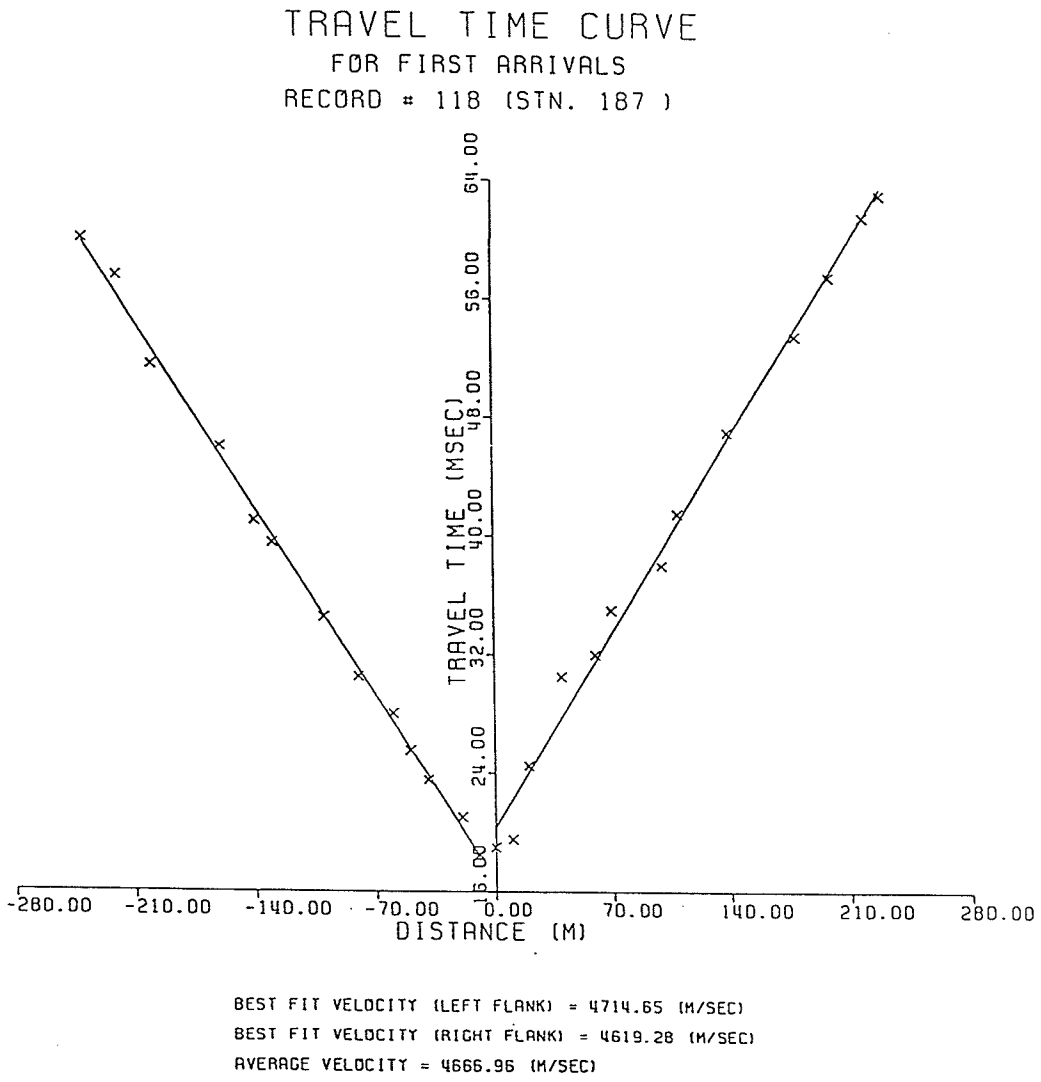

Figure 6.18: Traveltime curve of the first arrivals for the central portion of the line. The near surface velocity is obtained from the inverse slope of the RMS best fit line.

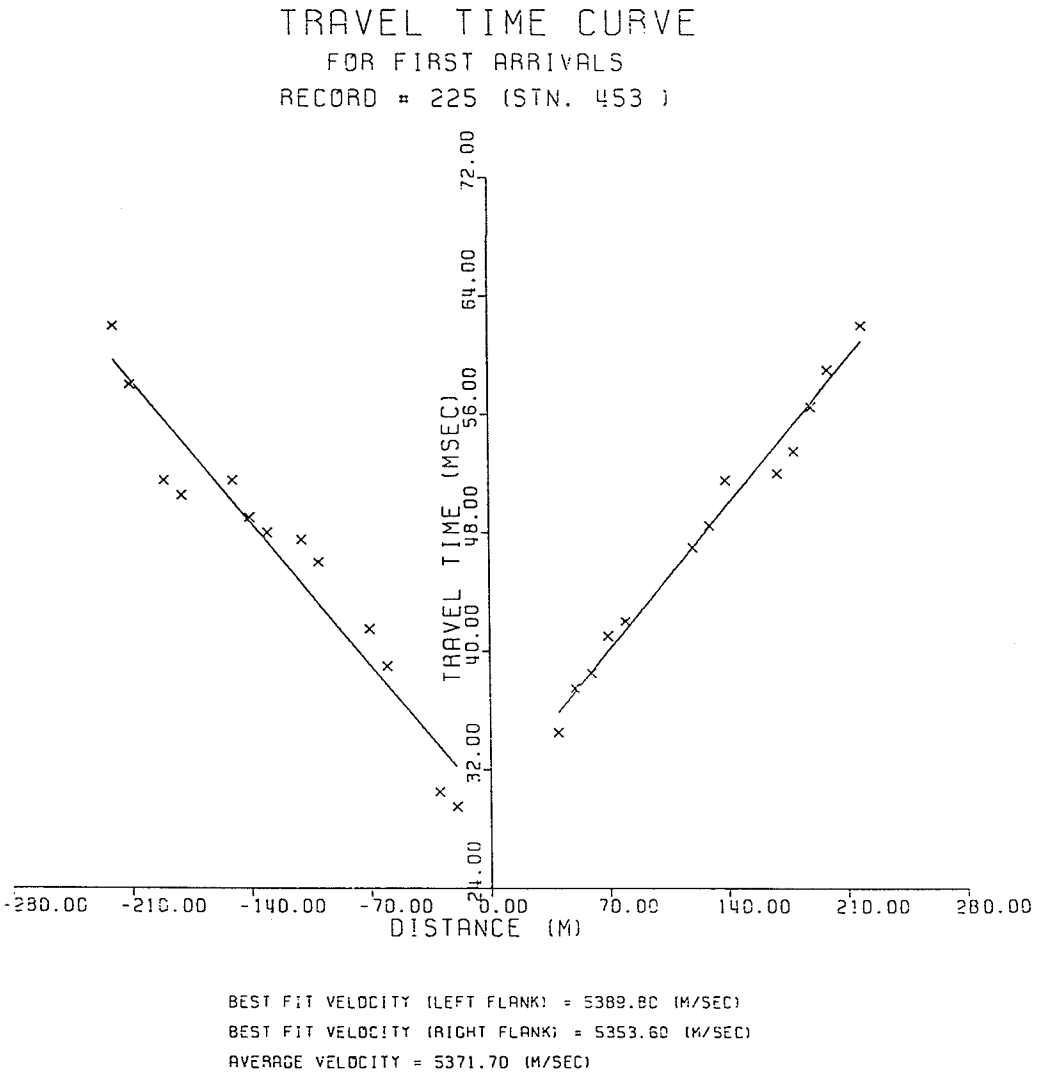

Figure 6.19: Traveltime curve of the first arrivals for the southern portion of the line. The computed average near surface velocity is 5371 m/s.

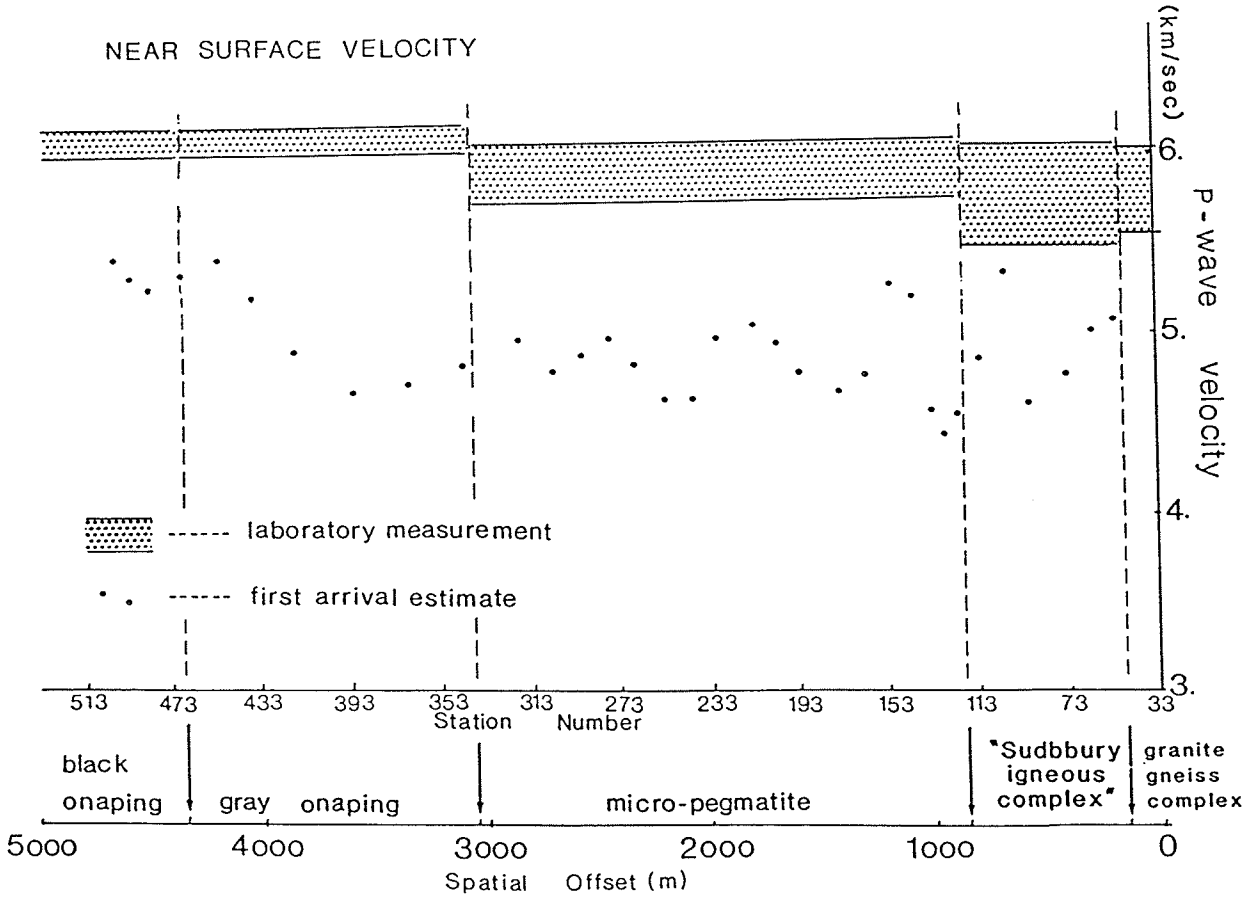

Figure 6.20: Near surface velocity along the line L85S1. The dots represent velocities obtained from first arrivals. The solid lines are the laboratory results (Moon et al., 1990) .

6.3.2 Dip-moveout processing and interpretation

From the fact that the limbs of the igneous complex in the North Range dip up to 30°–50° southward (Card and Hutchinson, 1972; Dressler, 1984), it was concluded that surface velocity dependent static correction, and partial prestack migration (dip-moveout) be applied to the data to improve the quality of final stacked section.

The final processing of the Sudbury reflection data included bandpass and velocity filtering, and surface dependent static correction in addition to previously discussed steps. The final revised velocity used during the main processing pass incorporated the result of the first arrivals.

To improve the quality of the final stack, a partial prestack migration based on Hale's (1984) algorithm was developed and applied on the Sudbury data. Detail description of the mathematical derivation, and discussion on the development of the DMO by Fourier Transform algorithm was given in detail in chapter 4. Results of prestack partial migration on theoretical synthetic data and the potential of this algorithm in improving the quality of the final stack section was also discussed. The following steps were performed to get the final DMO stack section. After the data went through the usual preprocessing steps, surface velocity dependent static correction was applied to the CSP gathers. Bandpass filter with a pass band of 20−110 Hz was also applied to the CSP gathers. Next, the data was sorted into CMP gathers for velocity analysis and NMO correction. After NMO correction and velocity analysis, the CMP gathers were sorted into common offset gathers. Each common offset gather was DMO corrected using an average velocity of 5000 m/s. The DMO corrected data was sorted back into CMP gathers. Subsequently, the gathers were stacked using the revised velocity. Finally, a 200 ms AGC window was applied to the data prior to displaying the section. Figure 6.21 shows a dip-moveout corrected stacked section for

the northern half of line. The final DMO stack section for whole line is given in figure 6.22. Interpretation of the DMO stack is shown as a line drawing in figure 6.23 (Moon et al., 1990). Application of partial prestack migration enhanced the S/N ratio, and reflector continuity also showed marked improvement compared to the stack section without DMO.

Interpretation of the final seismic section is based on known surface geology and a drill hole in the vicinity of the survey line (station 250). Information obtained from the mining area of Sudbury Basin was also incorporated. The final section revealed some discontinuous reflection segments on the northern part of the line dipping southward between the two way time (TWT) of 0.15 - 0.7 seconds. The reflection segments are repetitive in nature, which was also observed on several common shot gathers (Appendix B, record 20, 22). Moon et al. (1990) interpreted the repetitive reflections to be the combined effects of source geometry and local topography. Another possible explanation comes from Green and Mair (1983) who interpreted similar events from seismic surveys at Lac du Bonnet, Manitoba to be PS_nP phase. There are several prominet discontinuities dipping northward. These are interpreted as steeply dipping fault like structures. On the south end of the line southward dipping reflections are observed between TWT 0.2 - 0.7 seconds. In the middle of the line there is a region of very weak to no reflection, based on surface geology this was mapped as micropegmatite.

Although, the high resolution survey mapped several discontinuous reflection segments, geological verification could be confirmed only from one drill hole data. The micropegmatite-quartz gabbro interface did not show strong reflection to be a marker horizon, contrary to the prediction made by the theoretical forward modeling. In other words, the acoustic impedance contrast across the igneous complex contact is

not as significant as previous study suggested or the contact itself is not clear cut as modelled in the theoretical study. Due to the limited geological data available, further detailed geological interpretation will be left to the field and mining geologists working in the study area.

DMO Stack

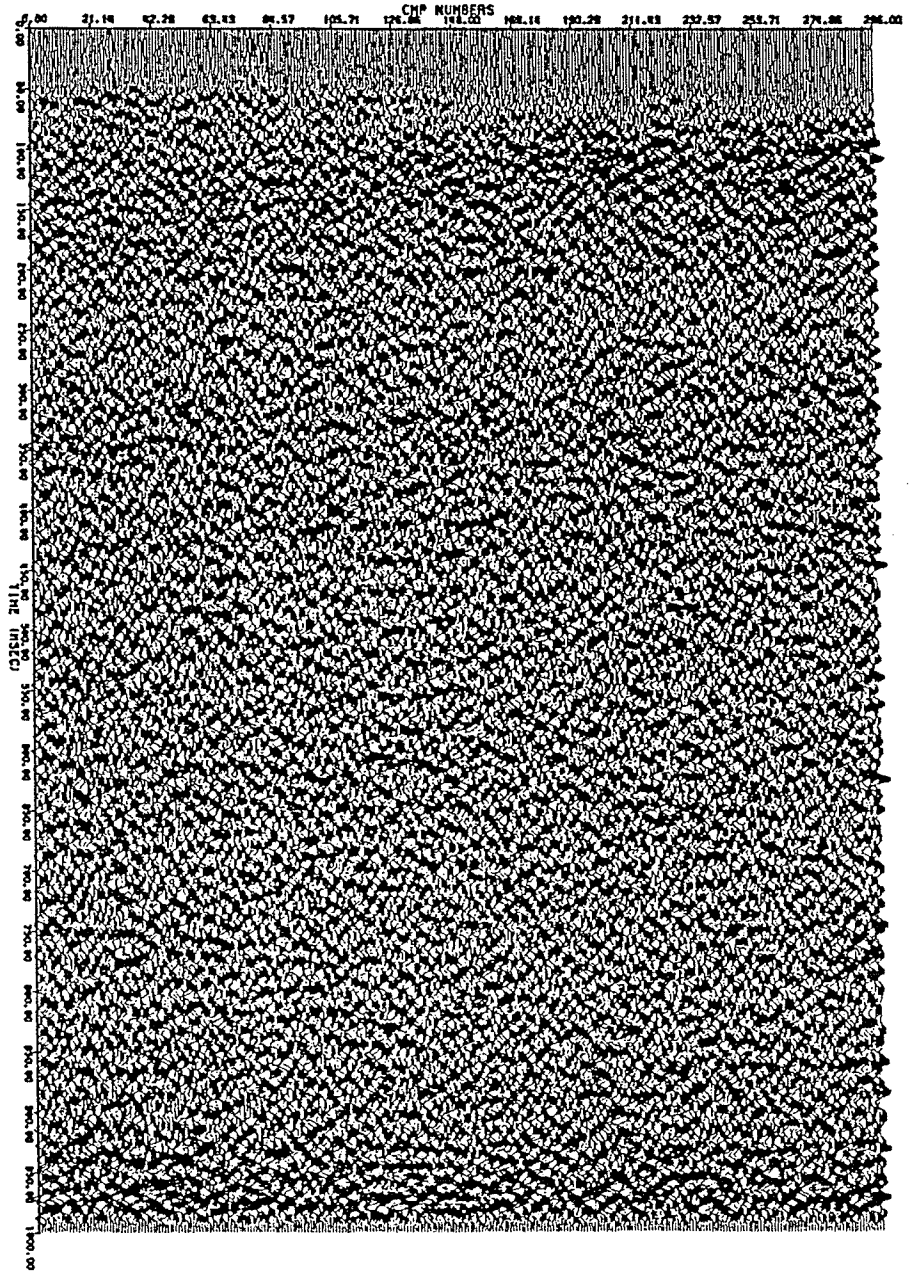

Figure 6.21: DMO stack section for the northern half of line L85S1. Compared to the section in figure 6.16, this section shows marked improvement. The prestack partial migration processed section shows some reflection segments dipping southward.

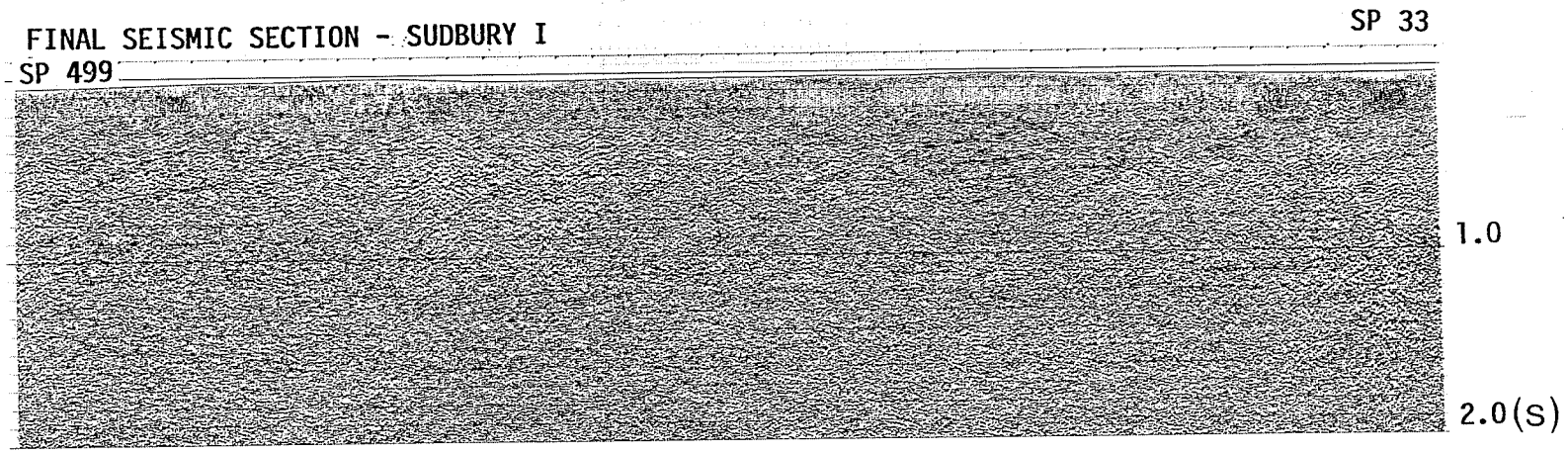

Figure 6.22: Stack section with prestack partial migration. Discontinuous reflections dipping southward are observed on the northern and on the southern part of the line. There is a quiet zone with very little reflections on the middle of the line.

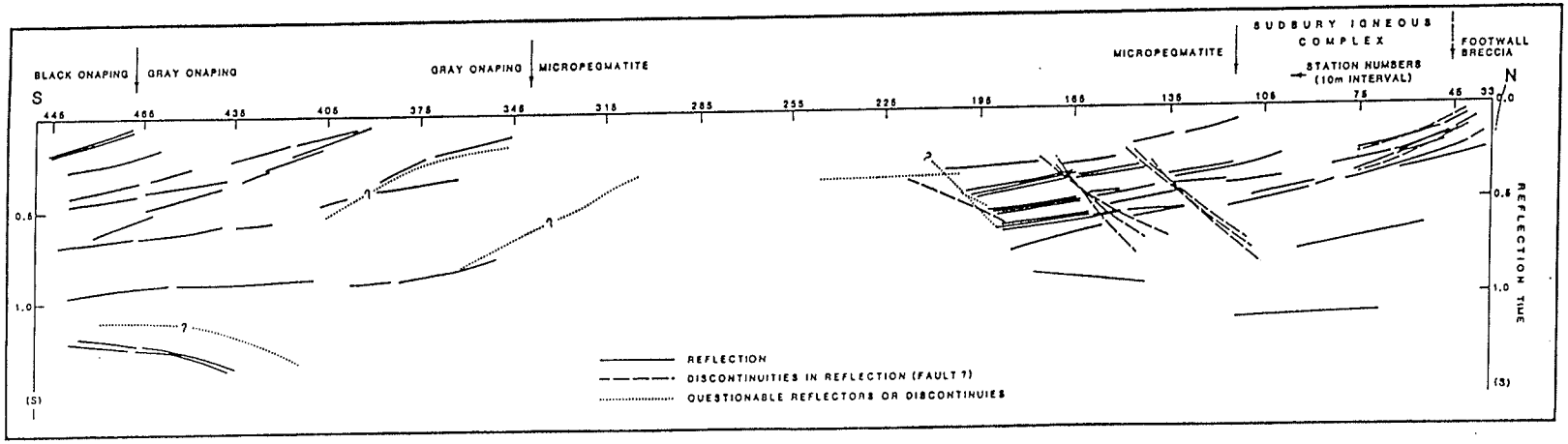

Figure 6.23: Interpretation of the DMO stack section shown in figure 6.22. Reflection segments dipping southward are observed on the northern as well as on the southern part of the line. The discontinuities dipping northward are interpreted as faults (Moon et al., 1990).

Chapter 7

Conclusions and Recommendations

Conventional seismic imaging software was originally developed for the oil exploration industry, and therefore, best suited for stratified soft rock environment. The software was ineffective when processing seismic data aquired in crystalline terrain. In this thesis several seismic imaging software have been developed applicable to hard rock environment with complex geology. The most significant contribution is the development of software for prestack partial migration (dip-moveout), wave equation modeling and migration and an innovative step-wise 2-D Fast Fourier Transform software for use in systems with limited core memory.

In the presence of dipping, curved and faulted reflectors, the CMP gather does not contain traces from the same CDP location, instead, the reflection points of the contributing traces are scattered in the updip direction. The prestack partial migration is a procedure which transforms the prestack data so that each CMP gather contains reflections from the same CDP location (Deregowski, 1986). Another important property of prestack partial migration is the correct treatment of events with conflicting dips. This is achieved by removing the dip dependence of the stacking velocity. Due to coherent stacking of dipping events, post-DMO stacks show improved

S/N ratio. The prestack partial migration software developed in this Master's thesis is based on Hale (1984) DMO theory. The programs have been tested successfully for both synthetic and real seismic data. Synthetic results confirmed Hale's theory that dip-moveout correction via prestack partial migration increases with increasing source-receiver offset (figure 4.10 and 4.12). The DMO correction is also large for early arrivals and decreases with increasing depth or travel time (figure 4.12).

The prestack partial migration discussed in this thesis is performed in frequency-wavenumber domain and requires efficient fast Fourier transform program to process large size seismic datasets. As part of this thesis research 2-D FFT software capable of handling very large dataset on limited core memory have been developed (Serzu and Moon, 1989(a)). The 2-D FFT algorithm is based on the paper by Anderson (1980). For smaller data sets there are a number of FFT subroutines in the public domain subroutine libraries which are more efficient than this particular software. The public domain subroutines however, are in-place by design and require the whole dataset to be on the systems real memory for processing. The advantage of the 2-D stepwise FFT is realized when the available computer memory is limited to handle the entire dataset. When using the stepwise FFT the dataset resides on direct access mass storage and the required core memory is a small fraction of the actual dataset. This software can handle both square and rectangular matrices, and it is also more efficient compared to similar subroutines which employ several tapes to hold intermediate steps. Table 4.1 shows the CPU time and core memory requirement for selected matrices.

To test the prestack partial migration software on synthetic dataset, modeling and migration programs have been developed. The wave equation modeling and migration programs are based on the phase shift theory by Gazdag (1978(a)). The impulse response of Hale's prestack partial migration operator is an ellipse. The wave equa-

tion Phase Shift migration of the DMO operator produced the theoretically predicted semi-elliptical reflector as shown in figure 5.19. The partial differential equation of motion governing the modeling and migration processes are solved numerically by approximation. Synthetic data were migrated using the second and fourth order approximation as well as, using the asymptotic approximation. The asymptotic equation gave accurate migration results (figure 5.19).

The seismic reflection data recorded in the Sudbury basin of Ontario exhibited very low S/N ratio. The CSP gathers were dominated by high amplitude surface waves and air blasts. High frequency noise was also a problem with the data. The Final DMO processed section showed some discontinuous reflections dipping southward on the northern and on the southern part of the line. Discontinuities believed to be faults were also observed on the northern part of the line (figure 6.23). The reflections from the micropegmatite-quartz gabbro contact predicted by the theoretical forward modeling were not as strong as predicted to be a marker horizon. One possible explanation for the weak reflection arrivals among many others is, the assumed geology and the acoustic impedance contrast at depth might not be as predicted in the study of the forward modeling. The lack of strong reflections in the data could also be attributed to poor source and receiver ground coupling or to the limitations of the recording instruments to record the desired high frequency signal with integrity.

DMO or prestack partial migration operators are designed to compensate the effects of dip-moveout on the recorded data. However, if the S/N ratio is very poor to start with, prestack partial migration does not improve the quality of the final stack very much.

Assuming the acoustic parameters obtained during the forward modeling closely approximate the actual geologic conditions in the Sudbury basin, the following re-

commendations are suggested for future seismic data aquisition strategy in Sudbury Basin or in areas with similar crystalline environment.

1) Use of a single geophone per station instead of a cluster. This would eliminate the averaging effect of the recorded signal which can degrade the high frequency content of the data.

2) Geophones with low natural frequency (< 40 Hz) are not appropriate for recording frequencies greater than 200 Hz. Lower frequency geophones are also known to record parasitic frequencies (motion arising perpendicular to the direction of propagation) in the high resolution pass band (Knapp and Steeples, 1986(a)). Geophones with natural frequencies greater than 100 Hz have been available in the market for some time. The high frequency geophones can record frequencies upto 500 Hz with integrity. Therefore, in high resolution seismic experiment, in addition to fine temporal and spatial sampling it is also important that geophones with high natural frequencies be employed to increase the high frequency signal bandwidth.

3) The type of energy source, and source-ground coupling are some of the known factors which affect the quality of the recorded signal. For high resolution surveys explosive sources placed in deeper drillholes and tamped with sand and crushed rock are expected to produce lower amplitude ground roll and good source-ground coupling.

4) When using explosive sources, lowering the charge size is known to shift the recorded signal toward the high frequency end of the spectrum (Ziolkowski and Lerwill, 1979), decreasing charge sizes also reduces the S/N ratio, thus, optimum charge size must be used during high resolution surveys.

Application of high resolution reflection seismic in crystalline environment have made significant progress in the last few years. A carefully designed and processed high resolution survey has a good possibility of being effective tool in exploration

of deep seated ore bodies. However, more research is required to enable routine application of high resolution seismic in Precambrian terrain.

Bibliography

[1] Al Sadi, H.N., 1980, *Seismic Exploration*, Birkhauser Verlag, Basel.

[2] Anderson, G.L., 1980, A Stepwise Approach to computing the Multidimensional Fast Fourier Transform of Large Array, *IEEE Trans. Acoustics, Speech, and Signal Processing*, v. **28**, no. **3**, pp. 280–284.

[3] Applegate, J.K., Emilia, D.A., Neitzel,E.B. and Donaldson, P.R., 1982, High-resolution seismic study in the Gas Hills uranium district, Wyoming, *Geophysics*, v. **47**, no. **10**, pp. 1355–1374.

[4]* Bergland, G.D., 1982, A guided tour of the Fast Fourier Transform, *IEEE Spectrum*, v. **6**, no. **7**, pp. 41–52.

[5]* Berkhout, A.J., 1986, Seismic inversion in terms of pre-stack migration and multiple elimination : *Proceedings of the IEEE*, v. **74**, no. **3**, pp. 415–427.

[6]* Berkhout, A.J., 1985, *Seismic Migration–Imaging of acoustic energy by wave field extrapolation : A. Theoretical aspects*, Elsevier Science Publishing Co., Inc.

[7]* Berkhout, A.J., 1985, *Seismic Migration–Imaging of acoustic energy by wave field extrapolation : B. Practical aspects*, Elsevier Science Publishing Co., Inc.

[8] Bolondi, G., Loinger, E. and Rocca, F., 1982, Offset continuation of seismic sections : *Geophysical Prospecting*, v. **30**, pp. 813–828.

[9] Biondi, B. and Ronen, J., 1986, Shot profile dip moveout using log-stretch transform : *SEG annual meeting expanded technical abstracts with bibliography*, pp. 431–434.

[10] Biondi, B. and Ronen, J., 1987, Dip moveout in Shot profile : Geophysics, v. **52**, pp.1473–1482.

[11] Bracewell, R.N., 1986, *The Fast Fourier Transform and its Applications*, McGraw-Hill Book Co.

[12] Brigham, E.O., 1974, *The Fast Fourier Transform*, Prentice Hall, Eglewood Cliffs, New Jersey.

[13] Card, K.D., and Hutchinson, R.W., 1972, The Sudbury structure, its geological setting : *In New developments in Sudbury Geology* , J.V., Guy-Bray (editor), The Geological Association of Canada, special paper No. **10**, pp. 67–78.

[14]* Carswell, A. C., 1985, Multioffset VSP experiment for the mapping of fracture zones: *M.Sc. thesis*, University of Manitoba.

[15] Carswell, A.C. and Moon, W.M.,1989, Application of multi-offset VSP for fructture mapping in granite batholith : *Geophysics*, v. **54**, pp. 737–746.

[16]* Christie, P.A.F., Hughes, V.J. and Kennett, B.L.N., 1983, Velocity filtering of seismic reflection data : First Break, v. **1**, no. **3**, pp.9–24.

[17]* Chun, J.H., and Jacewitz, C.A., 1981, Fundamantals of frequency migration : *Geophysics*, v. **46**, pp. 717-773.

[18] Claerbout, J.F., 1970, Coarse grid calculations of waves in inhomogeneous media with application to delineation of complicated seismic structures : *Geophysics*, v. **35**, pp. 407–418.

[19]* Claerbout, J.F., and Doherty, S.M., 1972, Downward continuation of moveout corrected seismograms : *Geophysics*, v. **37**, pp. 741–768.

[20] Claerbout, J.F., 1976, *Fundamentals of Geophysical Data Processing*, Mcgraw Hill, New York.

[21] Claerbout, J.F., 1985, *Imaging the Earth's Interior*, Blackwell Scientific Publications, Oxford, London.

[22] Cooley, J.W. and Tukey, J.W., 1965, An algorithm for machine calculation of complex Fourier series, *Math. Computation*, v. **19**, pp. 297–301.

[23]* Cooper, H.W. and Cook, R.E., 1984, Seismic data gathering : *Proceedings of IEEE*, v. **72**, no. **10**, pp. 1266–1275.

[24] Dahle, A., Gjoystdal, H., Grammeltvedt, G., Soyland Hansen, T., 1985, Application of seismic reflection methods for ore prospecting in crystalline rock: *First Break*, v. **3**, No. **2**, pp. 9–16.

[25] Dence, M. R., 1978, *Sudbury and Brent Excursions, guide book*, Laurentian University, Sudbury, Ontario, pp. 1-28.

[26] Dietz, R.S., 1964, Sudbury structure as an astrobleme: *Journal of Geology*, v.**72**, pp. 412–434.

[27] Dietz, R.S., 1972, Sudbury astrobleme, splash emplaced sub-layer and possible cosmogenic ores: *New Developments in Sudbury Geology*, J. V. Guy-

Bray(editor), The Geological Association of Canada, special paper No. **10**, pp. 29–40.

[28] Deregowski, S.M., 1982, Dip moveout and reflector point dispersal : *Geophysical Prospecting*, v. **30**, pp. 318–322.

[29] Deregowski, S.M., and Rocca,F., 1981, Geometrical optics and wave theory of constant offset sections in layered media : *Geophysical Prospecting*, v. **29**, pp. 384–406.

[30] Deregowski, S.M., 1986, What is DMO ?, First Break, v. 4, no. **7**, pp. 7–24.

[31] Dressler, B.O., 1984, General geology of Sudbury, area, *The Geology and Ore Deposits of the Sudbury Structure*, edited by E.G., Pye, A.J., Nalbrett and P.E., Giblin, Ontario Geological Survey, Special volume **1**.

[32] Eklundh, J.O., 1972, A fast computer method for matrix transposing, *IEEE Trans. Comput.*, v. **C-21**, pp. 801–803.

[33]* Farr, J.B., 1977, How high is high resolution ? (abstract) : *Geophysics*, v. **42**, p. 150.

[34] French, B.M., 1967, Sudbury Structure, Ontario, Some petrographic evidence for origin by meteorite impact: *Science*, v. **156**, pp. 1094–1098.

[35] French, W.S., 1975, Computer migration of oblique seismic reflection profiles : *Geophysics*, v. **40**, pp. 961–980.

[36]* Gardner, G.H.F., 1982, *Migration of seismic data*, Geophysics reprints no. **4**, 462 p.

[37] Gazdag, J., 1978(a), Wave equation migration with the phase shift method : *Geophysics*, v. **43**, no. **5**, pp. 1343–1351.

[38] Gazdag, J., 1978(b), Extrapolation of seismic waveforms by Fourier methods : *IBM Journal of Research and Developments*, v. **22**, no. **5**, pp. 4881-486.

[39] Gazdag, J., 1980, Wave equation migration with accurate space derivative method : *Geophysical Prospecting*, v. **28**, pp. 60–70.

[40] Gazdag, J. and Sguazzero, P., 1984(a), Migration of seismic data by phase shift plus interpolation : *Geophysics*, v. **49**, no. **1**, pp. 124–131.

[41] Gazdag, J. and Sguazzero, P., 1984(b), Migration of seismic data : *Proceedings of IEEE*, v. **72**, no. **10**, pp. 1302–1315.

[42]* Gerald, C.F. and Wheatley, P.D., 1984, *Applied Numerical Analysis,* Addison Whesley Publishing Company.

[43]* Green, A.G., Anderson, N.L., and Stephenson, O.G., 1979, An expanding spread seismic reflection survey across the Snake Bay- Kakagi Lake Greenstone Belt, Northwestern Ontario: *Canadian Journal of Earth Sciences*, v. **16**, pp. 1599–1612.

[44] Green, A.G., 1981, Results of siesmic reflection survey across the fault zone between the Thompson Nickel Belt and the Churchill Tectonic Province, Northern Manitoba: *Canadian Journal of Earth Sciences*, v. **18**, pp. 13–25.

[45] Green, A.G. and Mair, J.A., 1983, Subhorizontal fractures in a granitic pluton: Their detection and implication for radioactive waste disposal, *Geophysics*, v. **48**, no. **11**, pp. 1428–1449.

[46]* Hajnal, Z. and Stauffer, M.R., 1975, The application of seismic reflection techniques for subsurface mapping in the Precambrian Shield near Flin Flon, Manitoba: *Canadian Journal of Earth Sciences*, v. **12**, pp. 2036–2047.

[47] Hale, I.D., 1983, Dip-moveout by Fourier transform : *Ph.D. Thesis*, Stanford University.

[48] Hale, I.D., 1984, Dip-moveout by Fourier transform : *Geophysics*, v. **49**, no. **6**, pp. 741–757.

[49]* Hron, F., and Kanasewich, E.R., 1971, Synthetic seismograms for deep seismic sounding studies using asymptotic ray theory: *Bulletin of Seismological Society of America*, v. **61**, pp. 1169–1200.

[50] Kelamis, P., and Kjartansson, E., 1985, Forward modelling in frequency space domain : *Geophysical Prospecting*, v. **33**, pp. 252–262.

[51]* Kanasewich, E.R., 1981, *Time Sequence Analysis in Geophysics*, University of Alberta Press.

[52] Knapp, R.W. and Steeples, D.W., 1986(a), High resolution common depth point profiling: Instrumentation, *Geophysics*, v. **51**, no. **2**, pp. 276–282.

[53]* Knapp, R.W. and Steeples, D.W., 1986(b), High resolution common depth point profiling: Field aquisition parameter design, *Geophysics*, v. **51**, no. **2**, pp. 283–294.

[54] Levin, F.K., 1971, Apparent velocity from dipping interface reflections : *Geophysics*, v. **36**, pp. 510–516.

[55] Lines, C.L. and Bleistein, N., 1988, Comparative anatomy of common offset dip-moveout : *Society of Exploration Geophysicists 58th Annual International Meeting and Exposition*, Expanded Abstracts of the Technical Program with Author's Bibliographies, v. **II**, pp. 1101–1105.

[56] Loewenthal, D., Lu, L., Roberson, R., Sherwood, J., 1976, The wave equation applied to migration : *Geophysical Prospecting*, v. **24**, pp. 380–399.

[57] Mair, J.A., and Green, A.G., 1981, High resolution seismic reflection profiles reveal fracture zones within a homogeneous granite batholith : *Nature*, v. **294**, pp. 439–442.

[58] Messfin, D., 1983, Seismic approaches for mineral exploration in the Sudbury Basin of Ontario : *M.SC. Thesis*, University of Manitoba.

[59] Messfin, D. and Moon, W., 1984, Seismic approaches for structural studies of the Sudbury Basin: *Geophysics*, v. **49**, pp. 1675–1689.

[60]* Mitra, S.K., and Ekstrom, M.P. (editors), 1978, Two-Dimensional digital signal processing, Dowden, Hutchinson and Ross Inc.

[61] Moon, W.M., Kublic, E., Serzu, M.H. and Krause, B., 1990, Application of high resolution seismic survey in Precambrian Shield exploration (Sudbury, Ontario): *Submitted to Geophysics.*

[62]* Napoleon, I., Heikkinen, P. and Mehrotra, S., 1979, Applicability of seismic reflection sounding in regions of Precambrian geology : *Geoexploration*, v. **17**, no. **1**, pp. 1–9.

[63] Notfors, C.D. and Godfrey, R.J., 1987, Dip moveout in the frequency–wavenumber domain : *Geophysics*, v. **52**, pp. 1718–1721.

[64]* Ongkiehong, L. and Askin, H.J., 1988, Toward the universal seismic aquisition technique : *First Break*, v. **6**, no., **2**, pp. 46–63.

[65]* Oppenheim, A.V. and Schafer, R.W., 1975, *Digital Signal Processing*, Prentice Hall, Eglewood Cliffs, New Jersey.

[66] Palmer, D., 1987, High resolution seismic reflection surveys for coal : *Geoexploration*, v. **24**, pp. 397–408.

[67]* Philip, S.S. and Sherwood, J.W.C., 1980, Depth migration before Stack : *Geophysics*, v. **45**, no. **3**, pp. 376–393.

[68]* Rigdon, H. and Hoover., G., 1987, Quantitative selection of seismic aquisition parameters : *The Leading Edge*, v. **6**, no. **1**, pp. 18–25.

[69] Robinson, E.A., 1983, *Migration of Geophysical Data*, IHRDC, Boston.

[70] Schneider, W.A., 1978, Integral formulation for migration in two and three dimensions : *Geophysics*, v. **43**, pp. 49–76.

[71] Serzu, M.H. and Moon, W.M., 1989(a), Two dimensional fast Fourier transform for large data matrices : *Computer Physics Communications*, v. **52**, no. **2**, pp. 333–336.

[72] Serzu, M.H. and Moon, W.M., 1989(b), Algorithm for Dip-moveout by Fourier Transform : *Computer Physics Communications*, v. **52**, no. **2**, pp. 337–344.

[73] Singleton, R.C., 1967, A method for computing the fast Fourier transform with auxiliary memory and limited high-speed storage, *IEEE trans. Audio Electroacoust.*, v. **AU-15**, pp. 91–97.

[74]* Smith, S.B., Shive, P.N. and Brown, S.K., 1977, Seismic velocity, reflection and structure of the crystalline crust, *American Geophysical Union, Monograph*, no. **20**, pp. 254–270.

[75] Speers, E.C., 1957, The age relation and origin of the Sudbury breccia: *Journal of Geology*, v. **65**, pp. 497–514.

[76] Steeples, D.W., Knapp, R.W. and McElwee, C.D., 1986, Seismic reflection investigations of Sinkholes beneath Interstate Highway 70 in Kansas, *Geophysics*, v. **51**, no. **2**, pp. 295–302.

[77] Stolt, R.H., 1978, Migration by Fourier transform : *Geophysics*, v. **43**, no. **1**, pp. 23–48.

[78] Stolt, R.H. and Benson, A.K., 1986, *Seismic migration : Theory and practice* : Geophysical Press, London–Amsterdam.

[79]* Tucker, P.M., 1982, Pitfalls revisited : *Society of Exploration Geophysicists Monograph*, no. **1**, Tulsa, OK.

[80]* Trorey, A.W., 1970, A simple theory of seismic diffractions : *Geophysics*, v. **35**, pp. 762-784.

[81] Whitmore, N.D., Samuel, H.G. and Adam, G., 1988 Two-dimensional poststack depth migration : a survey of methods : *First Break*, v. **6**, No. **6**, pp. 189–197.

[82]* Widess, M.B., 1975, How thin is a thin bed ? : *Geophysics*, v. **38**, pp. 1176–1180.

[83] Yilmaz, O. and Claerbout, J.F., 1980, Prestack partial migration : *Geophysics*, v. **45**, no. **12**, pp. 1753–1779.

[84]* Yilmaz, O., 1987, *Seismic Data Processing*, Society of Exploration Geophysicists, Tulsa, OK.

[85] Ziolkowski, A. and Lerwill, W.E., 1979, A simple approach to high resolution seismic profiling for coal : *Geophysical Prospecting*, v. **27**, pp. 360–393.

[ ]* References not quoted in the thesis but cited for general background information on seismic modeling and migration, FFT, prestack partial migration, and high resolution seismic.

Appendix

Appendix A

Computer Programs

To carry out the synthetic seismic modelling and the seismic data processing discussed in this study, several computer programs have been developed. Most of source code was written in Fortran 77. The Calcomp plotting subroutines have been utilized extensively to plot majority of the diagrams in this thesis. Some of the most important programs are briefly described in the following paragraphs.

READWRPLOT - Performs input/output task between two digital tapes storing seismic data. The input and output tapes are in SEG-Y format. The program also posesses the option of displaying selected common shot gathers as wiggle traces with or without shading the positive amplitudes.

STATICOR - Does static correction on common shot gathers and displays the data before and after correction for comparison.

BANDPASS - Performs bandpass filtering on CSP, CMP gathers and on CMP stacked data. The program has the option to display the input output gathers.

SORTOFFSET - Sorts the seismic data stored as CSP or CMP gathers into common offset gathers. The program uses a seismic data base which contains previously computed field geometry to sort the sesimic traces. Each seismic trace stored in the tape is associated with a particular shot nunmber, trace number, CMP (CDP) num-

ber and offset. The common offset gathers are input to the prestack partial migration program. The program has the option to display the output gathers.

CMPSORT- The program accoplishes CMP sorting by taking the common shot or common offset gathers as an input. Selected CMP gathers may be displayed if desired.

CMPSTACK - Performs NMO correction, trace interpolation, CMP stacking, AGC (Automatic Gain Control), and display. This program uses the output CMP gathers from the program CMPSORT as an input.

DMO (Dip-moveout) - The program performs partial prestack migration on common offset gathers. In the processes transforms the constant offset gathers in zero offset sections. This program requires NMO corrected data as input.

SW2DFFT (Stepwise Fast Fourier Transform) - Performs fast Fourier transform of large data matrices in stepwise fashion. The program is the practical implementation of the Anderson's method for 2-D case (Anderson, 1980).

WVMODEL - Wave equation zero offset modeling with the phase shift method. The program accomodates depth variable velocity.

DVSHIFT - Performs depth variable wave equation migration of zero offset (or post stack) data. The algorithm is based on Gazdaz's (1978(a)) phase shift method.

Appendix B

Sudbury seismic reflection data (Common Shot Gathers)

The following records are the partially preprocessed common shot gathers (SP. 33 to SP. 192) recorded on the northern part of the line L85S1. Most of the detail processing carried out in this study involved these gathers.

SUDBURY LINE S-1 85
REC = 1 (STN. = 33)

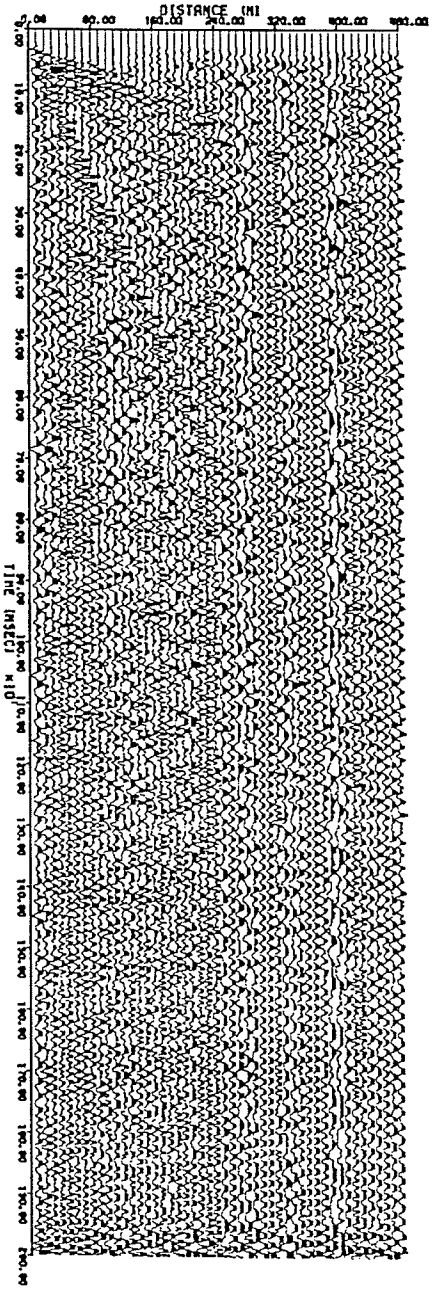

SUDBURY LINE S-1 85
REC = 2 (STN. = 35)

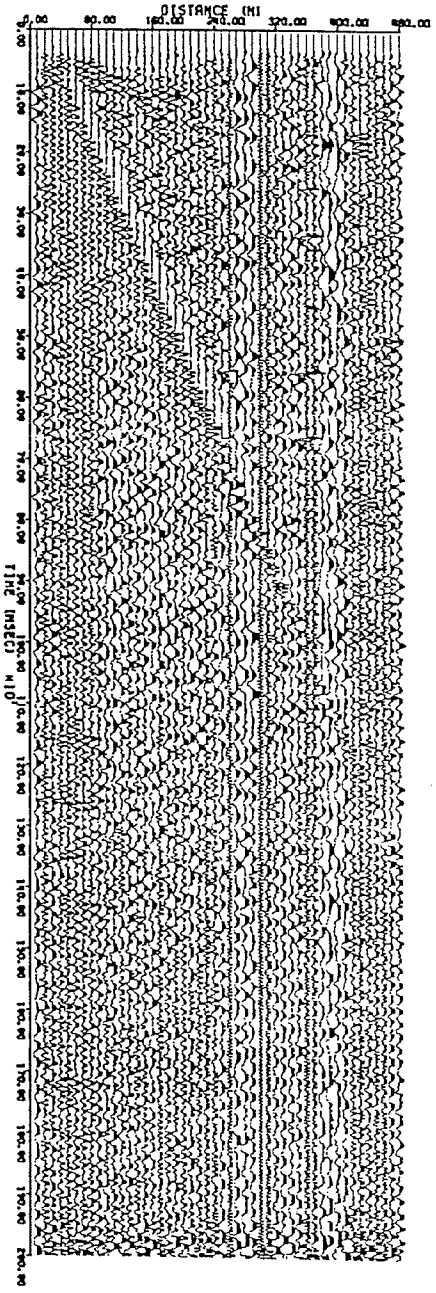

SUDBURY LINE S-1 85
REC = 3 (STN. = 37)

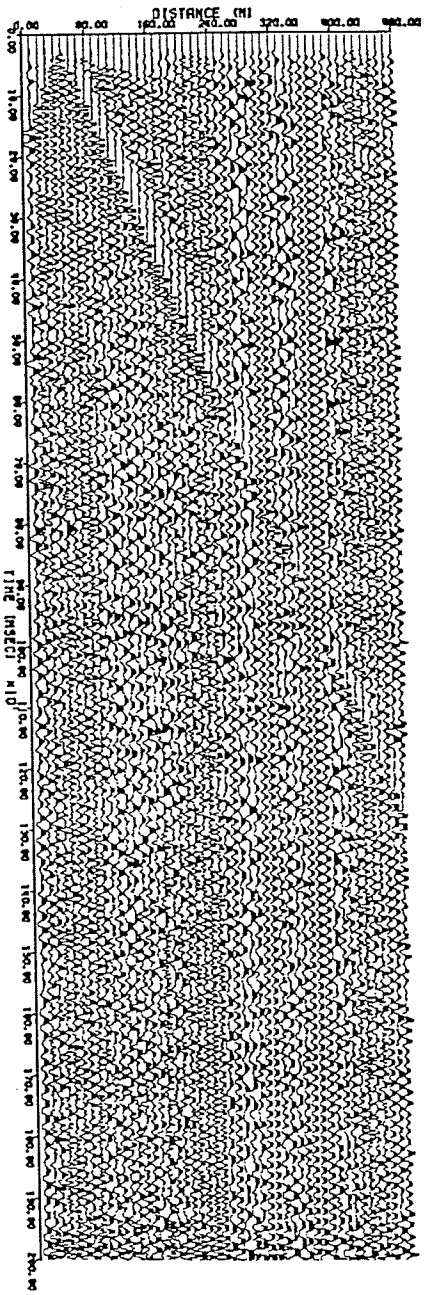

SUDBURY LINE S-1 85
REC = 4 (STN. = 39)

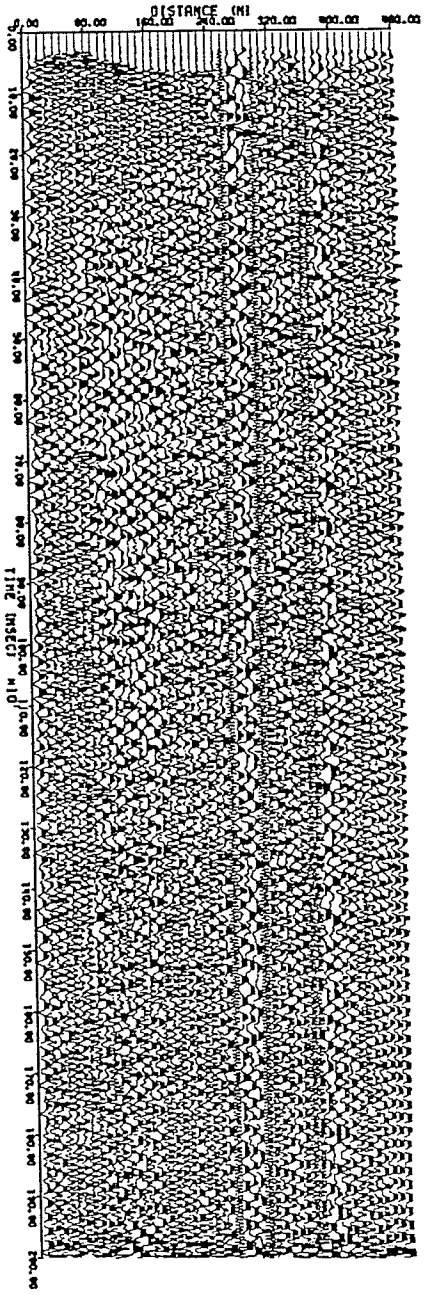

SUDBURY LINE S-1 85
REC = 5 (STN. = 41)

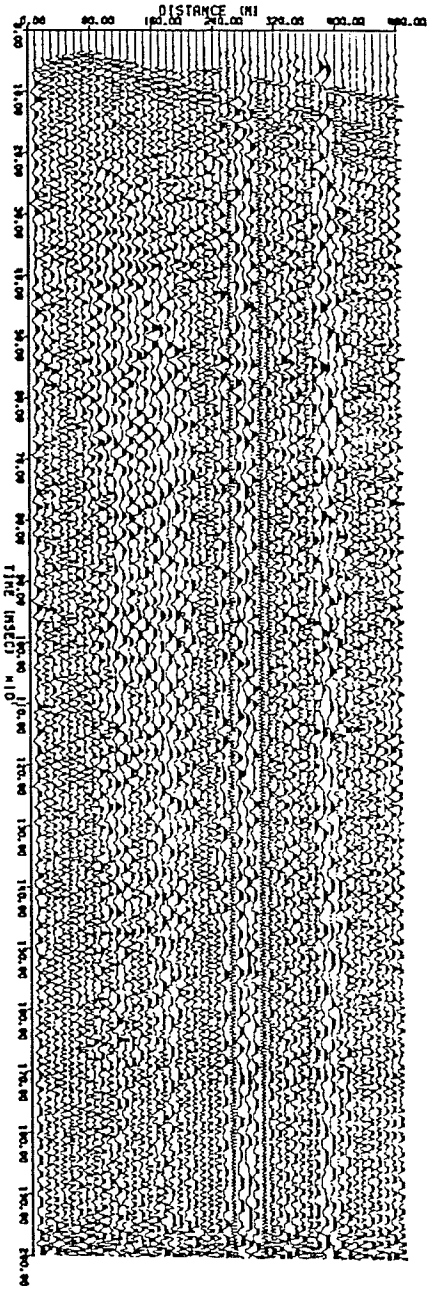

SUDBURY LINE S-1 85
REC = 6 (STN. = 49)

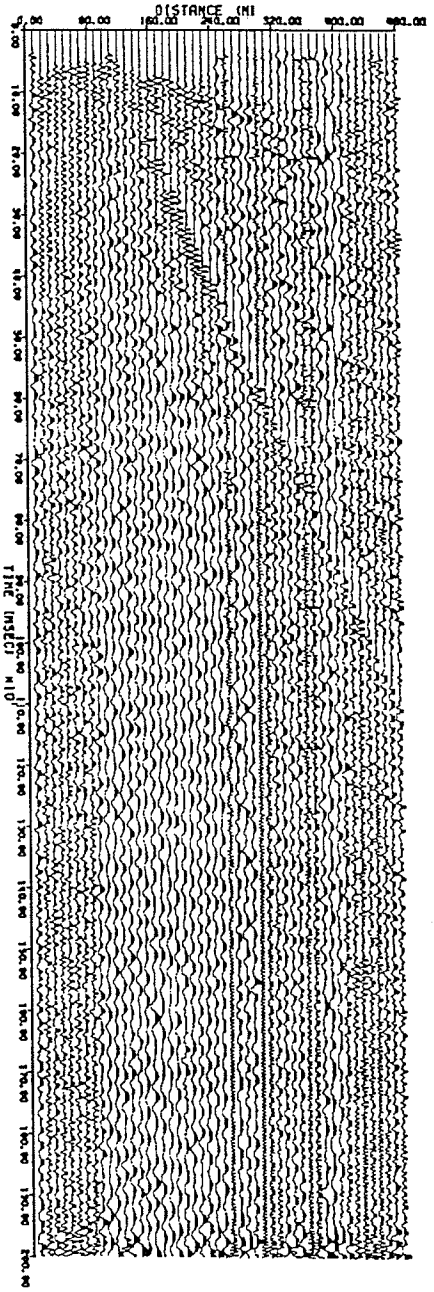

SUDBURY LINE S-1 85
REC = 7 (STN. = 45)

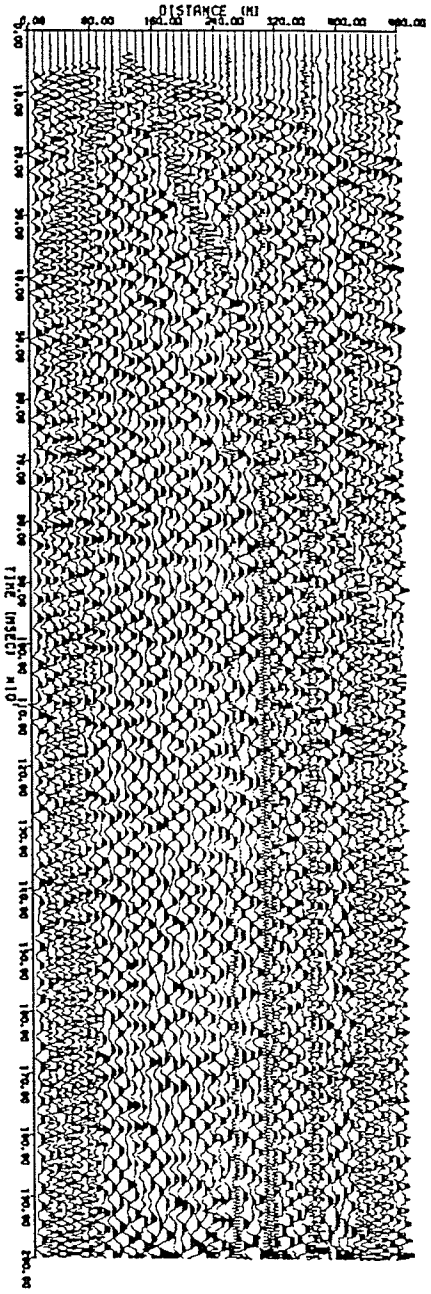

SUDBURY LINE S-1 85
REC = 8 (STN. = 47)

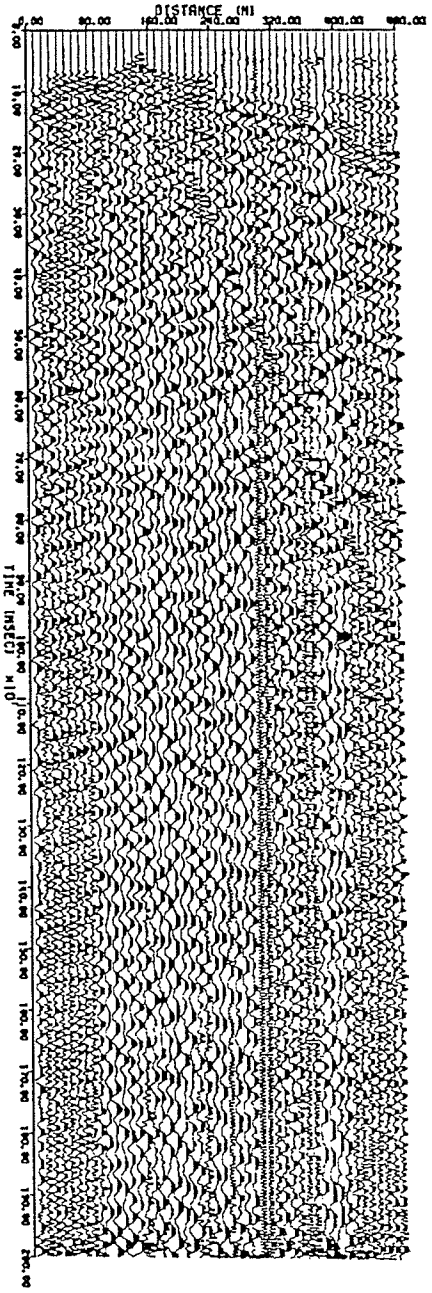

SUDBURY LINE S-1 85
REC = 9 (STN. = 49)

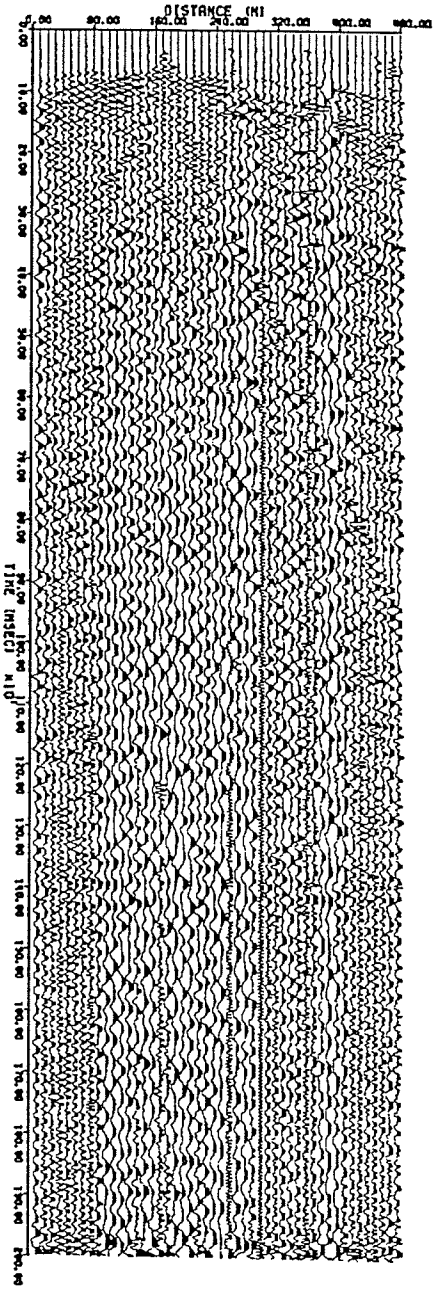

SUDBURY LINE S-1 85
REC = 10 (STN. = 51)

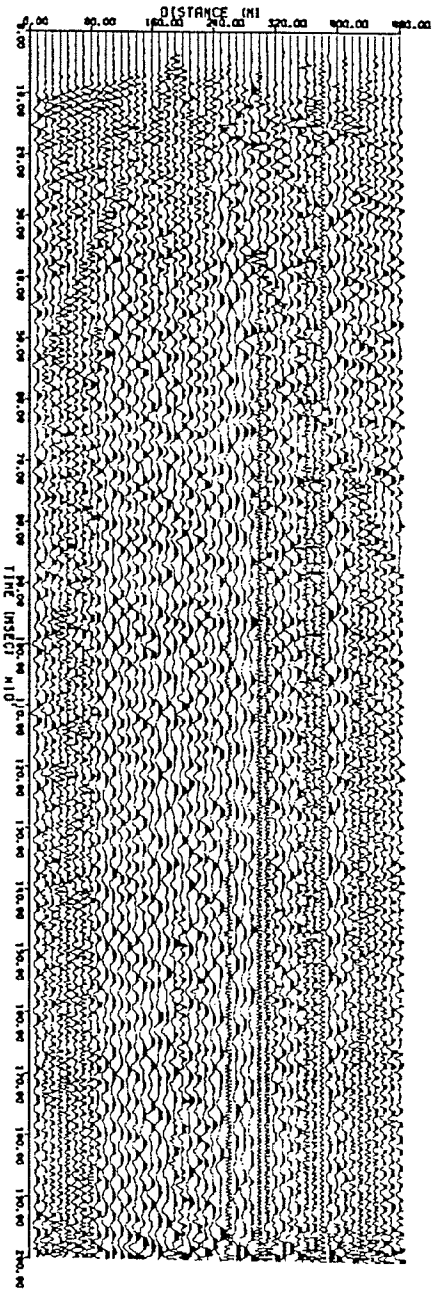

SUDBURY LINE S-1 85
REC = 11 (STN. = 53)

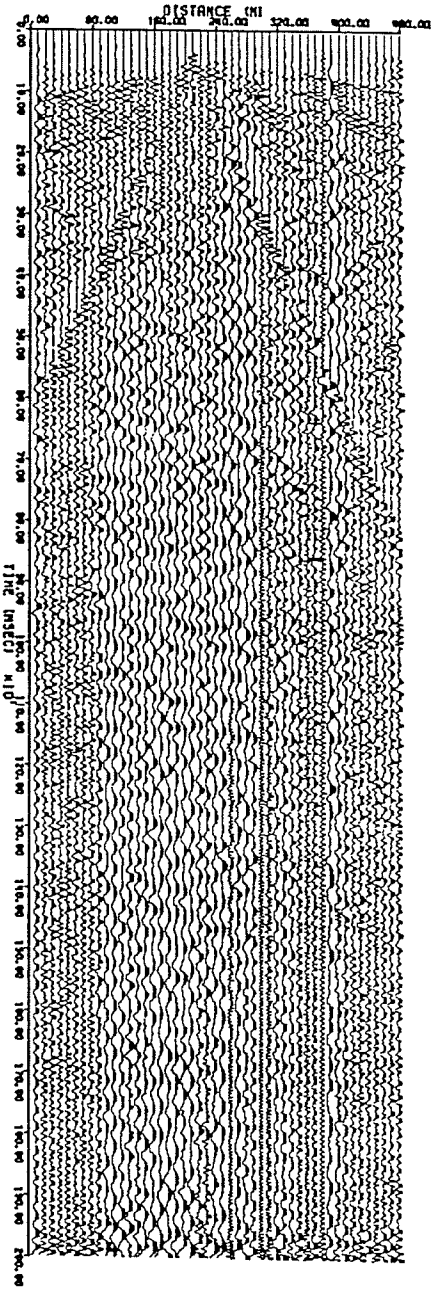

SUDBURY LINE S-1 85
REC = 12 (STN. = 55)

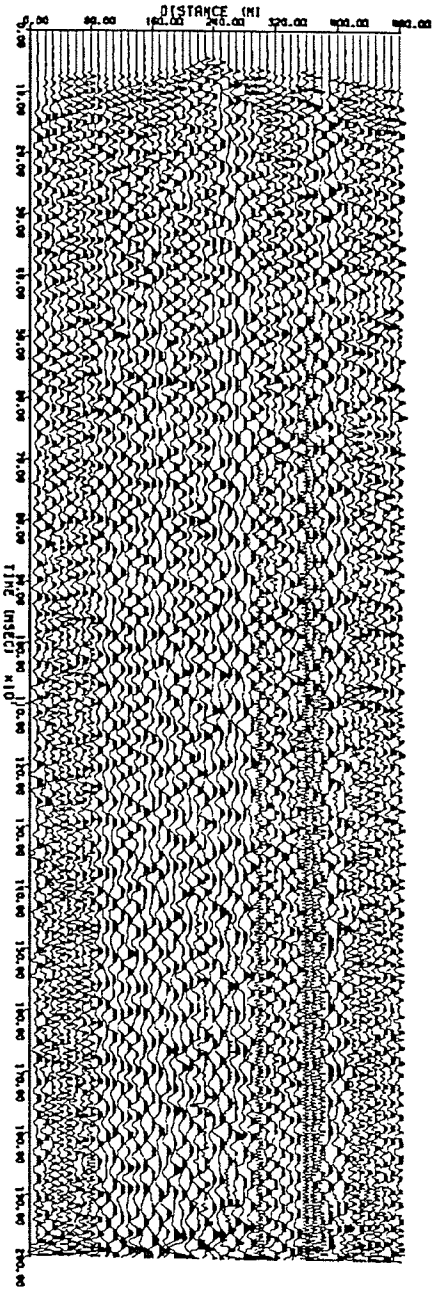

SUDBURY LINE S-1 85
REC = 13 (STN. = 57)

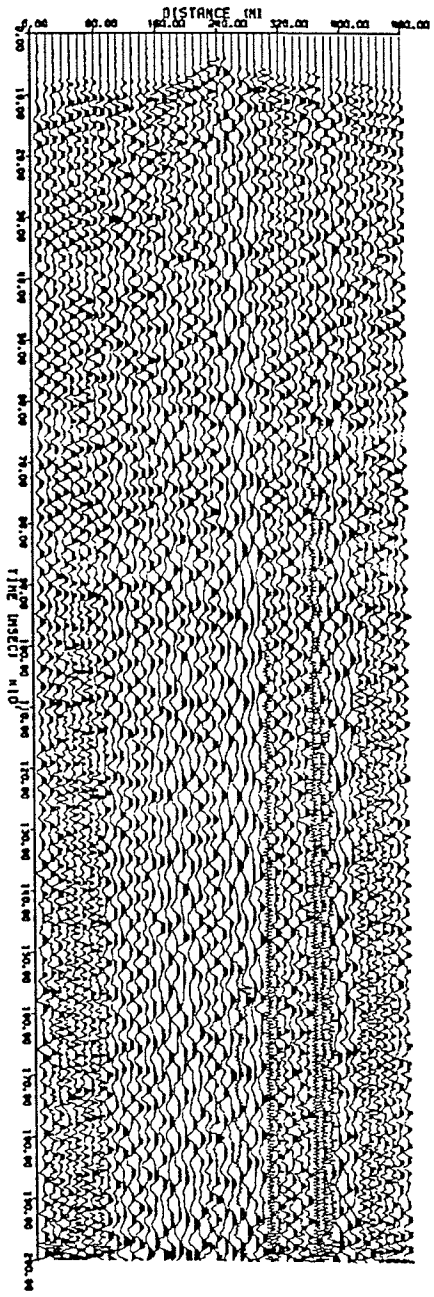

SUDBURY LINE S-1 85
REC = 14 (STN. = 59)

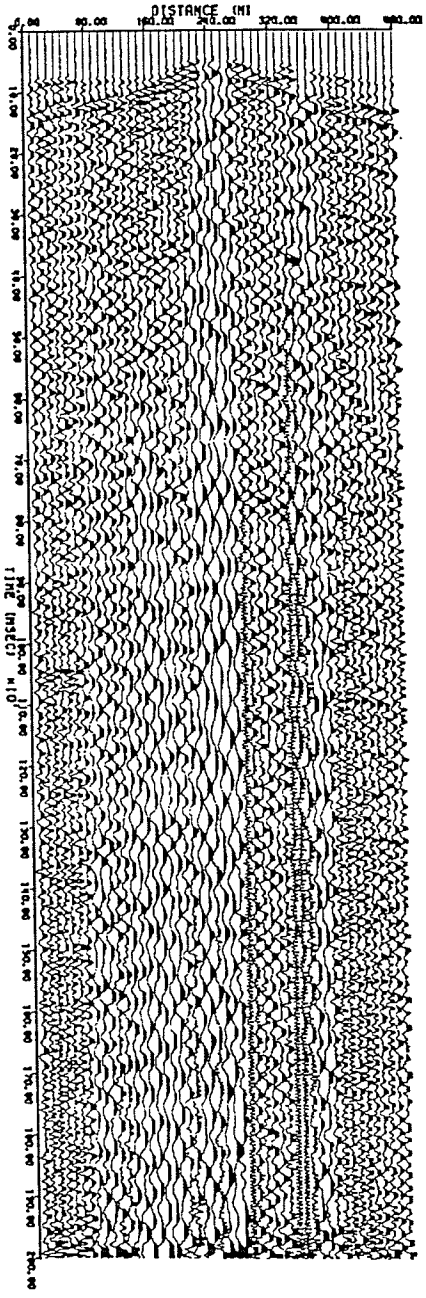

SUDBURY LINE S-1 85
REC = 15 (STN. = 61)

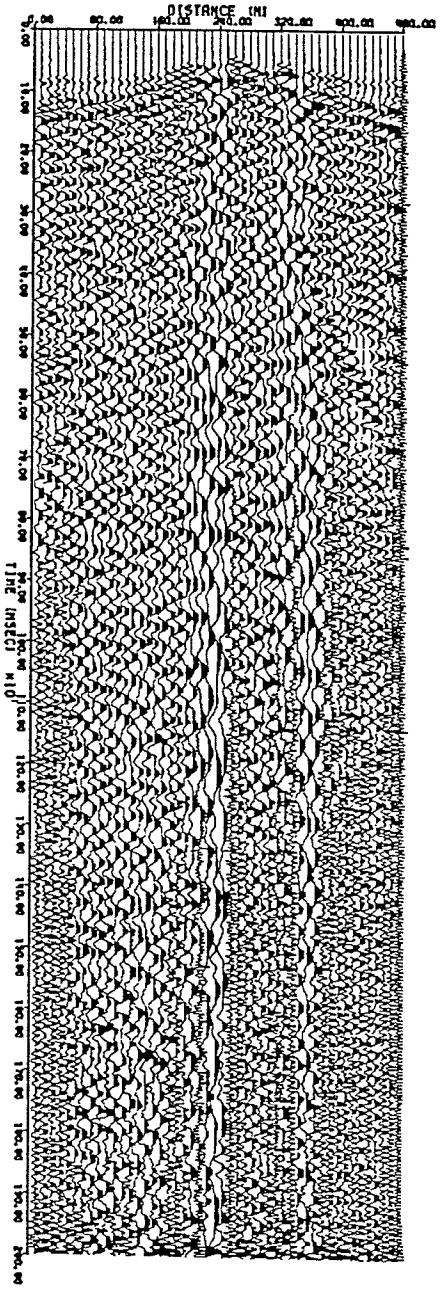

SUDBURY LINE S-1 85
REC = 16 (STN. = 63)

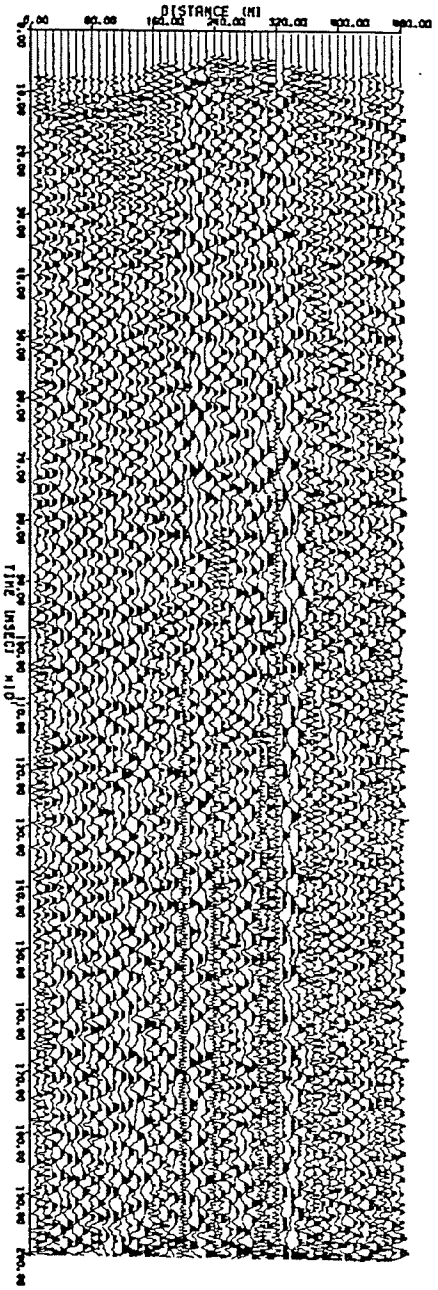

SUDBURY LINE S-1 85
REC = 18 (STN. = 67)

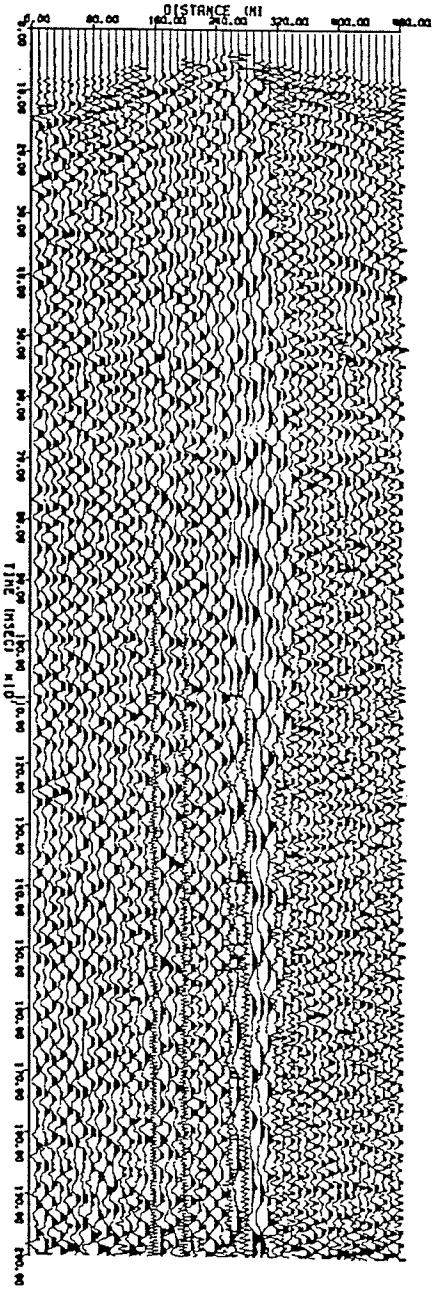

SUDBURY LINE S-1 85
REC = 17 (STN. = 65)

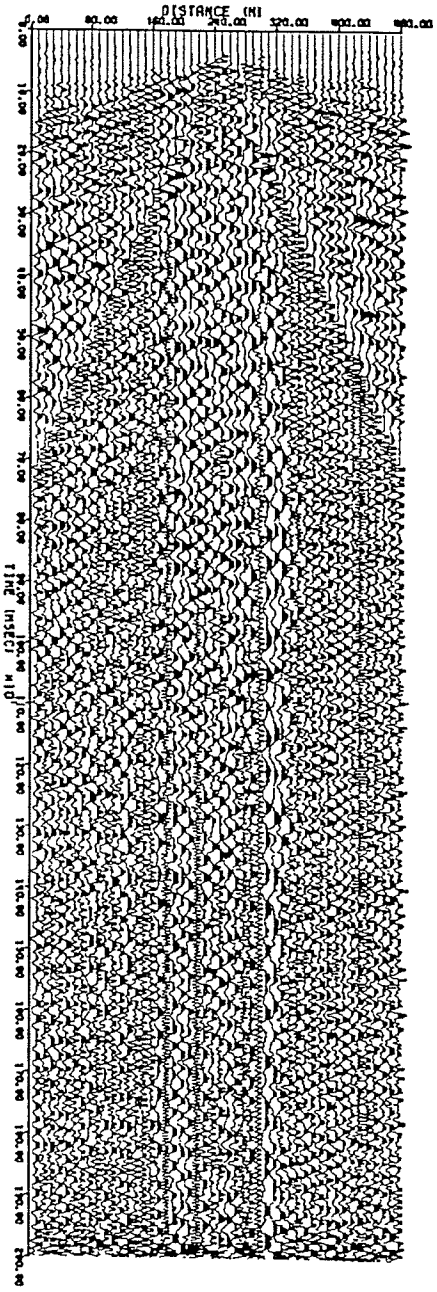

SUDBURY LINE S-1 85
REC = 19 (STN. = 69)

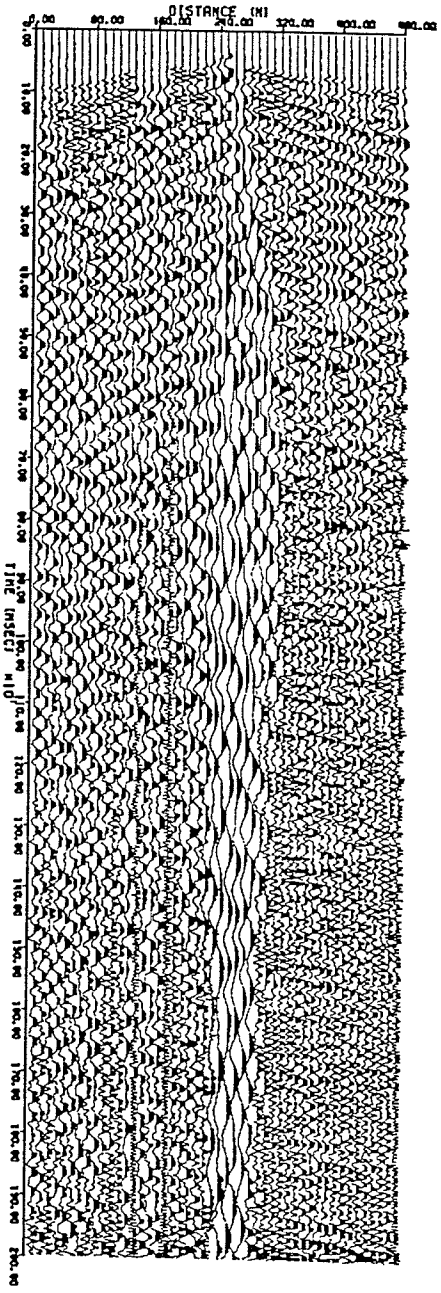

SUDBURY LINE S-1 85
REC = 20 (STN. = 71)

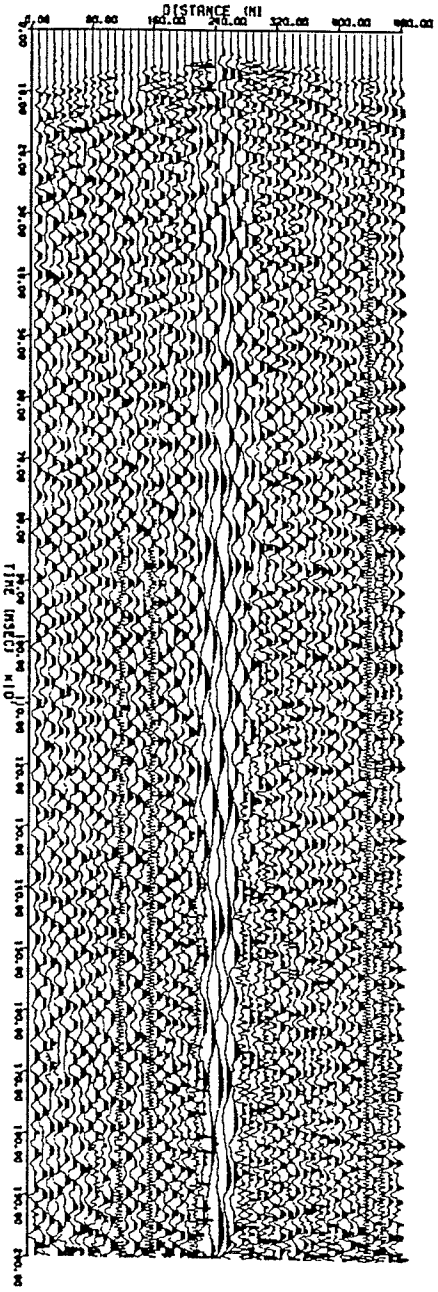

SUDBURY LINE S-1 85
REC = 21 (STN. = 73)

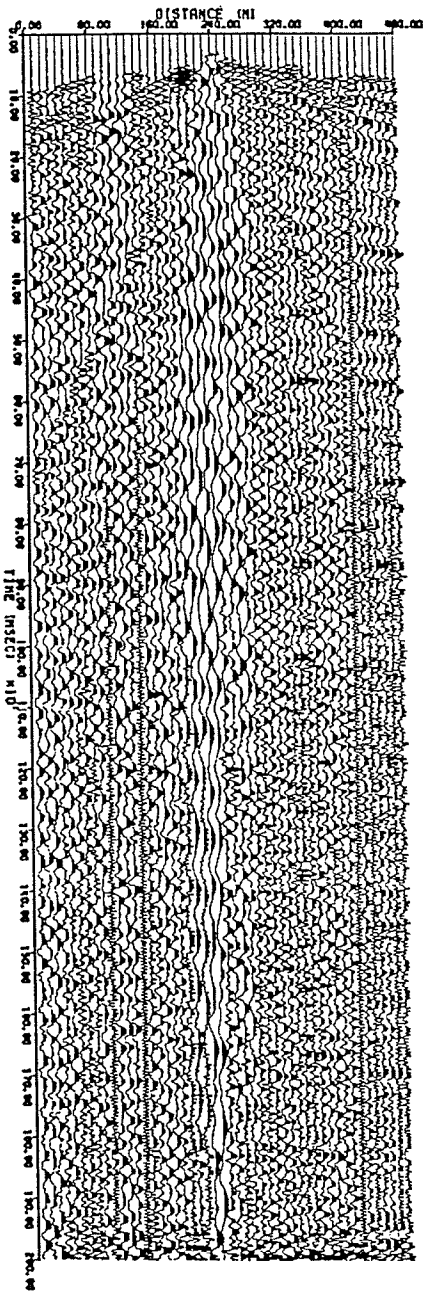

SUDBURY LINE S-1 85
REC = 22 (STN. = 75)

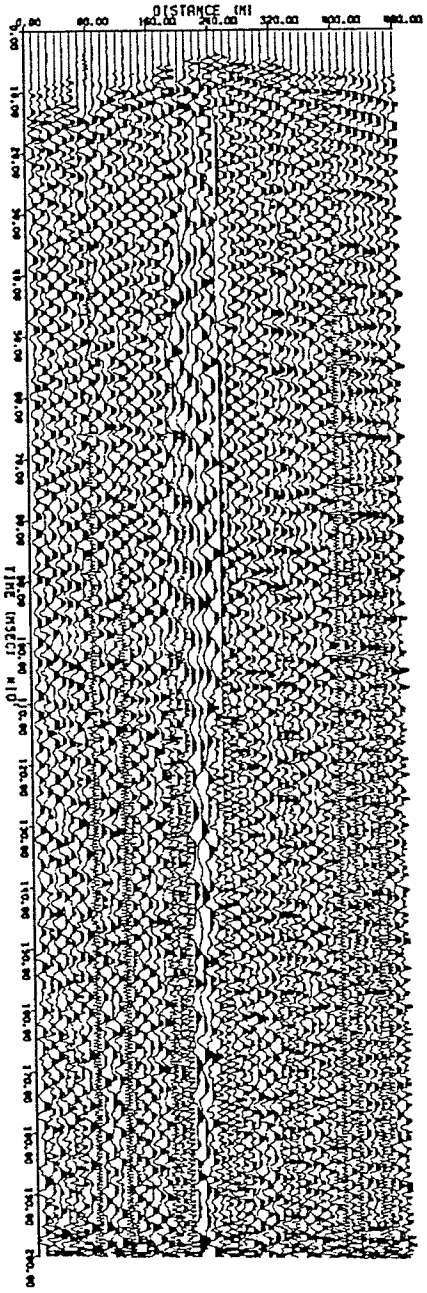

SUDBURY LINE S-1 85
REC = 23 (STN. = 77)

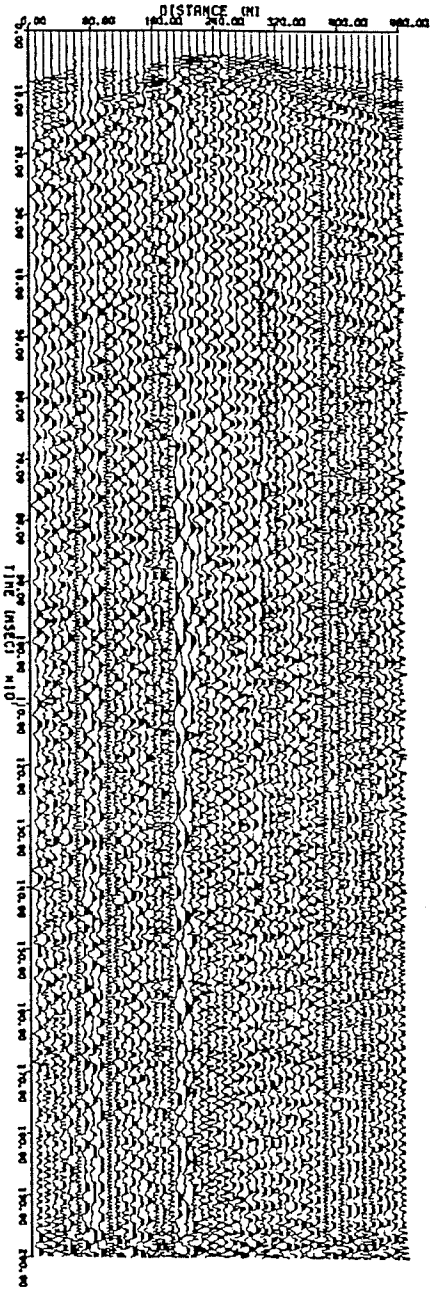

SUDBURY LINE S-1 85
REC = 24 (STN. = 79)

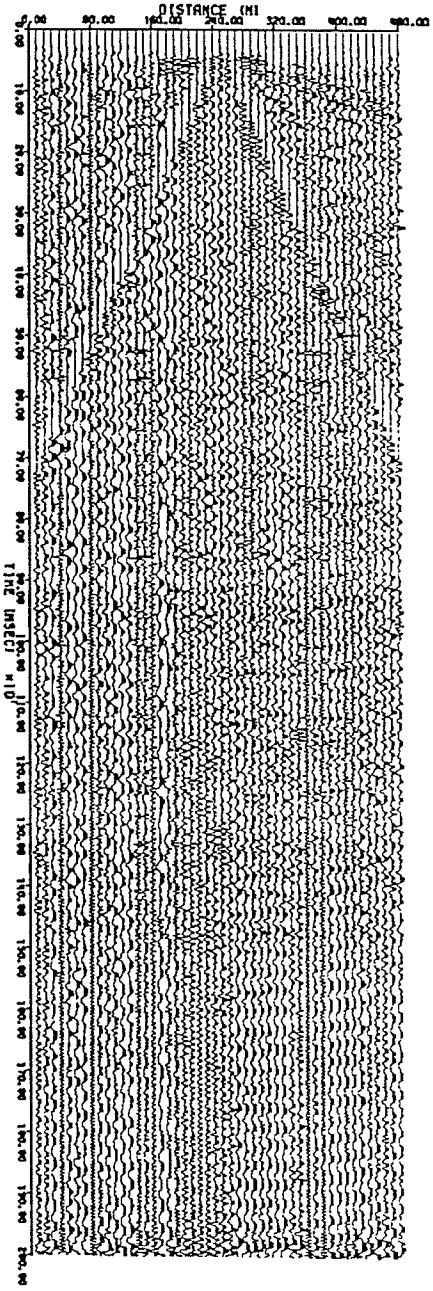

SUDBURY LINE S-1 85
REC = 25 (STN. = 81)

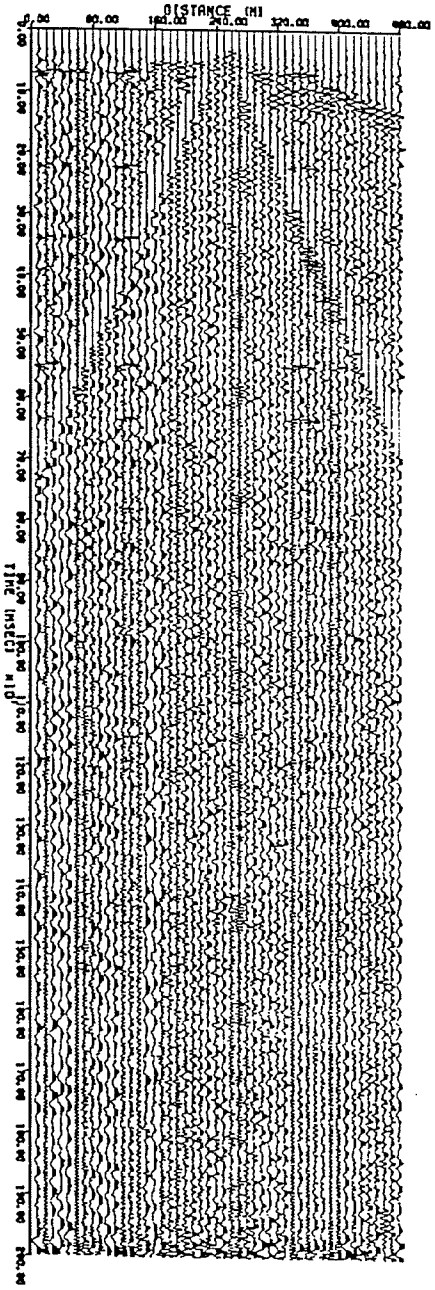

SUDBURY LINE S-1 85
REC = 26 (STN. = 83)

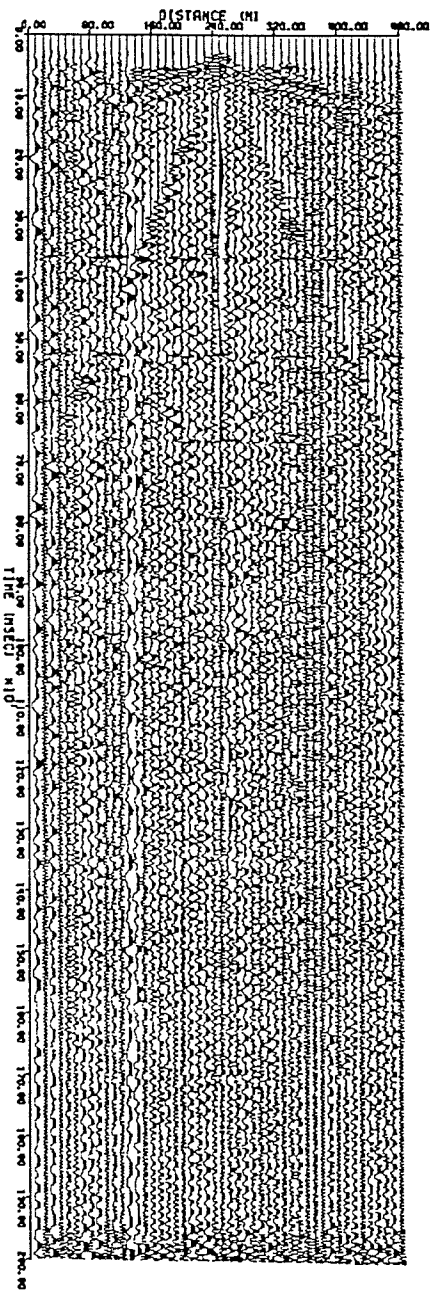

SUDBURY LINE S-1 85
REC = 27 (STN. = 85)

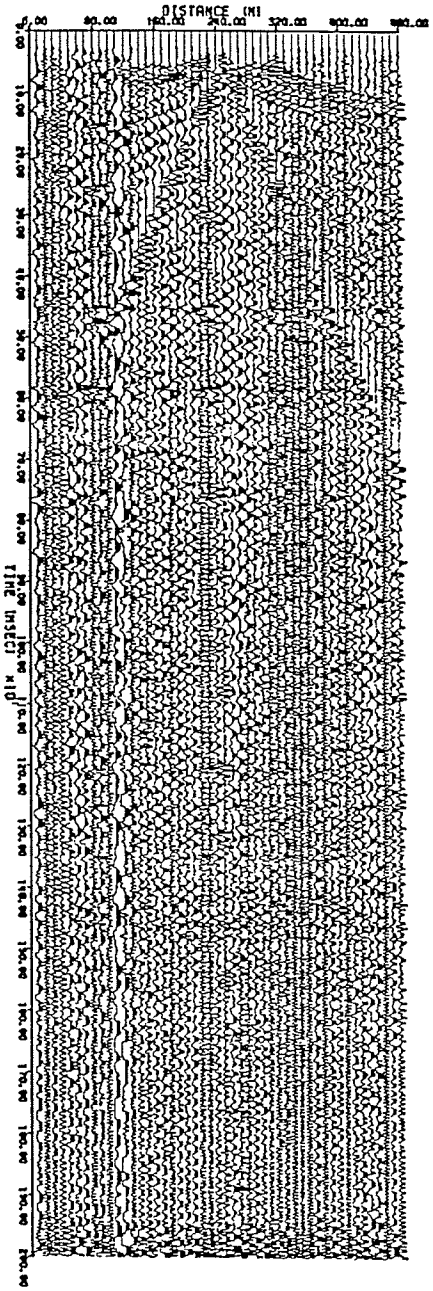

SUDBURY LINE S-1 85
REC = 28 (STN. = 87)

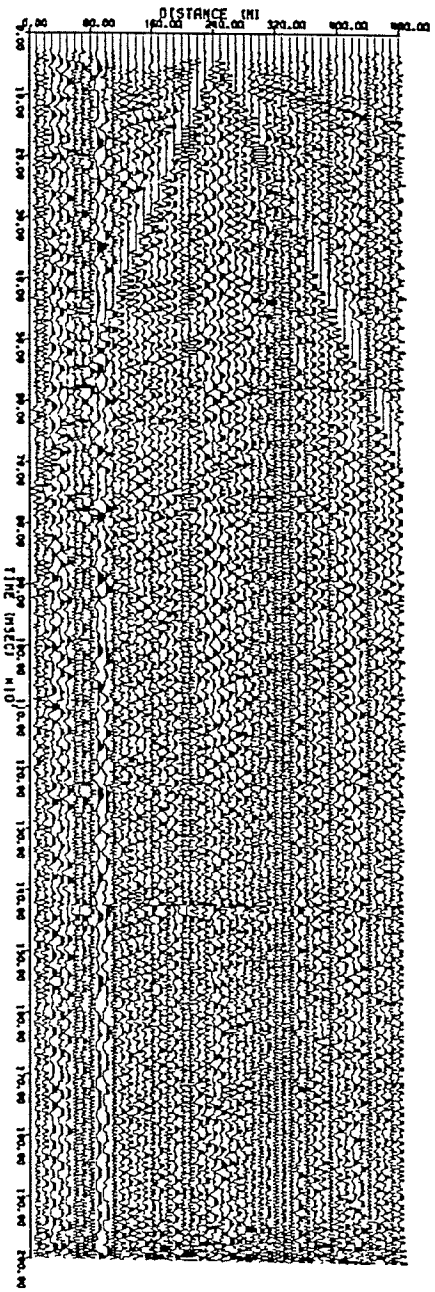

SUDBURY LINE S-1 85
REC = 29 (STN. = 89)

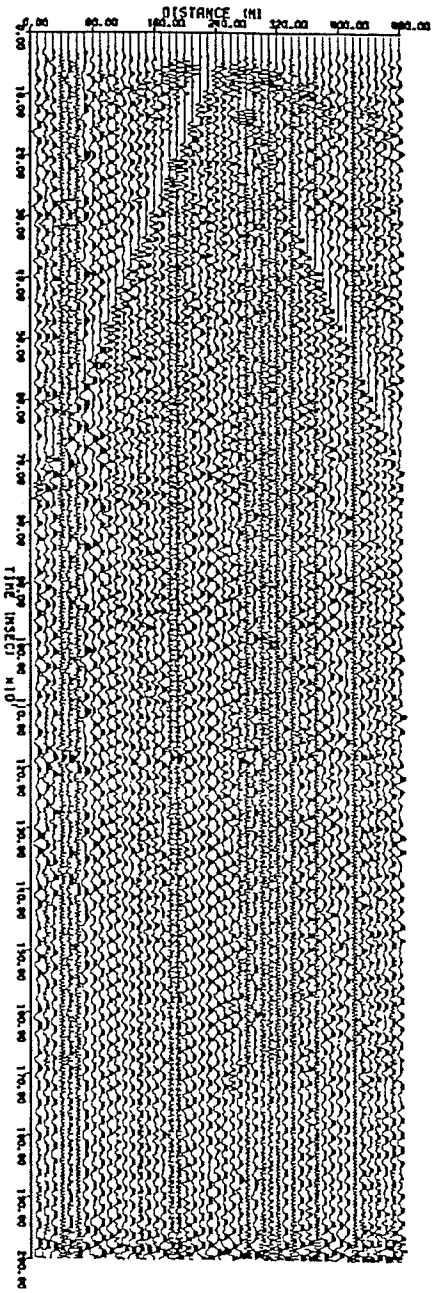

SUDBURY LINE S-1 85
REC = 30 (STN. = 91)

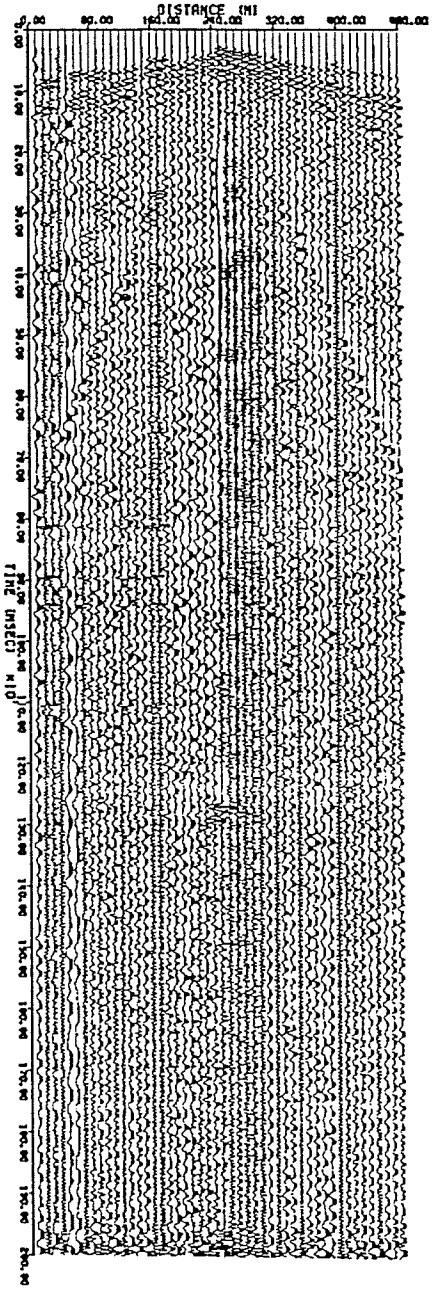

SUDBURY LINE S-1 85
REC = 91 (STN. = 93)

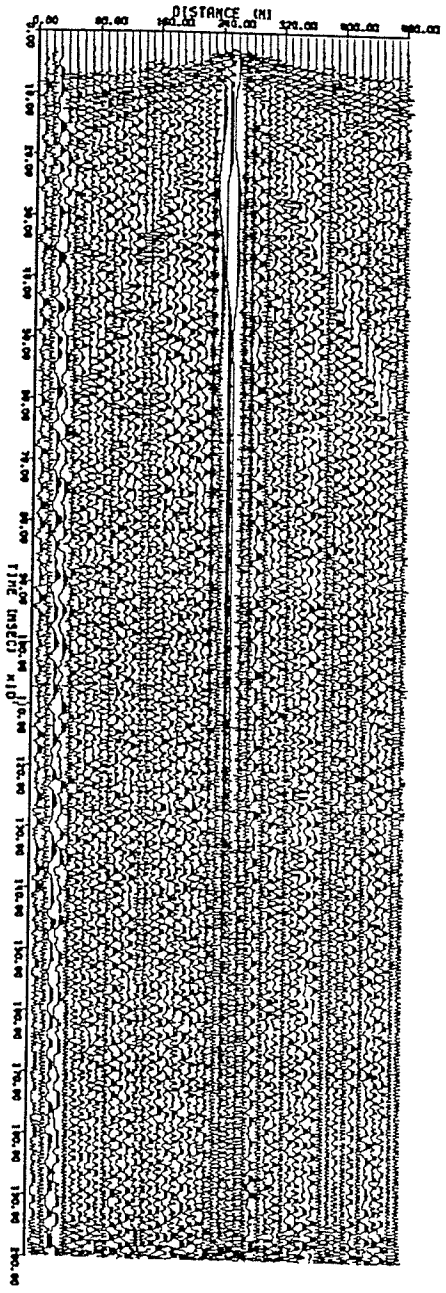

SUDBURY LINE S-1 85
REC = 92 (STN. = 95)

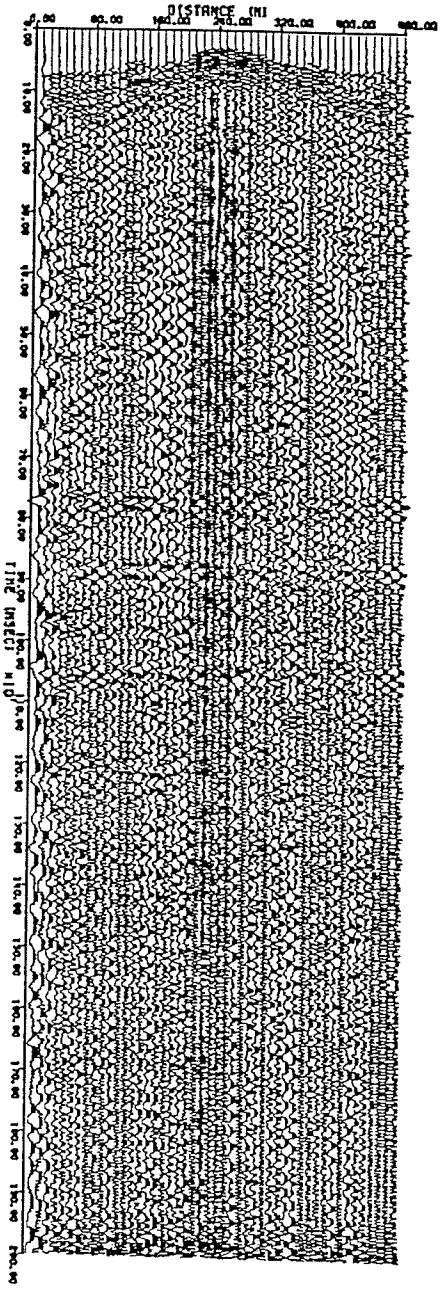

SUDBURY LINE S-1 85
REC = 33 (STN. = 97)

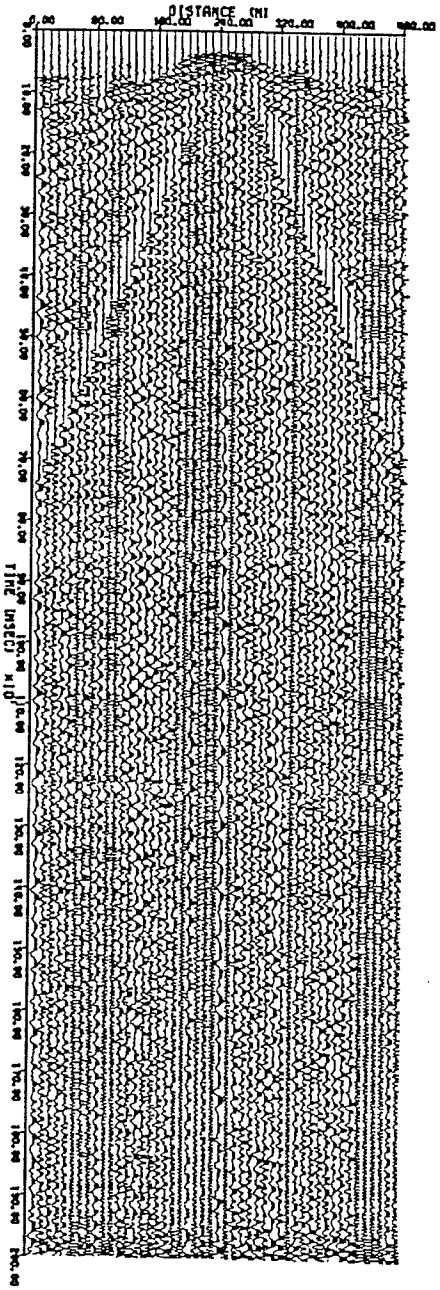

SUDBURY LINE S-1 85
REC = 34 (STN. = 99)

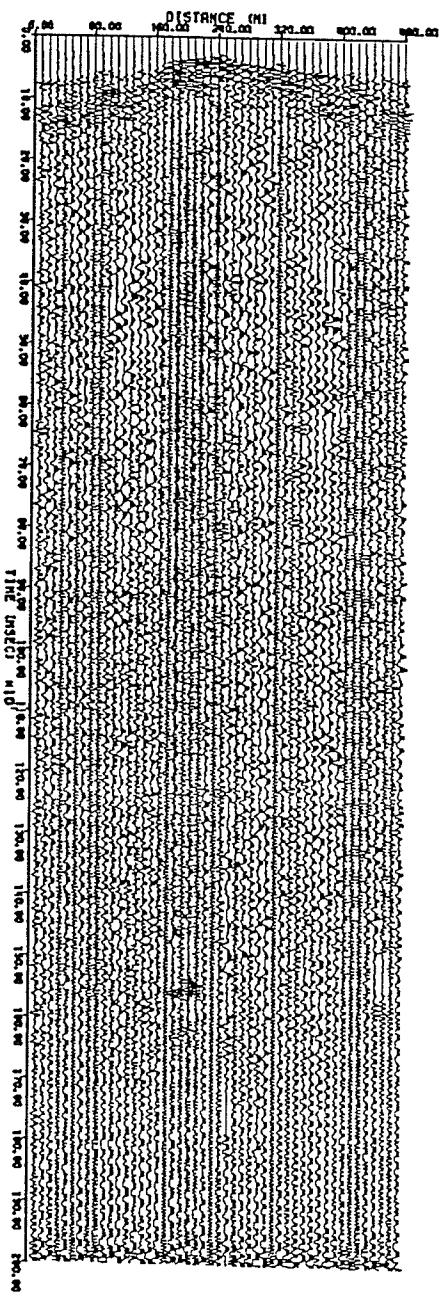

SUDBURY LINE S-1 85
REC = 33 (STN. = 97)

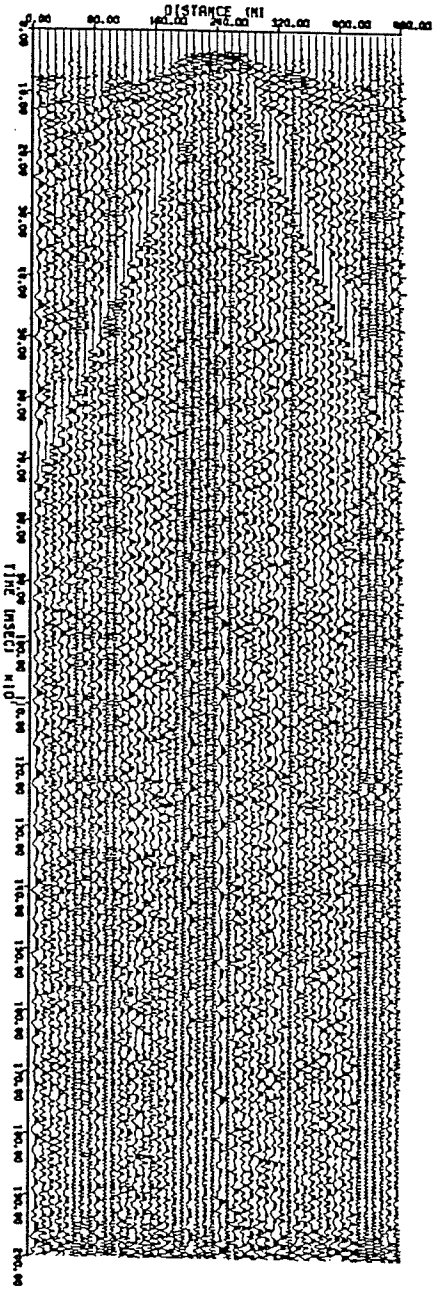

SUDBURY LINE S-1 85
REC = 34 (STN. = 99)

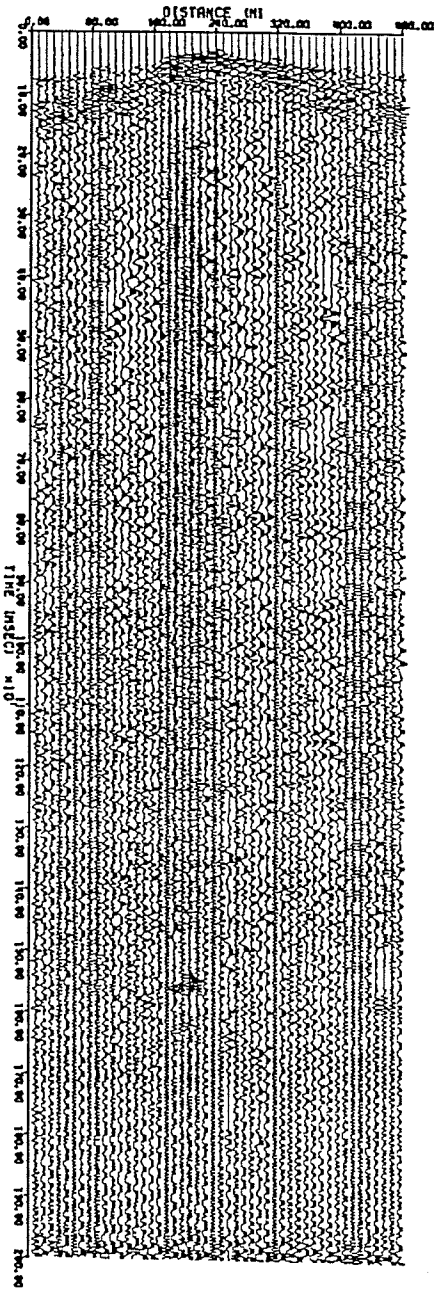

SUDBURY LINE S-1 85
REC = 35 (STN. = 101)

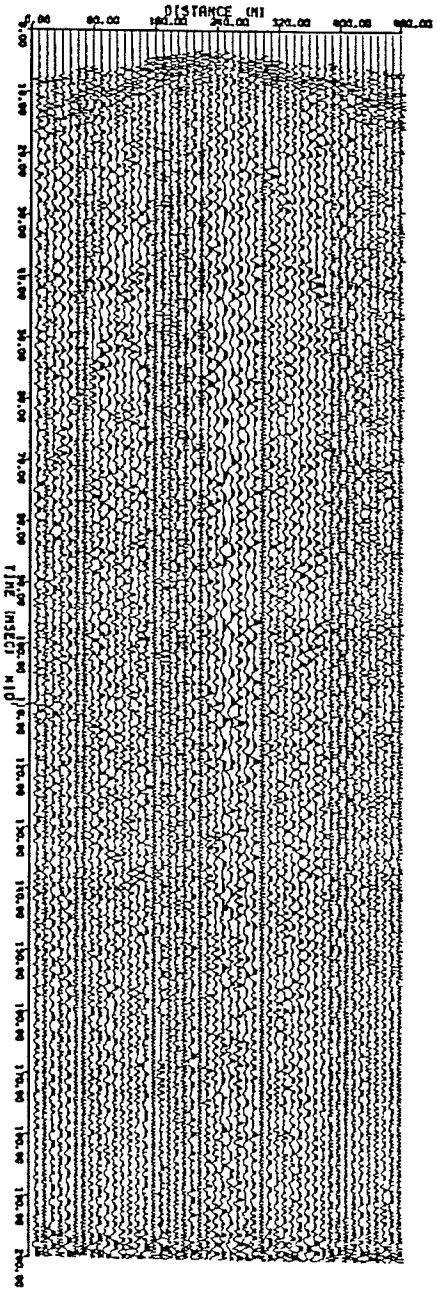

SUDBURY LINE S-1 85
REC = 36 (STN. = 103)

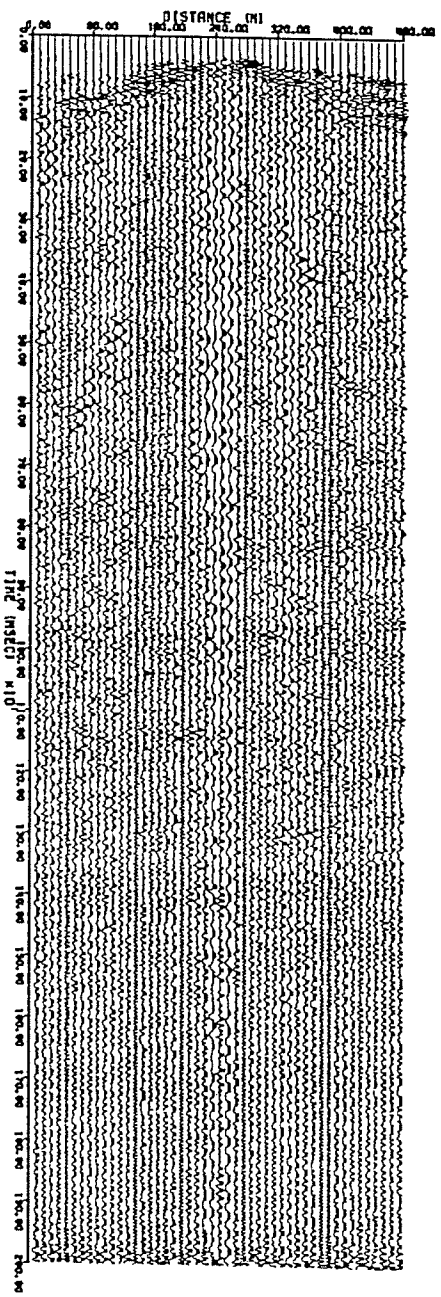

SUDBURY LINE S-1 85
REC = 37 (STN. = 105)

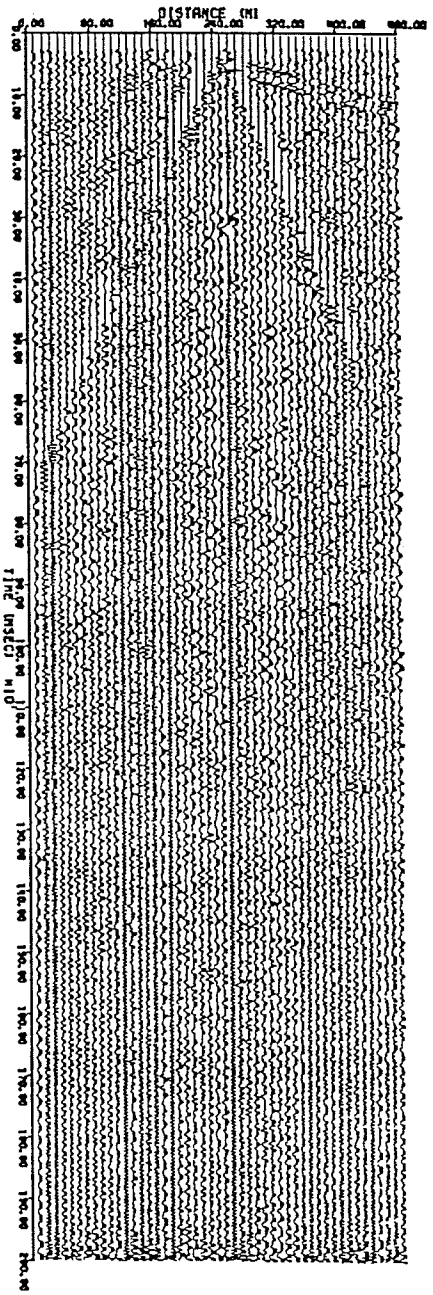

SUDBURY LINE S-1 85
REC = 38 (STN. = 107)

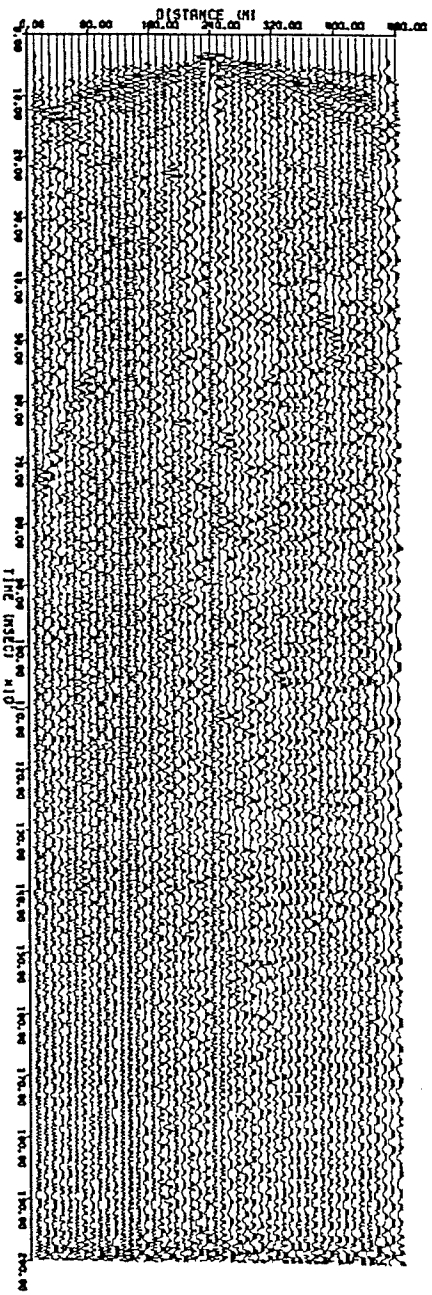

SUDBURY LINE S-1 85
REC = 39 (STN. = 109)

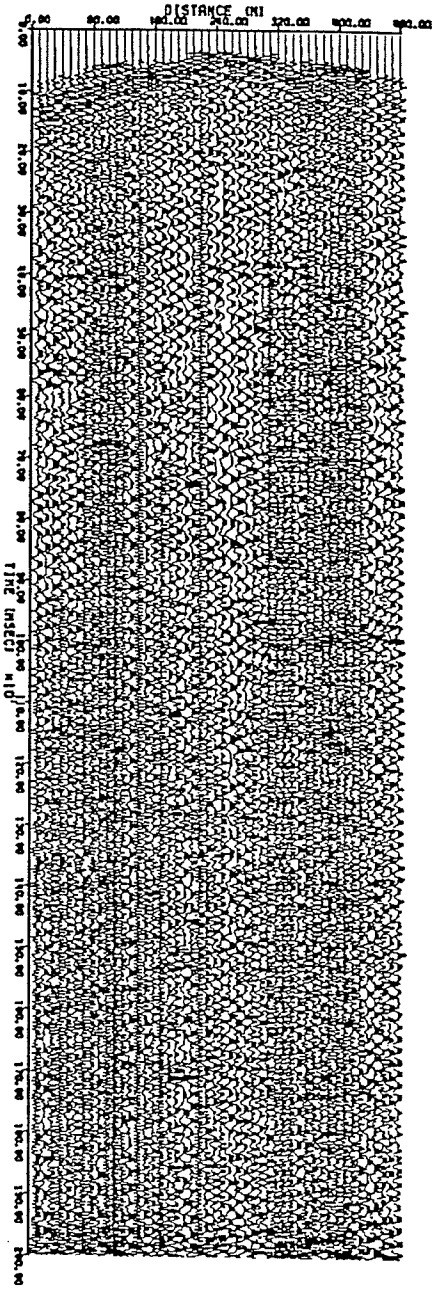

SUDBURY LINE S-1 85
REC = 40 (STN. = 111)

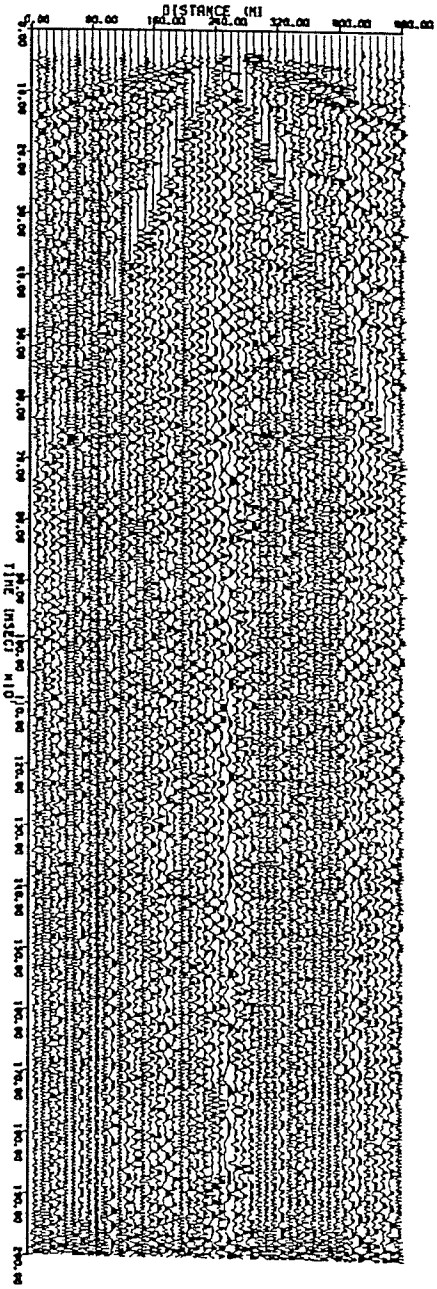

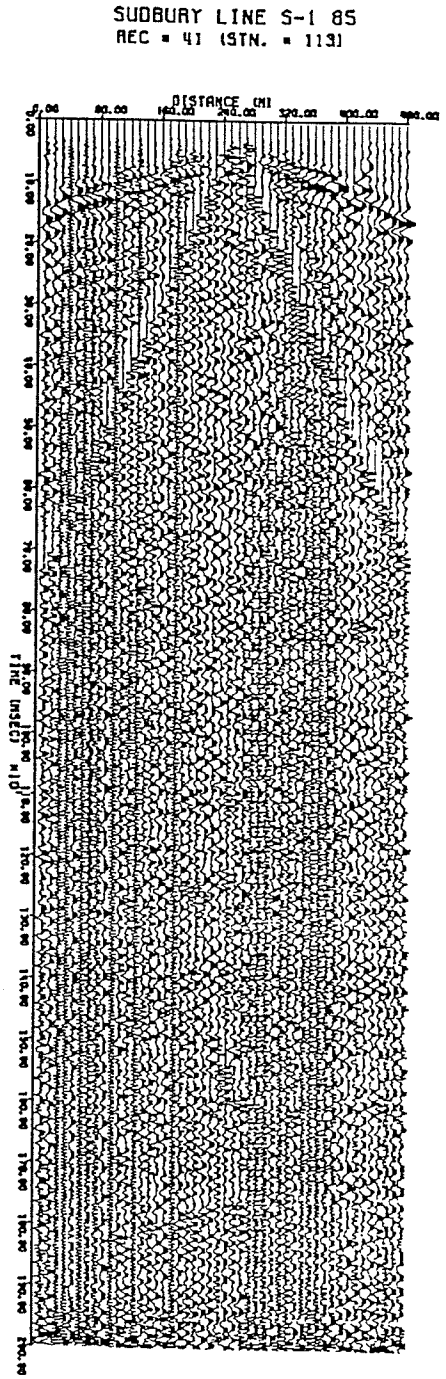
SUDBURY LINE S-1 85
REC = 41 (STN. = 113)
DISTANCE (MI

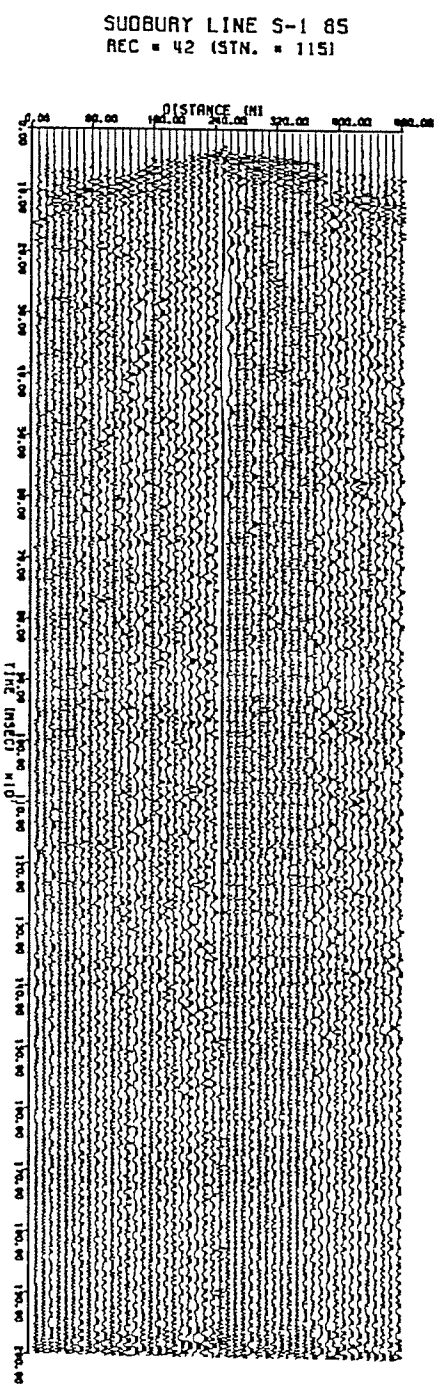
SUDBURY LINE S-1 85
REC = 42 (STN. = 115)
DISTANCE (MI

SUDBURY LINE S-1 85
REC = 43 (STN. = 117)

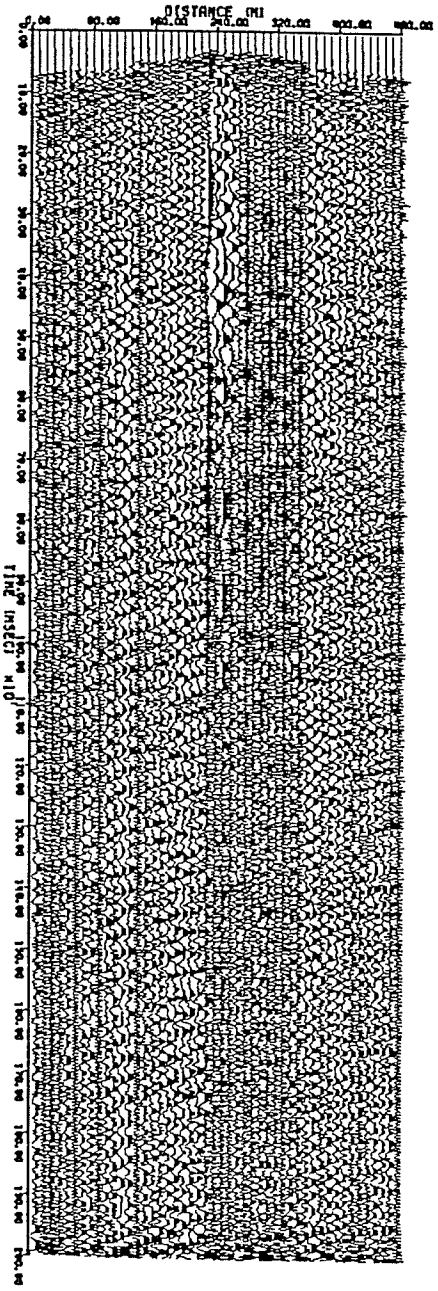

SUDBURY LINE S-1 85
REC = 44 (STN. = 119)

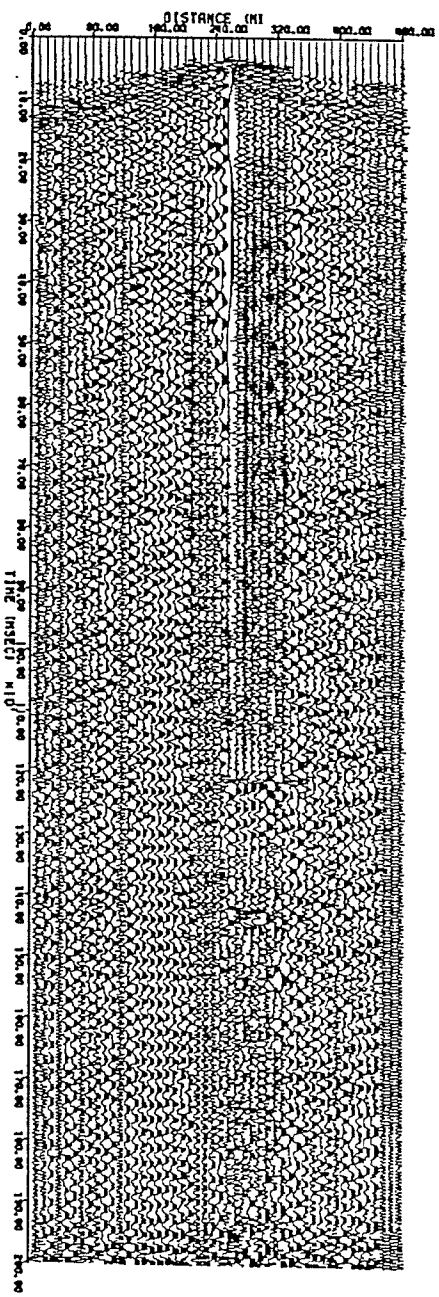

SUDBURY LINE S-1 85
REC = 45 (STN. = 121)

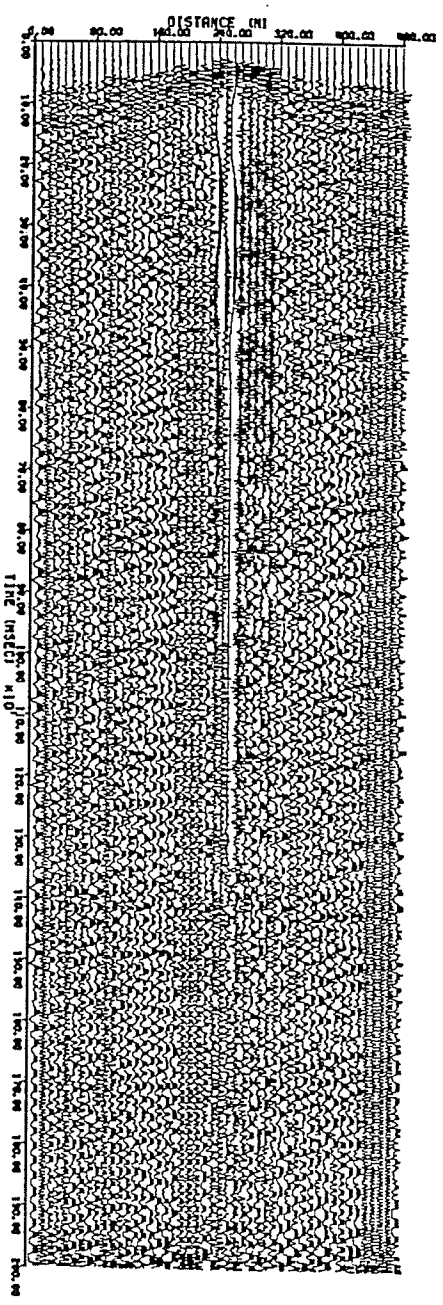

SUDBURY LINE S-1 85
REC = 46 (STN. = 123)

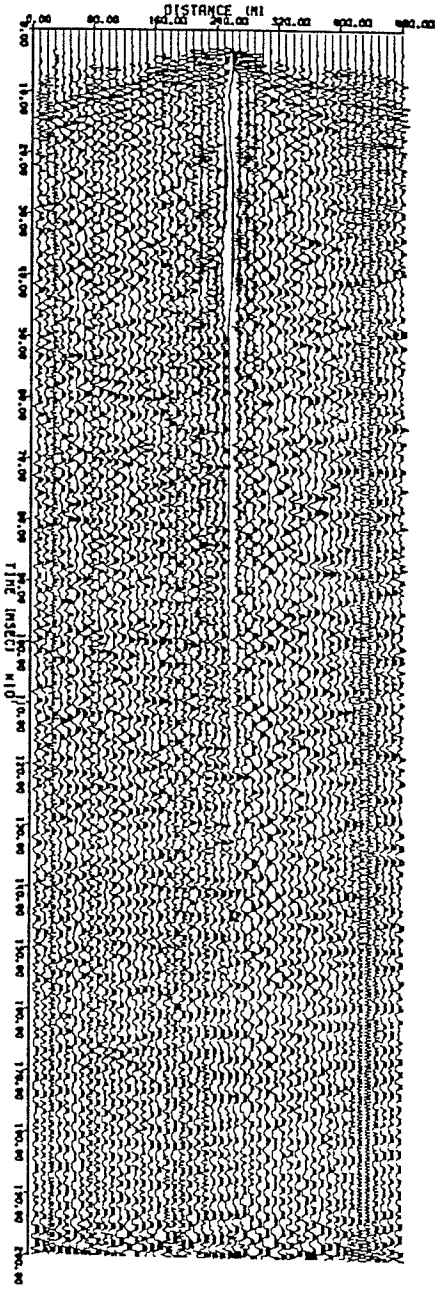

SUDBURY LINE S-1 85
REC = 47 (STN. = 125)

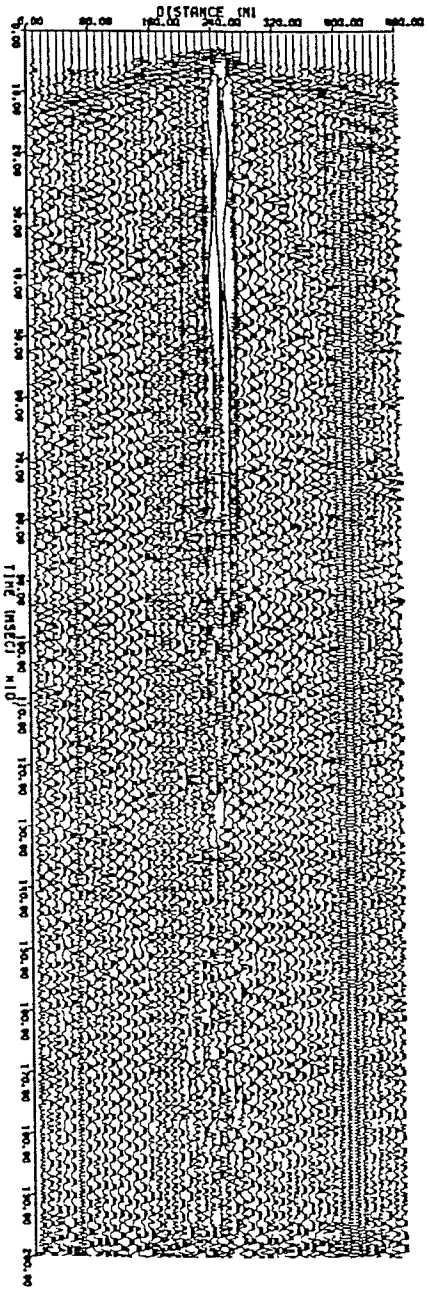

SUDBURY LINE S-1 85
REC = 48 (STN. = 127)

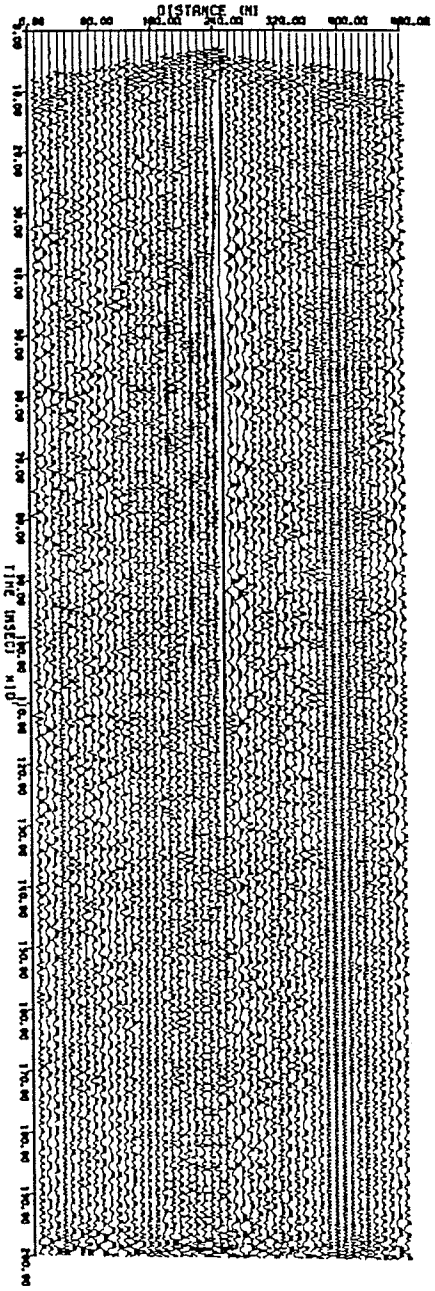

SUDBURY LINE S-1 85
REC = 49 (STN. = 129)

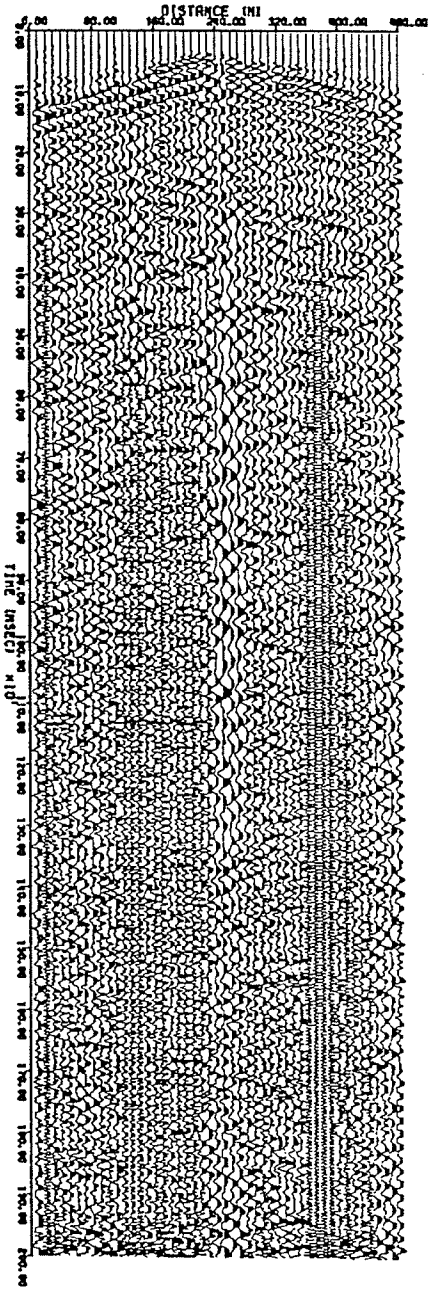

SUDBURY LINE S-1 85
REC = 50 (STN. = 131)

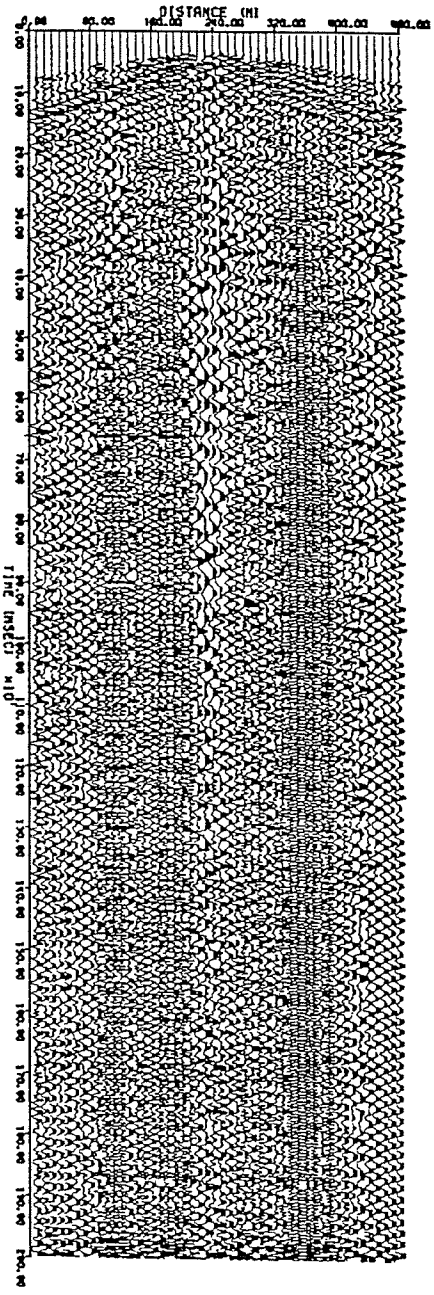

SUDBURY LINE S-1 85
REC = 51 (STN. = 133)

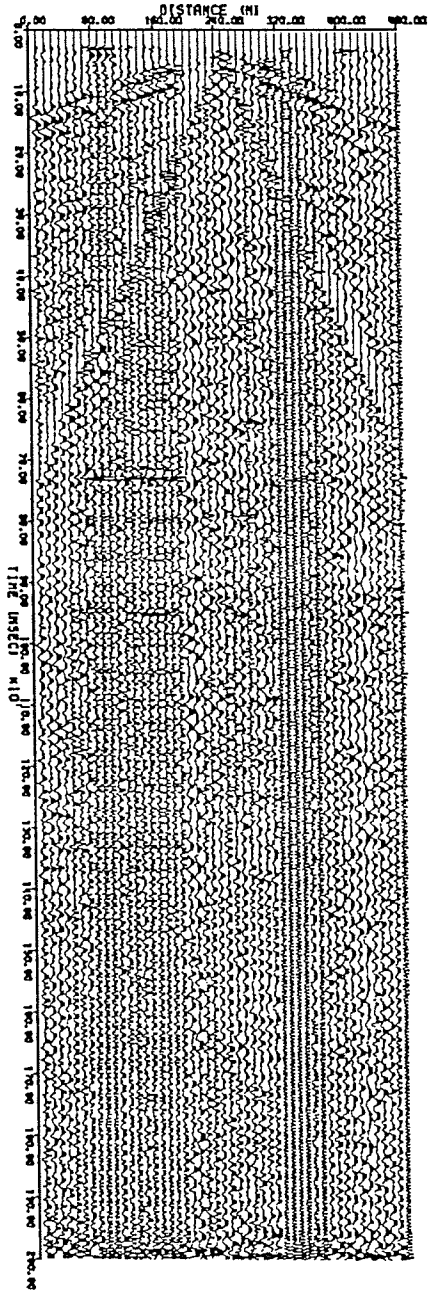

SUDBURY LINE S-1 85
REC = 52 (STN. = 135)

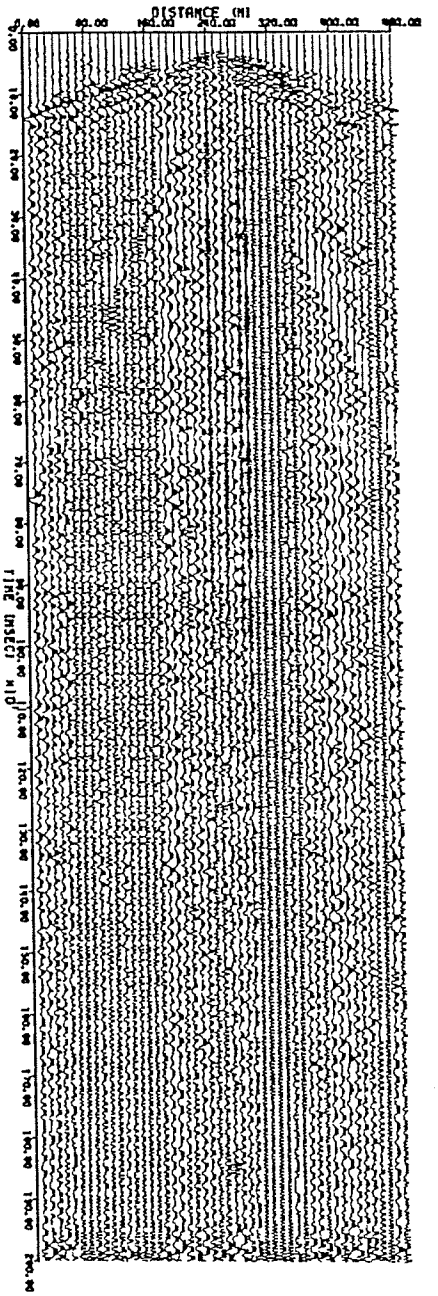

SUDBURY LINE S-1 85
REC = 53 (STN. = 137)

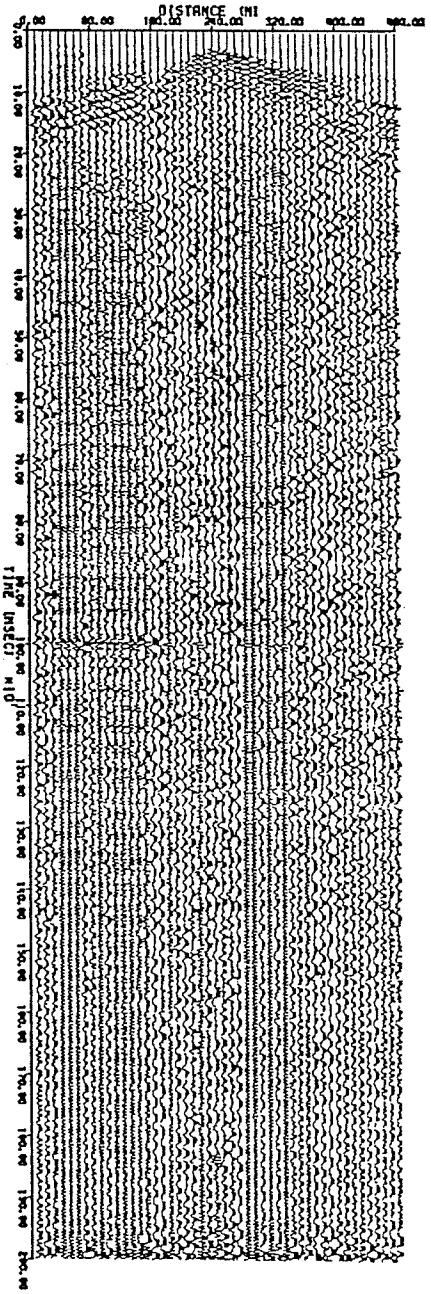

SUDBURY LINE S-1 85
REC = 54 (STN. = 139)

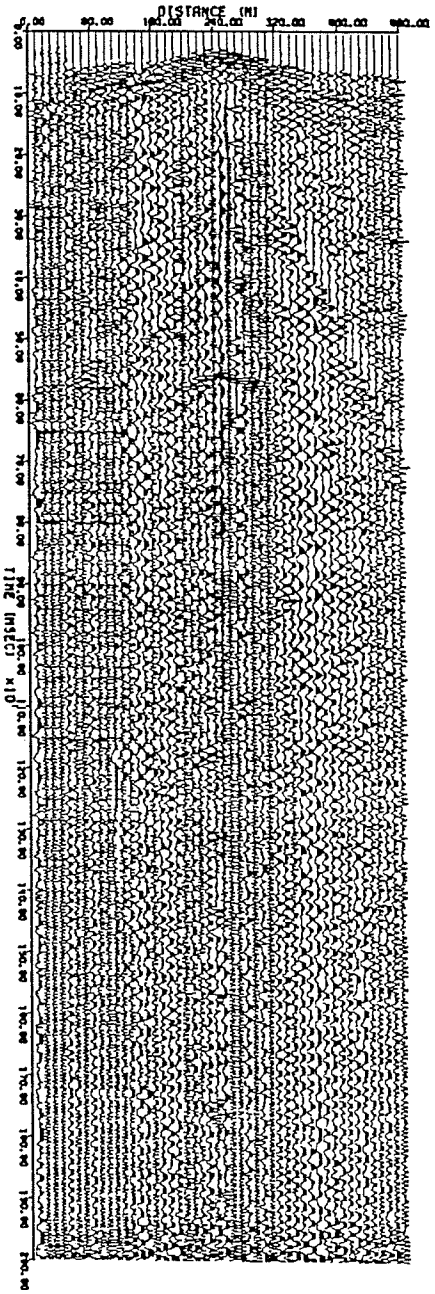

SUDBURY LINE S-1 85
REC = 55 (STN. = 141)

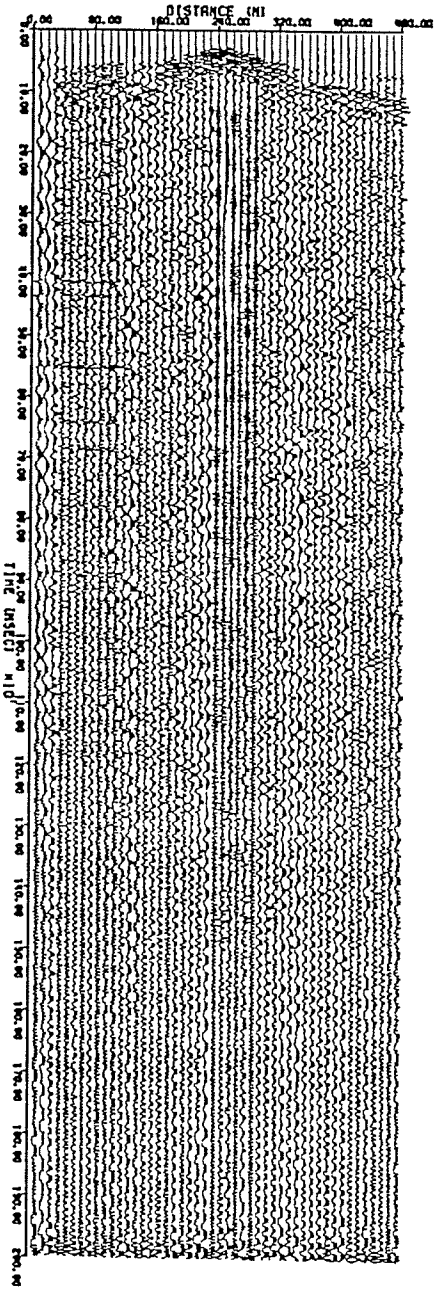

SUDBURY LINE S-1 85
REC = 56 (STN. = 143)

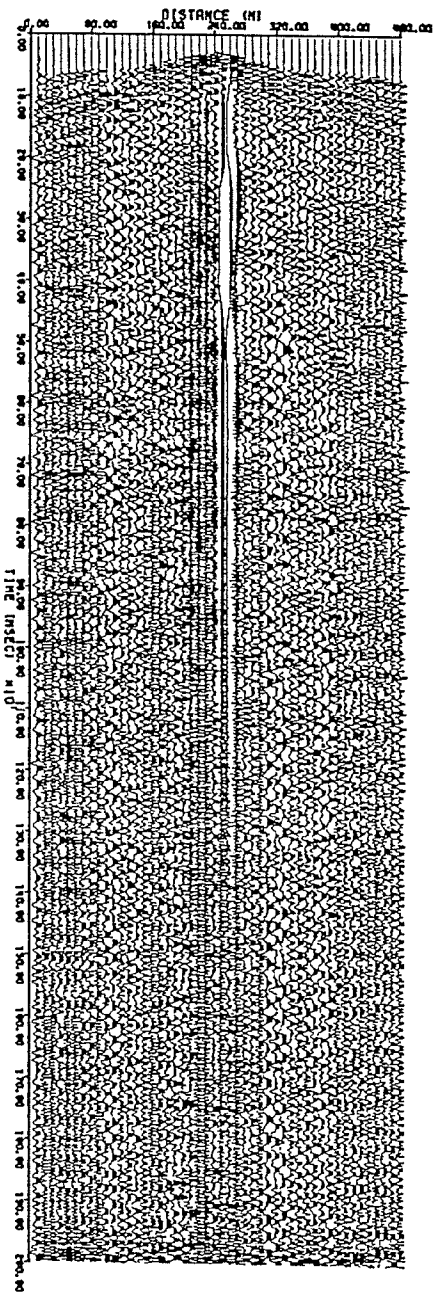

SUDBURY LINE S-1 85
REC = 57 (STN. = 145)

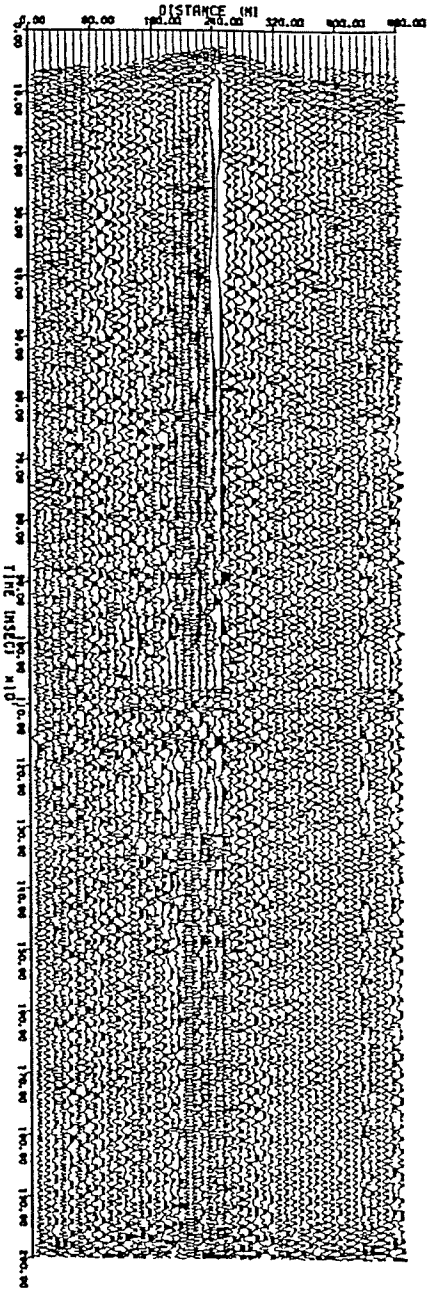

SUDBURY LINE S-1 85
REC = 58 (STN. = 147)

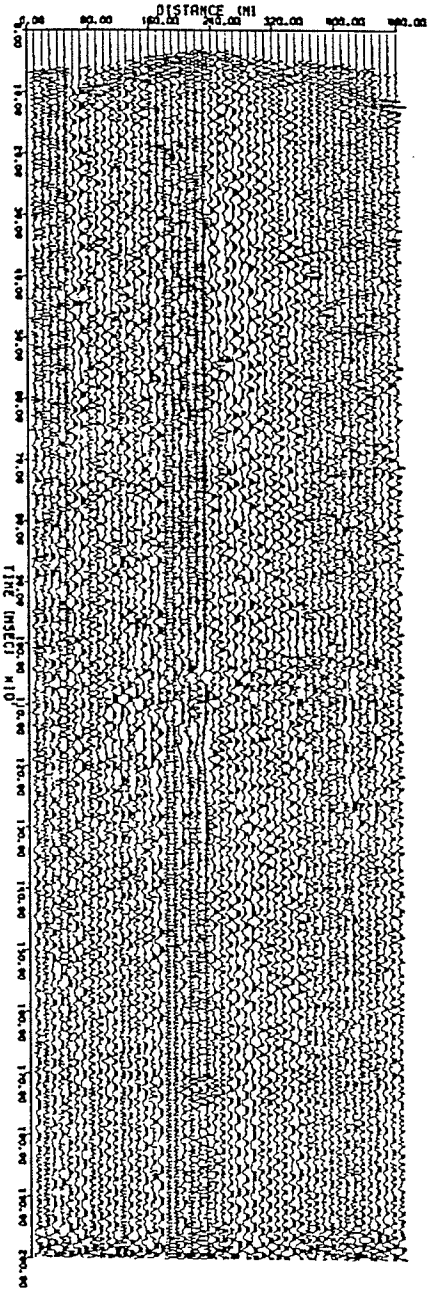

SUDBURY LINE S-1 85
REC = 59 (STN. = 149)

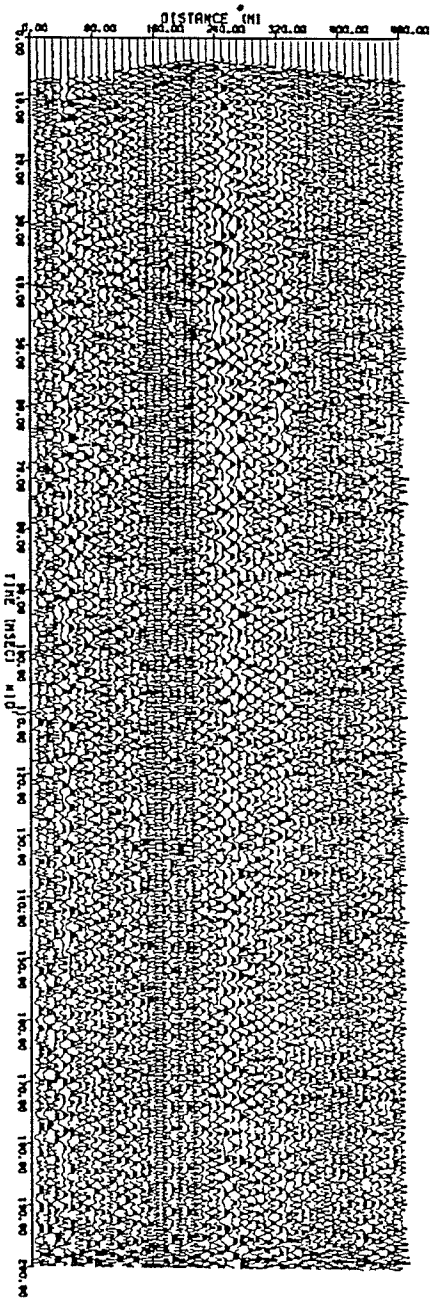

SUDBURY LINE S-1 85
REC = 60 (STN. = 151)

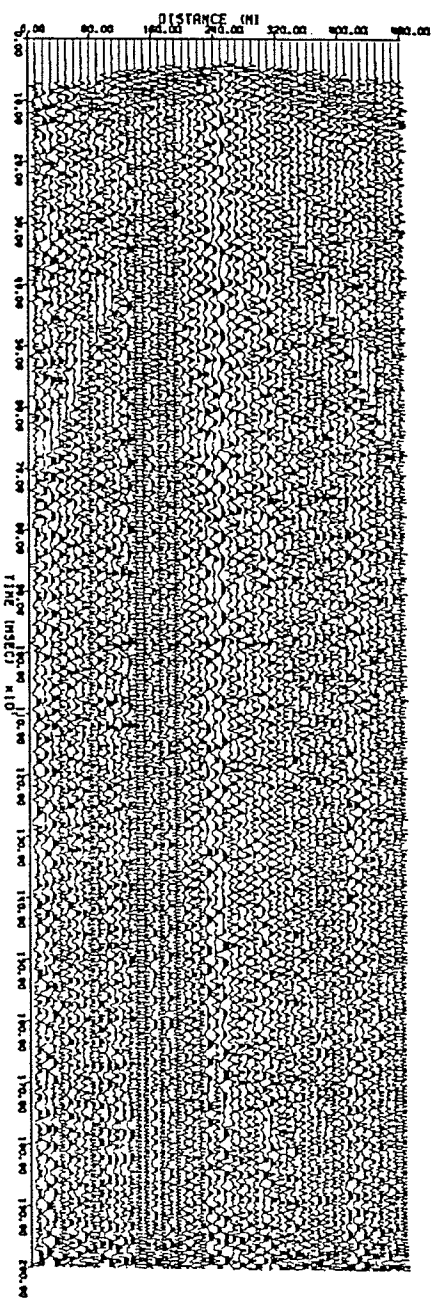

SUDBURY LINE S-1 85
REC = 61 (STN. = 153)

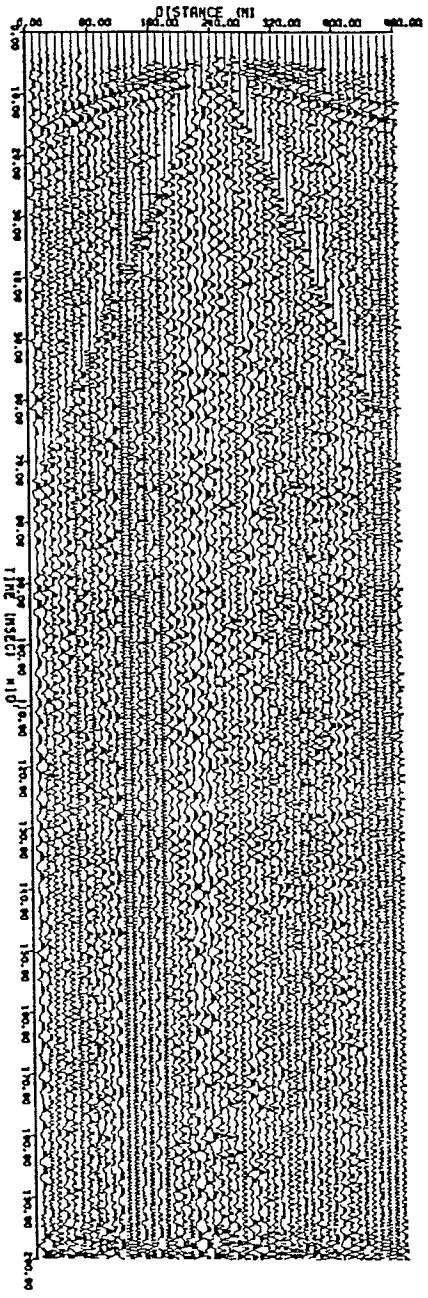

SUDBURY LINE S-1 85
REC = 62 (STN. = 155)

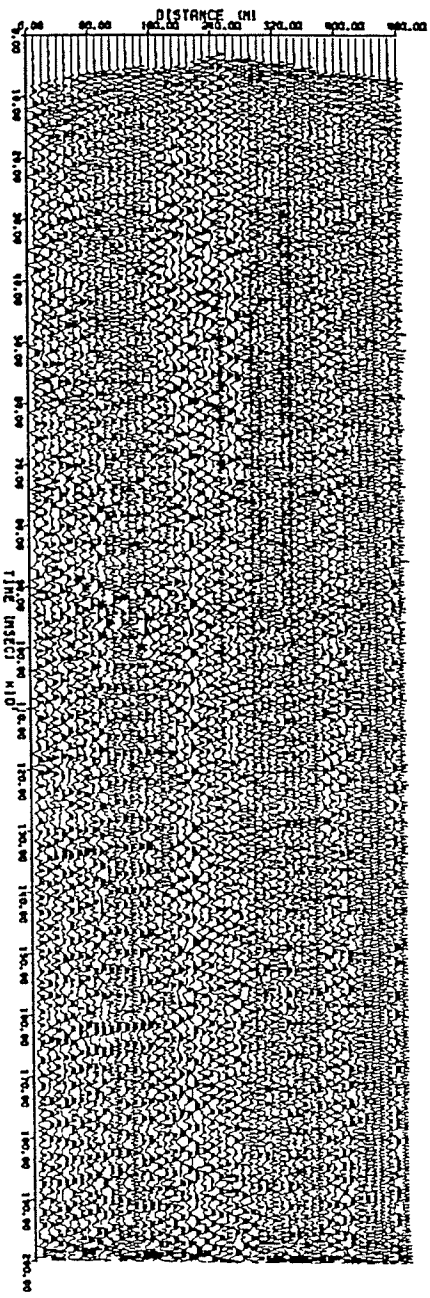

SUDBURY LINE S-1 85
REC = 63 (STN. = 157)

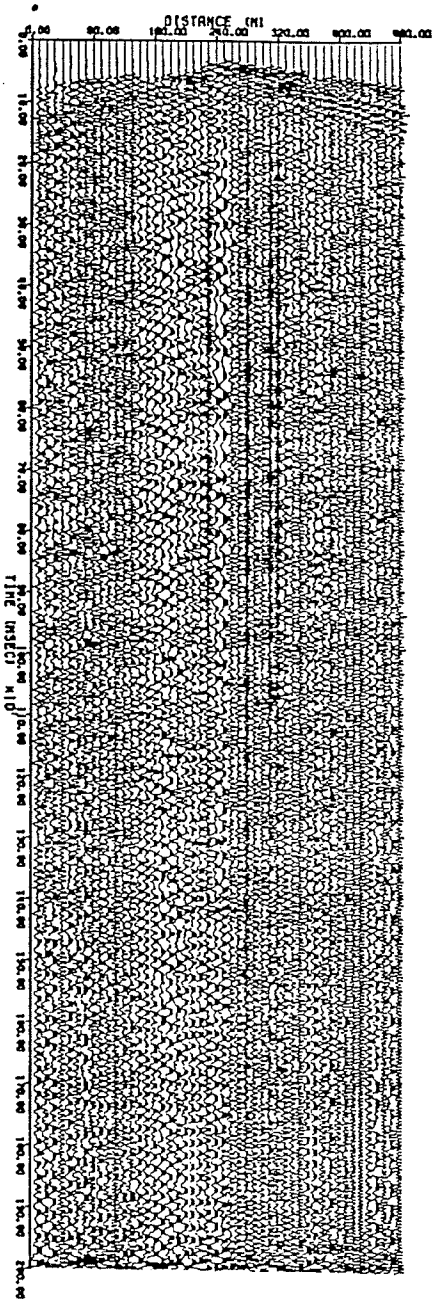

SUDBURY LINE S-1 85
REC = 64 (STN. = 159)

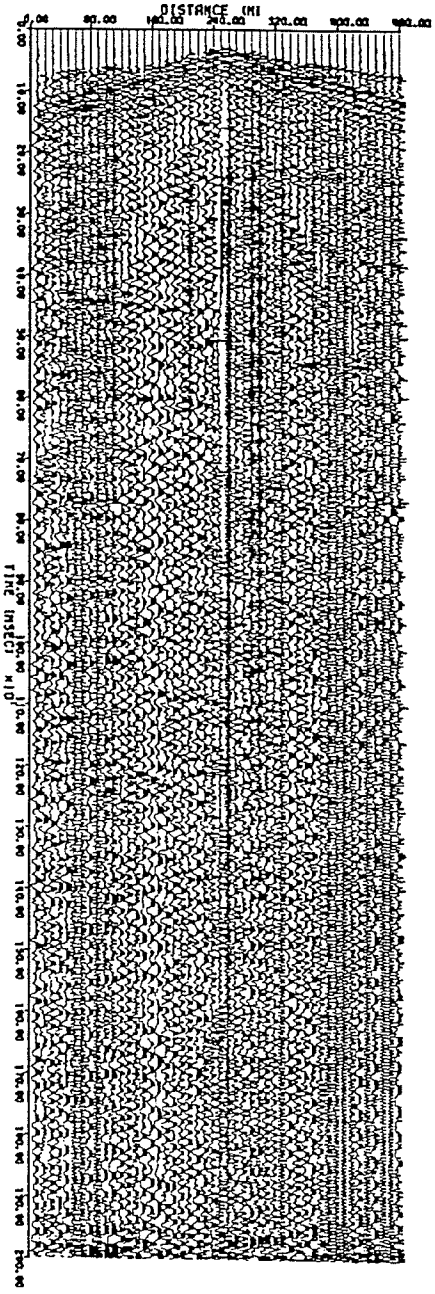

SUDBURY LINE S-1 85
REC = 65 (STN. = 161)

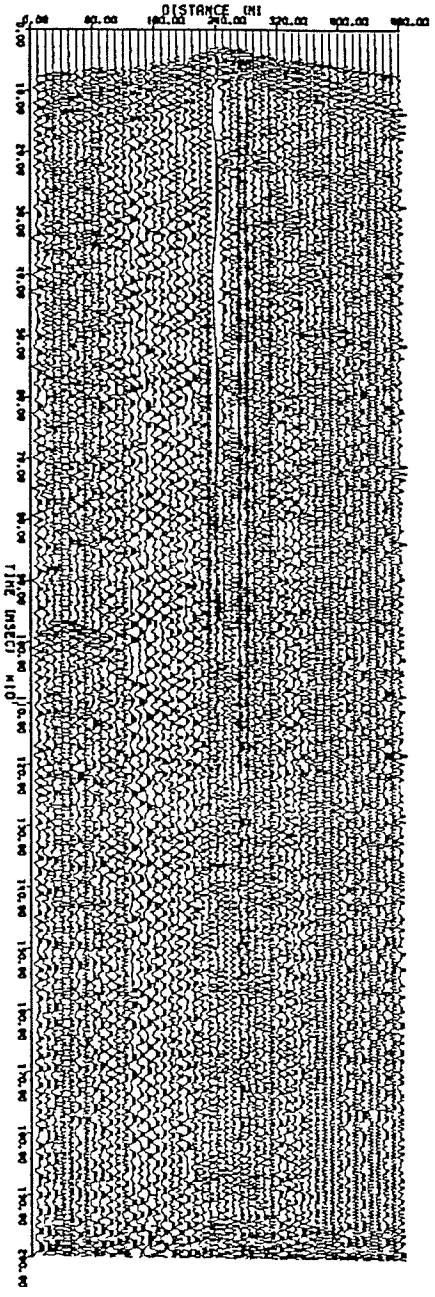

SUDBURY LINE S-1 85
REC = 66 (STN. = 163)

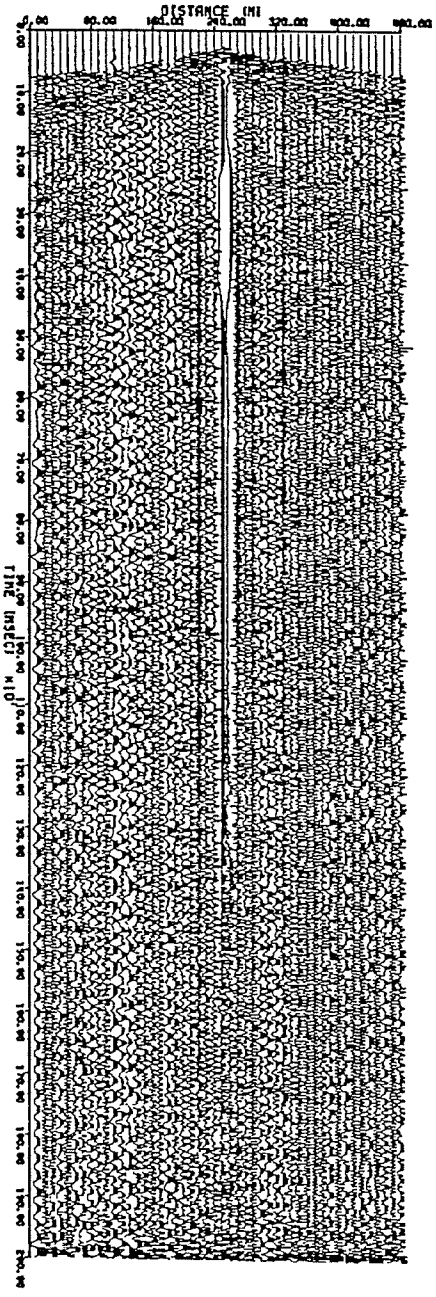

SUDBURY LINE S-1 85
REC = 67 (STN. = 165)

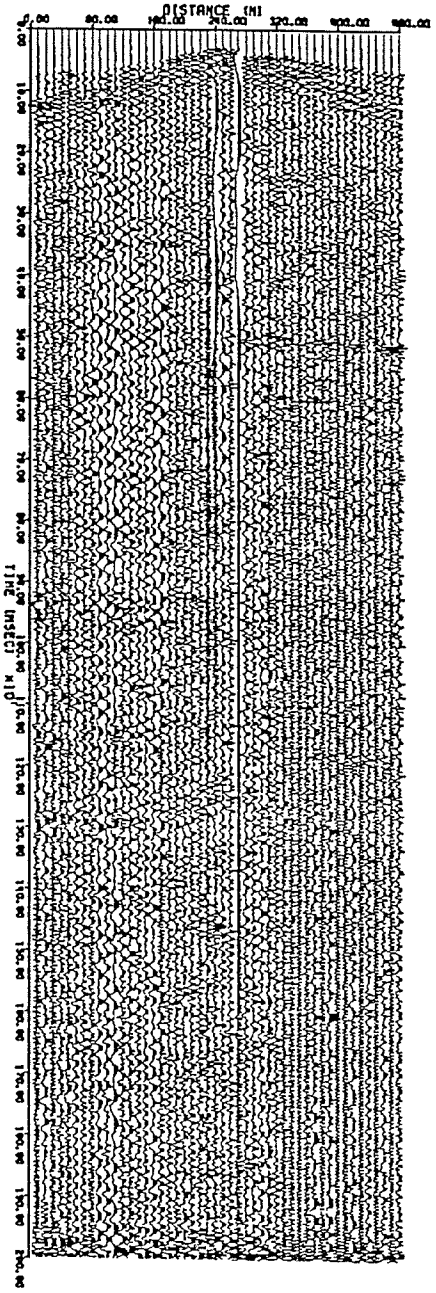

SUDBURY LINE S-1 85
REC = 68 (STN. = 167)

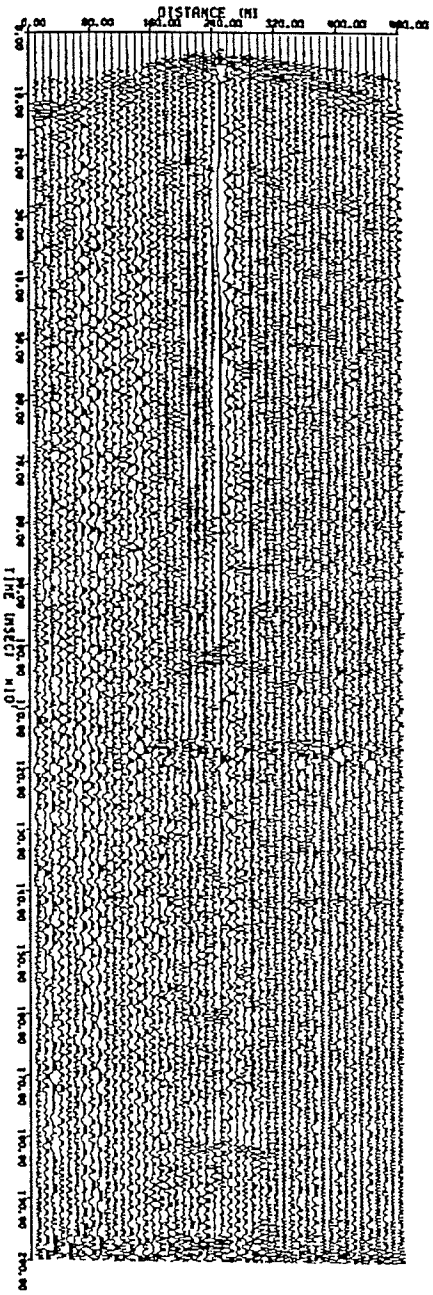

Appendix C

Copy of the manuscript for the algorithm Dip-moveout by Fourier transform

This following paper was published in *Computer Physics Communications* Journal (Serzu and Moon, 1989(b)). The accompanying computer program in Fortran can obtained from the Computer Program Library section of the Computer Physics Communications. The paper deals with software development for partial prestack migration discussed in chapter 4 of this thesis.

Dip Moveout by Fourier Transform

Mulugeta H. Serzu
and
Wooil M. Moon

Geophysics
The University of Manitoba
Winnipeg Manitoba R3T 2N2
Canada

April 4, 1988

Abstract

Seismic reflection survey is primarily designed to determine subsurface geological structures from the data recorded at the surface. Processing of seismic data undergoes several digital processing and beam forming steps, first to enhance the signal-to-noise ratio and then to construct the final digital image which is physically correct and geologically meaningful. Dip-moveout (prestack partial migration) is a processing step which corrects the dip filtering action of normal moveout (NMO) and stacking. Dip-moveout (DMO) eliminates the reflection point scattering associated with dipping reflectors by shifting the reflection event to its zero offset location.

In recent years several dip-moveout methods have been discussed in literature. This paper presents a DMO program (FORTRAN) and its long write-up based on the "Dip-moveout by Fourier transform" by Hale [7]. The program was tested with theoretical synthetic seismic data in which the expected DMO operator response was simulated.

Program Summary

Title of program : DMO

Computer : Amdahl 5870

Operating system : 370 MVS3

Programming language : VS Fortran 77

High speed storage required : the core memory requirement depends on size of the data. For 128×128 data matrix, the core memory requirement is 600K.

Number of bits on a byte : 8

Peripherals used : terminal, printer (line printer/Xerox laser printer)

Number of lines in the program : 841

Keywords : Dip-moveout (DMO), prestack partial migration, zero offset, common offset, common midpoint, common depth point, half offset, 2–D FFT.

Nature of physical problem

A surface linear recording array (multichannel) receives seismic reflection signals in such a way that the CDP display misplaces the dipping reflectors. Dip moveout corrects spatial distortion in the 2–D datasets.

Method of solution

The dip-moveout program is computd using Hale's method [7] in the frequency-wave-number $(f-k)$ domain. The transformation from the time-space $(t-y)$ domain to the $(f-k)$ domain is accomplished using a double integral. The integral with respect to the spatial variable is evaluted using 1–D fast Fourier transform, and the second integral with respect to the time variable is evaluated numerically using Simpson's method. The transformation

from the $f-k$ to the $t-y$ domain is performed using 2–D FFT.

Restrictions on the complexity of the program

The dimensions of the data matrix to be transformed have to be powers of 2. The data must be reordered into a constant offset section. Each constant offset section must be computed separately and placed back into a mass storage. When DMO processing involves a constant offset section too large to fit into the system's core memory, the 2–D FFT subroutine may be replaced by the stepwise 2–D FFT subroutine given by Serzu and Moon (1988) or any other similar subroutines.

Typical running time

For 128 by 128 data matrix (including plotting time)

Dip Moveout (DMO) : takes 1.0 minute and 18 seconds.

Long Write–up

Introduction

In the multichannel data processing, horizontal stacking consists of the summation of the traces of each common mid–point (CMP) gather after the normal moveout (NMO) correction. This CMP stacking improves signal-to-noise ratio by enhancing reflections with a particular slope while attenuating reflections with different slopes. The NMO velocity for a dipping reflector is greater than that for a horizontal reflector. This has been shown by Levin (1971) :

$$v_{NMO} = \frac{v}{\cos\phi} \tag{1}$$

where, ϕ is the reflector dip associated with the direction of source receiver offset. Equation (1) implies that the NMO correction for dipping events is best performed using a velocity v_{NMO} that is higher than the true velocity v. Unfortunately the conventional NMO and stack allow one choice of v for a particular CMP and travel time. As shown in figure 1, the reflection point dispersal associated with a dipping reflector increases as square of the half offset. In structurally complex formations, the correction of all dip angles becomes impossible and horizontal stacking loses its usefulness, and a fewer number of stacks are tolerated before the quality of the data is deteriorated rather than being enhanced. Under this circumstance migration before stack is the alternative.

Migration before stack has a sound theoretical foundation. However direct implementation requires simultaneous migration of large sets of common offset gathers. The large amount of computer memory and computing time required in migration before stack makes the technique very expensive and less practical. Migration before stack is a one-step process, and does not provide any intermediate results such as a CMP stacked section, which helps to identify false events on the migrated section.

To overcome some of the disadvantages of migration before stack a number of special purpose prestack techniques such as *DEVILISH* (dipping events velocity inequality licked by Sherwood), *prestack partial migration* (PSPM), *offset continuation*, *dip-moveout by Fourier transform*...etc. have been developed to suppress the dip selectivity of the NMO and stacking. Prestack partial migration process when combined with the conventional processing sequence yields approximately the result of the costly full migration before stack.

The approximations made in deriving the *Finite Difference* DMO algorithms ([2],[16]) break down at large offsets and steep dips. The prestack partial migration program being presented in this paper is based on Fourier transform implematation of the DMO theory

(Hale [7]). Constant NMO velocity is the only assumption made in developing DMO by Fourier transform. Unlike the finite difference counterparts, this algorithm is accurate for all dips and offsets.

Method of solution

Dip moveout theory

Consider a seismic experiment conducted over a constant velocity half–space having a single dipping reflector as shown in Fig. 1. Let us define the following variables :

ϕ – dip of reflector

h – half offset

t_o – zero offset two way travel time

t – travel time from source to receiver

v – velocity of the medium.

y – source receiver mid-point

y_o – the point where the dipping reflector meets the surface.

From triangle $ss'r$ the travel time t of the reflection from the dipping reflector can be written as (following the notatin of Hale [7]) :

$$t^2 = \frac{1}{v^2}\left[(\overline{ss'})^2 + (\overline{sr})^2 - 2(\overline{ss'})(\overline{sr})\cos\left(\frac{\pi}{2} + \phi\right)\right]. \qquad (2)$$

At the zero offset $s = r = y$, the travel time t_o is obtained from the triangle $y'yy_o$ where $\overline{yy'} = vt_o/2$ and

$$\sin\phi = \frac{t_o v}{2(y - y_o)} \quad , \tag{3}$$

and the zero offset travel time becomes

$$t_o = \frac{2}{v}(y - y_o)\sin\phi. \tag{4}$$

If we substitute equation (3) into (2) we obtain the Levin's NMO expression corrected for dip :

$$t = \sqrt{t_o^2 + \frac{4h^2\cos^2\phi}{v^2}}. \tag{5}$$

Let $p(t, y, h)$ denote seismograms recorded as a function of time t, midpoint y, and half offset h. Equation (5) then leads to the following transformation to zero offset from non-zero offset seismograms $p(t, y, h)$

$$p_o(t_o, y, h) = p\left(\sqrt{t_o^2 + \frac{4h^2\cos^2\phi}{v^2}}, y, h\right) \tag{6}$$

The dip corrected NMO may be performed in two steps. First we rewrite equation (5), the dip corrected NMO, as follows :

$$t = \sqrt{t_o^2 + \frac{4h^2}{v^2} - \frac{4h^2\sin^2\phi}{v^2}}. \tag{7}$$

No approximation have been made in deriving the above expression and it is accurate for small ϕ and dips up to 90°. The dip-moveout term in equation (7) is significant for large

offsets and steep dips and very minor for a gently dipping reflector. Substituting equation (4) into equation (5) and taking

$$\sin^2\phi + \cos^2\phi = 1 \tag{8}$$

NMO without dip correction becomes :

$$t = \sqrt{t_n^2 + \frac{4h^2}{v^2}} \tag{9}$$

where, t_n is the NMO time. From equation (5) and (9) we obtain another expression for dip corrected NMO time t_o :

$$t_n = \sqrt{t_o^2 - \frac{4h^2\sin^2\phi}{v^2}} \tag{10}$$

Equations (9) and (10) imply that the dip corrected NMO given in equation (6) may be evaluated in two steps : First use equation (9) to define NMO as :

$$p_n(t_n, h, y) = p\left(\sqrt{t_n^2 + \frac{4h^2}{v^2}}, y, h\right) \tag{11}$$

and then use equation (10) to define dip moveout (DMO) as :

$$p_o(t_o, y, h) = p_n\left(\sqrt{t_o^2 + \frac{4h^2\sin^2\phi}{v^2}}, y, h\right). \tag{12}$$

NMO is the transformation from recording time t to NMO time t_n . DMO is the transformation from NMO time t_n to zero offset time t_o .

Consider an example shown in Fig. 2 as a zero offset section. The slope of the reflection is given by :

$$\frac{\Delta t_o}{\Delta y} = \frac{2\sin\phi}{v}. \tag{13}$$

Substituting equation (13) into equation (12) we have

$$p_o(t_o, y, h) = p\left(\sqrt{t_o^2 - (\Delta t_o/\Delta y)^2\, h^2}, y, h\right) \tag{14}$$

where the evaluation of the DMO equation (14) does not require knowledge of velocity or dip. However equation (14) is impractical as $\Delta t_o/\Delta y$ must be obtained from the zero offset data. Another problem is that conflicting dips may exist for different events at given (t_o, y).

Equation (14) implies that a different DMO correction is needed for each different zero offset slope $\Delta t_o/\Delta y$. 2-D Fourier transform of t_o–y provides a particularly useful domain to apply to a dip-dependent process, because events having a particular dip in the (t_o,y) domain map into a single radial line in the (ω_o, k)domain given by :

$$\frac{k}{\omega_o} = \frac{\Delta t_o}{\Delta y} = \frac{2\sin\phi}{v} \tag{15}$$

2-D Fourier transform of $p_o(t_o, y, h)$ (ie. zero offset) is defined by :

$$P_o(\omega_o, k, h) = \int dt \exp(i\omega_o t_o) \int dy \exp(-iky)\, p_o(t_o, y, h) \tag{16}$$

Since we don't measure zero offset data (dip and velocity being unknown), we can express the above Fourier transform in terms of NMO data. Substituting (15) into (10) we obtain :

$$t_o = \sqrt{t_n^2 + \frac{4h^2 \sin^2\phi}{v^2}}$$

$$= \sqrt{t_n^2 + \left(\frac{\Delta t_o}{\Delta y}\right)^2 h^2}$$

$$= \sqrt{t_n^2 + \frac{(kh)^2}{\omega_o^2}} \quad . \tag{17}$$

Define

$$A = \frac{dt_n}{dt_o} = \frac{t_o}{t_n}$$

$$= \sqrt{1 + \left(\frac{\Delta t_o}{\Delta y}\right)^2 \frac{h^2}{t_n^2}}$$

$$= \sqrt{1 + \frac{k^2 h^2}{\omega_o^2 t_n^2}} \tag{18}$$

and

$$B = \omega_o t_n A$$

$$= \omega_o \sqrt{t_n^2 + \frac{(kh)^2}{\omega_o^2}} \quad . \tag{19}$$

Substitution of equation (18) into equation (16) gives

$$P_o(\omega_o, k, h) = \int dt\, A^{-1} \exp(iB) \int dy\, \exp(-iky) p_n(t_n, y, h) \tag{20}$$

Equation (15) provides a method for applying DMO correction for each slope $\Delta t_o/\Delta y = k/\omega_o$ in the zero offset section. Inverse Fourier transform of (20) gives the zero offset section $p_o(t_o, y, h)$, that is :

$$p_o(t_o, y, h) = \int d\omega_o \, \exp(-i\omega_o t_o) \int dk \, \exp(iky) \, P_o(\omega_o, k, h). \tag{21}$$

Application of DMO by Fourier transform

(1) Apply NMO using Equation (9) with velocity estimated from velocity analysis.

(2) Reorder the data into common offset!

(3) Take 1-D FFT of the NMO corrected data with respect to midpoint y.

$$p_n(t_n, y, h) - - - \text{ 1-D FFT} - - > p_n(t_n, k, h)$$

(4) Integrate over t_n for the left hand integral in (20) for all ω_o and k to obtain $P_o(\omega_o, k, h)$.

(5) Inverse 2-D FFT of $P_o(\omega_o, k, h)$ to obtain $p_o(t_o, y, h)$ which is the zero offset section.

$$P_o(\omega_o, k, h) - - - \text{ 2-D FFT}^{-1} - - > p_o(t_o, y, h).$$

(6) Repeat steps 3–5 until all the common offset sections are processed.

Subroutines

Subroutine Name		*Description*
NMO	:	Performs the normal moveout correction. Calls subroutine SPLINE to resample the points within each trace.
SPLINE	:	Given irregularly spaced traces this routine recomputes equally spaced traces. Subroutine SPLINE uses the output from subroutine CUBIC to do the actual cubic spline interpolation.
CUBIC	:	Given an array of travel times and the corresponding amplitudes, this routine returns an array of the second derivative at each point. CUBIC is given in Applied Numerical Analysis by Gerald and Wheatley (p.251–217).
FFT2	:	Computes the roots of a dataset. For instance if a dataset is composed of 128 (ie. 2^{r1}) columns each record with 1024 (equal to 2^{r2}) samples, FFT2 computes $r1$ and $r2$ and passes these values to FARWAR or INVERS subroutine according to the value of the parameter COND (if COND=1 FFT2 calls forward Fourier transform, otherwise inverse Fourier transform is assumed).
FFT	:	Performs 1–D fast Fourier transform
FORWAR	:	Performs Fourier transform of two dimensonal data in the row direction. The transform is carried out as a series of 1–D transforms by calling the subroutine FFT.

Subroutine Name		*Description*
INVERS	:	Computes the two dimensional Fourier transform as a series of 1–D FFT. This subprogram calls subroutine FFT.
DMOUT	:	Performs numerical integration with respect to the time variable t_n for all w_o and k (ie. computes the left hand integral in equation (25)). Calls subroutine INTEGR to do the actual integration.
INTEGR	:	Does numerical integration using Simpson's method. It is a slightly modified version of the subroutine given in Applied Numerical Analysis by Gerald and Wheatley (p. 280).
GRAPH	:	Creates plot of a seismic record. Calls the Calcomp plotting subroutine LINE, AXIS, SYMBOL, and NUMBER. (This subroutine may be replaced by any other user plotting subroutine).

Input/Output parameters and common block names

Common block name

There is one common block defined in the program.

INPUT : Originally holds the input data to be processed. At the end of computation, INPUT contains the NMO and DMO corrected output data.

Variable Dictionary		*Description*
COMTR	:	Complex valued two dimensional array, which holds the input common offset section before processing and the zero offset equivalent common offset section at output.
AMP	:	Real valued one dimensional array, reads a trace from external disk and assigns the trace to the real part of COMTR.
TRACE	:	Real valued one dimensional array, holds the NMO corrected and unevenly spaced trace.
INTAM	:	Real valued one dimensional working area, holds the interpolated and equally spaced trace.
TNMO	:	Irregularly spaced NMO time corresponding to values in array TRACE.
TTIME	:	Equally spaced travel time corrosponding to the interpolated amplitudes in array INTAM.
NT	:	Number of points per trace.
NRC	:	Number of traces.
VEL	:	Normal moveout velocity.
H	:	The shot reciever half offset.
DELTAT	:	Sampling interval in time.
DELTAX	:	Sampling interval in space (ie. receiver spacing).

Plotting parameters

Variable Name		*Description*
XLEN	:	Length of the X-axis
YLEN	:	Length of the Y-axis
TSTART	:	Starting value for the Time axis
XSTART	:	Starting value for the X-axis (receiver axis)
ICON1	:	Parameter which controls the plot of the original data : $=$ 1 plot is requested $\neq$ 1 plot is not required
ICON2	:	Parameter which controls the plot of NMO corrected data : $=$ 2 plot is requested $\neq$ 2 plot is not required
ICON3	:	Parameter which controls the plot of the NMO and DMO corrected data : $=$ 3 plot is requested $\neq$ 3 plot is not required
IB	:	Flag for shading positive amplitudes
HEIG	:	parameter which controls the maximum trace amplitude

Test Run

The dip moveout operator displays a semi-elliptical response to a common offset section seeded with a spike [7]. The DMO program was tested for a synthetic common offset section in which the data consisted of zeros everywhere except the centre trace. The centre trace was seeded with seven spikes 650 milliseconds apart. The theoretically expected semi-elliptical responses were obtained. Fig. 5 shows that DMO is very significant for early time and at large offsets. As the reflection time increases the response curve becomes sharper and sharper. At shorter offsets and longer travel times the DMO operator reduces to a spike.

Dip-moveout Performance

The dip-moveout process involves time shift in the f–k domain. In the forward direction, the two dimensional data is fast Fourier transformed with respect to spatial variable and numerically integrated with respect to time. Mapping back to the *time–space* domain is performed using 2-D FFT. This DMO program is slightly slower, but more accurate compared to the approximated DMO algorithms which are being proposed recently and employ the 2-D FFT to move in and out of the $f - k$ space. The following table shows sample CPU times for selected data matrices.

DMO CPU Time for three data matrices

Matrix size	*CPU Time (including plotting)*
64×64	17.0 second
128×128	1.0 minute and 18.0 second
256×256	7.0 minute and 21.15 second

References

[1] Berkhout,A.J., Seismic inversion in terms of pre-stack migration and multiple elimination : *Proceedings of the IEEE*, v. **74**, no. **3**, pp. 415–427,1986.

[2] Bolondi,G., Loinger,E., and Rocca,F., Offset continuation of seismic sections : *Geophysical Prospecting*, v. **30**, pp. 813–828,1982.

[3] Biondi,B., and Ronen,S., Shot profile dip moveout using log-stretch transform : *SEG annual meeting expanded technical abstracts with bibliography*, pp. 431–434,1986.

[4] Clearbout,J.F., Imaging the Earth's Interior : *Blackwell Scientific Publications*, 398 pp.,1985.

[5] Deregowski,S.M., Dip moveout and reflector point dispersal : *Geophysical Prospecting*, v. **30**, pp. 318–322,1982.

[6] Deregowski,S.M., and Rocca,F., Geometrical optics and wave theory of constant offset sections in layered media : *Geophysical Prospecting*, v. **29**, pp. 384–406,1981.

[7] Hale,I.D., Dip-moveout by Fourier transform : *Geophysics*, v. **49**, no. **6**, pp. 741–757,1984.

[8] Gazdag,J., Wave equation migration with the phase shift method : *Geophysics*, v.**43**, no.**5**, pp. 1343–1351,1978.

[9] Gazdag,J., and Sguazzero,P., Migration of Seismic data by phase shift plus interpolation : *Geophysics*, v. **49**, no. **1**, pp. 124–131,1984.

[10] Gazdag,J., and Sguazzero,P., Migration of seismic data : *Proceedings of IEEE*, v. **72**, no. **10**, pp. 1302–1315,1984.

[11] Gerald,C.F., and Wheatley,P.D., *Applied numerical analysis,* Addison Whesley publishing company,1984.

[12] Levin,F.K., Apparent velocity from dipping interface reflections : *Geophysics*, v. **36**, pp. 510–516,1971.

[13] Philip,S.S., and Sherwood,J.W.C., Depth migration before Stack : *Geophysics*, v. **45**, no. **3**, pp. 376–393,1980.

[14] Serzu,M.H., and Moon,W.M., Two dimensional fast Fourier transform for large data matrices : *Computer Physics Communications (in press).*

[15] Stolt,R.H., Migration by Fourier transform : *Geophysics*, v. **43**, no. **1**, pp. 23–48,1978.

[16] Yilmaz,O., and Clearbout,J.F., Prestack partial migration : *Geophysics*, v. **45**, no. **12**, pp. 1753–1779,1980.

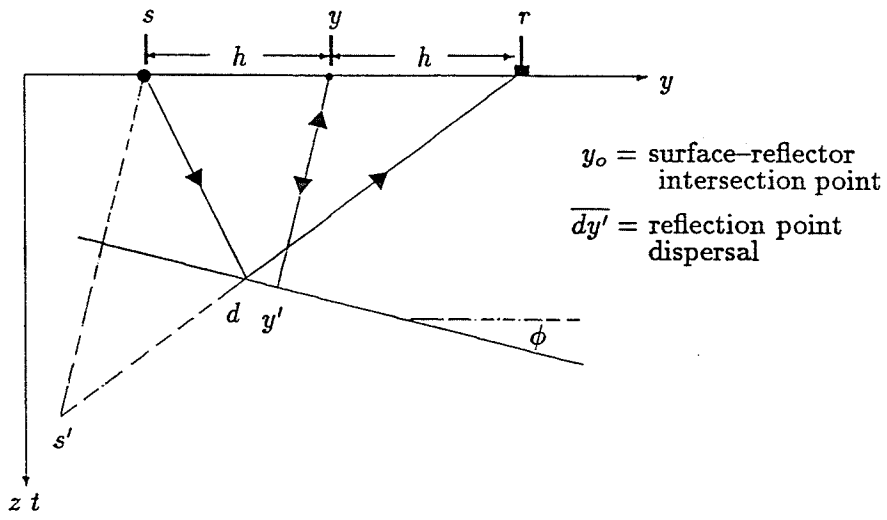

Figure 1: Seismic experiment conducted over a half-space with a constant velocity medium and a dipping reflector.

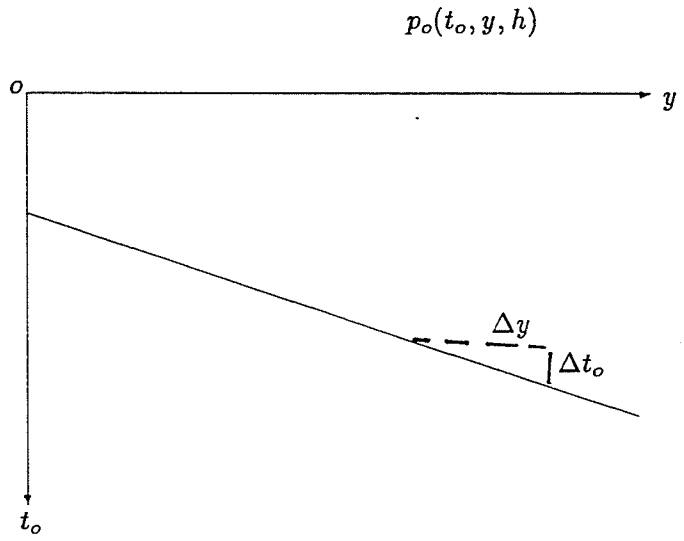

Figure 2: Zero offset section

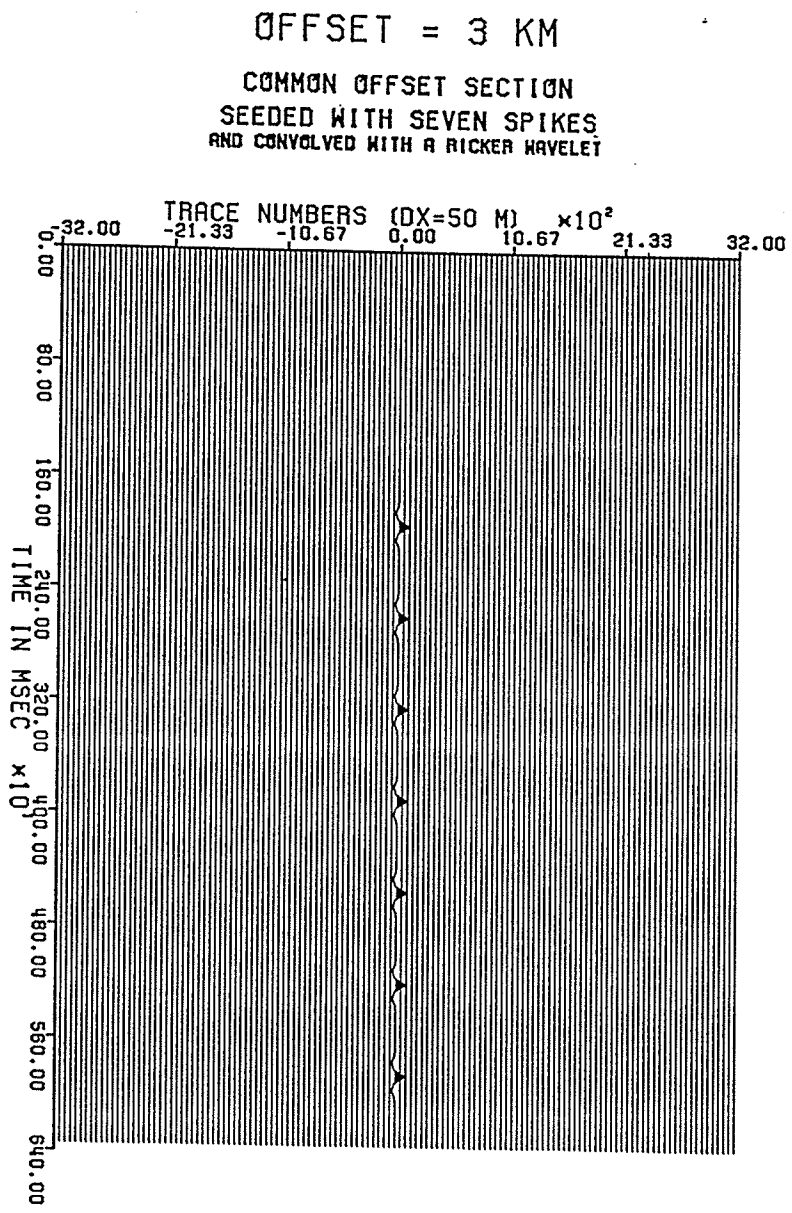

Figure 3: Common offset section seeded with seven spikes and convolved with a Ricker wavelet.

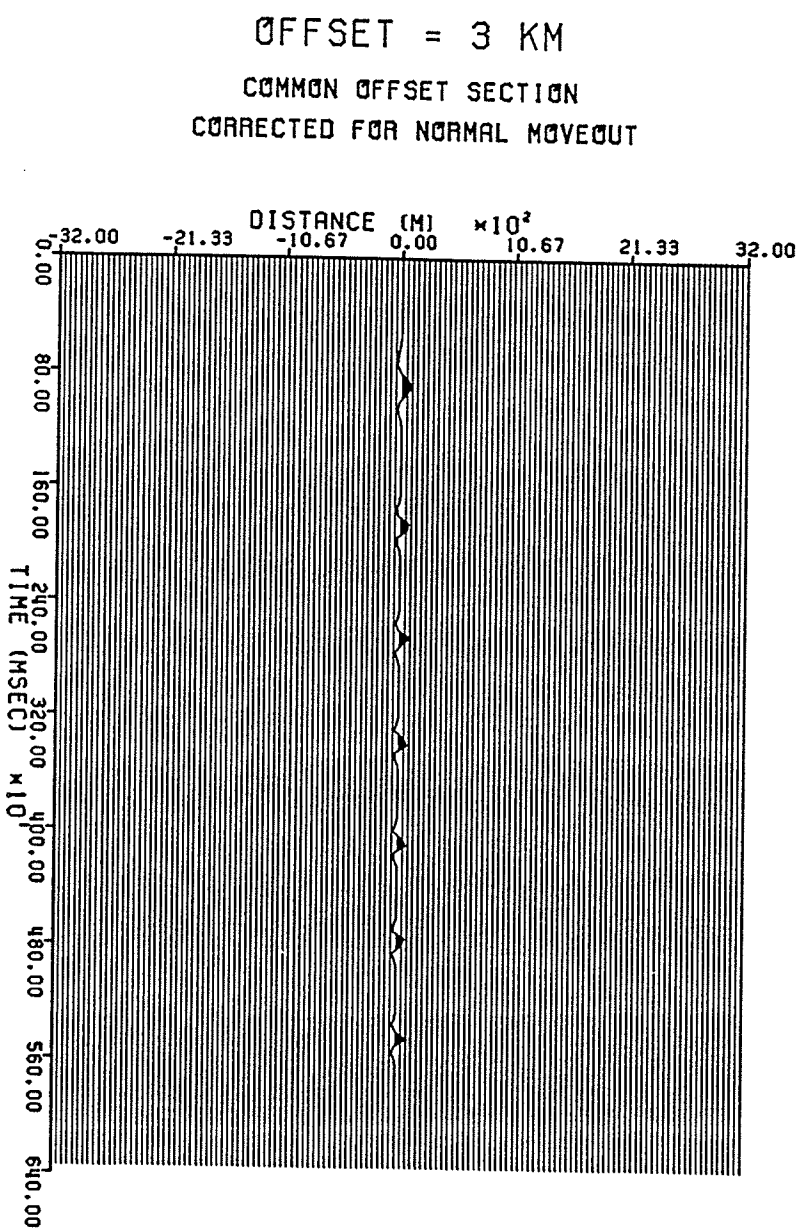

Figure 4: The common offset section given in figure 3 after NMO correction.

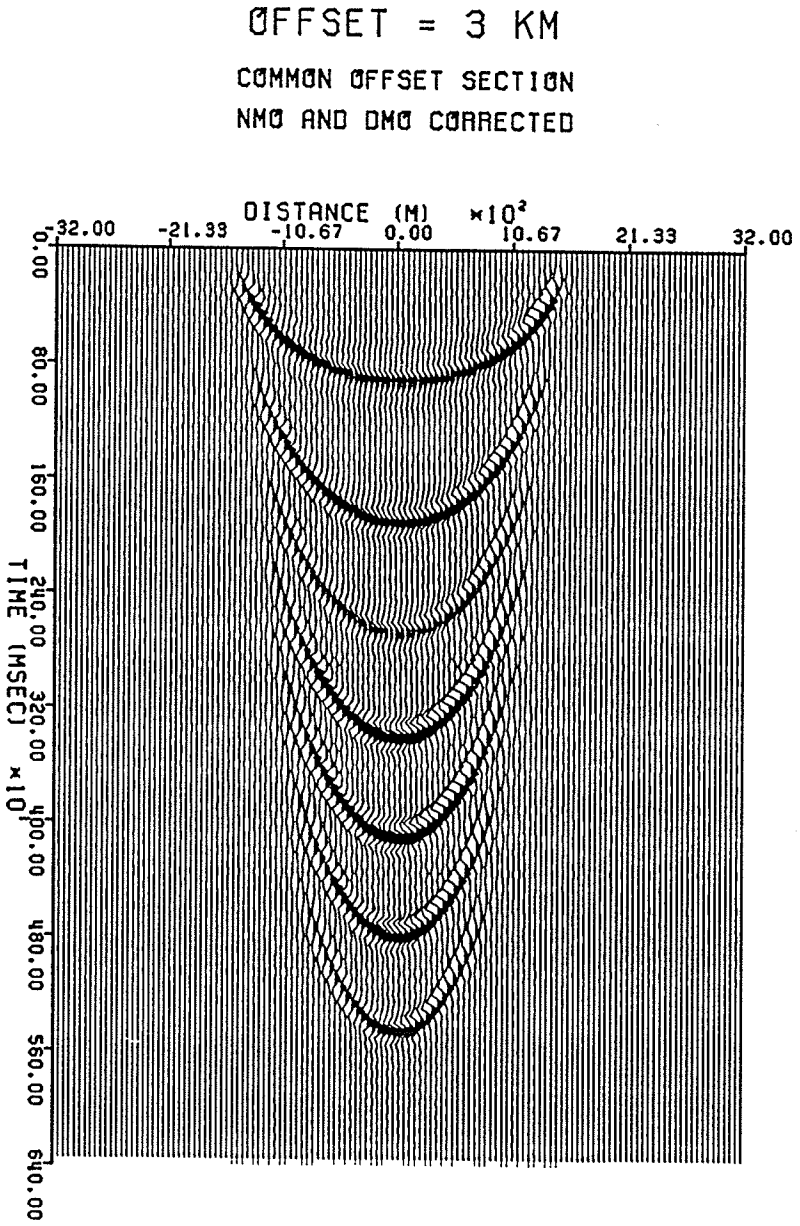

Figure 5: Common offset section after NMO and DMO correction.

Appendix D

Copy of the manuscript for the Stepwise 2-D Fast Fourier Transform for large datasets

This following paper deals with the Stepwise 2-D Fast Fourier Transform Program for large data matrices discussed in chapter 3 of this thesis. The paper was published in *Computer Physics Communications* Journal (Serzu and Moon, 1989(a)). The accompanying computer program in Fortran can obtained from the Computer Program Library section of the Computer Physics Communications.

TWO DIMENSIONAL FAST FOURIER TRANSFORM FOR LARGE DATA MATRICES

by

Mulugeta H. Serzu

and

Wooil M. Moon

Geophysics

The University of Manitoba

Canada R3T 2N2

Abstract

Most of the commonly used fast Fourier Transform subroutines require that the data matrix to be transformed to reside in the high speed core memory. This requirement is very prohibitive when the matrix to be transformed can not be accomodated into the system core memory. Hardware limitation makes the in-place FFT subroutines unsuitable for processing large data matrices.

In this paper we present a two dimensional FFT program (SW2DFFT) and its long write up. SW2DFFT is a Fortran program capable of handling large data matrices both square and rectangular in limited core memory. The program uses a stepwise approach in computing the large matrices based on the decomposed Cooley-Tukey algorithm (Anderson [1]). The number of arithmetic operations are exactly the same as the Cooley-Tukey method. The data matrix is stored externally in a direct access mass storage. A test run have been performed on a data matrix generated by numerically computing a two dimensional sine wave. Compared to other FFT algorithms ([2] p.164) gives accurate results.

Program Summary

Title of program : SW2DFFT

Computer : Amdahl 5780

Operating system : 370 MVS3

Programming language : Fortran IV (extended)

High speed storage required : the core memory requirement depends on size each subset. For 1024×1024 data matrix, in which a subset is made up of 32 columns (1024×32) the core memory requirement is 368K.

Number of bits on a byte : 8

Peripherals used : terminal, printer (line printer/Xerox laser printer)

Number of lines in the program : 428

Keywords : Fast Fourier Transform, implace computation, stepwise computation, 2-D FFT, rectangular data matrix

Nature of physical problem

Any problem that requires Fourier Transformation of a large 2-D data matrix.

Method of solution

The Discrete Fourier Transform (DFT) is computed using the decomposed Cooley–Tukey algortnineithm for Fast Fourier Transform [1]. The algortnineithm is implemented in decimation in time. The program avoids calling the complex function CMPLX and the Fast Fourier Transform is performed in two stages; A

and B.

Restrictions on the complexity of the program

The dimensions of the data matrix to be transformed has to be powers of 2. The data must reside in a direct access mass storage for efficient use of core memory.

Typical runnig time

For 256 by 256 data matrix

Stepwise FFT (SW2DFFT) : 33.90 sec

Usual FFT, [2], pp. 164 : 25.32 sec

LONG WRITE UP

Introduction

The Fast Fourier Transform (FFT) is an efficient method of computing the discrete Fourier transform (DFT). Because of its computational advantage the discrete Fourier transform have gained wide application in many fields of quantitative science.

The familiar Cooley–Tuckey algorithm as well as the canonic FFT algorithms require that the whole data matrix to be on hand (core memory) during computation. When the data matrix to be transformed is square and small enough to fit into the systems core memory, the two dimensional discrete Fourier transform is computed by repeated use of the one dimensional implace FFT algorithm, both in

column and row direction. However, if the data matrix can not be accomodated in the system's core memory, then, the implace FFT algorithms are not suitable to compute the discrete Fourier transform of the data matrix.

Here we present a long write up of the stepwise fast Fourier transform program (SW2DFFT). The SW2DFFT is a Fortran program capable of handling large data matrices both square and rectangular in limited core memory. The program uses a stepwise approach in computing large matrices. It is based on the decomposed Cooley–Tukey (decimation in time) alogithms [1].

Method of solution

The two dimensional discrete Fourier transform is given by :

$$X_{kl} = \sum_{j=0}^{N-1} \sum_{i=0}^{M-1} X_{ij}\, W_M^{ik}\, W_N^{jl} \qquad (1)$$

$$for \quad k = 0, 1, \cdots, M-1 \quad , \quad l = 0, 1, \cdots, N-1$$

where

$$W_N = e^{\frac{2\pi\sqrt{-1}}{M}}, \qquad W_M = e^{\frac{2\pi\sqrt{-1}}{N}}.$$

$\{X_{ij} |\ 0 \le i \le M-1 \quad and \quad 0 \le j \le N-1\}$ are complex data samples.

The inner sum in equation (1)

$$y_{kj} = \sum_{j=0}^{M-1} x_{ij} W_M^{ik} \quad for \quad k = 0, 1, \cdots, M-1 \tag{2}$$

is the columnwise Fourier transform. Since the the data matrix is stored columnwise a record from the data matrix is read and computed using one of the familiar FFT algorithms. The outer sum

$$X_{kl} = \sum_{j=0}^{N-1} y_{kj} W_M^{jl} \quad for \quad k = 0, 1, \cdots, M-1; l = 0, 1, \cdots, N-1 \tag{3}$$

is the discrete Fourier transform through the row and runs over every sample in the k^{th} row. In other words, if the data matrix does not fit into the core memory of the system, to obtain one row from the data matrix we have read every record (column) in the disk. This makes the implace FFT algorithms expensive as well as unsuitable for large data matrices. Anderson (1980) presented an algorithm which does not require the entire row to be implace at one time. This was done by rearrangement of the Cooley–Tukey FFT algorithm [1], [2].

For bit reversed input data ($N = 2^r$), that is

$$y_0([j_{r-1}, \cdots, j_0]) = x[j_0, \cdots, j_{r-1}] \tag{4}$$

the row transformation in binary form can be written as

$$y_r([l_{r-1},\cdots,l_0]) = \sum_{j_{r-1}=0}^{1} y_{r-1}([j_{r-1},l_{r-2},\cdots,l_0])\, W_N^{[l_{r-1},\cdots,l_0]j_{r-1}} \tag{5}$$

If $n = 2^s > 2$ is the number of samples that can be stored in real memory, then for each row we have N/n subsets. Each subset is composed of samples required to advance the data (row) s steps in the FFT algorithm. The equation required to do the partial transform is given below ([1]).

$$y_s([j_{r-1},\cdots,j_s,l_{s-1},\cdots,l_0]) = \sum_{j_{s-1}=0}^{1} \cdots \sum_{j_0=0}^{1} y_0([j_{r-1},\cdots,j_s,j_{s-1},\cdots,j_0]\cdots W^{[l_0]2^{r-s}} \cdots W^{[l_{s-1},\cdots,l_0]\,j_{s-1}\,2^{r-s}} \tag{6}$$

At stage one equation (6) partially transforms each subset and the result is written back to direct access mass storage. On the next stage the samples are chosen to allow each subset to advance another s steps in FFF algorithm. The process is repeated using equation (6). If the number of stages (r/s) is equal to two, on the first stage each subset is composed of $r-s$ common high order bits. At the second stage, each subset is made up of samples that can be advanced to the very last step of the FFT algorithm and it is given by

$$\{y_s([j_{r-1},\cdots,j_0]) \mid j_{2s-1},\cdots,j_s \text{ arbitrary; all other index bits constant }\}\ .$$

However, if the number of stages (r/s) is not an integer, there are fewer computational steps on the last stage. For instace, if the number of samples in each row is 32 which is equal to 2^5 and the number of samples in each subset is 8 (2^3) then r/s

is less than 2 which is rounded to 2. Two stages of three steps each make six steps (greater than the five required), hence, at the second stage we have to make sure that we calculate one less step, because for N equals to 2^r samples the full FFT algorithm requires only r computational steps.

Program structure

Main program

The main program reads the data matrix stored in bit reverse order one subset at a time. At every stage the program chooses records that would allow stepwise computation of the large data matrix. The chosen subset is passed to subroutine FFT2, and on return the intermidiate results are written back into the direct access disk storage.

Core memory requirement

For 1024 by 1024 complex data matrix, the core memory reqirement is about 32×1024 complex words (if each subset consists of 32 records). It is possible to minimize the core memory requirement by decreasing the size of a subset, hence, increasing the number stages.

Subroutines

1. FFT2 : computes the roots of a subset. For instance if a subset is composed of 32 (ie. 2^{r1}) columns each record with 1024 (equal to 2^{r2}) samples, FFT2 computes $r1$ and $r2$ and passes this values to DFT or IDFT subroutine according to value of the

parameter COND (if COND=1 FFT2 calls forward Fourier transform, otherwise inverse Fourier transform is assumed).

2. DFT : performs house keeping during Fourier transformation in the forward direction. This subroutine calls two user subroutines, BRIFFT and STPFFT.

3. IDFT : performs the same duty as DFT subroutine during computation of the inverse Fourier transform.

4. BRIFFT : is an implace FFT subroutine. This subroutine computes the discrete Fourier transformation in the column direction. BRIFFT calls function BITREV which return the power of the exponential weight (W_M^P). After the completion of computatin BITREV returns the index of the reordered data.

5. STPFFT : perfoms the FFT of a row in stepwise fashion, by repeated partial transform of each subset of the row. STPFFT calls the user supplied FLIP subroutine.

6. Flip : takes the index of a samples and returns the index of dual sample required for butterfly calculation. This subroutine also computes the power of the exponential weight given in equation (6).

Input parameters and common block names

All write/read passes to and from the direct access mass storage is unformatted. This was done to avoid unneccessary conversions.

Common block name

There is one common block defined in the program.

INPUT : holds the input data to the FFT subroutines and the output data after FFT computation.

Variable name	*Description*
AREAL and AIMAG	contains the real and the imaginary part of each subset
NCOL and NROW	are the dimensions of the data matrix
NS	number of columns in each subset
NSTAGE	number of stages required for the full FFT algorithm
NSUBS	number of subsets
NU	number of computational steps required to perform FFT in the column direction
SP	number of computational steps performed during row transform of a subset
INDEX	array that keeps track of the index of of each sample of a given record
COND	input option parameter = 1 F.T. of the data is to be computed = -1 inverse of the F.T. is to be computed

Application and performance

The two dimensional stepwise FFT program should be used when a need arises to perform FFT on large data matrix. For small and medium size matrices it is

slightly slower compaperd to the implace FFT subroutines. This is due to extra read/write pass required over the data. This program is much faster compared to similar programs which employ several tapes as external mass storage [6]. Unlike Eklunds method [5], there is no need to transpose the data matrix after processing is completed. The following table shows CPU time for two dimensional complex transforms.

CPU Time for two dimensional complex matrices

(for direct Fourier transform only)

Original matrix	Size of one subset	Minimum core requirement	CPU Time (sec)
64×64	64×8	76Kb	2.31
256×64	256×8	—	7.60
256×256	256×16	120Kb	33.90
1024×256	1024×16	—	121.73
1024×1024	1024×32	368Kb	597.88

Test Run

The test run output contains the title of the run, the two dimensional input data, the parameters and the computed forward Fourier transform of the data matrix.

Note

The test data is a two dimensional sine wave stored in a direct access data set in bit reverse order.

References

[1] G.L. Anderson,"A Stepwise Approach to computing the Multidimensional Fast Fourier Transform of Large Array," *IEEE Trans. Acoustics, Speech, and Signal Processing*, v. **28**, no. **3**, pp. 280–284,1980.

[2] G.D. Bergland, "A guided tour of the Fast Fourier Transform," *IEEE Spectrum*, v. **6**, no. **7**, pp. 41–52,1982.

[3] E.O. Brigham, The Fast Fourier Transform, *Eglewood Cliffs, NJ : Prentice Hall*, 1974.

[4] J.W. Cooley and J.W. Tukey,"An algorithm for machine calculation of complex Fourier series," *Math. Computation*, v. **19**, pp. 297–301,1985.

[5] J.O. Eklundh, "A fast computer method for matrix transposing," *IEEE Trans. Comput.*, vol. **C-21**, pp. 801–803,1972.

[6] R.C. Singleton, "A method for computing the fast Fourier transform with auxiliary memory and limited high-speed storage," *IEEE trans. Audio Electroacoust.*, v. **AU-15**, pp. 91–97,1967.